

**SIDE CHAIN ALKYLATION OF TOLUENE
WITH METHANOL OVER BASIC ZEOLITES**

NOVEL PRODUCTION ROUTE TOWARDS STYRENE?

Leden van de promotiecommissie:

Voorzitter / Secretaris:	Prof. dr. P.J. Gellings	(U. Twente)
Promotor:	Prof. dr. ir. L. Lefferts	(U. Twente)
Promotor:	Prof. dr. J.A. Lercher	(T.U. München)
Assistent-promotor:	Dr. J.G. van Ommen	(U. Twente)
Leden:	Prof. dr. ir. H. van Bekkum	(T.U. Delft)
	Prof. dr. ir. B. Weckhuysen	(U. Utrecht)
	Prof. dr. ir. W.P.M. van Swaaij	(U. Twente)
	Prof. dr. ir. A.B. de Haan	(U. Twente)
	Prof. dr. ing. G. Weickert	(U. Twente)
Deskundige:	Dr. G. R. Meima	(DOW Benelux BV)

Financial support of **CW/NWO** for the benefit of the workgroup 700.36.017 is gratefully acknowledged. This work was performed under the auspices of the Netherlands Institute for Catalysis Research (**NIOK**) and the Dutch Process Technology Institute Twente (**PIT**).

This publication has been supported financially by **CW/NWO**

Copyright © 2002 by Marco Rep, Hengelo (Ov), The Netherlands

ISBN 90 365 1816 4

Printing and binding by Océ Facility Services, Enschede

SIDE CHAIN ALKYLATION OF TOLUENE
WITH METHANOL OVER BASIC ZEOLITES

NOVEL PRODUCTION ROUTE TOWARDS STYRENE?

PROEFSCHRIFT

ter verkrijging van
de graad van doctor aan de Universiteit Twente,
op gezag van de rector magnificus,
prof. dr. F.A. van Vught,
volgens besluit van het College voor Promoties
in het openbaar te verdedigen
op woensdag 16 oktober 2002 te 13.15 uur

door

Marco Rep

geboren op 30 december 1970
te Zaandam

Dit proefschrift is goedgekeurd door de promotoren

Prof. dr. J.A. Lercher en Prof. dr. ir. L. Lefferts

en de assistent-promotor

Dr. J.G. van Ommen

*We do not inherit the earth from our ancestors;
we borrow it from our children.*

(anonymous)

To my parents and my brother

Summary

Styrene is an important monomer for the production of different types of (co-) polymers that are used in, e.g., toys, medical devices, food packaging, paper coatings etc. Styrene is produced with several different industrial processes. In 1998, the production of styrene monomer was approximately 21 million tons that are produced or used by more than 15,000 plants worldwide. Two of the largest production processes are described in Chapter 1 and both have their major drawbacks.

These drawbacks have prompted researchers (academic and industrial) to study other styrene synthesis routes. Two possible synthesis routes are introduced in Chapter 1. One of these possibilities is the side chain alkylation of toluene with methanol (MeOH) using basic zeolites. The toluene side chain alkylation reaction with methanol was first discovered by Sidorenko *et al.* (*Dokl. Akad. Nauk. SSSR* **1967**, 173, 132) in the mid sixties. Since then researchers all over the world have tried to improve the styrene productivity. Major drawbacks are the high methanol conversion to byproducts like CO, H₂, and dimethyl ether (DME) and the low yield of styrene.

This thesis describes our efforts to understand the fundamentals of the interaction between methanol and the zeolite host and its reaction with toluene.

In Chapter 2 a literature overview of the composition and structure of acidic and basic zeolites is given. Factors influencing acidity and basicity are discussed. Special emphasis is on alkali cation exchanged zeolites, also called basic zeolites. The basicity of zeolites was shown to be located on the zeolite framework oxygen centers adjacent to a framework aluminum center. Zeolite basicity increases with decreasing Si/Al ratio and within a given chemical composition of the zeolite framework with decreasing electrostatic potential of the charge balancing extra framework cation. Cation locations in basic FAU, MOR and MFI zeolites based on single crystal refinement and powder X-ray diffraction are also described. In Chapter 3, the general experimental equipment and procedures are described.

Our first attempt was to understand the adsorption structure of MeOH on basic zeolites (Chapter 4). Using i.r. spectroscopy it was observed that with increasing basicity of the framework oxygen centers (thus decreasing Si/Al ratio and decreasing electrostatic potential of the charge balancing cation) the interaction of the hydrogens of the hydroxy and methyl group of MeOH with the framework increased. Methanol adsorbed on Na- and Cs-MFI showed sharp OH and CH i.r. bands, while on Na-FAU(Y) a broad methanol OH i.r. band was observed. It was concluded that this was the result of increasing hydrogen bonding between methanol and the basic zeolite host. In the case of Na- and Cs-FAU(X), due to the high cation concentration and the proximity of adsorption sites, interaction between adsorbed methanol molecules contributes as well to the i.r. spectrum of adsorbed methanol. Furthermore, the high basicity of these basic FAU(X) zeolites, induces interaction between the CH group and the zeolite host. This increased interaction, however, did not result in increased binding energy. In Chapter 5 the possible location of the methanol adsorption complexes is given. MeOH-cation complexes in FAU(X) are located in the supercage, whereas in MOR and MFI they are found in the channels.

The high methanol conversion into DME, CO and H₂ is the subject of Chapter 6. It is concluded that DME is formed by reaction over the alkali cations in the zeolite *via* “surface” methoxy groups. Especially small cations catalyze the reaction efficiently. Methanol dehydrogenation yielding formaldehyde needs the concerted action of both the alkali cation and the zeolite oxygen centers and proceeds only over zeolites with high surface basicity. The MeOH hydroxy hydrogen combines with methyl hydrogen yielding gaseous H₂ and adsorbed formaldehyde (CH₂O). The adsorbed CH₂O decomposes *via* surface formate into CO and H₂. A mechanism is proposed that accounts for these observations.

In Chapter 7 it was observed that with the use of oxygen MeOH dehydrogenation was facilitated yielding surface formaldehyde at low temperatures. At low temperature ($T < 500$ K) the adsorbed formaldehyde species tend to dimerize to form methyl formate. At temperatures above 463 K formaldehyde decomposition and oxidation yielding CO₂, CO, and H₂ was observed. The use of O₂ also induced the formaldehyde production on weakly basic MFI catalysts, otherwise not active dehydrogenation catalysts.

In Chapter 8 a mechanism is presented that accounts for the reaction of toluene with methanol over basic FAU(X) zeolites yielding styrene. The formation of the carbon-carbon bond between formaldehyde and toluene resembles an aldol condensation reaction. Co-adsorption studies showed that the adsorption and activation of toluene is critical to enable the conversion to styrene and therefore strong basic sites are needed. Furthermore, strong basic sites are also necessary to dehydrogenate methanol to CH₂O. These requirements are met best with the choice of Rb- and Cs-FAU(X). However, very low styrene yields were obtained. This is mainly caused by the high MeOH decomposition into DME, CO and H₂ at temperatures where alkylation proceeds.

Therefore, it was tried to react formaldehyde and toluene at lower temperatures (Chapter 9), by using oxygen. Addition of oxygen yielded formaldehyde at lower temperatures and our hopes were that with increasing surface CH₂O concentration also the reaction with toluene would be facilitated, yielding more styrene. Slightly higher styrene selectivity was found, but mainly higher methanol conversion related to decomposition and oxidation. Thus it was concluded that activation of the toluene side chain over basic zeolites has to be improved, to yield more styrene.

This work has shown that the MeOH decomposition *via* surface formaldehyde and formate into CO and H₂ and the MeOH dehydration yielding dimethyl ether has to be diminished and the activation of toluene has to be improved before competitive technology can be developed based on these catalysts.

Samenvatting

Styreen is een belangrijk monomeer voor de produktie van verschillende soorten (co-) polymeren die bijvoorbeeld verwerkt worden in plastic speelgoed, medische toepassingen, verpakkings materiaal, papier coatings enz. Styreen wordt momenteel geproduceerd via verschillende industriële processen. In 1998 bedroeg de produktie van styreen ongeveer 21 miljoen ton en werd geproduceerd of gebruikt door 15.000 fabrieken wereldwijd. Twee van de belangrijkste processen worden beschreven in hoofdstuk 1 tezamen met de industriële tekortkomingen.

Deze tekortkomingen hebben industriële en academische onderzoekers ertoe aangezet om andere styreen synthese routes te onderzoeken. Twee mogelijkheden worden beschreven in hoofdstuk 1. Eén van deze mogelijkheden is de zijketen alkylering van toluen met methanol (MeOH) waarbij gebruik wordt gemaakt van basische zeolieten. De toluen zijketen alkylerings reactie met methanol werd ontdekt door Sidorenko *et al.* (*Dokl. Akad. Nauk. SSSR* **1967**, 173, 132) halverwege de jaren zestig. Sinds die ontdekking hebben onderzoekers over de hele wereld geprobeerd de styreen produktiviteit te verbeteren. De belangrijkste tekortkomingen zijn de hoge methanol conversie in de bijprodukten CO, H₂ en dimethyl ether (DME) en de lage opbrengst van styreen.

Dit proefschrift beschrijft onze inspanningen om de beginselen van de interactie tussen methanol en de zeoliet host en de reactie met toluen te begrijpen.

Hoofdstuk 2 beschrijft de zeoliet samenstelling en structuur van de zure en basische zeolieten, zoals gebruikt in dit proefschrift en is gebaseerd op literatuur onderzoek. De factoren die zuursterkte en basiciteit beïnvloeden worden besproken. Speciale aandacht wordt besteed aan de alkali cation uitgewisselde zeolieten, ook wel basische zeolieten genoemd. De basiciteit van zeolieten blijkt gelocaliseerd te zijn op de zuurstof centers van het zeoliet geraamte naast een aluminium center. De basiciteit van zeolieten neemt toe met afnemende Si/Al verhouding en binnen een bepaalde samenstelling van het zeoliet met afnemende electrostatische potentiaal van het lading stabiliserende cation dat geen onderdeel is van het zeoliet geraamte. Ook wordt hier de locatie van de cationen in basische FAU, MOR en MFI zeolieten beschreven welke is gebaseerd op één-kristal refinement en poeder diffractie. De algemene werkwijze en experimentele apparatuur zijn in hoofdstuk 3 beschreven.

Onze eerste aanpak van het probleem betrof de adsorptie structuur van methanol op basische zeolieten (hoofdstuk 4). Met behulp van infrarood spectroscopie bleek dat met toenemende basiciteit van de zuurstof centers in het zeoliet geraamte (dus met afnemende Si/Al verhouding en afnemende electrostatische potentiaal van het lading stabiliserende cation) de interactie van de waterstof atomen van de hydroxy en de methyl groep van methanol met het zeoliet geraamte toe nam. Methanol geadsorbeerd op Na- en Cs-MFI vertoonde scherpe methanol OH en CH infrarood banden, terwijl op Na-FAU(Y) een brede methanol OH infrarood band werd waargenomen. Dit is zeer waarschijnlijk het resultaat van waterstof brug vorming tussen MeOH en de zeoliet host. In het geval van Na- en Cs-FAU(X) bleek interactie tussen geadsorbeerde methanol moleculen, veroorzaakt door de hoge cation concentraties en de nabijheid van adsorptie plaatsen, ook aan het infrarood spectrum van

geadsorbeerd MeOH toe te voegen. Bovendien veroorzaakt de hoge basiciteit van deze basische FAU(X) zeolieten ook interactie tussen de CH groep en de zeoliet host. Echter de toegenomen interactie resulteerde niet in een toegenomen MeOH bindingsenergie. In hoofdstuk 5 wordt de mogelijke locatie van de MeOH-cation complexen beschreven. De MeOH-cation complexen in FAU(X) zijn gelocaliseerd in de supercage; in MOR en MFI worden deze in de kanalen gevonden.

De hoge methanol conversie in dimethyl ether, CO en H₂ is het onderwerp van hoofdstuk 6. DME wordt gevormd door reactie van MeOH over de alkali cationen in het zeoliet via “oppervlakte” methoxy groepen. Vooral kleine cationen katalyseren de reactie efficiënt. Methanol dehydrogenering levert geadsorbeerd formaldehyde en dit vereist de samenwerking van het alkali cation en de zuurstof centers van het zeoliet geraamte en verloopt alleen over zeolieten met een hoge basiciteit. De MeOH hydroxy waterstof combineert met een methyl waterstof en levert gasvormig H₂ en geadsorbeerd formaldehyde (CH₂O). Het geadsorbeerde CH₂O ontleedt in CO en H₂ via oppervlakte formiaat. Een mechanisme dat deze waarnemingen kan verklaren wordt voorgesteld.

Het gebruik van zuurstof vergemakkelijkt de MeOH dehydrogenering tot formaldehyde bij lage temperatuur. Dit is beschreven in hoofdstuk 7. Dimerisatie van geadsorbeerd CH₂O bij lage temperatuur (T < 500 K) leidde tot de productie van methyl formiaat. Bij temperaturen boven de 463 K werd formaldehyde ontleding en oxidatie waargenomen wat resulteerde in de vorming van H₂, CO en CO₂. Het gebruik van zuurstof leidde ook tot de vorming van geadsorbeerd formaldehyde op zwak basische MFI zeolieten, welke zonder zuurstof geen actieve katalysatoren voor MeOH dehydrogenering zijn.

In hoofdstuk 8 wordt een mechanisme voorgesteld dat de reactie van toluen met methanol over basische zeolieten wat leidt tot styreen kan verklaren. De vorming van de koolstof-koolstof binding tussen CH₂O en toluen lijkt op een aldol condensatie reactie. Coadsorptie studies toonden aan dat de adsorptie en activering van toluen belangrijk is om conversie naar styreen mogelijk te maken en dus zijn sterke basische sites nodig. Sterke basische sites zijn ook nodig voor de dehydrogenering van methanol tot formaldehyde. Deze vereisten worden gevonden in de zeolieten Rb- en Cs-FAU(X). Echter erg lage styreen opbrengsten worden verkregen. Dit wordt voornamelijk veroorzaakt door de hoge MeOH ontleding in DME, CO en H₂ bij de temperaturen waar ook toluen alkylering plaatsvindt.

Daarom is geprobeerd om toluen te laten reageren met formaldehyde bij lagere temperaturen (hoofdstuk 9). Toevoeging van zuurstof leidde tot CH₂O productie bij lagere temperatuur en onze hoop was dat met de toenemende CH₂O oppervlakte concentratie ook de reactie met toluen zou verbeteren, resulterend in meer styreen. Naast een kleine verbetering in de styreen productie werd voornamelijk hogere methanol conversie, gerelateerd aan ontleding en oxidatie, gevonden. Dus om meer styreen te produceren moet de activering van toluen worden verbeterd.

Dit werk heeft aangetoond dat omzetting van MeOH in de producten CO en H₂ via oppervlakte CH₂O en formiaat en in DME moet worden verkleind en dat activering van toluen moet worden verbeterd, voordat competitieve technologieën op basis van deze katalysatoren kunnen worden ontwikkeld.

Resumen

El estireno es un monómero importante para la producción de distintos tipos de (co)-polímeros usados en plásticos, aparatos médicos, producción de papel, etc. La producción de estireno se lleva a cabo a través de distintos procesos industriales. En 1998, la producción de estireno alcanzaba aproximadamente 21 millones de toneladas siendo utilizado en más de 15.000 plantas industriales en todo el mundo. Los dos mayores procesos industriales descritos en el Capítulo 1 presentan también sus desventajas. Estas desventajas han hecho que investigadores (a nivel académico e industrial) estudien otras rutas opcionales para la síntesis del estireno. Dos de estas posibles rutas se describen en el Capítulo 1. Una de ellas es la alquilación de la cadena lateral del tolueno con metanol (MeOH) sobre zeolitas básicas. La alquilación de la cadena lateral del tolueno fue descubierta por Sidorenko *et al.* (*Dokl. Akad. Nauk. SSSR* **1967**, 173, 132) a mediados de los años sesenta. Desde entonces, investigadores de todo el mundo han intentado aumentar la producción de estireno. Las mayores desventajas que estos procesos presentan son la elevada conversión de metanol en subproductos tales como CO, H₂, y dimetiléter (DME) y la baja conversión en estireno.

Esta tesis describe nuestros esfuerzos por entender la razón de la interacción entre el metanol y la zeolita y su reacción con el tolueno.

En el Capítulo 2 se describe la revisión bibliográfica sobre la composición y estructura de las zeolitas ácidas y básicas. Los distintos factores que afectan a la acidez y basicidad de las zeolitas son discutidos, haciendo especial énfasis en las zeolitas intercambiadoras de cationes, también llamadas zeolitas básicas, cuya basicidad depende de la relación Si/Al. Las posiciones de los cationes en distintos tipos de zeolitas básicas (FAU, MOR y MFI) también se describen en este capítulo.

Nuestro primer intento se centró en la búsqueda del mecanismo de adsorción del MeOH sobre la superficie de la zeolita (Capítulo 4). Con la ayuda de una técnica espectroscópica (i.r) se observó que al aumentar la basicidad en el entorno de los centros de oxígeno (por lo tanto aumentando Si/Al) se producía un aumento en la interacción de las moléculas de hidrógeno y de los grupos hidroxilo y metilo del MeOH con la zeolita. En el caso de la adsorción de MeOH sobre Na- y Cs-FMI, las bandas de infrarrojo de los grupos OH y CH fueron muy acentuadas, mientras que en el caso de Na-FAU(Y), se observó una banda ancha correspondiente a grupos OH. Se concluye, por tanto, que esto es el resultado del aumento de los enlaces del H entre el MeOH y la zeolita básica. En el caso de Na- y Cs-FAU(X), la elevada concentración de catión y a la proximidad entre centros activos y por tanto entre moléculas de metanol adsorbido, se observa también en el espectro de infrarrojo. Además, la elevada basicidad de las zeolitas tipo FAU(X), induce interacción entre el grupo CH y la zeolita misma. Sin embargo, esta elevada interacción, no resultó en un aumento en la energía de enlace.

En el Capítulo 5, se muestra la probable localización de los complejos de metanol adsorbidos. Los complejos MeOH-catión sobre FAU(X) se localizan en la estructura de la celda, mientras que en MOR y MFI se localizan en los canales.

El estudio de la elevada conversión de metanol en DME, CO y H₂ se lleva a cabo en el Capítulo 6. Se concluye que DME se forma como resultado de la reacción de cationes sobre la zeolita vía formación de “metoxy grupos sobre la superficie”, en los que cationes pequeños catalizarían la reacción. La deshidrogenación de metanol hacia formaldehído necesita la acción conjunta del catión y los centros de oxígeno en la zeolita, llevándose a cabo, por lo tanto, sólo sobre zeolitas que poseen elevado carácter básico. El hidrógeno del grupo hidroxilo del metanol se combina con el hidrógeno del metilo llevando a la formación de H₂ en estado gaseoso y formaldehído (CH₂O). El CH₂O adsorbido se descompone formando un compuesto intermedio en superficie (formato), descomponiéndose este último en CO y H₂. Se propone también el mecanismo sustentado por estas observaciones.

En el Capítulo 7 se discute sobre la deshidrogenación del metanol utilizando oxígeno. Además se observa la formación de formaldehído a baja temperatura. A bajas temperaturas la concentración de formaldehído adsorbido sobre la superficie se ve limitada por la producción de metilformato. A elevadas temperaturas se observa la descomposición de formaldehído en CO₂, CO y H₂. En el caso de MFI (catalizador no activo hacia la deshidrogenación), la presencia de O₂ induce también la formación de formaldehído.

En el Capítulo 8 se presenta un mecanismo que explicaría la reacción entre el tolueno y el metanol sobre FAU(X) para producir estireno: La formación del enlace C-C entre el formaldehído y el tolueno se asemeja a una reacción de condensación. Basándonos en estudios de adsorción se concluye que para obtener un buen catalizador que produzca estireno, se debe dar preferiblemente la adsorción de tolueno y el catalizador ha de tener suficiente carácter básico. De ahí que se haya escogido Rb- y Cs-FAU(X). Sin embargo, las conversiones de estireno son muy bajas. Esto se explicaría debido a la descomposición del metanol en DME, CO y H₂ en el rango de temperatura en el que la alquilación se produciría.

Se intentó hacer reaccionar el formaldehído y el tolueno con oxígeno a baja temperatura (Capítulo 9). Con ello se intentaba aumentar la concentración de formaldehído en superficie y por lo tanto facilitar la reacción con el tolueno, produciendo así más estireno. Como resultado, una pequeña mejora en la conversión a estireno se ha encontrado, aumentando significativamente la descomposición y oxidación de metanol. Se concluye así, que la activación de la cadena lateral del tolueno sobre zeolitas básicas para la producción de estireno necesita ser mejorada.

Este trabajo muestra que la descomposición del metanol en CO, H₂ (vía formación de formaldehído y formato) y la deshidratación del metanol en DME tiene que ser minimizada. Además, la activación del tolueno debe ser mejorada para hacer que esta reacción pueda competir con los procesos actuales de producción de estireno.

Contents

Chapter 1: <i>Introduction</i>	1
Chapter 2: <i>Materials</i>	27
Chapter 3: <i>Experimental</i>	43
Chapter 4: <i>Interaction of Methanol with Alkali Cation Exchanged Molecular Sieves: IR Spectroscopic Study</i>	59
Chapter 5: <i>Location of Methanol-Cation Adsorption Complexes in FAU, MOR and MFI</i>	75
Chapter 6: <i>Methanol Reaction over Basic Zeolites</i>	89
Chapter 7: <i>Oxydehydrogenation of Methanol over Basic Zeolites</i>	127
Chapter 8: <i>Alkylation of Toluene over Basic Catalysts - Key Requirements for Side Chain Alkylation</i>	157
Chapter 9: <i>Side Chain Methylation of Toluene: The Effect of Molecular Oxygen</i>	175
<i>Acknowledgements</i>	197
<i>Curriculum Vitae</i>	199
<i>List of Publications</i>	200

Parts of this thesis have been published and can be found in literature:

Chapter 4:

Interaction of Methanol with Alkali Metal Exchanged Molecular Sieves. 1. IR Spectroscopic Study (full length),

Rep, M; Palomares, A.E.; Eder-Mirth, G.; Van Ommen, J.G.; Rösch, N.; Lercher, J.A. *J. Phys. Chem. B* **2000**, *104*, 8624 as Part 1. (Part 2 is a DFT study on the adsorption of methanol on Si-O-Al clusters containing different Al concentrations and alkali metal cations; Vayssilov, G.; Lercher, J.A.; Rösch, N. *J. Phys. Chem. B* **2000**, *104*, 8614.)

Sorption of Methanol in Alkali Exchanged Zeolites (partially),

Rep, M; Palomares, A.E.; Van Ommen, J.G.; Lefferts, L.; Lercher, J.A. In *Proceedings of the 12th International Congress on Catalysis, Granada*; Corma, A., Melo, F.V., Mendioroz, S., Fierro, J.L.G., Eds.; Elsevier: Amsterdam, 2000; Vol. 130C, pp 2957-2962.

Chapter 6:

I.r. Study on the Reaction Path of Methanol Decomposition over Basic Zeolites (partially),

Rep, M; Van Ommen, J.G.; Lefferts, L.; Lercher, J.A. In *Proceedings of the 13th International Zeolite Conference, Montpellier*; Galarneau, A., Di Renzo, F., Fajula, F., Viedrine, J., Eds.; Elsevier: Amsterdam, 2001; Vol. 135, p 316.

Chapter 8:

Alkylation of Toluene over Basic Catalysts – Key Requirements for Side Chain Alkylation (full length),

Palomares, A.E.; Eder-Mirth, G.; Rep, M; Lercher, J.A. *J. Catal.* **1998**, *180*, 56.

Chapter 1

Introduction

Abstract:

Styrene is used as intermediate for the production of different polymers. Two different industrial processes produce the majority of the worldwide styrene throughput. The use of carcinogenic reagents, corrosive catalysts, energy demands or market needs have motivated the chemical industry to search for alternatives. Two new processes are described, that have theoretical potential to replace these industrial processes. Special emphasis will be on the use of heterogeneous zeolitic catalysts as catalysts for the selective direct synthesis of styrene *via* side chain alkylation of toluene with methanol. This Chapter will give an overview of the results obtained so far for the side chain methylation of toluene to produce styrene.

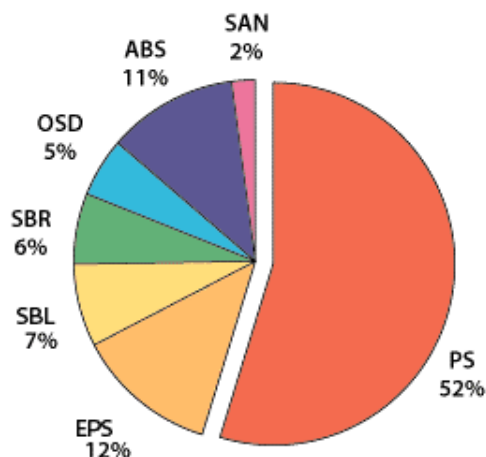
1.1 INDUSTRIAL PRODUCTION ROUTES TO STYRENE

As this thesis is mainly attributed to developing fundamental understanding of the selectivities obtained in the alkylation of toluene over basic zeolites, this paragraph will introduce styrene and its utilization in (co-) polymers, its commercial production (with major drawbacks) and novel production routes currently under investigation.

There is no direct end use for styrene. It is a well-known basic building block for the manufacture of a broad range of materials used in thousands of products throughout the world, e.g., pipelines, toys, package material, etc. The production of styrene monomer in 1998 was approximately 21 million tonnes, produced or used by more than 15,000 plants worldwide.

Commercially available polymers containing styrene as building block are collected in Figure 1.1 and Table 1.1. Figure 1.1 displays the market share for styrene in the

production of different polymers, whereas in Table 1.1 characteristics and common uses of these polymer plastics are compiled. Fig. 1.2 shows a Scanning Electron Micrograph of foamed polystyrene.



Polystyrene (PS); Expandable polystyrene (EPS); Acrylonitrile-butadiene-styrene (ABS); Styrene-acrylonitrile (SAN); Styrene-butadiene rubber (SBR); Unsaturated polyester resins (UPE); Styrene-butadiene latices (SBL); Other styrene related products (OSD)
Figure 1.1: Market share of styrene monomer in different polymers.

Table 1.1: Styrene-containing polymers, their characteristics and their usage [1,2,3].

(Co-) polymer	Characteristics	Usage
polystyrene	rigid, brittle, low strength	package material (CD, MC), toys
foamed polystyrene	lightweight, rigid	food package, protection, insulation
acrylonitril-butadiene-styrene	rigid, thermal resistance, glossy	toys, protection, chairs
acrylonitril-styrene	clarity, chemical resistance	auto lenses, medical devices
styrene-butadiene rubber	high-performance elastomers	shoe soles, conveyor belts
styrene-butadiene latex	thermal/chemical resistance	paper coating, carpet adhesive
styrene- <i>p</i> -divinylbenzene	ion-exchange material	separation or cleaning

1. Ege, S. *Organic Chemistry*, 2nd Edition; D.C. Heath and Company: Lexington, 1989; pp 1180-1181.

2. For more information and characteristics about styrene (co-)polymers: <http://www.designinsite.dk>

3. For more information and characteristics: <http://www.styreneforum.org/>

State of the art: commercial production of styrene.

In this paragraph, two major industrially employed production routes towards styrene, i.e., (1) adiabatic ethylbenzene (EB) dehydrogenation employed by ABBLummus/UOP (Classic SMTM process) and (2) the SMPO process employed by SHELL, will be presented. Major drawbacks of these reactions are discussed as well. Other processes for the production of styrene are, e.g., Toray's STEX process (extraction of styrene from pyrolysis gasoline) and Lurgi's isothermal EB dehydrogenation process, which will not be discussed here [4].

Adiabatic dehydrogenation of ethylbenzene

At present the most important industrial production route towards styrene (over 75% of all operating styrene plants) is the adiabatic catalytic ethylbenzene dehydrogenation. The process was discovered and developed by IG Farbe in 1931. Modified and improved technology was commercialised by, e.g., ABBLummus/UOP, an American styrene-producing company (Classic SMTM

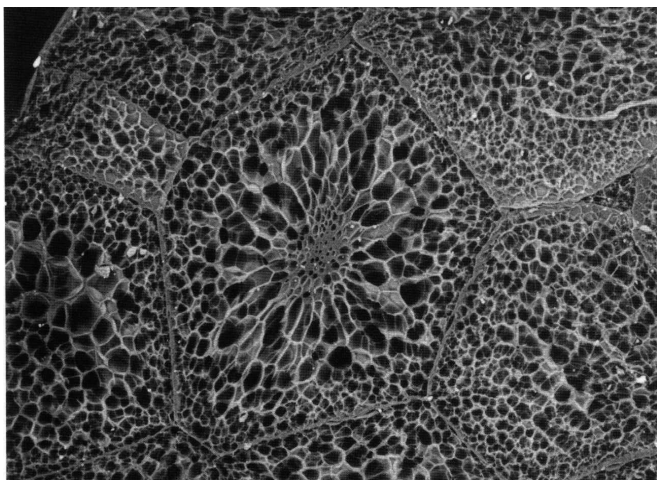


Figure 1.2: Foamed polystyrene; a SEM-picture (courtesy of JOEL Ltd.: Low Vacuum SEM Micrographs).

process). The reaction was previously performed over a potassium-promoted iron oxide catalyst (S-105, C-105, etc.) produced by Criterion Catalysts Corp., a SHELL company [5]. The Süd-Chemie Group now has the major share of the catalyst market with its G-64 and G-84 catalyst types. The average catalyst lifetime is approximately 1-2 years [5].

Evidence of an active potassium-ferrite phase, KFeO_2 , for the ethylbenzene dehydrogenation reaction

has been found [6]. However, more and more accepted in literature is that the active sites on these catalysts are not on the initial KFeO_2 surface one started with. Nowadays, a carbonaceous overlayer that is initially deposited on the surface and consists of carbon, oxygen and probably hydrogen is thought to be the active phase [7]. Only after its formation, the conversion rate is high. The active sites might be identified as being surface carbonyl and quinone groups [8,9]. These coke deposits arise from

4. a) Weissermel, K.; Arpe, H.J. *Industrial Organic Chemistry, Third Completely Revised Edition*; VCH Verlagsgesellschaft mbH: Weinheim, 1997; pp 335-342; b) James, D.H.; Castor, W.M. In *Ullmann's Encyclopedia of Industrial Chemistry*, 6th Edition (Electronic); Wiley-VCH Verlag GmbH, Weinheim, 2001.

5. Lee, E.H. *Catal. Rev.* **1973**, *8*, 285.

6. a) Meima, G.R.; Menon, P.G. *Appl. Catal. A: General* **2001**, *212*, 239; b) Holmlid, L.; Menon, P.G. *Appl. Catal. A: General* **2001**, *212*, 247.

7. Kuhrs, C.; Arita, Y.; Weiss, W.; Ranke, W.; Schlögl, R. *Topics Catal.* **2001**, *14*, 111.

8. Pereira, M.F.R.; Órfão, J.J.M.; Figueiredo, J.L. *Appl. Catal. A: General* **1999**, *184*, 153.

9. Mestl, G.; Maksimova, N.I.; Keller, N.; Roddatis, V.V.; Schlögl, R. *Angew. Chem.* **2001**, *113*, 2122.

the polymerization of the product styrene, which subsequently decompose on the catalyst surface to graphite-like structures *via* dehydrogenation. The presence of a Brønsted basic surface initiates this polymerisation of styrene to polystyrene [7]. Potassium doping also facilitates the gasification process of carbon deposits with steam. Steam reacts with carbon deposited on the catalyst surface (C) yielding carbon monoxide (CO) and carbon dioxide (CO₂) in a sequence of steps ($C + H_2O \rightarrow CO + H_2$ followed by $CO + H_2O \rightarrow CO_2 + H_2$). This process is catalyzed by K₂CO₃.

From the previous it is clear that there is a delicate equilibrium between the rate of coke build up, which is the active catalyst for ethylbenzene dehydrogenation, and the rate of coke gasification, necessary to prevent catalyst deactivation. Operation at more severe conditions, i.e. lower steam-to-aromatics (S/O) ratio ($< 7\text{-}12 \text{ mol}\cdot\text{mol}^{-1}$), higher reaction temperatures or the loss of gasification promoter (K₂CO₃) can result in an imbalance of this delicate balance of rates, leading to build up of coke and deactivation.

Figure 1.3 shows the flow scheme of a typical adiabatic ethylbenzene dehydrogenation plant as used by, e.g., ABBLummus/UOP, and contains the following process steps and units [4b]:

a superheater (1) for the generation of steam (temperature $\approx 993 \text{ K}$) to bring the system up to reaction temperature (approximately 913 K). The dehydrogenation unit (2), contains two adiabatic, fixed bed, radial flow reactors, and since during adiabatic reaction the process temperature drops, the outlet stream is reheated prior to passage through the second reactor. Fresh ethylbenzene feed is mixed with recycled ethylbenzene from the distillation system, vaporized and diluted with steam. The steam / ethylbenzene ratio fed to the reactors is chosen to give optimum yield with minimum utility cost. Conversion of ethylbenzene can vary with the system, but is often about 35 % in the first reactor and 65 % overall.

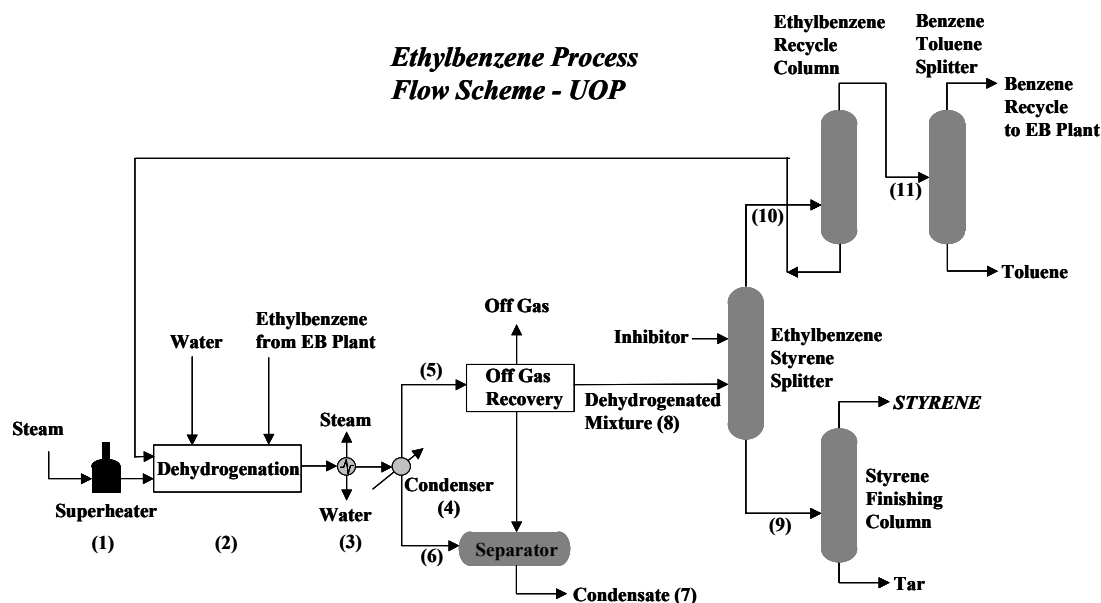


Figure 1.3: Flow scheme of a typical adiabatic ethylbenzene dehydrogenation plant.

The reactors are run at the lowest pressure that is safe (vacuum (0.5-0.8 atm) is needed, since the reaction is favored by low pressures). The reactor effluent is fed through an efficient heat recovery

system (3) to minimize energy consumption. Then it is condensed (4) and separated into vent (off) gas (5) and a steam condensate stream (6). The off gas stream (5), consisting mainly of hydrogen and carbon dioxide is compressed, processed through the off gas recovery section to recover aromatics, and used as fuel in the steam superheater or a feed stream for chemical hydrogen. The steam condensate (6) is steam-stripped, treated, and reused. The condensates from the condenser (4) and off gas recovery section (5) flow into the separator (7) where hydrocarbon and water phases are separated from each other. The dehydrogenated mixture is fractionated (8) to recover the styrene monomer product (9) and recycle ethylbenzene (10), as well as benzene, toluene and α -methylstyrene byproducts (11). Competing reactions degrade ethylbenzene to benzene (thermally) and styrene to toluene (catalytically) [4b]. To prevent styrene polymerization in the process equipment, inhibitors (usually free radical scavengers) are added.

Typical conversions of ethylbenzene (EB) up to 69%, styrene-selectivity of over 97 mol% and a styrene monomer purity of 99.85 wt% are obtained. This seems to be satisfying, however, there are also major drawbacks to be noted.

The ethylbenzene dehydrogenation reaction is thermodynamically limited; the overall reaction is endothermic (ΔH (873 K) = 124.9 kJ.mol⁻¹) with heat supplied by steam in the adiabatic reactors (reaction temperature over 873 K) [6,10]. Additionally, the high steam content in the feed acts as a diluent to shift the reaction to higher equilibrium conversions [6,10] and is also needed to prevent catalyst deactivation by coke (see before). Other catalyst deactivation processes include (1) loss and/or redistribution of potassium promoters, (2) change in oxidation state of the Fe₂O₃ due to metastable Fe-carbide formation and (3) physical degradation [6]. Also the production plant has some disadvantages, which consist mainly of the reactor operating under vacuum, the separation unit (consisting of four columns), the costly interstage reheater and the superheated steam requirements to perform the reaction. These are the main disadvantages.

To overcome some of these disadvantages ABBLummus/UOP has developed a new process based on the Classic SMTM Process called the SMART SMTM process [4]. In this process, molecular oxygen is added to the reactant feed and ethylbenzene is dehydrogenated using oxygen (this reaction yields water and styrene). By using oxygen (oxidative dehydrogenation), the reaction equilibrium is shifted forward through the partial pressure reduction of hydrogen. The heat released during oxidative dehydrogenation is supplied to the dehydrogenation reactions. This results in EB conversion of more than 80%, styrene monomer production with high purity (99.85 wt% minimum), as well as elimination of the costly interstage reheater and reduction of the superheated steam requirements.

Auto-oxidation of ethylbenzene, followed by dehydration (SMPO process)

The second major styrene production route in the world (about 15% of the total styrene production) is, e.g., used by Royal Dutch SHELL and uses a different approach to form styrene [4b].

10. Mimura, N.; Tuatara, I.; Saito, M.; Hattori, T.; Ohkuma, K.; Ando, M. *Catal. Today* **1998**, *45*, 61.

Styrene is produced, starting from ethylbenzene, together with propylene-epoxide; ethylbenzene is auto-oxidized by air to ethylbenzene hydroperoxide (90% selectivity): *l*-phenylethanol (also called methylphenylcarbinol or α -methylbenzyl alcohol) and acetophenone are also formed (5-7% selectivity). Conversion is held low (13%) to minimize byproducts. Oxygen transfer between the hydroperoxide (conversion \approx 100%) and propylene in the presence of a metallic catalyst than leads to the corresponding *l*-phenylethanol ($>$ 70% selectivity) and propene-epoxide (selectivity 70-85%). Liquid-phase molybdenum (ARCO) [5] or heterogeneous titanium catalyst (SHELL) [11] are used. To improve yields, acetophenone is hydrogenated to *l*-phenylethanol in the liquid phase. The catalyst is a mixture of ZnO and CuO. Approximately 90% of the acetophenone is converted, with 92% selectivity to *l*-phenylethanol. Subsequently, *l*-phenylethanol is dehydrated in the gas phase to styrene over titania/silica catalyst at 573 K. Titania/silica is used for the dehydration reaction, since it produces only small amounts of oligomeric material, which could deactivate the catalyst, and because of its high styrene selectivity. This process, which is called the SMPO process, was discovered in the mid 1970's by Halcon and improved by Royal Dutch SHELL [12]. Typical styrene monomer purity of 99.7 wt% is obtained. The styrene selectivity and ethylbenzene conversion obtained were, due to SHELL confidentiality legislation, not open to the public. Approximately 2-2.5 tons of styrene are produced per ton of propylene epoxide.

The flow scheme of a typical ethylbenzene auto oxidation plant contains the following process steps and units [11]:

(1) the auto-oxidation reactor where the oxidation of ethylbenzene with air or oxygen to ethylbenzene hydroperoxide takes place, and (2) an epoxidation reactor for the oxygen transfer from the obtained hydroperoxide to propene; both units are running continuously at 373-403 K and 20-50 bar. After this step unreacted propylene is separated from the propylene-epoxide/*l*-phenylethanol product mixture on a distillation column (3), followed by a second column (4) for the separation of propylene-epoxide and *l*-phenylethanol, and finally the dehydration reactor for the production of styrene.

Although the SMPO process is 'cleaner' than the conventional dehydrogenation route (less by-products) and much less energy intensive, the major drawback of this combined reaction is that the production of styrene is limited by the amount of propylene-epoxide globally needed for the manufacture of propylene glycol and polyurethanes; thus the propylene-epoxide demand controls the siting and capacity of these coproduct plants. In certain market conditions, styrene monomer can also be an unattractive co-product [13]. Therefore, SHELL is focusing on the potential of silver and gold catalysts for the direct epoxidation of propene to propylene-epoxide using propene, hydrogen and oxygen [13]. Another oxygen source, currently explored by SHELL, is cumene hydroperoxide from

11. Kieboom, A.P.G.; Moulijn, J.A.; Sheldon, R.A.; Van Leeuwen, P.W.M.N. In *Catalysis: An Integrated Approach, Second, Revised and Enlarged Edition*; Van Santen, R.A., Van Leeuwen, P.W.M.N., Moulijn, J.A., and Averill, B.A., Eds.; Elsevier: Amsterdam, 1999; pp 29-80.

12. Lange, J.P.; Mesters, C.M.A.M. *Appl. Catal. A: General* **2001**, *210*, 247.

13. Hesselink, W. *Shell Chemicals Magazine*, Second Quarter, 2001.

phenol plants [13]. Another drawback in the SMPO production plant is the high-pressure reactors (20-50 bar) that are used.

Thermal and free radical polymerization of styrene

A main problem after the production of styrene is that styrene undergoes undesirable thermal and free radical polymerization during storage, transportation, and particularly during processing. Such polymerization can cause fouling of distillation towers and other equipment used for processing the styrene monomers and can make styrene unfit for use without further treatment. Thus, to minimize polymerization, compounds that inhibit polymerization activity are commonly injected into the crude styrene containing feed to, e.g., the condenser or the distillation columns. Those styrene polymerization inhibitors can be divided into two groups: 1) "true inhibitors", which completely inhibit polymerization for the period of time during which they are present in the styrene stream and 2) "retarders", which do not stop polymerization, but only slow down the rate of polymer growth [14]. Inhibitors are most frequently free radical scavengers with a *1*-piperidinyloxy [14] or catechol [15] structure. For example, when *para*-tertiary-butylcatechol, abbreviated as *p*-TBC, is used at a *p*-TBC level of 12 mg kg⁻¹, a monomer lifetime of 6 months is predicted at ambient temperature; this falls to 3 months at 303 K [4b]. This inhibitor requires trace amounts of oxygen to keep it effective. Other inhibitors commonly used are: dinitrophenols (retarders) and nitroxides (true inhibitors). Unfortunately, dinitrophenols are extremely toxic and thus are nitroxides generally the preferred polymer inhibitor.

The production of ethylbenzene; starting material of styrene

As the production route towards and storage of styrene is not without disadvantages, as above-mentioned, also the production of its reactant on site, i.e., ethylbenzene, imposes some major environmental problems. Ethylbenzene is commercially produced *via* Friedel-Crafts alkylation of benzene and ethylene over homogeneous AlCl₃-HCl (Monsanto-process) [4b]. However, the use of benzene as reagent is restricted due to its impact on human health (carcinogenic); it thus needs special handling and storing. Also the use of the AlCl₃ catalyst is not without environmental risk, since it is very corrosive and contaminates the alkyl aromatic products with chlorinated compounds. Special precautions have to be taken to wash the catalyst out of the product. Furthermore, the use of the AlCl₃ catalyst in the ethylation of benzene leads to high yields of di- and tri-alkylated products, since the required product (ethylbenzene) is more reactive than benzene. Those di- and tri-alkylated products are, subsequently, recycled.

Nowadays, ABBLummus/UOP produces ethylbenzene by a zeolitic catalyst in liquid phase, for instance H-ZSM5 (Liquid Phase EBTM process) replacing the old AlCl₃-HCl process [16]. Recently, ABBLummus/UOP commercialised a new zeolitic alkylation catalyst named EBZ-500 for the liquid

14. a) Hyde, Z.; Lewis, V.E. *U.S. Pat. 5,910,232*, 1999, assigned to Nalco/Exxon Energy Chemicals, USA; b) Gatechair, L.R.; Merrill, J.T.; Li, S.-S.; Butler, J.R.; Winter, R.A.E. *Deutsch. Pat. 19811602*, 1998, assigned to Ciba Geigy A.G., Switzerland

15. Havlu, V.; Homola, L.; Sochor, J.; Pospicil, J. *C.S. Pat. 265083*, 1989, Czech Republic.

phase ethylbenzene process using lower benzene/ethylene ratio and less catalyst volume [16]. In contrast to ABBLummus/UOP, where the starting material ethylbenzene is produced in liquid phase, SHELL produces ethylbenzene on site *via* vapor phase alkylation of benzene with ethylene over H-ZSM5, using Mobil-Badger technology. These new technologies have a much lower tendency to form di- and tri-ethyl benzene.

1.2 NOVEL ROUTES TO STYRENE

As mentioned in the previous paragraph, the commercial production of styrene is restricted by environmental and thermodynamical limitations, by factory requirements and/or market limitations. This has invoked extensive research towards novel routes for the production of styrene; (1) less reaction steps, less use of toxic and hazardous chemicals etc., and (2) by utilization of cheaper raw materials (see Table 1.2). In this paragraph, two examples using basic zeolites that are potential candidates are introduced; (1) oxidative methylation of toluene with methane over alkali cation exchanged zeolites, and (2) methylation of toluene with methanol over alkali cation exchanged zeolites. Basic zeolites are zeolites of which the Brönsted acid sites have been exchanged with alkali metal cations (see Chapter 2).

Table 1.2: Market prices for reactants and products¹ [17].

Chemical ²	Market price (in \$/lb ³)
<i>benzene</i>	0.13
<i>ethylene</i>	0.23
toluene	0.11
methane	
methanol	0.06
formaldehyde	0.34
<u>styrene (poly-)</u>	<u>0.29 (0.41)</u>
<u>ethylbenzene</u>	<u>0.27</u>

¹. Running Average Price of Commodity Chemicals of the period '95-'98 given in \$/lb.

². Chemicals in italic are used in nowadays processes. Chemicals in normal are of new processes with potential industrial application, which are discussed in this paragraph. Obtained products are underlined.

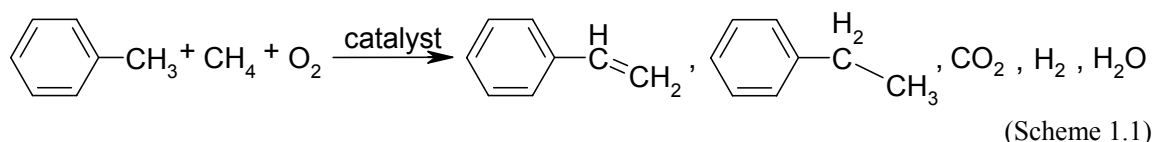
³. 1 lb = 1 pound = 0.454 kilogram.

16. Tanabe, K; Hölderich, W.F. *Appl. Catal. A: General* **1999**, *181*, 399.

17. Data taken from <http://www.chamotlabs.com/Documents/ChemRef.html#comp>

Oxidative methylation of toluene with methane over alkali cation exchanged and impregnated zeolites

Basic oxide catalysts are active catalysts for the oxidative toluene methylation (the methylation of toluene with methane in the presence of molecular oxygen) [18]. The reaction scheme is presented in Scheme 1.1.



Alkaline earth metal oxide catalysts promoted with alkali metal (hydr)oxide, alkali metal halide and bialkali metal(hydr)oxide were tested. Bialkali-promoted alkaline earth metaloxide, i.e., Na^+/Cs^+ -promoted CaO, were found to be the most stable (after 60 hrs time on stream only a 4% decrease in the toluene conversion was observed), the most selective (41%) and the most active (total C_8 -yield: 27%) catalysts for the production of styrene [18b].

Since then research has partially shifted to basic zeolites. Intriguing results had already been obtained for the oxidative coupling of methane to form C_2 -molecules (ethane and ethene) [19]. Other reasons for this interest in basic zeolites were the high surface area of zeolites, the high concentration of active sites and the possibility of changing easily the acid-base properties. Research has mainly focused on alkali metal cation exchanged and alkali and alkaline earth impregnated zeolites (containing metal-halide and oxide clusters) [20,21,22]. The most important results are summarized in Figure 1.4.

As can be seen in Figure 1.4, cesium-chloride impregnated NaX (CsCl-NaX(IMP)) was the most selective catalyst (total C_8 -selectivity = 88%) tested at 1023 K [20a]. No information on the styrene/ethylbenzene ratio was given. However, the highest toluene conversion, thus the highest activity, was obtained with 8wt% NaBr impregnated K-ZSM5 (8wt% NaBr/K-ZSM5), running at 973 K [21b] and with 12wt% BaO impregnated Na-X (12wt% BaO/Na-X) at 1023 K [22b] (76.3% and 32%, respectively). 8wt% NaBr/K-ZSM5 also had a high total C_8 -selectivity (76%) and styrene selectivity 69% [21b]. Of the ion exchanged samples, solid state Cs-X(SSIE), liquid phase Cs-X(LSIE), parent Na-X and liquid phase Cs-ZSM5(LSIE), Cs-X(SSIE) had the highest activity (19%) and total C_8 -selectivity (70%) [20,22a]. This is slightly less than results obtained for CsCl/Na-X(IMP). Cs-ZSM5(LSIE) had a higher activity and total C_8 -selectivity (13% and 51%, respectively) than Cs-X(LSIE) (8% and 40%, respectively), which had a higher total C_8 -selectivity than Na-X (30%)

18. a) Khan, A.Z.; Ruckenstein, E. *J. Chem. Soc., Chem. Commun.* **1993**, 587; b) Khan, A.Z.; Ruckenstein, E. *Appl. Catal. A: General* **1993**, 102, 233.

19. Kovacheva, P.; Arishtirova, K.; Davidova, N. *Appl. Catal. A: General* **1997**, 149, 277.

20. a) Arishtirova, K.; Kovacheva, P.; Davidova, N. *Appl. Catal. A: General* **1998**, 167, 271; b) Kovacheva, P.; Arishtirova, K.; Davidova, N. *Appl. Catal. A: General* **1999**, 178, 111.

21. a) Zhou, L.; Li, W.; Su, M.; Li, H.; Tao, K.; Hattori, H. *Appl. Catal. A: General* **1999**, 181, L1; b) Zhou, L.; Li, W.; Fu, Q.; Guan, N.; Zheng, S.; Tao, K. In *Proceedings of the 12th International Zeolite Conference, Baltimore*; Treacy, M.M.J., Marcus, B.K., Bisher, M.E., and Higgins, J.B., Eds.; Materials Research Society: Boston, 1999; Vol. 4, pp 2585-2588.

22. a) Kovacheva, P.; Arishtirova, K.; Vassilev, S. *Appl. Catal. A: General* **2001**, 210, 391; b) Arishtirova, K.; Kovacheva, P.; Vassilev, S. *Appl. Catal. A: General* **2001**, 213, 197; c) Kovacheva, P.; Predoeva, A.; Arishtirova, K.; Vassilev, S. *Appl. Catal. A: General* **2002**, 223, 121.

[20,22]. 12wt% BaO/Na-X was far more active and total C₈-selective (32% and 60%, respectively) than 13wt% MgO impregnated Na-X (12% and 50%, respectively) [22]. Furthermore, different halides appeared to promote either the production of ethylbenzene (NaCl) or styrene (NaBr) [21]. After 50 hrs of time on stream a 40-45% decrease in the toluene conversion over 8wt%NaBr/K-ZSM5 was observed; the total C₈-selectivity remained stable [21b]. 13wt% MgO impregnated Na-X (13wt% MgO/Na-X) catalyst was active for 24 hrs time on stream without any loss of activity and selectivity [22a]. These results emphasize the importance of the kind of modifying material.

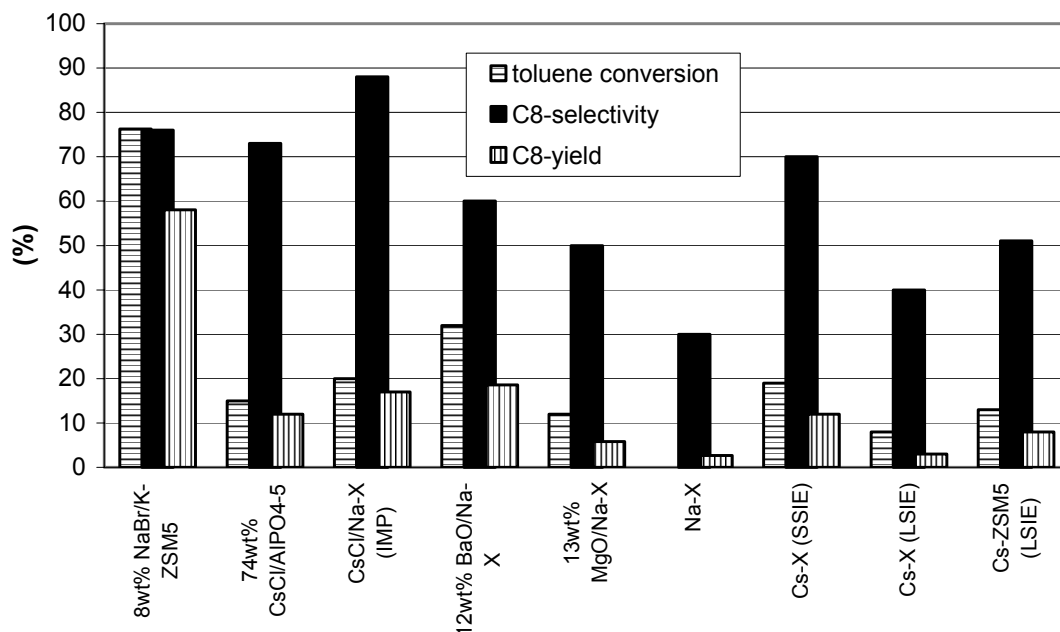
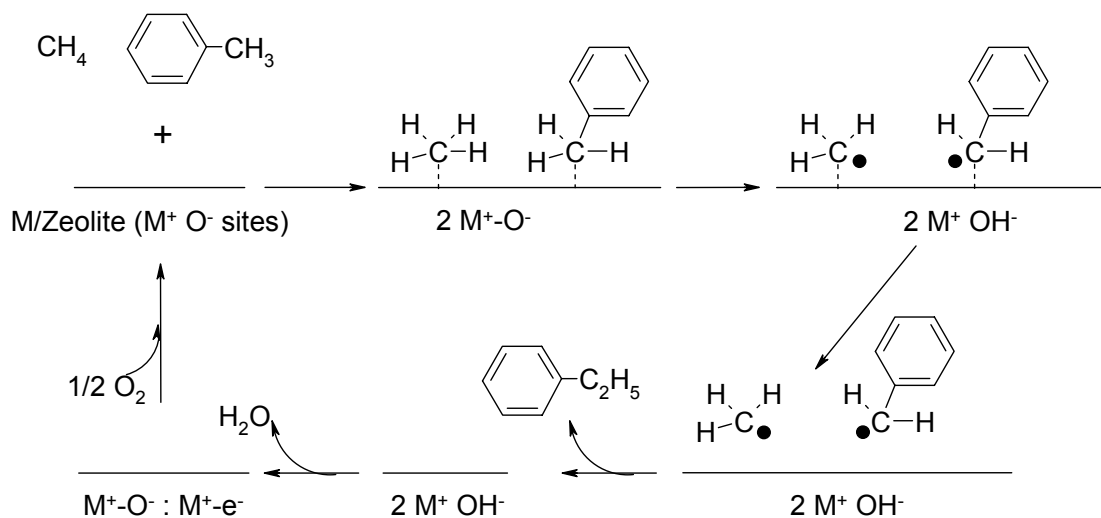


Figure 1.4: Oxidative methylation: catalysts and most important results. Results taken from Ref. [20-22].

The required characteristics necessary for the oxidative methylation of toluene of these catalysts, are still not clear. Usually high C₈-yields and C₈-selectivities were found with less basic material (with high Si/Al ratio, see also chapter 2) [20,21]. CO₂ Temperature Programmed Desorption (t.p.d.) studies showed that one of the most active and selective catalysts, CsCl/Na-X(IMP), had only moderate basicity [20a]. Also CsCl/AlPO₄-5, another active and selective catalyst, exhibited very poor basicity [20b]. Cs-ZSM5(LSIE) also showed high activity and selectivity although it has weak base sites [20b]. These results indicated that basicity is not the key factor for the oxidative methylation of toluene. Other t.p.d. experiments performed showed the presence of weak Lewis-acid centers (the cations) and moderately strong Lewis-base centers (the zeolite oxygens) [21a] and, recently, indication was found for the necessity of very strong Lewis-base centers [22b].

From the above it is clear that basicity alone cannot be the key to a strong promoting effect of the zeolite structure in the oxidative methylation of toluene. Another important factor leading to high activity and selectivity was concluded to be the dispersion of the impregnated oxide or halide phase and the cation location. Powder XRD showed very fine dispersion of the MgO phase in 13wt% MgO/Na-X,

and of the CsCl phase in Na-X and AlPO₄-5. According to Ref. [20] and [22], this leads to a high activity and selectivity.



The reaction mechanism for the oxidative methylation of toluene, yielding ethylbenzene, most likely proceeds *via* the cross coupling of methyl and benzyl radicals in the gas phase [23,24]. These radicals are generated by the abstraction of a hydrogen atom from methane and the methyl group of toluene, respectively, by the M⁺-O⁻ (M: alkali metal) site on the surface of the modified zeolites. This yields surface OH⁻ groups, which recombine to produce water, surface M⁺-O⁻ sites and M⁺-e⁻ sites. The M⁺-e⁻ sites are subsequently re-oxidized by molecular oxygen, yielding M⁺-O⁻ sites. The reaction mechanism is depicted in Scheme 1.2.

However, this mechanism has been proposed for the oxidative methylation of toluene over alkali promoted MgO, where the existence of M⁺-O⁻ sites was shown [24]. No literature reports concerning methyl and benzyl radical formation in alkali cation exchanged zeolites (under oxidative methylation conditions) were found. However, the high reaction temperatures reported in Ref. [20], [21] and [22] appear to be in favor of a radical mechanism and evidence for the oxygen exchange of alkali metal oxide clusters in Cs-X zeolites with ¹⁸O₂ (using ¹⁸O₂-temperature programmed desorption) [25] and of framework oxygen in basic natural stilbite with ¹⁷O-enriched water (using ¹⁷O solid state NMR) [26] was found.

Adebajo *et al.* have proposed another possible reaction pathway [27]. They claim a two-step mechanism for the oxidative methylation: (1) the intermediate formation of methanol by partial oxidation of methane, followed by (2) the methylation of the aromatic with methanol. However, this

23. Kim, H.; Suh, H.; Paik, H. *Appl. Catal. A: General* **1992**, *87*, 115.

24. a) Ito, T.; Wang, J.-X.; Lin, C.-H.; Lunsford, J.H. *J. Am. Chem. Soc.* **1985**, *107*, 5062; b) Lin, C.-H.; Wang, J.-X.; Lunsford, J.H. *J. Catal.* **1988**, *111*, 302.

25. Yagi, F.; Hattori, H. *Microporous Mater.* **1997**, *9*, 247.

26. Xu, Z.; Stebbins, J.F. *Geochim. Cosmochim. Acta* **1998**, *62*, 1803.

27. (a) Adebajo, M.O.; Long, M.A.; Howe, R.F. *Res. Chem. Intermed.* **2000**, *26*, 185; (b) Adebajo, M.O.; Howe, R.F.; Long, M.A. *Catal. Today* **2000**, *63*, 471.

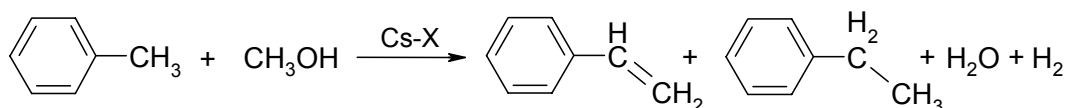
pathway of partial methane oxidation yielding intermediately formed methanol, was observed for the methylation of benzene in a high-pressure reactor at 673 K. The authors of Ref. [20-22], who performed the reaction at atmospheric pressure and much higher temperatures, report no such intermediates.

Careful studies showed that styrene is a secondary product formed by the oxidative dehydrogenation of ethylbenzene [21]. This was explained by the catalytic role of coke, resulting from the polymerization and decomposition of styrene, on the zeolites. Similar results were obtained for the oxidative coupling of methane, yielding ethane and ethylene [24].

The different results in oxidative toluene methylation activity, selectivity and yield obtained for the alkali cation exchanged X, Y and ZSM5 zeolites in Ref. [20] and [21] can be explained by the high electrostatic field exhibited by the alkali cations in the pores of ZSM5, compared to X and Y zeolites, on the activation of molecular oxygen [28]. It was found that interaction of the cation with molecular oxygen generates the formation of superoxide anions (O_2^-) and hydrocarbon radical cations by the transfer of electrons.

Alkylation of toluene with methanol over alkali cation exchanged zeolites

In the mid-sixties, Sidorenko *et al.* [29] reported high selectivities to styrene and ethylbenzene in the alkylation with methanol of toluene performed over moderately basic X zeolites with a low Si/Al ratio (see Scheme 1.3). The side chain methylation reaction of toluene currently receives a lot of attention, since it has theoretical potential as a novel route to styrene. This process is thermodynamically nearly zero, when the rates are properly balanced: methanol dehydrogenation yielding formaldehyde is endothermic while the reaction of toluene and formaldehyde is exothermic [30].



(Scheme 1.3)

High styrene selectivity at 698 K was only obtained with cations with a small electrostatic potential at the ion-exchangeable site, i.e., Cs^+ and Rb^+ [31]. Reaction over Li^+ and Na^+ cation exchanged X [31], as well as over alkali cation exchanged ZSM5 (MFI) [32], zeolites yielded ring alkylation preferentially, whereas K^+ cation exchanged X zeolites show intermediate selectivity [31]. This is presented in Fig. 1.5, which shows typical selectivities obtained with weak and moderately strong basic (alkali metal cation exchanged) ZSM5 and X zeolites, respectively. Giordano *et al.*

28. Panov, A.G.; Larsen, R.G.; Totah, N.I.; Larsen, S.C.; Grassian, V.H. *J. Phys. Chem. B* **2000**, *104*, 5706.

29. Sidorenko, Y.N.; Galich, P.N.; Gutyrya, V.S.; Il'in, V.G.; Neimark, I.E. *Dokl. Akad. Nauk. SSSR* **1967**, *173*, 132.

30. Shreiber, E.H.; Rhodes, M.D.; Roberts, G.W. *Appl. Catal. B: Environmental* **1999**, *23*, 9.

31. Palomares, A.E.; Eder-Mirth, G.; Lercher, J.A. *J. Catal.* **1997**, *168*, 442.

32. Vinek, H.; Derewinski, M.; Mirth, G.; Lercher, J.A. *Appl. Catal.* **1991**, *68*, 277.

reported a similar graph [33]. Although high selectivities were obtained, only low toluene conversions and styrene yields were reported [33].

The high styrene selectivity of these materials was related to a formed formaldehyde intermediate, resulting from the dehydrogenation of methanol [34,35]. Methanol dehydrogenation was claimed to be a result of the presence of strong basic, framework oxygen, sites with weak Lewis acidic centers (the cation) in the zeolite pores. Up to now the dehydrogenation mechanism over these type of materials remains a mystery.

The use of formaldehyde as alkylating species increased the alkylation activity and the styrene selectivity [34,35,36]. Recently, it was shown that not only methanol or formaldehyde can alkylate toluene on the side chain. Dimethoxycarbonate was used as alternative methylating agent with high styrene selectivity [37], whereas the use of isopropanol as toluene alkylating agent yielded isobutylbenzene [36]. The reaction is also not limited to the use of toluene, since it was reported that methanol also alkylated the side chain of ethylbenzene, yielding isopropylbenzene, effectively [38].

Ethylbenzene (EB), dimethyl ether (DME) and carbon monoxide (CO) are the major observed by-products during the side chain methylation of toluene. Ethylbenzene is thought to be formed by hydrogenation of the primary alkylation product styrene by hydrogens resulting from the dehydrogenation of methanol [34,35,39]. Sooknoi and Dwyer [40], however, proposed rapid hydrogenolysis of 2-phenylethanol (the intermediate formed by toluene alkylation with formaldehyde) by molecular hydrogen (4% H₂ in the feed) to yield ethylbenzene and water, since hydrogenation of styrene with 4% hydrogen in the feed, resulted only in very small amounts of ethylbenzene. Also the formation of small concentrations of xylenes [31] (see below) and higher aromatics, like isopropylbenzene (cumene) [41] and trimethylbenzene (mesitylene) [33], were reported as well (usually referred to as C₉-aromatics). CO is formed by the decomposition of intermediately formed formaldehyde over

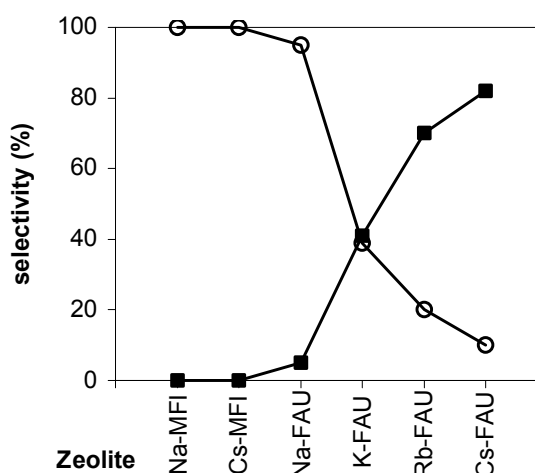


Figure 1.5: Methylation selectivity of toluene over alkali exchanged ZSM5 (MFI) and X (FAU) zeolites, yielding xylene (○) or styrene (■). [32,31].

33. Giordano, N.; Pino, L.; Cavallaro, S.; Vitarelli, P.; Rao, B.S. *Zeolites* **1987**, *7*, 131.

34. Yashima, T.; Sato, K.; Hayasaka, T.; Hara, N. *J. Catal.* **1972**, *26*, 303.

35. Itoh, H.; Miyamoto, A.; Murakami, Y. *J. Catal.* **1980**, *64*, 284.

36. Kumari Vasanthy, B.; Palanichamy, M.; Krishnasamy, V. *Appl. Catal. A: General* **1996**, *148*, 51.

37. Bal, R.; Sivasankar, S. In *Proceedings of the 12th International Congress on Catalysis, Granada*; Corma, A., Melo, F.V., Mendioroz, S., and Fierro, J.L.G., Eds.; Elsevier: Amsterdam, 2000; Vol. 130C, pp 2645-2650.

38. Huang, C.S.; Ko, A.-N. *Catal. Lett.* **1993**, *19*, 319.

39. Phillippou, A.; Anderson, M.W. *J. Am. Chem. Soc.* **1994**, *116*, 5774.

40. Sooknoi, T.; Dwyer, J. *Stud. Surf. Sci. Catal.* **1995**, *97*, 423.

41. Beltrame, P.; Fumagalli, P.; Zuretti, G. *Ind. Eng. Chem. Res.* **1993**, *32*, 26.

too basic sites, thereby lowering the methanol selectivity as methylating agent for side chain alkylation [42]. The formation of CO will be discussed in more detail below.

The intermediate and end products obtained during the reaction, 2-phenylethanol and styrene and ethylbenzene, respectively, were found to inhibit the reaction [40,41]. Also too high methanol concentrations in the feed inhibited the reaction [41].

1.3 OBSERVED SELECTIVITY IN TOLUENE ALKYLATION OVER ZEOLITES

High methanol conversions are observed during the side chain methylation of toluene over Cs⁺ and Rb⁺ exchanged X zeolites [33]. However, most of the methanol (MeOH) is decomposed to CO (selectivity: 39%), H₂ and dimethyl ether (selectivity: 34%) [42]. It is believed that CO formation is facilitated by the basicity of the framework oxygens of Cs-X, in the following sequence of steps: methanol dehydrogenation to intermediately formed formaldehyde (H₂CO), which, subsequently, decomposes into H₂ and CO (MeOH → H₂CO → CO + H₂).

Recently it was shown that methanol decomposition into CO and H₂ is also facilitated by the proximity of Lewis acid-base sites in alkali cation exchanged zeolites in addition to the high basicity of the framework oxygens. Zeolites Cs-L and Cs-β catalyzed the alkylation reaction (indicating sufficient zeolite basicity) with the simultaneous loss of much smaller amounts of CO and H₂, compared to Cs-X and Cs-Y zeolites. This was related to the much lower concentration of catalytic sites in Cs-L and Cs-β, compared to Cs-X and Cs-Y zeolites (which is related to the Si/Al ratio) [43]. The high methanol decomposition to CO and H₂ over Cs-X and Cs-Y zeolites could thus be explained by a *Cannizzaro* type disproportionation reaction, whereby two neighboring surface formaldehyde molecules react to a surface formate species and a surface methoxy species [44,45]; ¹³C-MAS NMR has shown that there is almost a 1:1 correspondence between the intensity of the surface formate resonance and the surface methoxide resonances on Cs-X [39]. The surface formate, subsequently, decomposes to CO and H₂ [46].

High methanol conversion yielding dimethyl ether (DME) was also observed over Cs-X zeolites (selectivity: 34%) [42]. This is related to the strong hydrogen bonding of the alcohol groups and the electrostatic field of the cation, which facilitates the methanol OH bond cleavage [47]. This is reflected well in the observed DME selectivities found for Na-X (62%) and Cs-X (34%) [42].

42. Archier, D.; Coudurier, G.; Naccache, C. In *Proceedings of the 9th International Zeolite Conference, Montreal*; Von Ballmoos, R., Higgins, J.B., and Treacy, M.M.J., Eds.; Butterworth-Heinemann: Boston, 1992; Vol. 2, pp 525-533.

43. Wieland, W.S.; Davis, R.J.; Garces, J.M. *J. Catal.* **1998**, *173*, 490.

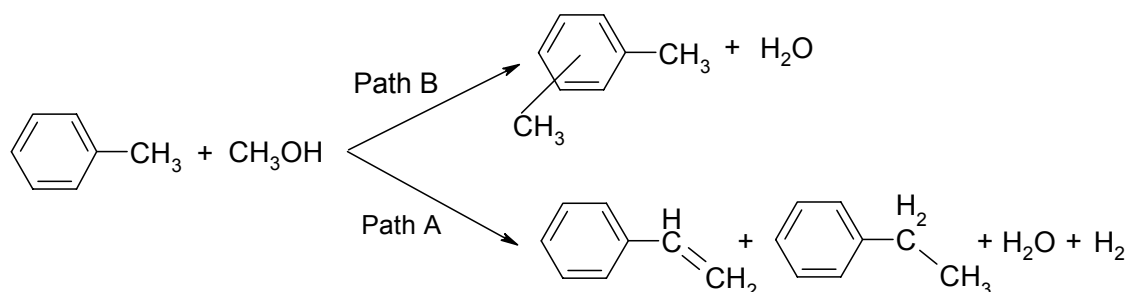
44. Busca, G.; Lamotte, J.; Lavalley, J.-C.; Lorenzelli, V. *J. Am. Chem. Soc.* **1987**, *109*, 5197.

45. Venuto, P.B.; Landis, P.S. *Adv. Catal.* **1968**, *18*, 259.

46. Rep, M.; Van Ommen, J.G.; Lefferts, L.; Lercher, J.A. In *Proceedings of the 13th International Zeolite Conference, Montpellier*; Galarneau, A., Di Renzo, F., Fajula, F., and Vedrine, J., Eds.; Elsevier: Amsterdam, 2001; Vol. 135, pp 316.

47. Kogelbauer, A.; Gründling, Ch.; Lercher, J.A. *J. Phys. Chem.* **1996**, *100*, 1852.

While Cs^+ and Rb^+ exchanged zeolites with a low Si/Al ratio were found to be active catalysts in the side chain methylation of toluene (path A; Scheme 1.4), zeolites exchanged with cations with a large electrostatic potential alkylated the toluene ring exclusively, yielding xylene (path B; Scheme 1.4) [31]. Also zeolites with a high Si/Al ratio were found to be selective in the production of xylene (path B; Scheme 1.4) [32].



(Scheme 1.4)

The reaction mechanism yielding xylene over these type of materials is not clear; supposedly, it proceeds *via* the formation of surface methoxy groups or highly activated methanol methyl groups. In a theoretical study, it was shown that interaction of methanol with alkali metal cations mainly weakens the bond between the oxygen and the methyl group yielding a highly activated methyl group [48] which, subsequently, can alkylate the toluene ring yielding xylenes. Thus by adjusting the Si/Al ratio and/or the cation, one can modify the selectivity in the alkylation reaction, ring *versus* side chain alkylation.

Toluene methylation performed over alkaline earth exchanged X and Y zeolites (containing Mg^{2+} , Ca^{2+} cations etc.) yield also xylenes (path B; Scheme 1.4) [49]. MgNa-X and MgNa-Y zeolites showed the highest activity. This high activity and xylene selectivity of alkaline earth exchanged X and Y zeolites is related to the presence of acidic surface hydroxyl groups (Brönsted acid sites), although these catalysts were prepared from Na-X and Na-Y zeolites. These Brönsted acid sites are formed by hydrolysis of water during the preparation, resulting from the strong electrostatic field imposed by the alkaline earth cation exchanged into the zeolite pores [50]. This produces basic alkaline earth metal hydroxyls and Brönsted acid sites [51]. Transition metal and rare-earth cation exchanged zeolites have also been used for the alkylation of toluene with methanol, showing a high preference for ring alkylation [52]; again, this is related to the presence of Brönsted acid sites resulting from water hydrolysis during the preparation. Also partially alkali cation exchanged materials (i.e., zeolites still containing residual Brönsted acid sites) were active ring alkylation catalysts and much more active than conventional protonic (H^+) zeolites [53]. The higher reactivity of these type of materials, compared to

48. Vayssilov, G.N.; Lercher, J.A.; Rösch, N. *J. Phys. Chem. B*, **2000**, *104*, 8614.

49. Galich, P.N.; Gutryra, V.S.; Sidorenko, Yu.N.; Il'in, V.G.; Neimark, I.E. *Dopov. Akad. Nauk Ukr. RSR* **1967**, *61*.

50. a) Ward, J.W. *J. Catal.* **1968**, *10*, 34; b) Ward, J.W. *idem* **1969**, *14*, 365.

51. Mirodatos, C.; Pichat, P.; Barthomeuf, D. *J. Phys. Chem.* **1976**, *80*, 1335.

52. a) Coughlan, B.; Carroll, W.M.; Nunan, J. *J. Chem. Soc., Faraday Trans. 1* **1983**, *79*, 281; b) Coughlan, B.; Carroll, W.M.; Nunan, J. *idem* **1983**, *79*, 297.

53. Sidorenko, Yu.N.; Galich, P.N. *Petrol Chem.* **1991**, *31*, 57.

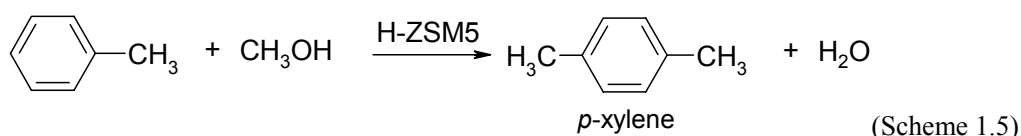
fully exchanged H^+ zeolites was reflected in the lower reaction temperatures needed, 483 K and 548 K, respectively (total xylene yield $\approx 25\%$). DFT calculations have shown that the higher activity of the partially cation exchanged materials is related to the higher acid strength of the residual Brönsted acid sites [54].

MgO-impregnated ZSM5 (MgO-ZSM5) zeolites have also been used for the toluene methylation showing a high preference for *p*-xylene [55]. On the other hand, bulk MgO (which is a basic catalyst) catalyses methylation of the methyl group of toluene (side chain methylation) [56]. Therefore, the high selectivity of MgO-ZSM5 for the formation of xylene is due to the high reactivity of the Brönsted acid sites of the ZSM5 zeolite. MgO-impregnation also influences the diffusional constraints of the different xylene isomers, thereby increasing the *p*-xylene selectivity.

From the previous it can be concluded that careful modification of the zeolites, i.e., ion-exchange, impregnation etc., has to be preformed to prevent formation of Brönsted acid sites inside the zeolite pores, since these Brönsted acid sites are far more active in the ring alkylation of toluene yielding xylenes, than the Lewis acid-base sites that catalyze the side chain alkylation of toluene (reaction temperature 483 K and 698 K, respectively).

The reaction mechanism of ring alkylation of toluene with methanol

As already said above, partially exchanged zeolites are very active catalysts for the ring alkylation of toluene with methanol. This high reactivity towards ring methylation is attributed to the presence of residual Brönsted acid sites inside the zeolite pores and is thought to proceed as found for fully exchanged H^+ zeolites [53]. The reaction mechanism for the formation of xylenes over acidic zeolites was studied using infrared [57], NMR [58] and molecular modeling techniques [59,60,61]. The reaction scheme is presented in Scheme 1.5.



The reaction mechanism is shown in Scheme 1.6. The general accepted idea for the reaction shown in Scheme 1.5 is that methanol adsorbs on a Brönsted acid site (Scheme 1.6: step 1). This interaction of methanol with a Brönsted acid site leads to the formation of a surface methoxy group,

54. Vayssilov, G.N.; Rösch, N. *J. Phys. Chem. B* **2001**, *105*, 4277.

55. a) Sotelo, J.L.; Uguina, M.A.; Valverde, J.L.; Serrano, D.P. *Ind. Eng. Chem. Res.* **1993**, *32*, 2548; b) Sotelo, J.L.; Uguina, M.A.; Valverde, J.L.; Serrano, D.P. *Appl. Catal. A: General* **1994**, *114*, 273; c) Sotelo, J.L.; Uguina, M.A.; Valverde, J.L.; Serrano, D.P. *Ind. Eng. Chem. Res.* **1996**, *35*, 1300.

56. Tanabe, K.; Takahashi, O.; Hattori, H. *React. Kinet. Catal. Lett.* **1977**, *7*, 347.

57. a) Mirth, G.; Lercher, J.A. *J. Phys. Chem.* **1991**, *95*, 3736; b) Rep, M.; Palomares, A.E.; Eder-Mirth, G.; Van Ommen, J.G.; Lercher, J.A. In *Proceedings of the DGMK-conference, Tagungsbericht 9903, Erlangen*; Emig, G., Rupp, M., and Weitkamp, J., Eds.; DGMK: Hamburg, 1999; pp 279-286.

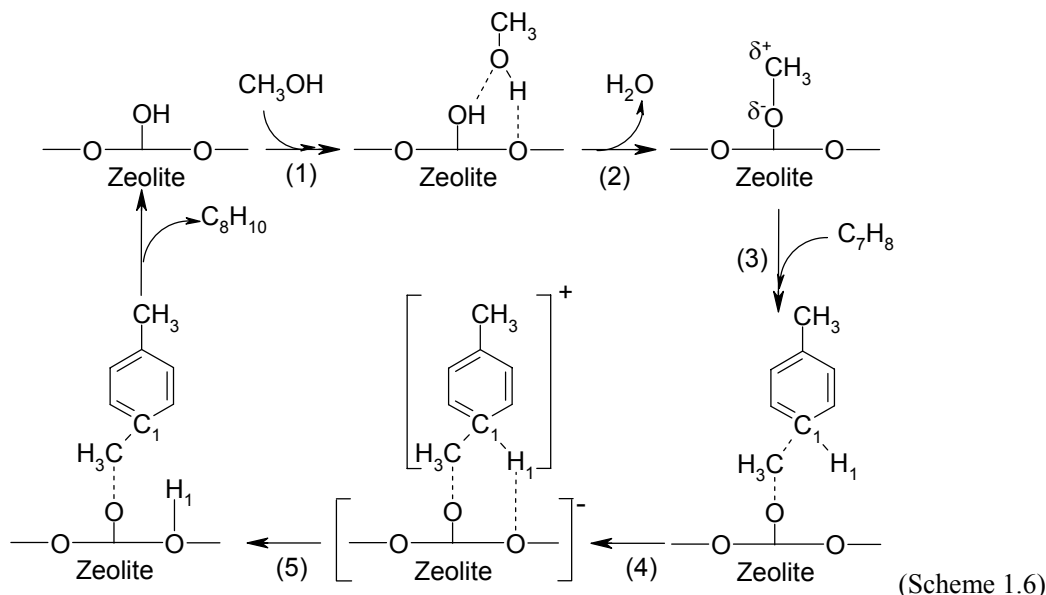
58. Izmailova, I.I.; Corma, A. *J. Phys. Chem. B* **1997**, *101*, 547.

59. Blaszkowski, S.R.; Van Santen, R.A. *J. Phys. Chem. B* **1997**, *101*, 2292.

60. a) Corma, A.; Zicovich-Wilson, C.; Viruela, P.M. *J. Phys. Org. Chem.* **1994**, *7* 364; b) Corma, A.; Sastre, G.; Viruela, P. M. *J. Mol. Catal. A: Chem.* **1995**, *100*, 75.

61. Waghmode, S.B.; Bharathi, P.; Sivasanker, S.; Vetrivel, R. *Microporous Mesoporous Mater.* **2000**, *38*, 433.

also called a methylcarbonium ion (CH_3^+) and water (Scheme 1.6: step 2). CH_3^+ (an electrophilic agent) is stabilized by the zeolite- O^- and reacts subsequently with the aromatic ring (Scheme 1.6: step 3 and 4), whereby the remaining zeolite- O^- group abstracts a leaving proton of the toluene ring, recreating the starting Brønsted acid site (Scheme 1.6: step 5). The formation of surface methoxy groups is also concluded to be the reactive species for the methanol to gasoline (MTG) process [62].



However, Sidorenko and Galich [53] proposed the formation of a methylene biradical ($:\text{CH}_2$) as the reactive methylating species. They opposed to the idea of a CH_3^+ ion being the ring alkylating species in the methylation of toluene, since the CH_3^+ ion was shown to be extremely stable, prohibiting its reaction with the toluene ring. The reason for this was not very clear [53]. A methylene biradical species is also claimed as alternative in the MTG process [62].

Gas phase analysis has shown that during the alkylation of toluene with methanol over acidic ZSM5 zeolites, besides *p*-xylene, also *ortho*- and *meta*-xylenes are formed within the pores of ZSM5. The existence of large cavities with an average diameter of 9 Å, formed by intersecting straight and sinusoidal channels, are thought to facilitate their formation. It was believed that since the pore size of ZSM5 is approximately 5.6 Å (the size of a benzene molecule), the diffusion of these bulky xylene isomers (*o*- and *m*-xylene) out of the zeolite pores is limited; experiments had shown that the diffusion rate of *p*-xylene was three orders of magnitude higher than of the other xylene isomers [63]. However, *in situ* i.r. experiments of the catalyst under working conditions suggest that in addition to the rate of product diffusion, a subtle balance between the intrinsic slow rate of alkylation and the high rate of isomerization exists, which determines the observed selectivity in combination to the diffusion rate of the different xylene isomers [64], as will be explained now in more detail.

62. Chang, C.D. In *ACS Symp. Ser.-Perspectives Molecular Sieve Science*; Flank, W.H., and Whyte, Jr., Th.E., Eds.; American Chemical Society: Washington, D.C., 1988; Vol. 368, pp 596-614.

63. Mirth, G.; Cejka, J.; Lercher, J.A. *J. Catal.* **1993**, *139*, 24.

64. a) Mirth, G.; Lercher, J.A. *J. Catal.* **1991**, *132*, 244; b) Mirth, G.; Lercher, J.A. *Idem* **1994**, *147*, 199.

If the diffusion rate of the different xylene isomers would determine the product selectivity, then xylene isomers inside the catalyst pores would be observed in their equilibrium concentration. However, *in situ* i.r. experiments showed that during the alkylation of toluene with methanol at 573 K mainly *meta*-xylene is formed within the pores of ZSM5 (transition state selectivity) [63]. The high surface concentration of *m*-xylene, due to diffusional constraints inside the pores and the acidity of the catalyst, results in a high isomerization rate towards *p*-xylene [63,64]. Since *m*-xylene isomerizes to approximately 66% *p*-xylene over H-ZSM5, the high selectivity to *p*-xylene is well explained by the isomerisation of the primary alkylation product, *m*-xylene, inside the pores [64b], in addition to the limited diffusion of *o*- and *m*-xylene.

This very high methylation selectivity towards *p*-xylene as observed with H-ZSM5 has led to the use of acidic ZSM5 zeolites as industrial catalysts for the selective methylation of toluene to *para*-xylene isomer [65]. Historically, the commercial production of xylene was performed over liquid sulfuric and hydrofluoric acid catalysts [65]. However, the highly corrosive and contaminating properties and low selectivities of these catalysts had motivated the chemical industry to search for alternatives.

1.4 SIDE CHAIN ALKYLATION OF TOLUENE: REACTION MECHANISM

Mechanistic research done by numerous research groups have resulted in many different reaction mechanisms explaining the observed side chain alkylation selectivity in the methylation of toluene with methanol. Most reaction mechanisms [31,36,39,66] are based on the mechanism proposed by Itoh *et al.* [35], which resembles an aldol type condensation.

Scheme 1.7 shows the reaction mechanism as proposed by Itoh *et al.* [35]. Interaction of toluene with a basic and an acidic site was claimed, i.e., a zeolite framework oxygen and an extra framework Lewis cation, respectively, yielding a highly activated methyl group, whereas formaldehyde only interacts with a Lewis acid site. The interaction of toluene with the basic framework oxygens increases the reactivity of the side chain (the side chain becomes negatively polarised), whereas simultaneous interaction with an acid site stabilises the toluene molecule [35]. When toluene is adsorbed only on an acid site, the toluene ring is highly activated towards ring-alkylation. The concerted zeolitic acid-base interaction with toluene needed during side chain alkylation was shown also by molecular modeling [67] and *in situ* poisoning of Cs-X catalysts during the methylation of toluene with an acid or base [68]. Co-feeding of the reactant mixture (toluene and methanol) with a basic compound (pyridine, 2,3-dimethyl pyridine or butyl amine) resulted in a sharp catalyst

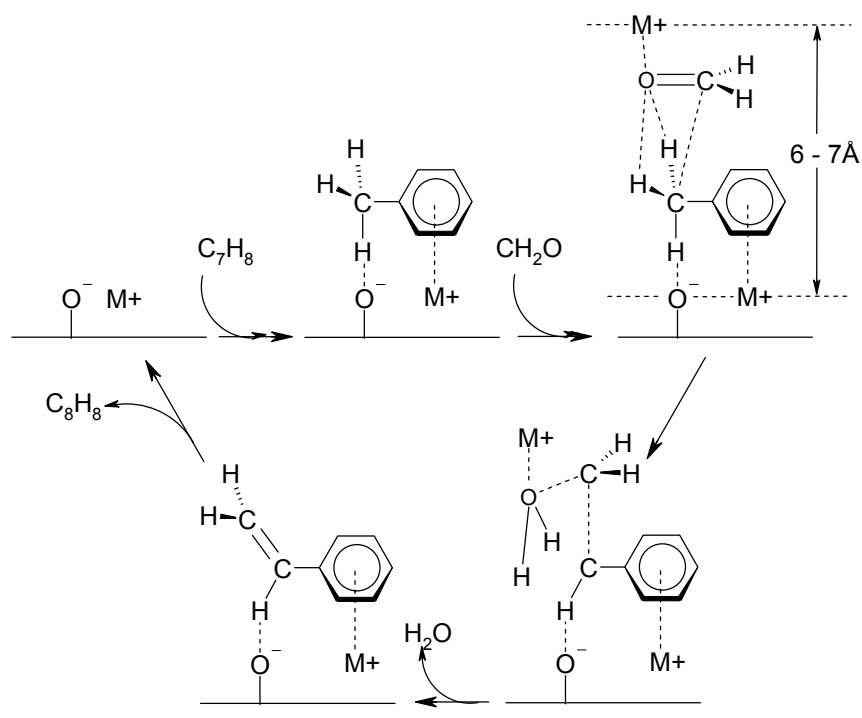
65. Smirniotis, P.G.; Ruckenstein, E. *Ind. Eng. Chem. Res.* **1995**, *34*, 1517.

66. Lacroix, C.; Deluzarche, A.; Kiennemann, A.; Boyer, A. *Zeolites* **1984**, *4*, 109.

67. Miyamoto, A.; Iwamoto, S.; Agusa, K.; Inui, T. In *Acid-Base Catalysis*; Tanabe, K., Hattori, H., Yamaguchi, T., and Tanaka, T., Eds.; Verlag Chemie: Weinheim, 1989; pp 497-504.

68. Borgna, A.; Sepulveda, J.; Magni, S.; Apesteguía, C. In *Proceedings of the 12th International Congress on Catalysis, Granada*; Corma, A., Melo, F.V., Mendioroz, S., and Fierro, J.L.G., Eds.; Elsevier: Amsterdam, 2000; Vol. 130C, pp 2621-2626

deactivation [68]. After acetic acid submission to the feed also a sharp catalyst deactivation was observed [68]. These results indicate that a cooperative action of acid-base pairs is needed for the side chain alkylation.



Many modifications of the side chain alkylation reaction mechanism have been proposed. Instead of formaldehyde as alkylating intermediate, a unidentate formate resulting from formaldehyde oxidation was proposed by King and Garces [69]. Lacroix *et al.* [66] and Garces *et al.* [70] have proposed proton abstraction from toluene yielding a phenylcarbanion, which is subsequently alkylated by formaldehyde. Sidorenko and Galich have claimed the formation of a biradical formaldehyde [53]. Garces *et al.* [70] have claimed a redox mechanism that involves alkali metal vapors formed *in situ* during the alkylation. These alkali metal vapors are formed by the reduction of alkali metal oxides, which result from the decomposition of metal carbonates during the activation inside the zeolite pores. However, this is highly unlikely if one considers the stability of alkali oxide and hydroxide clusters.

It was proposed by Sefcik that the high selectivity towards styrene and ethylbenzene could also be the result of the presence of Cs⁺ cations in the zeolite pores, which sterically hinder the formation of the transition states that lead to the products of ring alkylation [71]. NMR experiments showed inhibition of the toluene mobility in the pores of Cs-X [71]. This idea was rejected by Sidorenko and Galich [53]. An explanation was not given, but adsorption data reported by Bellat *et al.* showed even higher uptake rates for the adsorption of *p*-xylene in zeolites with more bulky cations; higher uptake rates were observed for the K-Y/*p*-xylene system than for the Na-Y/*p*-xylene system

69. King, S.T.; Garces, J. *J. Catal.* **1987**, *104*, 59.

70. Garces, J.M.; Vrieland, G.E.; Bates, S.I.; Scheidt, F.M. *Stud. Surf. Sci. Catal.* **1985**, *20*, 67.

71. Sefcik, M.D. *J. Am. Chem. Soc.* **1979**, *101*, 2164.

[72]. Also higher benzene mobility in Na-X compared to Na-Y was reported by Auerbach *et al.* despite the fact that Na-X has a much higher cation concentration per unit cell (see Chapter 2) compared to Na-Y which might hinder the mobility of benzene [73]. Thus the low toluene mobility observed in Cs-X by NMR cannot be explained solely by sterical hindrance imposed by the Cs⁺ cations in the zeolite pores.

However, the low toluene mobility observed by Sefcik could be explained by adsorption of toluene in the 12-membered ring (D₁₂) windows between adjacent supercages of Cs⁺ and Rb⁺ exchanged zeolite X as proposed by Xie *et al.* [74]. Toluene interacts *via* its hydrogens with the basic oxygens of the framework and is stabilized by migration of the counter cations to positions adjacent to the six oxygen atoms of the ring. This mode of adsorption might hinder the mobility of toluene. In Li-X and Na-X zeolites toluene interacts mainly *via* its aromatic ring with the cations. This trend was attributed to a decreasing Lewis acid strength and an increasing Lewis base strength of the framework oxygen atoms upon exchanging Na⁺ cations for K⁺, Rb⁺, and Cs⁺ cations [74,75]. High side chain selectivities during toluene methylation over Rb-X, Cs-X, Cs-Y and Cs-β zeolites was also reported [31,43], while literature reported benzene adsorption in the 12 membered ring windows of Cs-X [75], Rb-X, Cs-Y [76] and Cs-β [77] zeolites (based on infrared experiments). The diameter of the D₁₂ windows in X, Y and β zeolites is approximately 7.4 Å, large enough to host toluene (kinetic diameter 6.1 Å [33]). The high side chain selectivities during toluene methylation reported for Rb⁺ and Cs⁺ exchanged X and Y zeolites and Cs-β might thus be attributed to interaction of toluene with the pore wall, thereby sterically hindering an electrophilic attack on the hydrogen atoms. The CH₃-group (of toluene) may protrude from the D₁₂ window plane into the supercage where it is accessible for alkylation. A similar conclusion was drawn for the methylation of aniline over Rb⁺ and Cs⁺ exchanged X and Y zeolites [78]. The interaction of toluene with the framework oxygens is consistent with the calculations performed by Itoh *et al.* [35]. The environment surrounding the toluene molecules inside the zeolite pores during alkylation is still a matter of debate, but recently Garces *et al.* showed that indeed physical constraints do play an important role, since mesoporous basic alkali doped alumina was inactive in the side chain alkylation reaction [43], while alkali impregnated microporous carbon was active [79].

The activation of methanol and the dehydrogenation mechanism yielding formaldehyde by basic zeolites and its reaction in the alkylation of toluene towards styrene over basic zeolites is still a matter of debate. However, from the previous it becomes clear that a subtle balance between methanol

72. Bellat, J.-P.; Simonot-Grange, M.-H., *Zeolites* **1995**, *15*, 124.

73. Auerbach, S.M.; Bull, L.M.; Henson, N.J.; Metiu, H.I.; Cheetham, A.K. *J. Phys. Chem.* **1996**, *100*, 5923.

74. Xie, J.; Bousmina, M.; Xu, G.; Kaliaguine, S. *J. Mol. Catal. A: Chemical* **1998**, *135*, 187.

75. De Mallmann, A.; Barthomeuf, D. *Zeolites* **1988**, *8*, 293.

76. De Mallmann, A.; Barthomeuf, D. In *Proceedings of the 7th International Zeolite Conference, Tokyo*; Murakami, Y, Iijima, A., and Ward, J.W., Eds.; Elsevier: Tokyo, 1986; Vol. 28, pp 609-615.

77. Dzwigay, S.; De Mallmann, A.; Barthomeuf, D. *J. Chem. Soc., Faraday Trans.* **1990**, *86*, 431.

78. Su, B.L.; Barthomeuf, D. *Appl. Catal. A: General* **1995**, *124*, 73.

79. Wieland, W.S.; Davis, R.J.; Garces, J.M. *Catal. Today*. **1996**, *28*, 443.

(activation and) dehydrogenation, toluene activation and zeolite structure is needed, when yielding styrene (and ethylbenzene).

1.5 CATALYST IMPROVEMENT

This paragraph will describe attempts to increase the methanol selectivity (at the expense of the undesired decomposition reactions to CO and H₂ and dimethyl ether) and the styrene yield in the alkylation reaction, since these are reported to be very low [33]. In the first part, zeolites are discussed which are modified with alkali metaloxide clusters. In the second part alkali metal cation exchanged zeolites with (1) occluded metals, like copper or silver, (2) transition metaloxides, e.g., iron-molybdenumoxide, and (3) boron modified zeolites will be discussed. In the final part of this paragraph, a short outlook is presented into other possible zeolite catalysts that might be tested in the near future, since they have potential applicability as dehydrogenation catalysts, combined with the confining space and surface basicity of zeolites.

Alkali metal cation impregnated zeolites

It was claimed that the methanol dehydrogenation ability and the toluene side chain methylation selectivity are directly proportional to the basicity of alkali metal cation exchanged zeolites and the proximity of acid-base sites. This basicity is directly related to the Si/Al ratio and the topology of the zeolite (see Chapter 2). Introduction of metal oxide clusters into the zeolite pores increases the zeolite basicity and thus promotes the side chain methylation of toluene [42,80,81]. However, substantial amounts of methanol are decomposed to carbon monoxide over such strong basic material, limiting the use of methanol as alkylating agent [42,80]. Thus occlusion of alkali metal oxide clusters inside the zeolite pores is not the answer to more active and selective catalysts.

Dual catalysts

The effect of occluded boron on the alkylation of toluene over Cs⁺ exchanged X zeolites was studied by Guo *et al.* [82] and Das and Pramanik [83], while Archier *et al.* [42] investigated the effect of occluded boron in CsO modified Cs-X zeolites. Boron is known to enhance the *in situ* formation of formaldehyde from methanol [84]. However, boron impregnated on Cs⁺ exchanged X zeolites decreases the alkylation activity slightly, compared to Cs-X, and even different effects are found on the C₈-selectivity, given as the styrene/ethylbenzene ratio. While in the case of Guo *et al.* [82] this ratio is

80. Hathaway, P.E.; Davis, M.E. *J. Catal.* **1989**, *119*, 479.

81. Usachev, N. Ya.; Lapidus, A.L.; Usacheva, O.N.; Savelyev, M.M.; Krasnova, L.L.; Minachev, Kh.M. *Petrol. Chem.* **1993**, *33*, 291.

82. a) Guo, W.G.; Zhang, Z.W.; Liang, J.; Cai, G.Y.; Chen, G.Q. In *Proc. Int. Conf. Pet. Ref. Petrochem. Process.*; 1991; Vol. 3, pp 1459-1465; b) Guo, W.G.; Zhang, Z.W.; Liang, J.; Cai, G.Y.; Chen, G.Q. *Chin. Chem. Lett.* **1993**, *4*, 873.

83. (a) Das, N.K.; Pramanik, K. *J. Indian Chem. Soc.* **1997**, *74*, 701; (b) Das, N.K.; Pramanik, K. *J. Indian Chem. Soc.* **1997**, *74*, 705.

84. Unland, M.L.; Baker, G.E. *U.S. Pat. 4,115,424*, 1978, assigned to Monsanto Company.

enhanced while using boron impregnated Cs-X, Das and Pramanik [83] found a decreasing effect on this ratio with the impregnation of boron, compared to Cs⁺ exchanged X zeolites. No explanation for these effects is given. A possible explanation for the lower alkylation activity can be the increasing acidity of the samples upon impregnation with boron and different preparation methods.

When using boron impregnated Cs-X zeolites containing CsO-clusters, the effect was significant. Boron impregnation was shown by Archier *et al.* [42] to have an increasing effect on the toluene alkylation selectivity and activity, compared to CsO impregnated Cs-X zeolites, since it increases the dehydrogenation abilities for methanol and diminishes the unselective decomposition of formaldehyde into carbon monoxide and molecular hydrogen [84]. They concluded that the incorporation of boron resulted in the formation of B₂Cs₂O₄-species inside the zeolite channels, resulting in a lower overall basic strength of the CsO cluster, which decreases the decomposition activity into CO and molecular hydrogen and thus enhances the methylation of toluene.

The dual performance of boron-cesium exchanged and modified zeolites together with copper- or silver oxide catalysts in the side chain methylation of toluene, has been tested by Lacroix *et al.* [66] in a flow of molecular hydrogen (reaction temperature 673 K). The intrazeolitic Cu- and Ag-oxide clusters are reduced to metallic Cu and Ag *in situ* (reduced Cu- and Ag-metals are known materials to dehydrogenate methanol to formaldehyde [85,86]). By using molecular H₂, high yields of ethylbenzene are found, resulting from the *in situ* hydrogenation of styrene, thus at the expense of selective styrene formation. When performed in Ar or N₂ instead of H₂, high yields of styrene are obtained, while the total C₈ yields decreased slightly; reduction of the Cu or Ag-oxides is performed *in situ* by the formation of molecular hydrogen from the dehydrogenation of methanol over boron. Yields of secondary products like CO, CO₂ and dimethyl ether (DME) are reported as well. Only catalysts with impregnated CsO clusters (with occluded boron and copper more than boron occluded alone) were found to be active for the production of large amounts of CO. However, Archier *et al.* [42] showed that also Cs⁺ exchanged X zeolites decomposed MeOH to CO. This might be due to the use of H₂ as carrier gas. A reaction mechanism is presented which involves the presence of molecular H₂ necessary for scission of the C-O bond of intermediately formed, surface bound, phenylethanal, releasing styrene and ethylbenzene into the gas phase. The presence of gas phase H₂ diminished the formation of coke, thus increasing the catalyst lifetime.

Das and Pramanik [83b] also investigated the performance of a dual catalyst containing iron molybdenum oxide (Fe-Mo oxide) deposited on Cs⁺ exchanged zeolites, modified with and without boron. Fe-Mo oxide catalysts are known to be active for the dehydrogenation of methanol to formaldehyde in the presence of oxygen [87] and are used on a commercial scale. It was found that dual catalysts, containing Fe-Mo oxide deposition were already active at 598 K, while single Cs⁺ exchanged

85. Fisher, I.A.; Bell, A.T. *J. Catal.* **1999**, *184*, 357.

86. Yang, C.; Meng, Zh. *Shiyou Xuebao, Shiyou Jiagong* **1992**, *8*, 43.

87. Faliks, A.; Yetter, R.A.; Floudas, C.A.; Bernasek, S.L.; Fransson, M.; Rabitz, H. *J. Phys. Chem. A* **2001**, *105*, 2099.

catalysts exhibit catalytic activities only at temperatures higher than 648 K. This is probably related to the concerted interaction of the Cs⁺ exchanged zeolite and the incorporated Fe-Mo oxide with toluene. Direct toluene alkylation with formaldehyde over Cs⁺ exchanged X zeolites did not significantly lower the reaction temperature [34]. By incorporating Fe-Mo oxide onto the Cs⁺ exchanged zeolite, styrene yield and selectivity was enhanced with a factor of 1.5 and 1.2, respectively, compared to single zeolites (reaction temperature 698K). Most striking was the further enhancement of the styrene/ethylbenzene ratio, which was increased by a factor of 4.5. The extra addition of boron to the zeolite did not further increase the activity and selectivity. No effects are reported on the production of dimethyl ether (DME), CO, CO₂, H₂O and H₂. Interesting to note is that no oxygen was present during the catalytic testing.

This paragraph clearly indicates that most research has been focused solely on the improvement of the catalysts in the *in situ* methanol dehydrogenation during the side chain methylation of toluene. It is interesting to note that work performed by Das and Pramanik [83b] implies that toluene activation can be increased by impregnation with transition metals resulting in lower alkylation temperatures; however, this was not further investigated.

Future catalysts

Since the observation by Garces *et al.* [70] of *in situ* formed alkali metallic vapor as active species during the alkylation of toluene, a new class of basic zeolitic catalysts might be the alkali metal atom impregnated zeolites. Several groups have investigated these novel type of catalysts in: 1) the isomerization of *I*-butene [88], 2) the side chain alkylation of toluene with ethylene [89], 3) the side chain alkenylation of *o*-xylene with butadiene [89] and 4) the aldol condensation of acetone [90]. Catalytic tests have shown that these alkali metal exchanged zeolites exhibit a much stronger basicity than CsO-impregnated Cs-zeolites, which in turn possess a higher basicity than Cs⁺ exchanged zeolites [91].

Alkali metal exchanged zeolites are prepared by the thermal decomposition of alkali metal azide (M⁺-N₃) on the external zeolite surface, after which the metal clusters migrate to the zeolites internal [92]; depending on the heating rate, decomposition of the supported azide results in ionic clusters (fast heating rates; $\approx 25 \text{ K} \cdot \text{min}^{-1}$) or neutral metal clusters (slow heating rates; $\approx 1 \text{ K} \cdot \text{min}^{-1}$) [93].

88. Hannus, I.; Kiricsi, I.; Béres, A.; Nagy J.B.; Förster, H. *Stud. Surf. Sci. Catal.* **1995**, *98*, 81.

89. Davis, R.J.; Doskocil, E.J.; Bordawekar, S. *Catal. Today* **2000**, *67*, 241.

90. a) Martens, L.R.; Vermeiren, W.J.; Huybrechts, D.R.; Grobet, P.J.; Jacobs, P.A In *Proceedings of the 9th International Congress on Catalysis, Calgary*; Phillips, M.J., and Ternan, M., Eds.; The Chemical Institute of Canada: Ontario, 1988; Vol. 1, pp 420-428; b) Martens, L.R.M., "Sodium Clusters in Zeolites", PhD thesis, Katholieke Universiteit Leuven, Leuven, Belgium, 1987.

91. a) Bordawekar, S.; Davis, R.J. *J. Catal.* **2000**, *189*, 79; b) Doskocil, E.J.; Davis, R.J. *J. Catal.* **1999**, *188*, 353.

92. Hannus, I.; Beres, A.; Nagy, J.B.; Halasz, J.; Kiricsi, I. *J. Mol. Struct.* **1997**, *410/411*, 43.

93. Interesting detail occurring during the preparation method is that the impregnated alkali metal azide can exchange with the cation in the zeolite at the exchangeable position, resulting in the formation of mixed clusters, i.e., clusters of the exchanged cation (neutral and ionic), and clusters of the impregnated metal azide. This was shown to occur for both K-X (and Cs-X) impregnated with Na- (or Cs-) azide, where, after impregnation and thermal

Another way of impregnating zeolites with alkali metal clusters is by introducing alkali metal vapor by evaporation of solid alkali metal particles. This procedure is followed by Seff and coworkers [94] and Anderson *et al.* [95] and appears to yield only cationic clusters, e.g., Na_3^{2+} cluster, which exhibit a very high conductivity at room temperature [95,96]. The structure of the alkali metal clusters, i.e., neutral and ionic, has been successfully elucidated by using Electron Spin Resonance (ESR) Spectroscopy [91b,95].

TABLE 1.3: Alkali metal impregnated zeolites as catalysts in the side chain methylation of toluene, compared to conventional modified zeolites [97].

	CsXOH ^a	CsX-Na ^b	CsXB ^c	CsXB-Na ^d
6 hrs time on stream (698 K)				
methanol conversion (%)	15	45	15	8.5
styrene yield (%)	0.7	4.3	5	3.5
ethylbenzene yield (%)	0.25	4.1	0.35	1.1
total selectivity (%) ^e	6.3	18,6	36	54
15 hrs time on stream (698 K)				
methanol conversion (%)	nr ^f	40	12	5.5
styrene yield (%)	nr	4	3.1	2.7
ethylbenzene yield (%)	nr	3.8	0.1	0.65
total selectivity (%) ^e	nr	19,5	27	60

^a. CsXOH: unwashed Cs-X exchanged with CsOH, probably containing CsO-clusters.

^b. CsX-Na : CsXOH sample is mechanically mixed with sodium-azide and heated.

^c. CsXB: CsXOH impregnated with boric acid.

^d. CsXB-Na: CsXB impregnated with sodium metal using sodium vapor deposition.

^e. with respect to methanol conversion. ^f. nr: not reported.

So far only one reference was found concerning the use of alkali metal impregnated zeolites in the side chain methylation of toluene. In a 1989 patent, Barthomeuf and Quenach de Quivillic reported Cs-X impregnated with sodium metal to be active and selective catalysts for this reaction [97]. Table 1.3 compiles the most important findings and compares them with zeolites impregnated with CsO

treatment, neutral and ionic K-clusters were observed, together with neutral Na- (or Cs-) clusters [Xu, B.; Kevan, L. *J. Phys. Chem.* **1992**, *96*, 2642.

94. a) Sun, T.; Seff, K.; Heo, N.H.; Petranovskii, V.P. *J. Phys. Chem.* **1994**, *98*, 5768; b) Shibata, W.; Seff, K. *J. Phys. Chem. B* **1997**, *101*, 9022.

95. Anderson, P.N.; Armstrong, A.R.; Porch, A.; Edwards, P.P.; Woodall, L.J. *J. Phys. Chem.* **1997**, *101*, 9892.

96. Nozue, Y.; Kodaira, T.; Ohwashi, S.; Terasaki, O.; Takeo, H. *Mater. Sci. Eng.* **1996**, *A217/218*, 123.

97. Barthomeuf, D.; Quenach de Quivillic, V. *U.S. Pat. 5,068,483 (Eur. Pat. 389530)*, 1989, assigned to Elf Aquitaine, France, and Centre National de la Recherche Scientifique, France.

clusters or boron. Most surprising was the increase in methanol selectivity with time on stream of the alkali metal impregnated zeolites. The methanol selectivity usually decreases with time on stream when using more conventional CsO and boron modified zeolites (compare zeolites CsX-Na, CsXB, and CsXB-Na after 6 hrs and 15 hrs time on stream). Only when a Na⁺ exchanged zeolite impregnated with sodium metal was used a very low activity and selectivity was observed. Also the occlusion of boron in the zeolite has a negative impact on the performance of the alkali metal impregnated catalyst (compare CsX-Na and CsXB-Na in Table 1.3). The reason for this is unclear.

In a separate study it was shown that the occluded metals were the active phase for the dehydrogenation of methanol to yield formaldehyde. Metallic sodium was tested in the gasphase dehydrogenation of methanol by Ruf and Emig [98]. They found that this catalyst (typical TON of 500-700 were found) at temperatures above 423K (the sublimation point of solid atomic sodium) converted methanol to formaldehyde (conversion: 5% (523 K) - 76% (1058 K); selectivity: > 80%). Only stoichiometric amounts of molecular hydrogen and very small amounts of carbon monoxide are found. No water is formed during this reaction. Unclear was, whether sodium was provided atomically or as small clusters to the gas phase.

Despite these interesting results there are also drawbacks to be noted. Sodium metal catalyzes the dehydrogenation of methanol to formaldehyde, but how stable, i.e., thermodynamically or chemically, are these neutral alkali metal clusters? The presence of molecular oxygen in the feed deactivates the active sites as was shown for the side chain ethylation of toluene over Na- and Cs-metal impregnated zeolites [91a]. This has been attributed to the irreversible formation of superoxide anions (O₂⁻) attached to a Na⁺ cation and formed by the electron transfer from atomic metal clusters to the chemisorbed oxygen molecule [90b]. Also the presence of carbon dioxide blocks any appearance of basic activity as was found for *n*-olefin isomerisation [90b]. Other deactivating agents have so far not been reported; however, water that is formed during the reaction probably deactivates the active sites as well, yielding NaOH. Additionally, too high reaction temperatures could result in evaporation of the metallic phase inside the zeolite pores, resulting in a lowering of the catalytic activity with time on stream.

1.6 CONCLUDING REMARKS, SCOPE AND OUTLINE OF THIS WORK

A literature survey introducing the toluene side chain alkylation as a candidate for the replacement of the industrially employed styrene routes was given. Two possible candidates were reviewed: 1) oxidative toluene methylation with methane and 2) direct toluene methylation with methanol. Only the direct toluene methylation with methanol was investigated in this thesis. It was shown that Rb⁺ and Cs⁺ exchanged X zeolites were among the best zeolites tested for the direct methylation of toluene to produce styrene. Introduction of basic alkali oxide clusters increased the

98. a) Ruf, S.; Emig, G. *Appl. Catal. A: General* **1997**, *161*, L19; b) Ruf, S.; May, A.; Emig, G. *Appl. Catal. A: General* **2001**, *213*, 203.

alkylation activity, but also increased the methanol decomposition to CO and H₂. Occlusion of methanol dehydrogenation catalysts, like Fe-Mo oxide, Cu and Ag, yielded high toluene methylation activities. Furthermore, also the toluene alkylation mechanism has been elucidated.

The results presented here indicate a very delicate balance between the Lewis acid and base strength and density of active sites, and the zeolite structure in the side chain methylation of toluene: 1) toluene adsorption in the 12 membered ring windows due to hydrogen bonding in addition to cation- π interaction activates the methyl group of toluene and 2) methanol dehydrogenation over base sites yields formaldehyde. Furthermore, residual Brønsted acid sites are far more active than the Lewis acid-base sites that catalyse the side chain alkylation of toluene and must be avoided.

However, the selective methanol dehydrogenation yielding formaldehyde and the unselective decomposition into CO and H₂ is not yet understood. Therefore the research described in this thesis was aimed at gaining more insight into the methanol dehydrogenation and decomposition mechanisms. Understanding the methanol adsorption structure on these materials has been proven to be of vital importance (Chapter 4 and 5). Chapter 6 reports results obtained for the methanol dehydrogenation and decomposition mechanisms. Since molecular oxygen appeared to increase the surface concentration of formed formaldehyde (Chapter 7), we also investigated the side chain methylation of toluene in the presence of traces of oxygen to increase the methylating activity (Chapter 9) and compared the results obtained with those obtained in the absence of oxygen (Chapter 8).

Chapter 2

Materials

Abstract:

This Chapter describes the molecular sieves, i.e., zeolites, used in this work. A summary of the topology of the used zeolites, based on a literature survey will be given, whereby the emphasis will be on alkali metal cation exchanged aluminosilicates.

2.1 INTRODUCTION

Zeolites are ordered, crystalline solid materials with a very well defined microporosity. They have unique properties, such as high surface area, high concentration of active sites, narrow pore size distribution, small pores, etc., which make them very suitable for catalysis and sorption. In the previous chapter some examples of catalysis have been shown. Most famous are H-ZSM5 zeolites (MFI topology) and USY (FAU topology) used in the petrochemistry by, e.g., UOP, Mobil and BP [1].

All silica zeolites, e.g., silicalite-1, consist of no other than $[\text{SiO}_4]$ tetrahedra (although some impurities of Na and Al are found) [2]. The tetrahedra are linked together at the corners by shared oxygen ions to form an ordered framework with n -dimensional pores, e.g., $n = 1$ (TON and MOR zeolite), $n = 2$ (FER zeolite) and $n = 3$ (MFI and FAU zeolite) and different internal diameters (for examples see Ref. [3,4,5]). Since zeolites are usually composed of $[\text{SiO}_4]$ and $[\text{AlO}_4]^-$ tetrahedra arranged in various geometric patterns, they are also called aluminosilicates. Another often used name is molecular sieves, as zeolites are used for the separation of for example n - and *iso*-paraffins [6].

Isomorphous substitution of $[\text{SiO}_4]$ tetrahedra for $[\text{AlO}_4]^-$ tetrahedra introduces negative charges into the framework which are compensated by positive, extra framework, counterions, such as protons, monovalent cations or multivalent cations, which do not take part as tetrahedral atoms in the zeolite framework, as Si and Al do. By using counterions with different cation radius, modifications in pore size diameter are introduced. For example zeolite LTA has pore size diameters of 3, 4 and 5 Å, when exchanged with either K^+ , Na^+ or Ca^{2+} cations, respectively [7].

Based on the assumption that adjacent negative charges, i.e., an aluminum atom having another aluminum atom in its second coordination sphere, are less stable than isolated ones, this is virtually excluded. This aluminum avoidance rule is called Loewenstein's rule, named after W. Loewenstein who, in 1954, was the first to underline the importance of the Al-O-Al rule [8]; aluminosilicates in general do not have Si/Al ratio < 1 ; zeolites LTA and LSX have the lowest silicon to aluminum (Si/Al) ratio possible (Si/Al ≈ 1).

The description of zeolites is usually based on the silicon to aluminum ratio (Si/Al ratio) and framework structure (pore size, dimension, extra framework ions etc.) [9]. Up to now 133 natural and

-
1. a) Dyer, A., *An Introduction to Zeolite Molecular Sieves*, 1st Edition; John Wiley and Sons: Chichester, 1988; b) Tanabe, K.; Hölderich, W.F. *Appl. Catal. A: General* **1999**, *181*, 399.
 2. a) Zecchina, A.; Bordiga, S.; Spoto, G.; Marchese, L.; Petrini, G.; Leofanti, G.; Padovan, M. *J. Phys. Chem.* **1992**, *96*, 4985; b) Pelmenschikov, A.G.; Morosi, G.; Gamba, A.; Zecchina, A.; Bordiga, S.; Paukshitis, E.A. *J. Phys. Chem.* **1993**, *97*, 11979.
 3. a) Davis, M.E. *Ind. Eng. Chem. Res.* **1991**, *30*, 1675; b) Davis, M.E. *Acc. Chem. Res.* **1993**, *26*, 111.
 4. a) Csicsery, S.M. *Zeolites* **1984**, *4*, 202; b) Ramôa Ribeiro, F. *Catal. Lett.* **1993**, *22*, 107.
 5. Breck, D.W., *Zeolite Molecular Sieves. Structure, Chemistry, and Use*, 1st Edition; John Wiley and Sons: New York, 1974.
 6. Kieboom, A.P.G.; Moulijn, J.A.; Sheldon, R.A.; Van Leeuwen, P.W.M.N. In *Catalysis: An Integrated Approach, Second, Revised and Enlarged Edition*; Van Santen, R.A., Van Leeuwen, P.W.M.N., Moulijn, J.A., and Averill, B.A., Eds.; Elsevier: Amsterdam, 1999; pp 29-80.
 7. White, J.C.; Nicholas, J.B.; Hess, A.C. *J. Phys. Chem. B* **1997**, *101*, 590.
 8. Loewenstein, W. *Am. Miner.* **1954**, *39*, 92.
 9. Baerlocher, Ch.; Meier, W.M.; Olson, D.H., *Atlas of Zeolite Framework Types*, 5th Edition; Elsevier: Amsterdam, 2001.

synthetic zeolite types are characterized and catalogued [9], of which only zeolites with the FAU, MOR and MFI topology will be discussed here, since these are the zeolites used in Chapters 4-9.

Brönsted acidic zeolites (see Fig. 2.1), thus having a proton at the ion-exchangeable site (depicted as SiO(H)Al), are well described in literature [10,11]. Quantum chemical calculations have shown that the acid strength of these Brönsted acid sites, which is usually described by the heat of deprotonation (E_{DP}) or proton affinity (PA) lies in the order of 1150 to 1210 $\text{kJ}\cdot\text{mol}^{-1}$ [12]. Increasing E_{DP} results in a decreasing acid strength, in other words a decreasing ability of the framework to donate a proton.

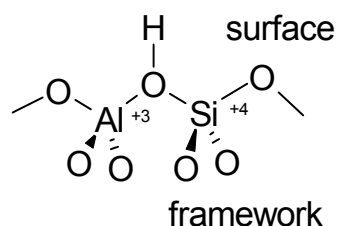


Figure 2.1: Brönsted acid site.

The acid strength increases with increasing Si/Al ratio. Decreasing aluminum content of the framework results in an increasing Si-O bond strength of the Si-O(H)-Al bridge and thus a decreasing OH bond strength (lower E_{DP}). For example, calculations have shown that the E_{DP} of SiO(H)Al groups in H-Y (Si/Al = 47) is 20-30 $\text{kJ}\cdot\text{mol}^{-1}$ lower than H-Y (Si/Al = 2.7) [12]. However, this acidity dependence on the Si/Al ratio is only observed up to a certain value, i.e., the critical Si/Al ratio (Si/Al_c ≈ 15) [12a]. Above this number the framework Al atoms are separated enough that they do not appear in the second nearest neighbor shell surrounding the Si (of the first shell) and thus do not influence each

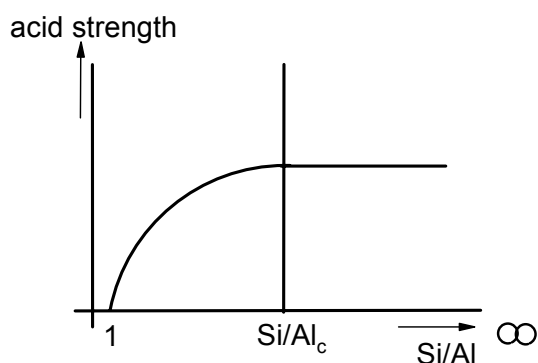


Figure 2.2: Brönsted acid strength as a function of Si/Al ratio.

other. Therefore the acid strength does not change (see Figure 2.2) [10]. However, since the total amount of acid sites decreases, the overall reaction rate decreases as well. Also the bond angle in the framework of the Si-O-Al bridging group, thus the framework topology, influences the acid strength. This becomes evident when the acid strength of dealuminated H-Y is compared with H-ZSM5 of similar high Si/Al ratio; the acid strength of dealuminated Y is higher [12]. These findings show

that the frameworks electrostatic field, defined by the Madelung Potential (i.e., the summation of all geometric (attractive and repulsive) interactions), has a large effect on the acidity of Brönsted acid sites and thus also on the sorption and catalytic properties [13]. Although the notation Brönsted acid sites suggests a large ionicity of the framework hydroxyl group, the chemical OH bond is regarded as being

10. Averill, B.A.; Rietjens, I.M.C.M.; Van Leeuwen, P.W.M.N.; Van Santen, R.A. In *Catalysis: An Integrated Approach, Second, Revised and Enlarged Edition*; Van Santen, R.A., Van Leeuwen, P.W.M.N., Moulijn, J.A., and Averill, B.A., Eds.; Elsevier: Amsterdam, 1999; pp 109-208.

11. a) Kramer, G.J.; Van Santen, R.A. *J. Am. Chem. Soc.* **1993**, *115*, 2887; b) Van Santen, R.A.; Kramer, G.J. *Chem. Rev.* **1995**, *95*, 637.

12. a) Eichler, U.; Brändle, M.; Sauer, J. *J. Phys. Chem. B* **1997**, *101*, 10035; b) Brändle, M.; Sauer, J. *J. Am. Chem. Soc.* **1998**, *120*, 1556.

13. a) Limtrakul, J.; Khongpracha, P.; Jungstutiwong, S.; Truong, T.N. *J. Mol. Catal. A: General* **2000**, *153*, 155; b) Limtrakul, J.; Jungstutiwong, S.; Khongpracha, P. *J. Mol. Struct.* **2000**, *525*, 153.

predominantly covalent [11a].

Determination of the acid strength and acid site concentration in Brønsted zeolites can be easily done by a variety of methods [14]. Most commonly used are calorimetry, temperature programmed desorption and infrared spectroscopy, which involve the use of weakly basic probe molecules, like CO, NH₃, pyridine or benzene. In calorimetry, the higher the acid strength the higher the heat of adsorption of the probe molecule. In infrared spectroscopy, the shift of the framework OH stretching vibrations ($\Delta\nu_{\text{OH}}$) upon adsorption of probe molecules to lower wavenumbers is proportional to the acid strength of the Brønsted acid site. The larger $\Delta\nu_{\text{OH}}$ the higher the acid strength. In t.p.d. experiments, the desorption temperature is a function of the acid strength of the acid site.

While for acid zeolites the compensating counterion of the negatively charged framework oxygens is the proton, in basic zeolites this counterion is a metal cation (see Figure 2.3). Growing numbers of examples are known, like Cs⁺, Tl⁺ or Ni²⁺ exchanged zeolites [15,16]. These zeolites contain a Lewis acid site, the metal cation, and a Lewis base site, the framework oxygen, and are thus called basic zeolites. The binding force between the cations and the negatively charged framework is of electrostatic nature and depends on attractive framework-cation interaction as well as on repulsive cation-cation interaction of neighboring cation sites.

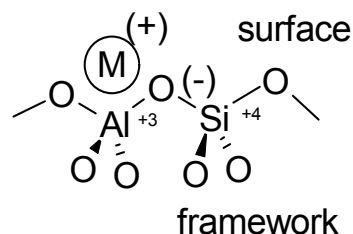


Figure 2.3: Lewis acid-base site in cation exchanged zeolites

For the determination of the basicity (basic strength) and concentration of basic sites, CO₂ has been considered as probe molecule. However, due to its high acidic character, it forms stable adducts with a large variety of surface oxygen ions exhibiting various basic strengths. The search for weakly acidic probe molecules is, therefore, ongoing. Other probe molecules proposed are CO, N₂, H₂, pyrrole, chloroform, etc. [17]. Also test reactions, e.g., dehydrogenation / dehydration [18,19], isomerization of *n*-butenes [20], methylbutynol dehydration / cleavage [21], etc. are employed. However, all these techniques have not led to a uniform description of basic site concentration and strength or to make a reliable classification of the basic materials.

X-ray photoelectron spectroscopy (XPS) as a direct method for measuring zeolitic O_{1s}

-
14. a) Farneth, W.E.; Gorte, R.J. *Chem. Rev.* **1995**, *95*, 315; b) Lercher, J.A.; Gründling, Ch.; Eder-Mirth, G. *Catal. Today* **1996**, *27*, 353; c) Brunner, E. *Catal. Today* **1998**, *38*, 361; d) Busca, G. *Catal. Today* **1998**, *41*, 191.
 15. a) Barthomeuf, D.; Coudurier, G.; Vedin, J.C. *Mater. Chem. Phys.* **1988**, *18*, 553; b) Barthomeuf, D. *Stud. Surf. Sci. Catal.* **1991**, *65*, 157; c) Barthomeuf, D. *Catal. Rev.- Sci. Eng.* **1996**, *38*, 521.
 16. Mortier, W.J., *Compilation of Extra Framework Sites in Zeolites*; Butterworth Scientific Ltd.: Guildford, 1982.
 17. Lavalley, J.C. *Catal. Today* **1996**, *27*, 377.
 18. a) Yashima, T.; Suzuki, H.; Hara, N. *J. Catal.* **1974**, *33*, 486; b) Nagy, J.B.; Lange, J.-P.; Gourgue, A.; Bodart, P.; Gabelica, Z. *Stud. Surf. Sci. Catal.* **1985**, *20*, 127; c) Concepción-Heydorn, P.; Jia, C.; Herein, D.; Pfänder, N.; Karge, H.G.; Jentoft, F.C. *J. Mol. Catal. A: Chem.* **2000**, *163*, 227.
 19. Aramendia, M.A.; Boráu, V.; Jiménez, C.; Marinas, J.M.; Porras, A.; Urbano, F.J. *React. Kinet. Catal. Lett.* **1998**, *65*, 25.
 20. Tsuchiya, S. In *Acid-Base Catalysis*; Tanabe, K., Hattori, H., Yamaguchi, T., and Tanaka, T., Eds.; Verlag Chemie: Weinheim, 1989; pp 169-182.
 21. a) Huang, M.; Kaliaguine, S. *Catal. Lett.* **1993**, *18*, 373; b) Meyer, U.; Hoeldrich, W.F. *J. Mol. Catal. A: Chem.* **1999**, *142*, 213.

binding energies has resulted in a better description of basic strength [22,23,24]. A decrease in O_{1s} binding energy can be interpreted as an increase in basicity (electron density) of oxygen. Detailed evaluation of XPS binding energies have shown that the trends observed for O_{1s} binding energies in different zeolites, i.e, different Si/Al ratios and/or extra framework cations, relates to the Madelung Potential of the zeolite framework (which is affected by the incorporation of different Al concentrations, bond lengths and angles) [25]. A similar conclusion was reached for the description of Brønsted acid zeolites (see above).

Recently, quantum chemical calculations are also applied to basic zeolites [26,27,28,29,30], resulting in a better description of basic strength along different samples and it describes the negative charge on the individual oxygen atoms of the framework [27,28].

A rather simple technique to calculate the basic properties of metal cation exchanged zeolites has been developed [31], based on the electronegativities [32] of the individual atoms in the zeolite. From the general zeolite composition, e.g., $(Me^{2+}Me^+)_n Si_{192-n} Al_n O_{384} \cdot m H_2O$ for FAU [9], and the zeolites chemical composition it is possible to determine the theoretical unit cell composition (see also Chapter 3). This allows one to calculate the average negative charge on the framework oxygens as a measure of the average framework basicity using the following equations [31]:

$$S_{int} = (S_p^p \cdot S_Q^q \cdot S_R^r \cdot S_T^t)^{1/(p+q+r+t)} \quad (\text{Eq. 2.1})$$

for a compound $P_p Q_q R_r T_t$ where S_{int} is the Intermediate Sanderson Electronegativity of compound $P_p Q_q R_r T_t$, S_X is the Sanderson Electronegativity of element X [32] and X is the number of atoms of element X in the compound $P_p Q_q R_r T_t$ and

$$-\delta_O = (S_{int} - S_O) / [2.08(S_O^{1/2})] \quad (\text{Eq. 2.2})$$

where $-\delta_O$ is the average negative charge of the framework oxygens and S_O is the Sanderson Electronegativity of oxygen. Decreasing S_{int} , and thus increasing $-\delta_O$, is indicative of an increasing basicity of the framework. Note that the calculated $-\delta_O$ is an average of the oxygen negative charge of

-
22. Vinek, H.; Noller, H.; Noller, H.; Ebel, M.; Schwarz, K. *J. Chem. Soc., Faraday I* **1977**, *73*, 734.
 23. Stöcker, M. *Microporous Mater.* **1996**, *6*, 235.
 24. a) Huang, M.; Adnot, A.; Kaliaguine, S. *J. Am. Chem. Soc.* **1992**, *114*, 10005; b) Xie, J.; Huang, M.; Kaliaguine, S. *Appl. Surf. Sci.* **1997**, *115*, 157.
 25. Grünert, W.; Muhler, M.; Schröder, K.-P.; Sauer, J.; Schlögl, R. *J. Phys. Chem.* **1994**, *98*, 10920.
 26. a) Ferrari, A.M.; Neyman, K.M.; Rösch, N. *J. Phys. Chem. B* **1997**, *101*, 9292; b) Vayssilov, G.N.; Staufer, M.; Belling, T.; Neyman, K.M.; Knözinger, H.; Rösch, N. *J. Phys. Chem. B* **1999**, *103*, 7920.
 27. Vayssilov, G.N.; Rösch, N. *J. Catal.* **1999**, *186*, 423.
 28. Heidler, R.; Janssens, G.O.A.; Mortier, W.J.; Schoonheidt, R.A. *J. Phys. Chem.* **1996**, *100*, 19728.
 29. Buttefey, S.; Boutin, A.; Mellot-Draznieks, C.; Fuchs, A.H. *J. Phys. Chem. B* **2001**, *105*, 9569.
 30. Deka, R.Ch.; Roy, R.K.; Hirao, K. *Chem. Phys. Lett.* **2000**, *332*, 576.
 31. Mortier, W.J. *J. Catal.* **1978**, *55*, 138.
 32. Sanderson, R.T. *J. Am. Chem. Soc.* **1983**, *105*, 2259.

the bulk material, however, it provides a tool to differentiate between zeolitic materials. Additionally, trends obtained using Eq. 2.1 and 2.2 are in good agreement with XPS measurements of the O_{1s} binding energy [23].

Bonds of large cations, like Na⁺ to Cs⁺, to framework oxygens are mainly ionic. However, a small contribution of covalent bonding can not be excluded. By interaction with the zeolite framework the partial atomic charges are decreased. Li⁺ bonding to the framework oxygens has a high covalent character and this covalency increases with increasing Al content of the framework [13,26a]. The presence of negative and positive charges within the zeolite framework does not only influence the Madelung potential, also the potential energy surface (PES) of the zeolite, thus the sum of the repulsive and attractive (electrostatic, inductive and dispersive) interactions of the zeolite framework, is largely influenced by a change in the basicity of the framework oxygens (which is related to the electrostatic potential of exchanged cations and Si/Al ratio), thus to the electric field inside the zeolite cavities, the cation location etc. Sorption and catalytic effects are therefore effected by a change in the potential energy surface (PES).

Although in the previous part the emphasis was upon aluminosilicates, also incorporation of trivalent boron, gallium or iron into the zeolite framework instead of aluminum has been performed. This results in a modification of the acid strength, as found experimentally [33,34,35] and theoretically [36,37]. Zeolites containing Al were found to be most acidic, whereas those containing B were the least acidic. Also zeolites containing Ge and Al [38] or Ti and Al (or Ga) [39], are known; Ge and Ti thus replacing framework Si. It was found that zeolites containing Ge had stronger basic sites than the corresponding Si analogous [38].

2.2 ZEOLITE TOPOLOGY AND CATION LOCATION IN FAU, MOR AND MFI

This paragraph will describe the topology of the three zeolites used in this thesis, i.e., FAU (X and Y), MOR and MFI (ZSM5). The emphasis will be on the locations of extra framework alkali metal cations in these zeolites, as determined by X-ray powder diffraction (XRD) [40] and single crystal refinement [41]. As the use of probe molecules can distort the location of the cations in the zeolite pores (especially in Y zeolites), when the cation-sorbate interaction is stronger than the cation-sorbent

33. Domokos, L., "Skeletal isomerization of *n*-butene over medium pore zeolites", PhD thesis, University of Twente, Enschede, The Netherlands, 2000.

34. Raj, A.; Sudhakar, J.R.; Kumar, R. In *Proceedings of the 9th International Zeolite Conference, Montreal*; Van Ballmoos, R., Higgins, J.B., and Treacy, M.M.J., Eds.; Butterworth-Heinemann: Boston, 1992; Vol. 2, pp 551-558.

35. Chu, C.T.-W.; Chang, C.D. *J. Phys. Chem.* **1985**, *89*, 1569.

36. Deka, R. C.; Tajima, N.; Hirao, K. *J. Mol. Struct.: THEOCHEM* **2001**, *535*, 31.

37. Chatterjee, A.; Iwasaki, T.; Ebina, T.; Miyamoto, A. *Microporous Mesoporous Mater.* **1998**, *21*, 421.

38. Concepción-Heydorn, P.; Jia, C.; Herein, D.; Pfänder, N. Karge, H.G.; Jentoft, F.C. *J. Mol. Catal. A: Chem.* **2000**, *163*, 227.

39. Anderson, M. W.; Rocha, J.; Lin, Z.; Philippou, A.; Orion, I.; Ferreira, A. *Microporous Mater.* **1996**, *6*, 195.

40. a) Mortier, W.J.; Van den Bossche, E.; Uytterhoeven, J.B. *Zeolites* **1984**, *4*, 41; b) Mortier, W.J.; Bosmans, H.J.; Uytterhoeven, J.B. *J. Phys. Chem.* **1972**, *76*, 650; c) Lin, J.-C.; Chao, K.-J.; Wang, Y. *Zeolites* **1991**, *11*, 376.

(framework oxygen) interaction (the framework oxygens are considered to be a weak ligand [42]), infrared spectroscopy studies using probe molecules as H₂, N₂, CO and pyrrole [17] are not included. This paragraph will thus mainly discuss results obtained using X-ray studies of dehydrated zeolites. In Table 2.1 the cation locations and site occupation in the different used zeolites are compiled. Paragraph 2.3 will briefly describe the influence of adsorbates on the site occupation and location of cations in metal exchanged zeolites.

Caution, however, has to be taken into account concerning the exact location and site concentration of cations reported in literature, compared to our experiments. It was shown by Mortier *et al.* that the number of extra framework cations at a certain location is a function of the dehydration / activation procedure used and the presence of adsorbate [40a,42,43].

Zeolite Faujasite (FAU)

The Faujasite framework topology is shared by the synthetic zeolites, X and Y, and the natural faujasite. The main difference between X and Y is the Si/Al ratio: the latter richer in silicon. The Si/Al ratio of zeolite X varies from ≈ 1 to 1.5 and of zeolite Y from greater than 1.5 to 3. Ultra stable Y zeolites (USY) have Si/Al ratio greater than 3 to ∞ and are usually dealuminated by severe steaming or acid leaching ($(\text{NH}_4)_2\text{SiF}_6$ or SiCl_4 treatment) [44].

One unit cell forming part of the three dimensional pore system of

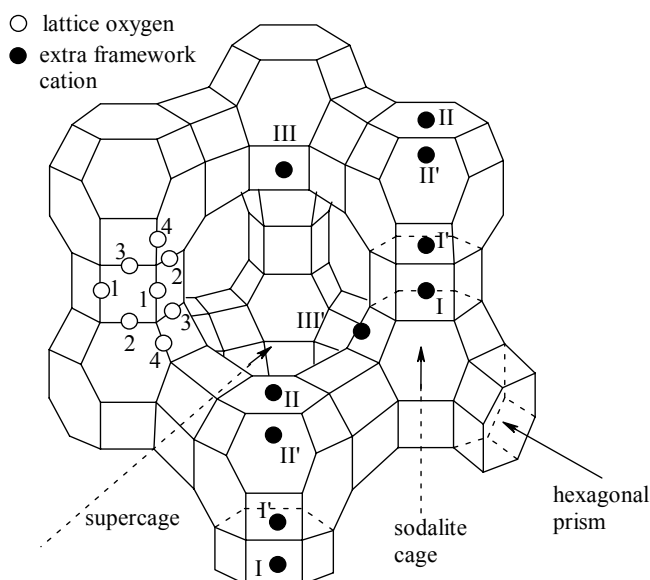


Figure 2.4: Framework structure of Na-FAU (X and Y). Cation locations are shown by Roman numerals I to III' (for details see text). The different oxygen atoms, which are involved in the bonding of the extra framework cations are indicated by the numbers 1 to 4. Cation sites are in accordance with Smith [46]. Drawing has been taken from Ref. [41c].

41. a) Olson, D.H. *Zeolites* **1995**, *15*, 439; b) Zhu, L.; Seff, K. *J. Phys. Chem. B* **1999**, *103*, 9512; c) Lee, S.H.; Kim, Y.; Kim, D.-S.; Seff, K. *Bull. Korean Chem. Soc.* **1998**, *19*, 98; d) Shepelev, Yu.F.; Butikova, I.K.; Smolin, Yu.I. *Zeolites* **1991**, *11*, 287.

42. Dendooven, E.; Mortier, W.J.; Uytterhoeven, J.B. *J. Phys. Chem.* **1984**, *88*, 1916.

43. a) Mortier, W.J. *J. Phys. Chem.* **1977**, *81*, 1334; b) Van Dun, J.J.I.; Mortier, W.J.; Uytterhoeven, J.B. *Zeolites* **1985**, *5*, 257.

44. Triantafillidis, C.S.; Evmiridis, N.P. *Ind. Eng. Chem. Res.* **2000**, *39*, 3233.

TABLE 2.1: Cations per site per Unit Cell of the different used zeolites, as deduced from X-ray crystallographic data (see for site numbering Figures 2.4 to 2.6). See the text for further details.

Sample	Reference	Si/Al	Location (see Figure 2.4)					
			Site I	Site I'	Site II	Site II'	Site III	Site III'
FAUjasite								
Na ₈₈ -X	41a	1.18	2.9	29.1	0	31	0	29.8
K _{86,5} -X	40b	1.22	9.2	13.6	0	25.6	0	38.2
Rb ₇₁ Na ₂₁ -X	41c	1.09	4.5 (Rb ⁺) 7.0 (Na ⁺)	8.9 (Rb ⁺)	2.6 (Rb ⁺)	17.7 (Rb ⁺) 12.7 (Na ⁺)	32.9 (Rb ⁺)	5.2 (Rb ⁺)
Cs _{46,1} Na _{49,5} -X	41d	1.11	1.0 (Cs ⁺) 12.5 (Na ⁺)	5.6 (Cs ⁺) 5.0 (Na ⁺)	1.6 (Cs ⁺)	32 (Na ⁺)	0	37.9 (Cs ⁺)
Na ₅₇ -Y	40a	2.37	7.0	13.8	0	29.4	0	0
MORdenite								
Na ₈ -MOR10	46	5	3.1	0	0	2.6	1.5	
Na-MOR20		10			Not determined; probably located in site I (3.3) and site IV (1.7).			
MFI (ZSM5)								
Main channel at intersection			Location (see Figure 2.6)			In nanosize cavities (defects)		
Li/Na-ZSM5	63,65	11	Not determined; probably located in both.					
Cs-ZSM5	40c	26	2.28 (Cs ⁺)			0		

faujasite zeolites consists of 8 supercages, 8 sodalite cages and 16 hexagonal prisms (see Fig. 2.4) [45]. Each supercage is connected via a 12-membered oxygen ring (D_{12}) window (= 24-membered ring, consisting of Si, Al, O): diameter D_{12} ring = 7.4Å; internal 6-membered (D_6) oxygen ring windows (thus a 12-membered Si, O, Al ring) diameter D_6 : 2.4Å). From the sodalite-cages entry to the hexagonal prism is possible. Hexagonal prisms connect the sodalite-cages, surrounding the supercages.

For the synthetic FAU samples 5 sites have been located numbered with Roman numerals I to III', according to Smith [46]. Site I is in the hexagonal prism (or double 6 ring (D_6R)) coordinated to three oxygens (O3) at either site of the prism [47]. XRD gives only an averaged site I location [28]. Site I' is found inside the cuboctahedron (also called the sodalite- or β -cage) close to the oxygen atoms of the six membered ring facing the hexagonal prism. There are 16 sites I and 32 sites I' per unit cell. Simultaneous occupation of the sites I and I' does not occur, because of repulsive forces of the cations in these positions. The general accepted equation for the cation population of site I and I' is [41a]:

$$n(\text{I}) + \frac{1}{2}m(\text{I}') \leq 16 \quad (\text{Eq. 2.3})$$

where n is the number of cations in site I and m is the number of cations in site I'. The occupation of site I and I' is related to the Si/Al ratio, as was shown by Fuchs *et al.* [29]. The number of cations in the hexagonal prism (site I) decreased with decreasing Si/Al ratio. Mortier *et al.* [40b] showed that for K^+ exchanged zeolites of different Si/Al ratio the site I occupation goes through an optimum with decreasing Si/Al ratio. Furthermore, with decreasing Si/Al ratio, one or two sites I' per unit cell are possible; site I_1' and I_2' , of which site I_2' is more drawn to the center of the sodalite cage [41a,48]. Also the size of the cation is of influence on the occupation of site I and I' (see Table 2.1). Increasing the cation radius from $K^+ \rightarrow Cs^+$ makes site I less favorable for these large cations. This is related to the large steric hindrance imposed by the cations.

Sites II and II' share the six-ring of the sodalite-cages facing the large supercage: site II' is inside the sodalite-cage, II is in the large cavity. There are 32 of sites II and II' per unit cell. Site II' is never found to be occupied by Na^+ cations; in dehydrated FAU zeolites this site is vacant, probably related to electrostatic repulsion induced by site I'; in hydrated zeolites this site is occupied by H_2O [40a]. Some occupation has been found for Rb^+ and Cs^+ cations (see Table 2.1) and this is probably related to the low energy barrier for crossing this 6-ring (approximately 10 $\text{kJ}\cdot\text{mol}^{-1}$ for Na^+ cations [26b]).

Increasing cation radius from $Na^+ \rightarrow Cs^+$ makes the alkali cation too large to fit in the plane of the six membered oxygen ring of site II; the cation is thus displaced to a great extend into the large

45. Eulenberger, G.R.; Shoemaker, D.P.; Keil, J.G. *J. Phys. Chem.* **1967**, *71*, 1812.

46. Smith, J.V. In *Adv. Chem. Ser.-Molecular Sieve Zeolites*; Flanigen, E.M., Sand, L.B., Eds.; American Chemical Society: Washington, DC, 1971; Vol 101; pp 171-200.

47. Engelhardt, G. *Microporous Mater.* **1997**, *12*, 369.

48. Takaishi, T. *Zeolites* **1996**, *17* 389.

supercage [49], approximately 0.8Å and 1.55Å for K⁺ [50] and Rb⁺ [41c], respectively, compared to Na⁺ (0.38Å), and imposing more sterical hindrance. This results in a different potential energy surface inside the cavities which effects the sorption properties [50].

For zeolites with Si/Al ratio of 1, site III is on the edge of the four-membered rings inside the supercage [29,40a,48] and are coordinated to supercage oxygens number 4 (O4 (see Fig. 2.4)). Crystallographic data has revealed that all cations in site III are moderately shifted to positions called site III' (three of such sites were detected called III₁', III₂', and III₃' [48]), because of the lower symmetry of the framework. This is caused by the usually higher Si/Al ratio in the zeolite samples. Sites III and III' are only to be occupied for FAU samples with a very low Si/Al ratio. Decreasing the Si/Al ratio, increases the number of possible site III and III' positions [40b], which is reported to be 48 and 96 respectively, for X with Si/Al ratio 1.09 (due to crowding, all 96 sites may not be available). Calculations have shown a low binding energy for cations in this site (approximately 40 kJ.mol⁻¹ less than for cations in site II), which decreases with increasing Si/Al ratio (reducing the Al centers in the four-membered ring from 2 to 1 reduces the binding energy of sodium with 16 kJ.mol⁻¹ [26,29]). Because of the local geometry of the framework, a cation in site III has a lower number of nearest-neighbor oxygen centers and thus is coordinatively less saturated than cations in site II. This results in a lower binding energy for cations in site III. Thus it is evident that sites III and III' become less occupied with increasing Si/Al ratios as was found experimentally with Y zeolites compared to X zeolites [40a].

Fig. 2.4 shows also the location of the oxygen atoms in the framework of FAU, which are numbered 1 to 4. XPS can not be used to differentiate between oxygens with different electron densities, however, theoretical calculations have shown that these framework oxygen atoms all are of different electronegativity [27,28]. Supercage oxygens number 1 (O1) and 4 (O4) are the most basic, whereas oxygen number 2 (O2) is the least basic. O1 and O4 are also the most softest oxygens, i.e. the most easiest to polarize. As adsorption of molecules and catalytic reactions occur almost exclusively in the supercages, the basicity of faujasite-type zeolites is determined by these oxygens.

For Na-X, Na⁺ cations were found in site I, I', II and III' (see Table 2.1) [41a]. For Na-Y no cations are found in site III or III' [40a]. Table 2.1 also compiles the concentration of cations per site per unit cell for K⁺, Rb⁺ and Cs⁺ exchanged faujasites, as found in literature. Note, however, that in most cases the Si/Al ratio is lower than the zeolites used in this study. From Table 2.1 it may also be concluded that exchange of Na⁺ in site I and I' for Rb⁺ or Cs⁺ cations of faujasite is only partially possible. This is related to the large cation radius and the large solvation complexes in water during the ion exchange [41d,51]. 100% exchange has only been reported using solid state ion exchange [52].

49. Huber, S.; Knözinger, H. *Appl. Catal. A: General* **1999**, *189*, 239.

50. Lachet, V.; Buttefey, S.; Boutin, A.; Fuchs, A.H. *Phys. Chem. Chem. Phys.* **2001**, *3*, 80.

51. a) Sherry, H.S. In *Ion Exchange - A Series of Advances*; Marinsky, J.A., Ed.; Marcel Dekker, Inc.: New York, 1969; Vol. 2, pp 89-133; b) Sherry, H.S. In *Adv. Chem. Ser.-Molecular Sieve Zeolites*; Flanigen, E.M., Sand, L.B., Eds.; American Chemical Society: Washington, DC, 1971; Vol 101; pp 350-379.

52. Weitkamp, J.; Ernst, S.; Hunger, M.; Röser, T.; Huber, S.; Schubert, U.A.; Thomasson, P.; Knözinger, H. In *Proceedings of the 11th International Congress on Catalysis-40th Anniversary, Baltimore*; Hightower, J.W., Delgass, W.N., Iglezi, E., and Bell, A.T., Eds.; Elsevier: Amsterdam, 1996; Vol. 101, pp 731-740.

Zeolite Mordenite (MOR)

“Large pore” mordenite is a one dimensional zeolite consisting of main channels (build up by a 12 membered oxygen ring (aperture 6.5 x 7.0 Å)) and side channels (two eight-membered oxygen ring windows, which indicate the beginning and the end of the side-channel). The eight-ring window at the intersection of the side channel and the main channel is a round shaped window, allowing small molecules and cations to enter (aperture $\approx 4.8 \times 3.7\text{Å}$). However, the eight-ring window, which lies at the intersection of the side channel and the inside eight-ring of the MOR, is very distorted, resulting in an ellipsoidal shaped ring with the smallest ring-width of around 1.3 Å and therefore allowing only small molecules like H₂ to diffuse through [53].

Single crystal refinement of dehydrated Na-MOR10 (Si/Al = 5) has revealed 5 different sites for cation location [54] (see Figure 2.5). Three coordination sites are located in the side channel, namely site II, III and IV. Site II is located in the window of the side channel and the inside 8-ring. Site III is located on the surface of the side channel midway between the periphery of two 8-rings which girdle the side pocket and is only occupied by divalent cations and site IV is situated in the intersection between the side channel and the main channel. Site I and site I' (total displacement of 0.53Å, perhaps of repulsive forces between adjacent cations) are situated in the 8-ring between two side channels and are only occupied by cations with a radius

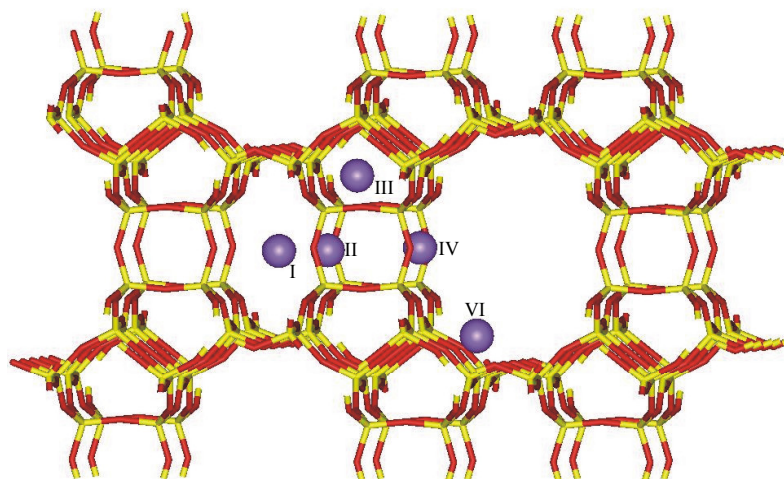


Figure 2.5: Framework structure of mordenite, with cation sites shown (see text for details about locations). The cation locations and site names are the same as given by Ref. [54] and cited references therein (sites I and I' are designated by site I). Mordenite framework has been drawn, using the InsightII Program, courtesy of MSI.

smaller than 1.3Å, like Na⁺ and Ca²⁺ cations [54]. Site VI is situated above the side channel in the main channel. Because the sites I and II are only 2.65Å apart, simultaneous occupancy of I and of II is unlikely. Also sites IV and VI are close enough (3.5Å) to inhibit simultaneous occupancy, while repulsive interaction between sites II and IV displaces cations of site IV to locations further inside the main channel. Na⁺ cations in Na-MOR10 have been found in site I and I', IV and VI; site occupation 3.1 (I/I'), 2.6 (IV) and 1.5 (VI) respectively (see Table 2.1).

53. a) Kustov, L.M.; Kazansky, V.B. *J. Chem. Soc., Faraday Trans.* **1991**, 87, 2675; b) Bordiga, S.; Garrone, E.; Lamberti, A.; Zecchina, A.; Otera Arean, C.; Kazansky, V.B.; Kustov, L.M. *J. Chem. Soc., Faraday Trans.* **1994**, 90, 3367.

54. Schlenker, J.L.; Pluth, J.J.; Smith, J.V. *Mat. Res. Bull.* **1979**, 14, 751.

As to our knowledge, no crystallographic data is available on the cation positions in Na-MOR20 (Si/Al = 10). However, we propose that site VI in the main channel is much less occupied (or empty) in Na-MOR20 compared to Na-MOR10, based on the following. By comparing articles concerning FAU structures with different Si/Al ratios, it is evident that sites located at the wall (site III) become less occupied with increasing Si/Al ratios. This is caused by the fact that these sites at the wall have a much lower coordination number and thus also a much smaller binding energy [26,29,55]. A similar situation arises for site VI in MOR zeolites with increasing Si/Al ratios. While in site I and IV the cations are surrounded by basic oxygens in a near planar coordination (site I) or one-sided coordination (site IV), the cations in site VI are poorly coordinated. Furthermore, gravimetric adsorption studies of *n*-alkanes on acidic H-MOR20 have shown that only one third of the present acid sites is situated in the main channel [56]. In line with the above mentioned discussion we expect the Na⁺ cations to be located only in site I and IV. Each unit cell of Na-MOR20 contains theoretically a maximum of 5 Na⁺ cations (from the general zeolite composition for MOR, (Me²⁺Me⁺)_{n/2}Si_{48-n}Al_nO₉₆.mH₂O [57], and the Si/Al ratio (Si/Al = 10) it is possible to determine the theoretical Na⁺ content), this accounts for approximately 3.3 and 1.7 cations, in site I (and I') and IV, respectively.

Zeolite MFI

Single crystal X-ray refinement has also been used to study the framework of MFI (ZSM5) [58,59,60]. “Medium pore” MFI has an effective three-dimensional channel defined by 10-membered ring openings (see Figure 2.6). Straight channels parallel to [010] have openings defined by 10-membered rings of size 5.4 x 5.6Å. Intersecting this channel at right angles is a sinusoidal channel along [100] with 10-membered ring openings of 5.1 x 5.5Å. The straight channels are connected to other straight channels by these sinusoidal channels. The framework pore walls of the sinusoidal channel are made of five rings with at the bottom a four ring and at the top a six ring

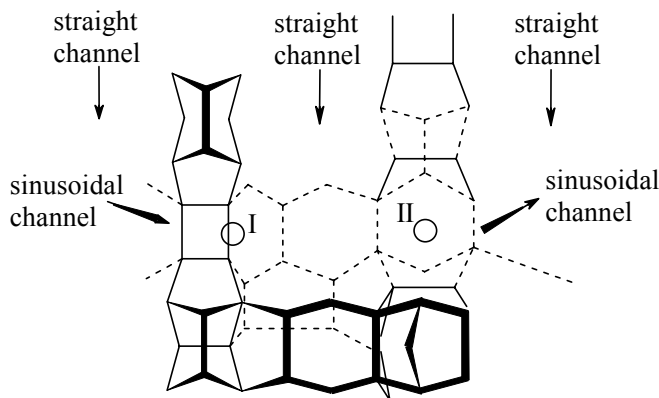


Figure 2.6: View of the [100] plane of MFI (ZSM5) with cation sites I and site II (see text for details). Drawing has been taken from Ref. [61].

55. Simon, U.; Flesch, U. *J. Porous Mater.* **1999**, *6*, 33.

56. Eder, F.; Stockenhuber, M.; Lercher, J.A. *Stud. Surf. Sci. Catal.* **1995**, *97*, 495.

57. Baerlocher, Ch.; Meier, W.M.; Olson, D.H., *Atlas of Zeolite Framework Types*, 5th Edition; Elsevier: Amsterdam, 2001.

58. Olson, D.H.; Kokotailo, G.T.; Lawton, S.L.; Meier, W.M. *J. Phys. Chem.* **1981** *85*, 2238.

59. Lermer, H.; Draeger, M.; Steffen, J.; Unger, K.K. *Zeolites* **1985**, *5*, 131.

60. a) Van Koningsveld, H.; Van Bekkum, H.; Jansen, J.C. *Acta Cryst.* **1987**, *B43*, 127; b) Van Koningsveld, H.; Jansen, J.C.; Van Bekkum, H. *Zeolites* **1990**, *10*, 235.

[60b,61]. Diffusion in the [001] direction can readily take place between the overlapping channels parallel to [100] and [010].

Although for MOR and FAU zeolites all alkali cation locations are well documented, little is known about the location of the alkali cations in MFI zeolites from single crystal refinement and powder XRD studies. This is related to the small amount of cations in MFI crystals, which makes them difficult to detect by powder diffraction [61]. Therefore, most studies make use of i.r. spectroscopy and probe molecules [53]. I.r. studies of H₂ and CO adsorption on Na-MFI [53] and X-ray crystal structure refinement of Cs-MFI [40c], indicate that the cations are preferentially located at the intersections of the sinusoidal and straight channels [40c] at the edge of a 4-membered ring (just inside the sinusoidal channel in the 10-membered ring window). This site is called site I and is shown schematically in Figure 2.6. X-ray crystal structure refinement of the as-synthesized ZSM5 sample has shown that the tetrapropyl-ammonium cation (TPA) [60a,62], which is used as the template molecule during MFI synthesis, is also located at the intersection. Additionally, small cations, like Li⁺ [63], Na⁺ [64] and Ba²⁺ [65] and Ni²⁺ [66] are also found in small cavities above the sinusoidal channel (site II), where they are shielded by the framework oxygens. MAS-NMR studies of Na-MFI showed a very small occupancy of this location (10%) [64]. That this position is not observed for dehydrated Cs⁺ using XRD, is probably related to the large Pauling's crystal radius of the Cs⁺ cation compared to Li⁺ ($r(\text{Cs}^+)$: 1.67Å and $r(\text{Li}^+)$: 0.68Å) as suggested by Katoh *et al.* [63]. As to our knowledge no crystallographic data has yet been published about the locations of the other cations used in this thesis.

Silicalite-1 is isostructural to ZSM5 zeolite with its silica content approaching 100% (it is the Al free member of the MFI series). Silicalite-1 exhibits shape selectivity behaviour (similar to MFI) and has little or no catalytic activity at higher temperatures. It is highly hydrophobic and hence it adsorbs organic molecules over water.

2.3 SORPTION EFFECT

Numerous studies have been performed to determine the effects of adsorbates during catalysis and sorption on zeolite structures, e.g., changes in geometry of the zeolite framework, extra framework cation shifts, interactions of sorbates with extra framework cations and zeolite framework oxygens etc. This paragraph will mainly describe results obtained for sorption of water, ammonia, benzene etc., in alkali metal and earth-alkali metal cation exchanged zeolites. Since multivalent cation exchanged zeolites are of more interest for sorption and catalysis, adsorbate adsorption is more often described [43,67,68].

61. Huddersman, K.D.; Rees, L.V.C. *Zeolites* **1991**, *11*, 270.

62. Chao, K.-J.; Lin, J.-C.; Wang, Y.; Lee, G.H. *Zeolites* **1986**, *6*, 35.

63. Katoh, M.; Yamazaki, T.; Ozawa, S. *Bull. Chem. Soc. Jpn* **1994**, *67*, 1246.

64. Ohgushi, T.; Niwa, T.; Arakia, H.; Ichino, S. *Microporous Mater.* **1997**, *8*, 231.

65. Esemann, H.; Förster, H.; Geidela, E.; Krause, K. *Microporous Mater.* **1996**, *6*, 321.

66. Liu, Z.; Zhang, W.; Yin, Q.; Lü, G. *Stud. Surf. Sc. Catal.* **1986**, *28*, 415.

67. Zhen, S.; Seff, K. *Microporous Mesoporous Mater.* **2000**, *39*, 1.

Water adsorption on zeolites has been shown to have a large impact on the cation concentration and site location in zeolites, implying a large cation-sorbate interaction energy. During water adsorption in Na-Y migration of Na⁺ cations from sites I, I' and II to positions in the supercage (probably close to site III; note that this site is unoccupied in dehydrated Y zeolites) has been reported to occur [40a]. However, the precise locations of these cation-water complexes could not be verified by XRD, because of their too low average occupancy to be detected. Similar results have been reported for hydrated K-Y [69] and hydrated Na⁺-, K⁺-, Rb⁺- and Cs⁺ exchanged X zeolites [41d,70]. Even at 723K in the presence of water, site I' was preferred over site I, while in the absence site I is the preferred site.

Cation movement upon ammonia sorption has also been reported for Ca-Y and X zeolites [42,71]. However, important differences were noted. Whereas NH₃ sorption on Ca-Y moves the cations from site I and site I' to the supercage [42], on Ca-X only small changes for Ca²⁺ cations in site II have been reported [71]. No effect on Ca²⁺-ions in site I was observed [71]. Excess ammonia molecules in Ca-X tend to form hydrogen bonds with adsorbed molecules and the lattice oxygens, rather than to penetrate the sodalite cage. This is probably related to the high basicity of the zeolite framework.

Similar results were obtained for benzene, which adsorbs in the 12-membered ring windows between the supercages without any cation interaction [72]. Benzene sorption on K⁺ cations in K-Y had no effect on the cation location and site concentration [43b]. In the case of Ca-Y, Ca²⁺ cations of site I' were found to have moved to more favorable positions inside the supercage [42], indicating a much higher Ca²⁺-benzene, i.e., cation- π [73], interaction energy than for K⁺-benzene, which could be related to the higher electrostatic potential of the Ca²⁺ cations. Note that since the benzene molecule has a kinetic diameter of 5.85Å [4a], it can not penetrate the sodalite cage (window: 2.4Å) and thus the interaction is of a long range order (> 4.73Å) [29]. Benzene adsorption on Ca-X shows no interaction of benzene with the cations in site I, only with cations in site II [72]. Benzene interacts only with 22 of the 30 Ca²⁺ cations of site II, which are displaced (0.55Å) into the supercage towards benzene.

2.4 CONCLUDING REMARKS

It has been shown that different Si/Al ratios, alkali metal cations and zeolite topology influences the basicity of the zeolite oxygens and the location of the cation. Overall one can conclude that the basicity of the zeolites increases with increasing framework aluminum contents and decreasing electrostatic potential of the counterion. The average basicity of the different zeolite samples can be calculated using Eq. 2.1 and Eq. 2.2 and can be used for comparing the different zeolite samples.

Furthermore, it was shown that the strength of interaction between sorbent and sorbate (cation

68. a) Jang, S.B.; Jeong, M.S.; Kim, Y.; Han, Y.W.; Seff, K. *Microporous Mesoporous Mater.* **1998**, *23*, 33; b) Bae, M.N.; Kim, Y.; Seff, K. *Microporous Mesoporous Mater.* **1998**, *26*, 101 c) Kim, M.J.; Jeong, M.S.; Kim, Y.; Seff, K. *Microporous Mesoporous Mater.* **1999**, *30*, 233.

69. Mortier, W.J.; Bosmans, H.J.; Uytterhoeven, J.B. *J. Phys. Chem.* **1971**, *75*, 3327.

70. Olson, D.H. *J. Phys. Chem.* **1970**, *74*, 2758.

71. Jang, S.B.; Jeong, M.I.; Kim, Y.; Song, S.H.; Seff, K. *Microporous Mesoporous Mater.* **1999**, *28*, 173.

72. Yeom, Y.H.; Kim, A.K.; Kim, Y.; Song, S.H.; Seff, K. *J. Phys. Chem.* **1998**, *102*, 6071.

and/or zeolite oxygens) changes with Si/Al ratio and extra framework metal cation. This is related to changes in the potential energy surface (PES) of the zeolite and has implications for characterization, sorption and catalysis. The formation of the metal-sorbate complexes changes the location of the bare cations, by moving them further away from the zeolite framework. Additionally, temperature treatments also can change cation locations. Therefore, one has to be careful with extrapolating data of dehydrated zeolites to zeolites loaded with adsorbate, since cation movement can be expected.

73. a) Dougherty, D.A. *Science* **1996**, *271*, 163; b) Ma, J.C.; Dougherty, D.A. *Chem. Rev.* **1997**, *97*, 1303.

Chapter 3

Experimental

Abstract:

In this chapter the general experimental procedure is described; i.e., the setups of the infrared spectroscopic experiments, the temperature programmed desorption experiments, the thermogravimetric experiments, and the catalyst testing experiments as well as the information that can be deduced from them. The experimental sections of following chapters will only contain information that is either specific for the experiments or deviate from the general procedure. Also the used materials, their preparation and characterization are described here.

3.1 CATALYSTS PREPARATION AND REACTANTS

Catalysts preparation

In the previous two chapters X and Y zeolites of the FAU framework topology were denoted by their capitals X or Y. We have chosen in the next chapters the following abbreviations in order to stress the similarity in framework, but to emphasize the difference in Si/Al ratio and thus the cation concentration and location in the two zeolites. For X type zeolites was chosen: FAU(X); for Y type zeolites: FAU(Y).

Alkali cation (Na^+ , K^+ , Rb^+ and Cs^+) exchanged FAU(X) zeolites (silicon/aluminum ratio of 1.3) were prepared from a commercial Na-FAU(X) zeolite (Fluka; Lotnr. 69856) by exchanging with 0.025 M aqueous solutions of sodium, rubidium and cesium acetate and potassium oxalate (obtained from Merck) at 353 K (solid/liquid ratio = 15 g.l^{-1}), as described in a previous paper [1]. For a detailed characterization see Palomares *et al.* [1]. A special prepared Cs-FAU(X) sample was used, denoted Cs-FAU(X2); main difference with Cs-FAU(X) is the extra framework cation content (Na^+ and Cs^+). Preparation was according to above mentioned procedure and followed by extensive washing. Figure 3.1 shows a Scanning Electron Micrograph (SEM) of the parent Na-FAU(X) zeolite (commercial Fluka).

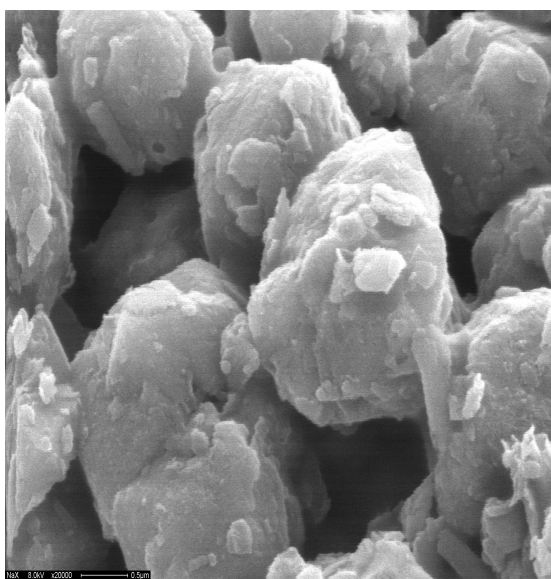


Figure 3.1: SEM image (magnification 20,000x) of the parent Na-FAU(X) (commercial Fluka; Lotnr. 69856), showing agglomerates of 1.4-1.5 μm .

MFI (ZSM5) with a Si/Al ratio of 36 was kindly supplied by Dr. M. Derewinski of the *Polish Academy of Sciences* (Krakow, Poland). The parent MFI zeolite was synthesized according to a Mobil patent [2] and subsequently exchanged with 0.1 M alkali nitrate solutions (Li^+ , Na^+ , K^+ and Cs^+) at 368 K for 12 hours [3]. Mordenite samples in the Na-form, with a Si/Al ratio of 4.9 and 10.1 (Na-MOR10 and Na-MOR20, respectively) were obtained from the Japanese Catalysis Society. Detailed analysis and characterization of both molecular sieves are reported by Kogelbauer *et al.* [4] and Sawa *et al.* [5].

Na-FAU(Y) (Si/Al ratio of 2.8) was obtained from Degussa (Lotnr. 36BB14). Samples were activated *in situ* prior to adsorption / reaction either in vacuum or in excess helium (He) flow (Praxair 5.0). The use of different materials with different characteristics demanded also different activation procedures (mainly depending on the removal of adsorbed CO_2 , which is more difficult in alkali cation exchanged FAU(X) compared to MFI zeolites), after which the sample was cooled down to the desired measurement

1. Palomares, A.E.; Eder-Mirth, G.; Lercher, J.A. *J. Catal.* **1997**, *168*, 442.
2. Argauer, R.G.; Landolt, R.G. *U.S. Pat.* 3.702.886, 1972, assigned to Mobil Oil Corporation.
3. Derewinski, M.; Haber, J.; Ptaszynski, J.; Lercher, J.A.; Rumlplmayer, G. *Stud. Surf. Sci. Catal.* **1986**, *28*, 957.
4. Kogelbauer, A.; Gründling, C.; Lercher, J.A. *J. Phys. Chem.* **1996**, *100*, 1852.
5. Sawa, M.; Niwa, M.; Murakami, Y. *Zeolites* **1990**, *10*, 532.

temperature (see Table 3.1 for the activation procedures).

In Table 3.1 the chemical composition of the exchanged zeolites determined by X-ray fluorescence (on a Philips PW 1480) are compiled together with the BET specific surface area of the samples (BET measurements were performed on a Micromeritics ASAP 2400). The Si/Al values indicate that the samples lose some silica during ion-exchange, compared to the parent materials. From the Chemical Composition and the general zeolite composition, e.g., $(\text{Me}^{2+}\text{Me}^+)_{n/2}\text{Si}_{192-n}\text{Al}_n\text{O}_{384}\cdot m\text{H}_2\text{O}$ for FAU [6], it was possible to determine the theoretical unit cell composition. This allowed us to calculate the average negative charge on the framework oxygens as a measure of the average framework basicity using Equations 2.1 and 2.2 shown in Chapter 2 (see Table 3.1).

From the BET surface area analysis (see Table 3.1) it is clear that by exchanging the Na^+ cations present in the parent FAU(X) zeolite with larger alkali metal cations, as K^+ or Rb^+ etc., the pore size dramatically drops with increasing cation radius. When exchanging Na^+ for Cs^+ a reduction of approximately 33% is apparent. This is to be expected as a consequence of the larger cation radius of Cs^+ ($r(\text{Cs}^+)$: 1.67Å) compared to Na^+ ($r(\text{Na}^+)$: 0.98Å) and is in agreement with Yagi *et al.* [7] who reported a decrease of approximately 27%.

The theoretical unit cell composition of Cs-FAU(X2) as calculated from the XRF results was $\text{Na}_{33.9}\text{Cs}_{38.1}\text{Si}_{105.2}\text{Al}_{86.8}\text{O}_{384}$. It can be seen from the unit cell configuration that not all framework oxygen centers (assigned by the number of present Al centers) are balanced by extra framework alkali cations (approximately 17%); the difference could be 14.8 protons per supercage in Cs-FAU(X2). 14.8 protons resemble $0.86 \text{ mmol}\cdot\text{g}^{-1}$ Brönsted acid sites. It was shown by Engelhardt *et al.* [8] that washing K-FAU(X) zeolites with water introduced some acidity into the catalysts. However, i.r. spectra of the activated catalyst and after pyridine adsorption revealed no Brönsted acid sites, while NH_3 t.p.d. revealed only a small number of weakly acidic sites ($0.013 \text{ mmol acid sites}\cdot\text{g}^{-1}$), which were attributed to the residual Na^+ cations. CO_2 t.p.d. experiments (see Fig. 3.2) showed a slightly higher CO_2 desorption temperature with Cs-FAU(X2) compared to Cs-FAU(X) indicating slightly higher sample basicity, compared to Cs-FAU(X). Also a larger desorbing CO_2 concentration from Cs-FAU(X2) compared to Cs-FAU(X) was observed. This is most likely due to the effect of the smaller concentration of Cs^+ cations in Cs-FAU(X2).

CO_2 adsorption monitored by i.r. spectroscopy revealed that this higher basicity can not be attributed to occluded alkali oxide clusters, since these are not present; CO_2 adsorption on occluded alkali

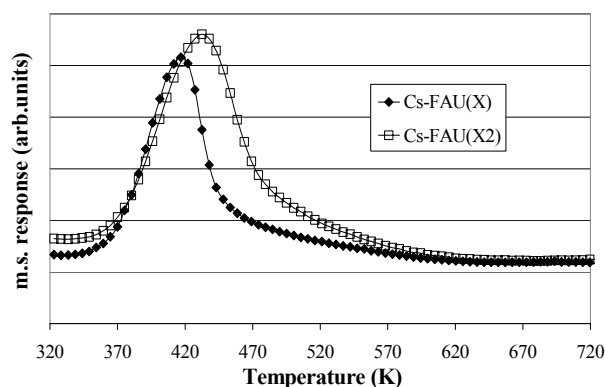


Figure 3.2: T.p.d. of CO_2 adsorbed on Cs-FAU(X) and Cs-FAU(X2).

6. Baerlocher, Ch.; Meier, W.M.; Olson, D.H., *Atlas of Zeolite Framework Types*, 5th Edition; Elsevier: Amsterdam, 2001.
7. Yagi, F.; Kanuka, N.; Tsuji, H.; Kita, H.; Hattori, H. *Stud. Surf. Sci. Catal.* **1994**, *90*, 349.
8. Engelhardt, J.; Szanyi, J.; Valyon, J., *J. Catal.* **1987**, *107*, 296.

TABLE 3.1: Compilation of zeolites, their activation procedures (*in situ* prior to all treatments) Chemical Composition, BET specific surface area, calculated unit cell composition, calculated average charge on the oxygen of the lattice ($-\delta_0$ (using Eq. 2.1 and 2.2)) and the electrostatic potential of the exchanged cation (e/r).

Zeolites	Chemical Composition (mol%)							BET				
	SiO ₂	Al ₂ O ₃	Li ₂ O	Na ₂ O	K ₂ O	Rb ₂ O	Cs ₂ O	Si/Al	(m ² /g)	Unit cell composition	$-\delta_0$	e/r (Å ⁻¹)
MFI (ZSM5)												
Activation procedure: 10 K.min ⁻¹ to 773K, 1 hr												
Li-MFI	97.3	1.4	1.1	0.1				35.7	321	H _{0.29} Li _{2.14} Na _{0.19} Al _{2.62} Si _{93.49} O ₁₉₂	0.161	1.67
Na-MFI	97	1.4		1.1				34.6	307	H _{0.60} Na _{2.10} Al _{2.70} Si _{93.47} O ₁₉₂	0.162	1.05
K-MFI	97.4	1.3		0.1	1.2			36.9	312	H _{0.10} K _{2.24} Na _{0.19} Al _{2.53} Si _{93.47} O ₁₉₂	0.164	0.75
Cs-MFI	97.3	1.3		0.1		1.2		36.5	306	H _{0.08} Cs _{2.28} Na _{0.20} Al _{2.56} Si _{93.44} O ₁₉₂	0.168	0.59
MORdenite												
Activation procedure: 10 K.min ⁻¹ to 773K, 1 hr												
Na-MOR20	90	4.9		5.1				9.2	n.d.	Na _{4.34} Al _{4.34} Si _{143.66} O ₉₆	0.192	1.05
Na-MOR10	82.3	9.1		8.6				4.5	n.d.	Na _{8.14} Al _{8.14} Si _{139.86} O ₉₆	0.224	1.05
FAUjasite												
Activation procedure: 10 K.min ⁻¹ to 773K, 2 hrs												
Na-FAU(Y)	73.2	13.3		13.5				2.8	641	Na _{50.5} Al _{50.5} Si _{141.5} O ₃₈₄	0.274	1.05
Na-FAU(X)	56.2	21.9		21.9				1.28	591	Na _{84.1} Al _{84.1} Si _{107.9} O ₃₈₄	0.317	1.05
K-FAU(X)	51.4	21.7		8.6	18.2			1.18	472	K _{73.7} Na _{34.8} Al _{87.9} Si _{104.1} O ₃₈₄	0.362	0.75
Rb-FAU(X)	54.6	21.6		9.3		14.5		1.26	428	Rb _{56.9} Na _{36.5} Al _{84.8} Si _{107.2} O ₃₈₄	0.378	0.67
Cs-FAU(X)	52.4	20.9		10.0			16.7	1.25	394	Cs _{68.1} Na _{40.8} Al _{85.2} Si _{106.8} O ₃₈₄	0.384	0.59
Cs-FAU(X2)	60	24		9		11		1.25	394	Cs _{38.1} Na _{33.9} Si _{105.2} Al _{86.8} O ₃₈₄	0.33	0.59

oxide clusters yields carbonate species, which show i.r. signals around 1570 and 1380 cm^{-1} (carbonate bands assigned to zeolite framework oxygen centers next to alkali metal cations show i.r. signals around 1650, 1380 and 1330 cm^{-1}) [9,10].

Above results for Cs-FAU(X2) could be explained as follows: most likely during the exchange and extensive washing procedure weak Brønsted acid sites have been introduced in the sample, which during calcinations have dehydrolysed the sample, yielding extra framework alumina, as shown by Kim *et al.* [11]. The XRD diffractograms of Cs-FAU(X) and Cs-FAU(X2) were found similar within the experimental limits of the XRD spectrometer. No peak broadening or lower intensities of peaks were observed for Cs-FAU(X2) compared to Cs-FAU(X), which could indicate framework collapse. Both samples showed an increased background, indicating amorphous material.

Silica (ref. F5, Lotnr. 71646) and γ -alumina (ref. 000-1.5E) were obtained from *AKZO Chemicals*, (The Netherlands). Silicalite-1 (microporous crystalline silica with a channel structure similar to that of MFI zeolite) was obtained from the *Technical University of Eindhoven, Department for Inorganic Chemistry and Catalysis*. Prior to reaction these materials were activated *in situ* in a He flow by increasing the temperature by 10 $\text{K}\cdot\text{min}^{-1}$ to 773 K for 1 hr. Subsequently the sample was cooled down to the desired reaction temperature. These materials are used in Chapter 6.

In Chapter 7 comparison was made with cesium solid state ion exchanged zeolite FAU(Y) and hydrotalcite. Cesium solid state ion exchanged zeolite FAU(Y) was obtained from Prof. Dr. H.G. Karge of the *Fritz Haber Institut der Max Planck Gesellschaft* (Berlin, Germany). The Si/Al ratio of the zeolite was 2.6 and 100% of Cs^+ exchange was reached. Hydrotalcites with Al/(Al+Mg) ratios of 0.33 and 0.2 and MgO with a specific surface area of 200 m^2/g were obtained from Prof. A. Corma of the *Instituto de Tecnologia Quimica* of Valencia (Spain).

Reactants

Methanol (p.a.), paraformaldehyde, formic acid (99% purity) and toluene (p.a.) were obtained from Merck. Paraformaldehyde has sufficient formaldehyde (CH_2O) vapour pressure at 293 K (1.93 mbar) [12]. Dimethyl ether, an O_2 / He mixture (20% O_2) and an O_2 / Ar mixture (20% O_2) were obtained from Praxair. Methanol-OD was obtained from Janssen Chimica. Carbon dioxide and ammonia for sample basicity and acidity analysis, respectively, were obtained from Hoekloos and Praxair, respectively. All reactants were used without further purification. Ethylbenzene (Merck), styrene (Merck) and xylene isomers (Fluka (*o*- and *p*-) and Aldrich (*m*-; > 99% purity)) were used for calibration of the reactor setup, i.e., determination of the respective response factors r_{f_i} . Calibration of the reactor setup was also performed with higher alkylated benzene derivatives (i.e., isopropylbenzene (cumene; Across) and 1,3,5-trimethylbenzene (mesitylene; Fluka)) and the permanent gasses H_2 and dimethyl ether (Praxair) and CO (Hoekloos).

9. Yagi, F.; Tsuji, H.; Hattori, H. *Microporous Mater.* **1997**, *9*, 237.

10. Hathaway, P.E.; Davis, M.E. *J. Catal.* **1989**, *116*, 263.

11. Kim, J.T.; Kim, M.C.; Okamoto, Y.; Imanaka, T. *J. Catal.* **1989**, *115*, 319.

12. a) Walker, J.F., *Formaldehyde*, 3rd Edition; Reinhold Publishing Corporation: New York, 1964; b) Helander, K.G. *Biotech. Histochem.* **2000**, *75*, 19.

3.2 ADSORPTION - DESORPTION STUDIES

For understanding catalytic activity and reaction mechanisms between reactants and catalyst, it is essential to identify the surface species during adsorption and reaction. Several techniques are employed to identify such surface reaction intermediates and characteristics. One of the most frequent used methods is infrared (i.r.) spectroscopy. By i.r. spectroscopy, the molecule is observed through its internal vibrational motions: any perturbation due to the zeolitic environment modifies the vibrational bands. It is easy to verify in this way whether the molecule retains its original structure or if it has been modified by interaction with the zeolite (physical or chemical adsorption processes). Generally, shifts of stretching vibration bands to higher wavenumbers indicate strengthening of bonds compared to the free molecule, while shifts to lower wavenumbers indicate weakening of these same bonds. The technique measures the wavelengths at which molecules, surface groups or adsorbed molecules, absorb light in the infrared region (2.5-16 μm or more commonly used 4000-625 cm^{-1}). Specific regions in which these surface groups absorb i.r. light can be assigned to different functional groups of a surface molecule [13,14,15,16], whereby isotopic labeling of the specific groups the characteristics significantly changes. Wavelengths at which absorption occurs correspond to stretching vibration, rotation or deformation (bending) motions of these groups, which can then be used as fingerprints of the present surface molecules, thus facilitating its characterization. For a more comprehensive understanding of i.r. spectroscopy, the interested reader is referred to Ref. [17,18]. Other *in situ* sorption techniques used here are temperature programmed desorption and thermogravimetry and will be discussed in this Paragraph. Catalytic performance testing (gas phase analysis and surface species monitored by i.r. spectroscopy) is subject of Paragraph 3.3.

Infrared (i.r.) Spectroscopy Studies

The zeolite powder was pressed into self-supporting wafers and analyzed *in situ* during all treatments (i.e., activation and sorption) by means of transmission absorption i.r. spectroscopy using a BRUKER Vector22 or a BRUKER IFS88 FT-IR spectrometer (spectral resolution set to 4 cm^{-1}). The spectra were recorded in the transmission absorption mode from 4000-1000 cm^{-1} with a time resolution of 30 s. For the activation, adsorption and desorption experiments, a stainless steel cell equipped with i.r. transparent windows which could be evacuated to pressures below 10^{-6} mbar was used [19]. The vacuum system used for the i.r. measurements is shown in Figure 3.3. In Figure 3.4 a schematic representation of the

13. Herzberg, G. *Molecular Spectra and Molecular Structure II. Infrared and Raman Spectra of Polyatomic Molecules*; D. van Nostrand Company, Inc.: Princeton, 1964.

14. Socrates, G. *Infrared Characteristic Group Frequencies*, 2nd Edition; John Wiley and Sons: Chichester, 1994.

15. Colthup, N.B.; Daly, L.H.; Wiberly, S.E. *Introduction to Infrared and Raman Spectroscopy*, 3rd Edition; Academic Press: San Diego, 1990.

16. Williams, D.H.; Fleming, I. *Spectroscopic Methods in Organic Chemistry*, 4th Edition; Mc Graw-Hill Book Company: London, 1989; pp 29-62.

17. Niemantsverdriet, J.W. *Spectroscopy in Catalysis - An Introduction*; VCH Verlagsgesellschaft mbH: Weinheim, 1995; pp 193-208.

18. Sherman Hsu, C.-P. In *Handbook of Instrumental Techniques for Analytical Chemistry*; Settle, F.A., Ed.; Prentice Hall, Inc.: New Jersey, 1997; pp 247-283.

19. Jentys, A.; Warecka, G.; Lercher, J.A. *J. Mol. Catal.* **1989**, *51*, 309.

used i.r. cell is shown. The self-supporting zeolite wafer is placed between two golden concentric cylinders (the sample holder), which could be heated to approximately 773 K by the surrounding heating wires.

Prior to adsorption experiments, the sample was activated by heating up to elevated temperatures to desorb water and CO₂ (see Table 3.1 for the activation procedures). Then the equipment was cooled down to the adsorption temperature. The activated zeolite wafer was contacted with the appropriate pressure (10^{-3} to 1 mbar) of adsorbate via a dosing valve at constant

temperature ($T = 323$ K). After adsorption - desorption equilibrium was achieved (monitored by time resolved i.r. spectroscopy), the adsorbate pressure was increased stepwise, allowing intermediate adsorption - desorption equilibrium to establish. For the coadsorption experiments, the catalyst was first equilibrated with one reactant at a partial pressure of $5 \cdot 10^{-3}$ mbar. Subsequently, the equilibrated material was exposed to $5 \cdot 10^{-3}$ mbar of the second reactant until adsorption - desorption equilibrium was reached (while keeping the partial pressure of the first reactant constant). When adsorption - desorption equilibrium was established the sample was evacuated for one hour at similar temperature. The adsorbed molecules remaining on the catalyst were removed by temperature programmed desorption (rate $10 \text{ K} \cdot \text{min}^{-1}$, up to 773 K), while analyzing the desorbing species by mass spectroscopy.

All i.r. spectra presented in this thesis are difference spectra, i.e., the spectrum of the activated zeolite is subtracted from the spectrum of the zeolite with the adsorbed molecules. In this kind of presentation all i.r. bands pointing upwards increased in intensity and all pointing downwards decreased in intensity, upon adsorption of adsorbate (compared to the activated zeolite). Analysis and deconvolution of the spectra were performed using

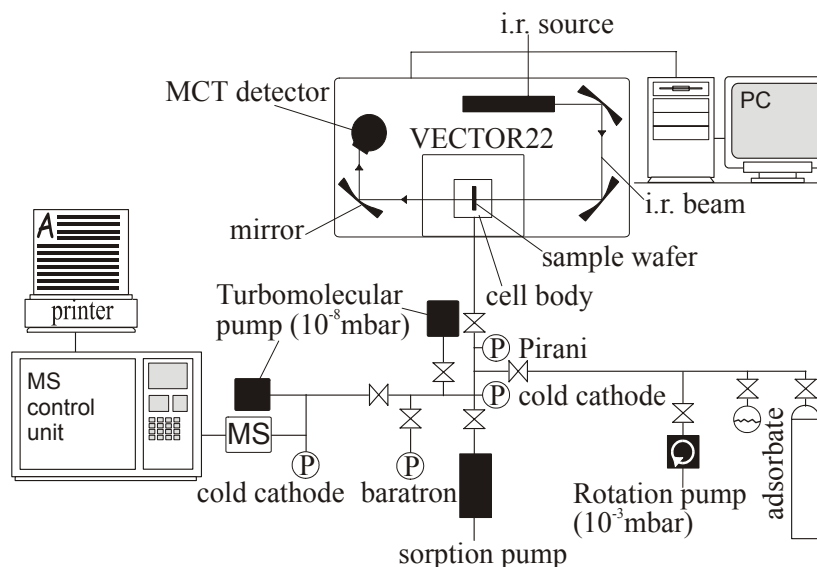


Figure 3.3: Schematic representation of the high vacuum BRUKER Vector22 i.r. system. Baratron: MKS BARATRON 628A, MS: mass spectrometer Spectramass Dataquad 100.

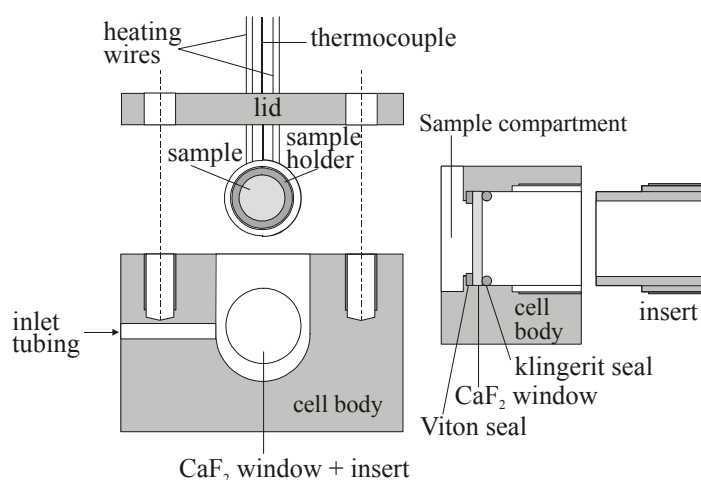


Fig. 3.4: Schematic representation of the high vacuum i.r. cell (front view (left)) and cross section of the CaF₂ window plus seals (right).

Grams/32 Spectral Notebook Software from Galactic Industries Corp. (version 4.01). The most characteristic bands observed during MeOH (Chapter 4), DME (Chapter 6), toluene (Chapter 8) etc. adsorption are attributed to hydroxy group stretching vibrations ($3700\text{--}3100\text{ cm}^{-1}$) [14], stretching vibrations of the C-H group ($3100\text{--}2840\text{ cm}^{-1}$) [14], C=C stretching vibrations ($1610\text{--}1480\text{ cm}^{-1}$) [16], O-H deformation vibrations [15] or C-O-H bending vibrations [13] ($1400\text{--}1350\text{ cm}^{-1}$) and C-H deformation vibrations of the methyl group ($1480\text{--}1450\text{ cm}^{-1}$) [13-16].

Temperature Programmed Desorption Studies (t.p.d.)

To study qualitatively the adsorption bond strength, a home made temperature programmed desorption (t.p.d.) setup connected to a UHV chamber with a mass spectrometer (BALZERS QMS 200 F) was used for the desorption experiments. Figure 3.5 shows a schematic drawing of the temperature programmed desorption setup. During a typical t.p.d. experiment, 20-30 mg of alkali metal cation exchanged zeolites was loaded in a quartz glass tube (quartz was used to avoid adsorption of gases). After activation at 10^{-3} mbar (see Table 3.1 for the used activation procedures), the activated powders were exposed to 7 mbar sorbate at 323 K. When adsorption - desorption equilibrium was reached, the sample was evacuated for several hours at 10^{-3} mbar to remove the excess and weakly held molecules. Then t.p.d. with an increment of $10\text{ K}\cdot\text{min}^{-1}$ to 973 K was started. Data collection was performed using BALZERS Quadstar 4.22 software package (version 6.02). Simple evaluation of the results was performed using Microsoft Excel.

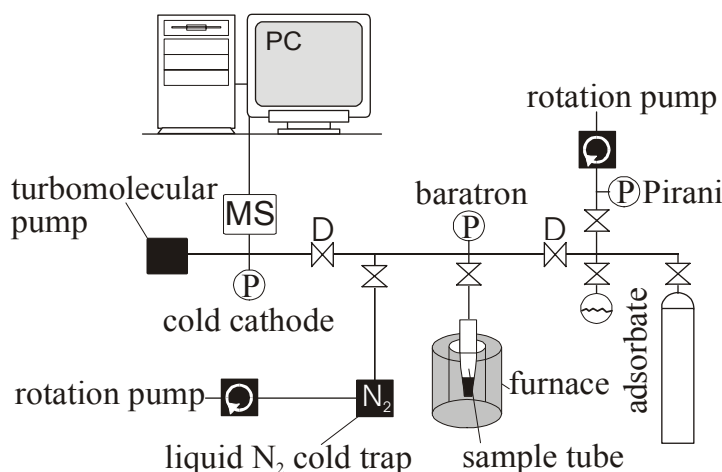


Figure 3.5: Schematic drawing of the vacuum t.p.d. setup. Lines were kept at 110°C to avoid condensation. D: dosing valve, baratron: Balzers CMR273, MS: mass spectrometer BALZERS QMS 200 F.

(see Table 3.1 for the used activation procedures), the activated powders were exposed to 7 mbar sorbate at 323 K. When adsorption - desorption equilibrium was reached, the sample was evacuated for several hours at 10^{-3} mbar to remove the excess and weakly held molecules. Then t.p.d. with an increment of $10\text{ K}\cdot\text{min}^{-1}$ to 973 K was started. Data collection was performed using BALZERS Quadstar 4.22 software package (version 6.02). Simple evaluation of the results was performed using Microsoft Excel.

Temperature programmed desorption (or temperature desorption spectroscopy (t.d.s.)) is also frequently used in surface science and catalysis; after calibration it can be used to determine surface coverages of adsorbates and to evaluate the activation energy of desorption [20,21]. Here results obtained by t.p.d. were only used to acquire information about the adsorbed amount and adsorption strength (qualitatively). For a more comprehensive description of t.p.d. experiments and analysis, the interested reader is kindly referred to Ref. [20,21].

Adsorbate t.p.d. was used to study the effect of the zeolite and exchanged cation on the adsorption and decomposition of the sorbate, especially in the case of formic acid t.p.d. (Chapter 6). More details about specific masses (m/z) followed as a function of temperature will be given in the respective Chapters.

The determination of the acid site concentrations was done by integrating the m/z 17 peaks in the

20. a) *Idem* as Ref. [17], pp 24-35; b) De Jong, A.M.; Niemantsverdriet, J.W. *Surf. Sci.* **1990**, 233, 355.
21. Falconer, J.L.; Schwarz, J.A. *Catal. Rev. - Sci. Eng.* **1983**, 25, 141.

spectra of the ammonia t.p.d. (adsorption temperature 423 K and 1 hr at adsorption - desorption equilibrium) between 450 and 925 K and comparison to a standard (H-ZSM-5-11, Union Carbide (H^+ concentration: $0.149 \text{ mmol.g}^{-1}$); NH_4 -FER, Tosoh Co. (H^+ concentration: 2.05 mmol.g^{-1})). Both samples are free of extra framework alumina and Al^{3+} induced Lewis acid sites as confirmed by ^{27}Al MAS-NMR and pyridine adsorption, respectively.

Thermogravimetric and Calorimetric Studies

To study sorption capacities of the used catalysts, a modified SETARAM TG-DSC 111 apparatus [22] was used for the thermogravimetric and calorimetric analysis (see Figure 3.6). The instrument consists of four main parts: the balance, the calorimeter, the vacuum system and a mass spectrometer. The sample compartments (crucibles) are fixed to the arms of the balance via suspension wires and are hanging without physical contact into the sensitive part of the calorimeter. The balance is an opto-electrical symmetrical microbalance with a detection limit of 10^{-6} g (the accuracy of the gravimetric measurements was $\pm 5\%$). The crucibles, the suspension wires and the inner part of the calorimeter are made out of quartz to avoid adsorption of gases. The calorimeter consists of two heat flow meters. One is used as reference element to eliminate a possible impact of thermal fluctuations and changes in the thermo conductivity of the gas phase on the heat signal.

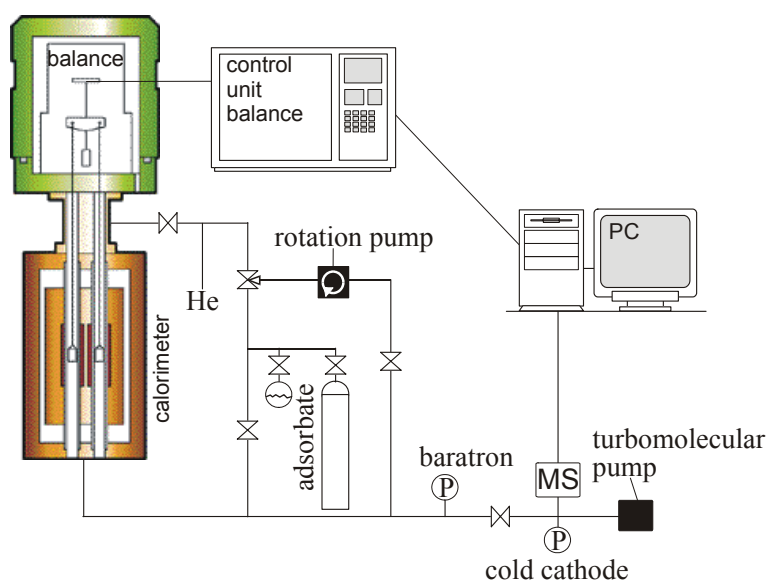


Figure 3.6: Schematic representation of the TGA vacuum system. MS: mass spectrometer BALZERS QMG 420, baratron: MKS BARATRON 122A. Balance: courtesy of SETARAM France.

The analog voltage signal of the calorimeter (μV) has to be calibrated to obtain the proper value for the heat flux (mW) inside the calorimeter. As the calibration factor S ($\mu V/mW$) changes with temperature and pressure, it has to be determined at different temperatures under the same conditions as in the sorption experiments. Calibration of the Setaram TG-DSC 111 micro calorimeter (type Tian-Calvet) using generated known thermal effects at known temperatures was described by Stockenhuber [23] and comprises two calibration methods: 1) for lower temperatures (typically $T < 400 \text{ K}$) an electrical heater gives heat pulses of known electrical power and duration (Joule effect calibration) and 2) phase transitions of different inorganic solids over the temperature range 380-1060 K (heating above transition temperatures with linear heating rates of $< 5 \text{ K.min}^{-1}$ and measuring the heat evolved). The output signal of the

The analog voltage signal of the calorimeter (μV) has to be calibrated to obtain the proper value for the heat flux (mW) inside the calorimeter. As the calibration factor S ($\mu V/mW$) changes with temperature and pressure, it has to be determined at different temperatures under the same conditions as in the sorption experiments. Calibration of the Setaram TG-DSC 111 micro calorimeter (type Tian-Calvet) using generated known thermal effects at known temperatures was described by Stockenhuber [23] and comprises two calibration methods: 1) for lower temperatures (typically $T < 400 \text{ K}$) an electrical heater gives heat pulses of known electrical power and duration (Joule effect calibration) and 2) phase transitions of different inorganic solids over the temperature range 380-1060 K (heating above transition temperatures with linear heating rates of $< 5 \text{ K.min}^{-1}$ and measuring the heat evolved). The output signal of the

22. Stockenhuber, M.; Lercher, J.A. *Microporous Mater.* **1995**, *3*, 457.

23. Stockenhuber, M., "Gravimetric and calorimetric investigations of the acidic properties of molecular sieves", PhD thesis, Technical University of Vienna, Vienna, Austria, 1994.

calorimeter (μV) could then be correlated to the known heat effect (mW) inside the calorimeter by the calibration factor S . The accuracy of the calorimetric measurements was $\pm 2 \text{ kJ}\cdot\text{mol}^{-1}$. See for more information concerning calorimetry in the study of heterogeneous catalysis also Ref. [24].

The samples were pressed to thin wafers (in the same way as for i.r. spectroscopic measurements) to avoid loss of sample when applying to vacuum and subsequently broken into small platelets. For a typical experiment, approximately 15 mg of these platelets were charged into the quartz sample holder of the balance and were activated *in situ* by heating in vacuum ($p < 10^{-6}$ mbar) according to the procedure described in Table 3.1.

Methanol adsorption studies (Chapter 4) were carried out between 10^{-3} -13 mbar equilibrium pressures at 323 K. The pressure was recorded with a BARATRON pressure transducer (type 122A). The equilibration was followed by means of weight changes, where typical equilibration times differed from 1 hour to several hours. The adsorption isotherms were determined gravimetrically.

Toluene was discontinuously dosed into the closed balance system and equilibrated with the zeolite surface at 303 K (Chapter 8); the equilibration was followed by means of heat flow and weight changes. The experiments were carried out in the pressure range from 10^{-3} to 1 mbar. The adsorption isotherms were determined gravimetrically simultaneously with the differential enthalpies of adsorption, which is defined as the heat evolved due to adsorption of a gas admitted in small quantities into a closed system at constant temperature and volume [24]. The heat flow measured after the admission of a differential amount of toluene to the sample was integrated over time, correlated to the mass uptake, and divided by the calibration factor S resulting in the differential adsorption enthalpy. Reversibility was checked through desorption of the aromatics induced by evacuation of the system at several points in one experiment. The initial heat of adsorption is used to compare the strength of the interactions between sorbed molecules and different samples as the contribution of sorbate-sorbate interactions can be neglected at zero coverage.

3.3 REACTION STUDIES

Catalytic Measurements using Infrared Spectrometry

The zeolite powder was pressed into self-supporting wafers (approximately $3\text{-}4 \text{ mg}\cdot\text{cm}^{-2}$) and analyzed *in situ* during all treatments (i.e., activation, sorption and reaction) by means of transmission absorption i.r. spectroscopy. The i.r. spectra were recorded with 4 cm^{-1} spectral resolution using a Fourier transform i.r. spectrometer (NICOLET 20SXB FT-IR) which was equipped with an MCT (HgCdTe) detector. 120 scans per spectrum were recorded. An i.r. reactor cell (CaF_2 windows) equipped with $1/16''$ gas in-and outlet tubings (located at either side of the i.r. reactor cell) and with a volume of 1.5 cm^3 , which approximates a continuously stirred tank reactor [25] was used. The cell is equipped with a heatable sample

24. a) Cardona-Martinez, N.; Dumesic, J.A. *Adv. Catal.* **1992**, *38*, 149; b) Solinas, V.; Ferino, I. *Catal. Today* **1998**, *41*, 179.

25. Mirth, G.; Eder, F.; Lercher, J.A., *J. Appl. Spectrosc.* **1994**, *48*, 194.

holder (see also Figure 3.2). The heating wires and thermocouple are coated with a thin layer of gold (40 μm) to prevent any gas phase reactions catalyzed by their presence. Gas phase analysis was performed using a BALZERS OMNISTAR GSD 300 O₂ mass spectrometer. The flow system used for the measurements is described in Figure 3.7.

Zeolite wafers, after activation (see Table 3.1) in excess flowing helium (19 ml/min;

Praxair, 5.0), were contacted with different partial pressures of reactant in helium by switching V1 at reaction temperature. Supelco OMI-2 Indicator Tube was used to dry and purify helium from water and O₂ prior to inlet. Liquid reactants were added to the dried carrier gas stream through a septum by means of a syringe pump (Cole Parmer 74900) or *via* the “reactant” inlet (when molecular O₂ or DME were used) controlled by a Brooks MFC 5850E (0-5 ml.min⁻¹). When adsorption - desorption equilibrium was achieved (monitored by time resolved i.r. spectroscopy), the temperature programmed reaction is started (5 K.min⁻¹ up to 773 K).

Catalytic Measurements

Catalytic testing [26] was carried out in a conventional plug (down) flow reactor under atmospheric pressure, and is presented in Figure 3.8. The catalyst was pelletized, crushed and sieved to obtain particles in the range of 0.3-0.6 mm. It was used as is without binder to eliminate its contribution to the catalytic performance. The catalyst particles were placed into a quartz reactor tube (with an inner diameter of 5 mm and about 50 cm long from gas inlet to outlet) and held by a fritted quartz disk at the bottom and a quartz wool plug at the top of the catalyst bed (the total amount of catalyst in each experiment was approximately 50 mg, resulting in a typical catalyst bed length of 3-5 mm). The reactor tube was placed concentrically in a vertical quartz tube of 2 cm inner diameter, on the outside of which an electric heating wire was wound (the oven): the catalyst bed was held at the isothermal zone of the oven. The oven temperature was controlled *via* a thermocouple (nickel-alumel) placed on the outside of the reactor. An additional thermocouple, placed on the top of the catalyst bed (in a quartz enclosure ($\varnothing_{\text{outer}} = 4$ mm) to avoid

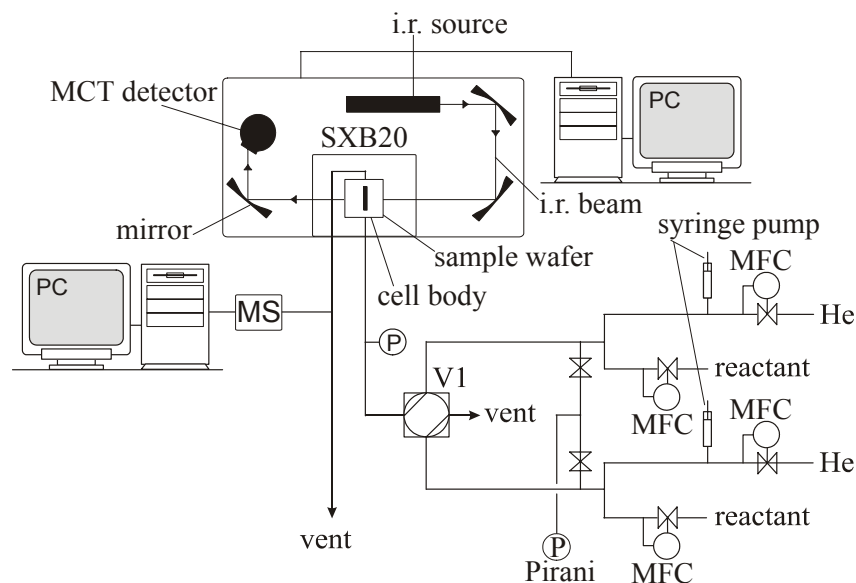


Figure 3.7: Schematic drawing of the flow cell NICOLET 20SXB IR system. All lines are kept at 80°C to avoid condensation. MS: mass spectrometer BALZERS OMNISTAR GSD 300 O₂, MFC: Brooks mass flow controller, V1: four port switching valve.

26. Dautzenberg, F.M. In *ACS Symp. Ser.-Characterization and catalyst development: An interactive approach*; Bradley, S.A., Gattuso, M.J., Eds.; American Chemical Society: Washington, DC, 1988; Vol. 411; pp 99-119.

its contribution to the catalytic activity and to minimize the empty reactor volume), was used to measure the actual temperature which was found to differ not more than 10 K at 698 K.

The catalyst was activated *in situ* in stream 1 by temperature increment of $10 \text{ K}\cdot\text{min}^{-1}$ up to 773 K and kept there for 1 to several hours in large excess of Ar flow (Praxair, 5.0). The sample was subsequently cooled down to reaction temperature. In the mean time the feed mixture (stream 2) was flowed *via* the by-pass line. After stabilization of at least 80 minutes the feed composition was analyzed *via* the GC sampling system. The reaction was started by switching V1 from pure argon flow (stream 1) to a reactant mixture (stream 2). Depending on the type of experiment, different partial pressures of methanol and/or toluene in argon were used in the range of 10-45 mbar. These were fed into the system prior to the reactor by using glass saturators that are filled with reactant and held at a constant temperature by using a Lauda RMS6 or a Grant LTD6 thermostat. Reactant flows were created by flowing Ar ($0\text{-}50 \text{ ml}\cdot\text{min}^{-1}$) as carrier gas. Different vapor pressures of methanol and toluene were set by lowering or increasing the temperatures of the saturators. Calibration of the vapor pressure (in moles) as function of the temperature was done by gas chromatograph by correlating them to known injected amounts. Accuracy of our experiments was checked

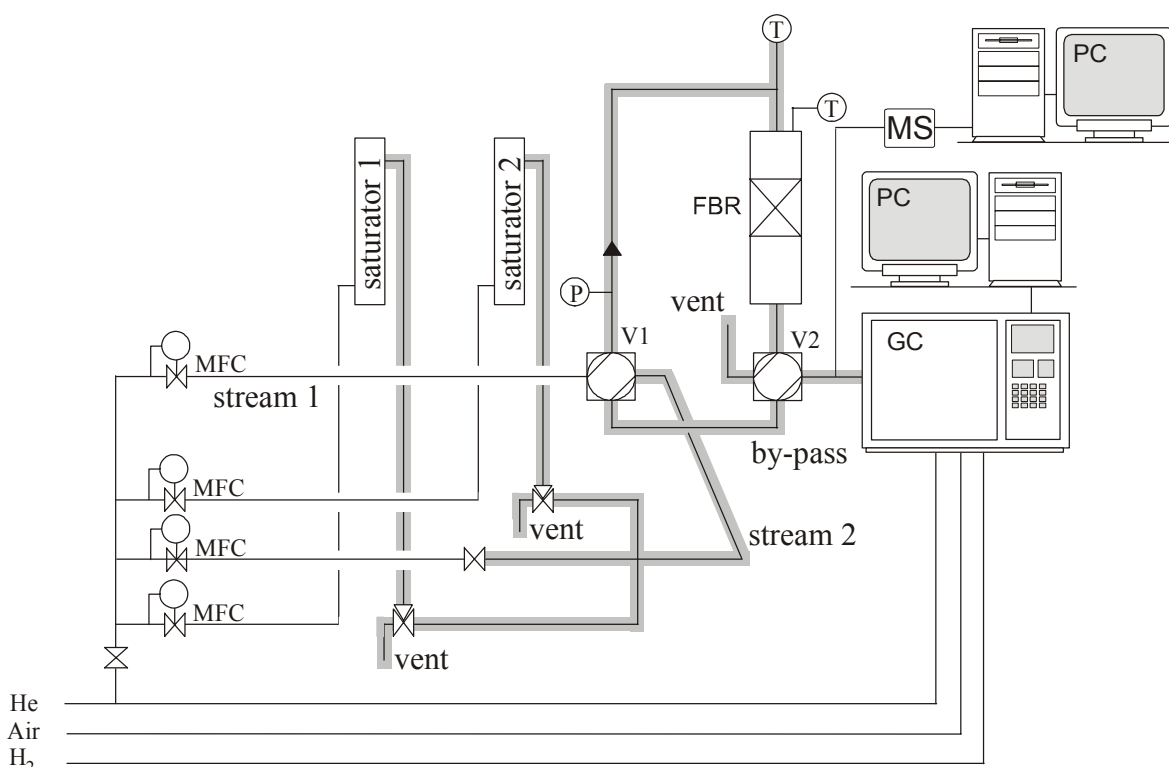


Figure 3.8: Schematic drawing of the kinetic setup used for catalytic testing. Saturators are filled with reactant and held at a constant temperature. Shaded lines were kept at 120°C to avoid condensation. FBR: fixed bed reactor, V1, V2: four port switching valves, MS: mass spectrometer BALZERS OMNISTAR GSD 300 O2, MFC: Brooks mass flow controller.

with standard tables for methanol and toluene vapor pressures as a function of temperature [27]. Different reactant flows diluted by different Ar flows (while keeping the total flow constant) then resulted in different partial pressures of the reactants. Blank experiments could be performed to check for unchanged reactant flows and partial pressures during the experiment, by using the by-pass line.

27. Weast, R.C. (Ed.) *Handbook of Chemistry and Physics*, 64th Edition; CRC Press: Cleveland, 1983; pp D217-D218.

The effluent stream was analyzed on-line by gas chromatography using a Varian 3300 gas chromatograph equipped with a 10 m packed CP-SIL 5CB (ID 0.53 mm; film thickness 5 μm) and a 25 m CP-WAX 52CB fused silica WCOT (ID 0.53 mm; film thickness 2 μm ; WCOT: wall coated open tube) column in serial for the separation of the “heavy” compounds, which were detected by FID. A packed molsieve 13X 6 ft stainless steel (ID 1/8”; 60 mesh) column is used for the separation of CO, CO₂ and H₂ which are detected by TCD. Simultaneous on-column injection and measurement is possible by using a switching valve (see Figure 3.9). Undesired pressure jumps, which were likely to be caused by switching valve V2, were avoided by providing almost identical flow rates and pressures in both gas lines (approximately 3 ml.min⁻¹). Because of the low carrier flow rate through the columns, adding of argon (make up) before the TCD was needed to ensure a proper functioning of the same TCD (total flow of 11 ml.min⁻¹ needed).

Due to the limiting properties of the setup (Ar as carrier gas, chosen GC columns, and capillary column (limited heating range)) accurate gas chromatographic measurements of H₂O, CO and CO₂ could not be done.

The program used to run the GC was configured as follows: at time t_0 the GC is started externally by Chromatography Station for Windows (DataApex version 1.7), followed after 10 seconds by the injection (switch V1). The GC then runs isothermally at 37 °C for 6 minutes, before heating starts (at time t_3). 5.7 minutes (at time t_2) after starting the GC program,

switch V2 connects the capillary columns with the FID. This means that the capillary and the molsieve columns are switched from running serial to parallel. The following temperature program was used after 6 minutes: 5 K.min⁻¹ from 37 to 190 °C. Figure 3.9 shows a schematic drawing of the here described analysis procedure. The same Chromatography Station for Windows was used to analyze the data.

Data evaluation

Evaluation of the gas composition of the effluent gas stream (conversions (X), yields (Y) and selectivities (S)) were performed as follows. Conversion of methanol (X_{MeOH}) and toluene (X_{toluene}) and yield of any product (Y_{product}) was calculated as usual and is formulated as:

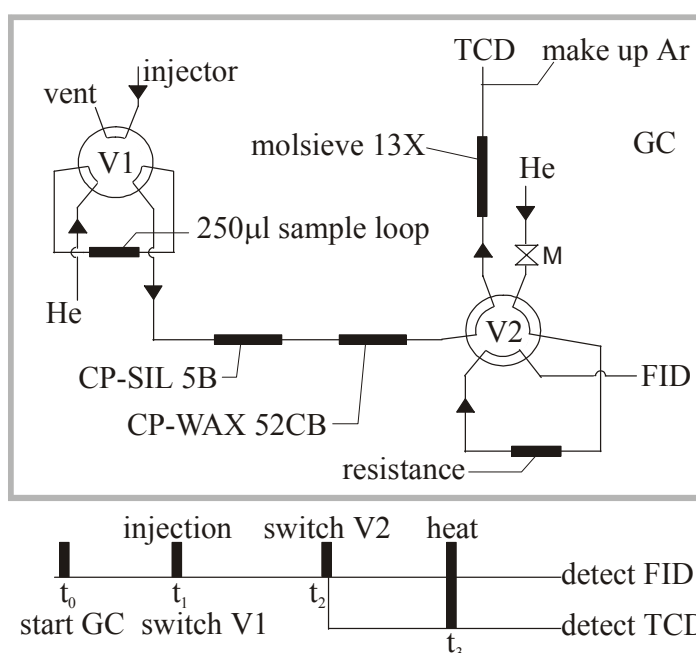


Figure 3.9: Analysis system installed in the Varian 3300 GC (top) and the time sequence (bottom). Drawing represents valve position between t_1 and t_2 . V1, V2: 6 port switching valve, TCD, FID: detector types, M: metering valve.

$$X_{MeOH} = ((N_{MeOH,in} - N_{MeOH,out}) / N_{MeOH,in}) \times 100\% \quad (\text{Eq. 3.2})$$

$$= 1 - (N_{MeOH,out} / N_{MeOH,in}) \times 100\% \quad (\text{Eq. 3.2b})$$

$$Y_{product} = N_{product} / N_{MeOH,in} \times 100\% \quad (\text{Eq. 3.3})$$

where N_i is calculated from the GC response signal (area of the FID or TCD peak) using the response factors for individual components (i) and converted into mols.

Selectivity (S_i) was calculated from yield and conversion according to the conventions [26]:

$$S_{product} = Y_{product} / X_{MeOH} \times 100\% \quad (\text{Eq. 3.4})$$

Similarly the conversion of toluene and yield and selectivity on basis of toluene was calculated using Equations 3.5-3.7.

$$X_{toluene} = ((N_{toluene,in} - N_{toluene,out}) / N_{toluene,in}) \times 100\% \quad (\text{Eq. 3.5})$$

$$Y_{product} = N_{product} / N_{toluene,in} \times 100\% \quad (\text{Eq. 3.3})$$

$$S_{product} = Y_{product} / X_{toluene} \times 100\% \quad (\text{Eq. 3.4})$$

The aromatic selectivity ($AS_{alkylation}$) was calculated as the ratio of selective alkylation products (side chain or ring alkylation) per total alkylation products (side chain+ring alkylation) (Equation 3.8).

$$AS_{alkylation} = Y_{side\ chain\ or\ ring\ alkylation} / Y_{total\ alkylation} \times 100\% \quad (\text{Eq. 3.8})$$

The W/F in $g_{catalyst} \cdot s \cdot mol^{-1}$ (Eq. 3.9) and WHSV (weight-hourly-space-velocity) in h^{-1} (Eq. 3.10) were calculated as follows ($mol_{reactant}$ and $g_{reactant}$ were calculated from the partial pressure *via* the *ideal gas equation*):

$$W/F = g_{catalyst} \times (mol_{reactant} \cdot time^{-1})^{-1} \quad (\text{Eq. 3.9})$$

$$WHSV = (g_{catalyst})^{-1} \times (g_{reactant} \cdot time^{-1}) \quad (\text{Eq. 3.10})$$

Acknowledgment. Dr. G. Eder-Mirth is gratefully acknowledged for the making of Figure 3.4. Special thanks go to B. Kamp for the outstanding help and devoted dedication for building the analysis GC, Ing. A. Hovestad for designing the columns and last but not least to H. Veldhuis for building the reactor setup. J. Talman of ELTN is thanked for the maintenance of the high vacuum setups used. The author is grateful for receiving the samples used in this thesis from Dr. M. Derewinski, the Japanese Catalysis Society, Technical University of Eindhoven, AKZO Chemicals, Prof. Dr. H.G. Karge and Prof. A. Corma. Special thanks go to Ing. J.A.M. Vrieling for measuring XRF, and to Ing. V. Skolnik and Dipl. Ing. (FH) X. Hecht of the Technische Universität München for measuring the BET specific surface areas of the here introduced samples. M. Smithers of the Centrum voor Materialen Onderzoek (CMO) of the University of Twente is thanked for measuring the SEM image of Na-FAU(X). Drs. J. González Raya is gratefully acknowledged for the synthesis of the sample Cs-FAU(X2).

Chapter 4

Interaction of Methanol with Alkali Cation Exchanged Molecular Sieves: I.r. Spectroscopic Study

Abstract:

The adsorption of methanol over various alkali metal cation exchanged zeolites (MFI, MOR and FAU) was studied by *in situ* i.r. spectroscopy and gravimetry. Lower Si/Al ratios (increasing the polarity of the zeolite lattice) strengthened the interaction between methanol hydrogens, i.e., hydroxy (OH) as well as the methyl (CH₃) hydrogens, and the framework oxygen. Similarly, the total interaction of the methanol CH₃ and OH groups with the framework oxygen was stronger as the atomic weight of the alkali cation increased (in FAU(X)). This strengthened hydrogen bonding did not lead to an overall higher heat of adsorption. This suggests that the most important interaction occurs between the electron lone-pair donor function of methanol (i.e., the oxygen) and the electron pair acceptor function of the zeolite (i.e., the alkali metal cation). The methanol adsorption complexes in the zeolite pores are discussed.

4.1 INTRODUCTION

The directed and localized interaction of polar molecules with hydroxy groups and metal cations and the oxygen atoms of pore walls of a molecular sieve has been seen to be most important for the nature of the sorbate-sorbent bonding and its activation in catalytic transformations. Consequently, the interaction of small polar molecules such as methanol with acidic zeolites, such as H-MFI (H-ZSM5), have been thoroughly investigated leading to a profound understanding of subtle details of the sorbent - sorbate interactions [1,2,3,4,5].

It has been observed that methanol molecules tend to form ring-like hydrogen bonded structures. When the protons of the Brønsted acid hydroxy groups of the zeolites were exchanged for alkali cations [1] the interaction appeared to be very localized, the methanol oxygen atom assuming the role of the electron pair donor site and the alkali cation that of the electron pair acceptor site. At least for zeolites with a low concentration of framework aluminum such as MFI the zeolite pores appear to act like an inert environment containing the Lewis acid sites (exposed alkali cations). This situation changes and becomes increasingly more complex when materials with higher concentrations of alkali cations (higher concentrations of aluminum in the zeolite lattice) are considered. This is connected with the complexity of the possible interactions and the inherent coupling of the density of sites and the acid-base properties. In such cases the preliminary experiments so far indicate strong interactions between the oxygens of the pore walls and the sorbed polar molecules as well as intermolecular hydrogen bonding between sorbed molecules. Consensus whether or not this leads to cleavage of some polar bonds (formation of alcoholate species at ambient temperatures) is not reached [6,7,8].

Thus, we decided to systematically study the non-reactive interaction of methanol with three molecular sieves (MFI (ZSM5), MOR and FAU (X and Y)) containing various alkali metal cations and to compare this with theoretical calculations. With respect to the various molecular sieves, comparisons will be made for Na⁺ ion exchanged molecular materials containing varying concentrations of tetrahedrally coordinated alumina in the lattice. The variations of the Si/Al ratio and the different exchanged cations induce marked variations in the concentrations of adsorption sites and the acid-base properties. For a given cation, the negative charge on the lattice oxygen increases with increasing aluminum concentration and for a given chemical composition of the lattice with increasing the atomic weight of the cation. The changes can be approximated by Sanderson's electronegativity equalization principle [9,10]. Such an approach is acceptable as it has been shown that variations in the zeolite

-
1. Mirth, G.; Lercher, J.A.; Anderson, M.W.; Klinowski, J. *J. Chem. Soc., Faraday Trans.* **1990**, *86*, 3039.
 2. Kotrla, J.; Nachtigallova, D.; Kubelkova, L.; Heeribout, L.; Doremieux-Morin, C.; Fraissard, J. *J. Phys. Chem. B* **1998**, *102*, 2454.
 3. Blaszkowski, S.R.; Van Santen, R.A. *J. Phys. Chem. B* **1997**, *101*, 2292.
 4. Haase, F.; Sauer, J. *J. Am. Chem. Soc.* **1995**, *117*, 3780.
 5. Haase, F.; Sauer, J. *Microporous Mesoporous Mater.* **2000**, *35-36*, 379.
 6. Bosáček, V. *J. Phys. Chem.* **1993**, *97*, 10732.
 7. Ziolk, M.; Czyniewska, J.; Lamotte, J.; Lavalley, J.C. *React. Kinet. Catal. Lett.* **1994**, *53*, 339.
 8. Salvador, P.; Kladnig, W. *J. Chem. Soc., Faraday Trans.* **1977**, *73*, 1153.
 9. Mortier, W.J. *J. Catal.* **1978**, *55*, 138.
 10. Sanderson, R.T. *J. Am. Chem. Soc.* **1983**, *105*, 2259.

framework type exert a much more subtle influence on the acid-base properties than variations of the chemical composition [11]. For the alkali cations, the electronegativity decreases with increasing atomic weight leading to increasing polarity of the lattice and base strength of the oxygens. Increasing the aluminum concentration in the lattice of the zeolite appears to increase the concentration and strength of basic sites available [12,13]. Thus, Cs-FAU(X) is the most and Na-MFI the least basic molecular sieve studied in this contribution. Great care has also been taken that inclusions, i.e., alkali (hydr)oxide clusters are absent in the samples studied in order to avoid contributions of basic species other than the ion exchanged zeolites.

Central to the experimental contribution will be the assignment of the three forms of adsorbed methanol observed also in earlier i.r. spectroscopic studies [14,15], i.e., (i) methanol with freely vibrating OH bonds, (ii) with hydrogen bonds to the zeolite walls and (iii) with additional strong intermolecular hydrogen bonding and the assessment of their variation in abundance with the structural and chemical changes in the molecular sieves investigated. These observations and interpretations were evaluated by theoretical calculations performed by Vayssilov *et al.* [16].

4.2 EXPERIMENTAL

Materials

Materials used were alkali metal cation exchanged MFI and FAU(X), and Na⁺ exchanged MOR20, MOR10 and FAU(Y), as described in Chapter 3. Detailed specifications of the used molecular sieves are compiled in Table 3.1.

Infrared Spectroscopy, Temperature Programmed Desorption and Thermogravimetric Studies

Experiments were performed according to the procedures described in Chapter 3. Infrared spectra were taken using a BRUKER IFS88 FTIR spectrophotometer.

4.3 RESULTS AND DISCUSSION

I.r. spectra of adsorbed methanol

The infrared spectra of methanol sorbed on Na-MFI (Na-ZSM5), Na-MOR, Na-FAU(Y) and Na-FAU(X) after equilibration at 1.10^{-3} mbar at 308 K are shown in Figure 4.1 (see also Table 4.1). Table 4.1 gives a more detailed list of all observed i.r. bands during methanol adsorption, of which some wavenumbers are not printed for clarity in Fig. 4.1. The MeOH i.r. bands obtained after sorption

11. Brändle, M.; Sauer, J. *J. Am. Chem. Soc.* **1998**, *120*, 1556.

12. Barthomeuf, D.; De Mallmann, A. *Stud. Surf. Sci. Catal.* **1988**, *37*, 365.

13. Vayssilov, G.N.; Rösch, N. *J. Catal.* **1999**, *186*, 423.

14. Izmailova, S.G.; Karetina, I.V.; Khvoshchev, S.S.; Shubaeva, M.A. *J. Colloid Interface Sci.* **1994**, *165*, 318.

15. Bonn, M.; Bakker, H.J.; Domen, K.; Hirose, C.; Kley, A.W.; Van Santen, R.A. *Catal. Rev.-Sci. Eng.* **1998**, *40*, 127.

16. Vayssilov, G.N.; Lercher, J.A.; Rösch, N. *J. Phys. Chem. B* **2000**, *104*, 8614.

on different alkali metal cation exchanged MFI and FAU are reported in Table 4.2 and 4.3, respectively. The low equilibrium pressure assures low coverage of methanol per alkali cation of the zeolite allowing us to better interpret the significant differences between the wavenumbers and shapes of the bands of the CH and OH stretching and deformation vibrations of adsorbed methanol. The details of these variations and the implications for the adsorption structures are discussed below. These interpretations are compared with detailed quantum chemical calculations, performed by Vayssilov *et al.* [16].

OH stretching vibrations

After equilibration of Na-MFI (Na-ZSM5) with 10^{-3} mbar methanol at room temperature, a sharp peak at 3612 cm^{-1} (width at half height of 55 cm^{-1}) assigned to the methanol OH stretching vibration was observed. The sharp band at a wavenumber close to that of the stretching vibration of a free OH group of methanol (3681 cm^{-1} [17]) indicates the presence of a rather unperturbed, freely vibrating hydroxy group. This suggests that the molecule interacts *via* the lone pair electrons of its oxygen center with the Na^+ cation of the zeolite and the hydroxy group points away from the lattice oxygens of the zeolite channel (see Fig. 4.2; Structure 1). These conclusions are supported

by the increase of the wavenumber of the OH band with decreasing electrostatic potential of the cation (see Table 4.2) which indicates that the strongest perturbation of the O-H band occurs with the metal cation of the highest Lewis acid strength (i.e., Li^+). The weak and broad band at approximately 3500 cm^{-1} is attributed to some additional methanol adsorption on the free hydroxy group of an already adsorbed methanol molecule [1]. This band

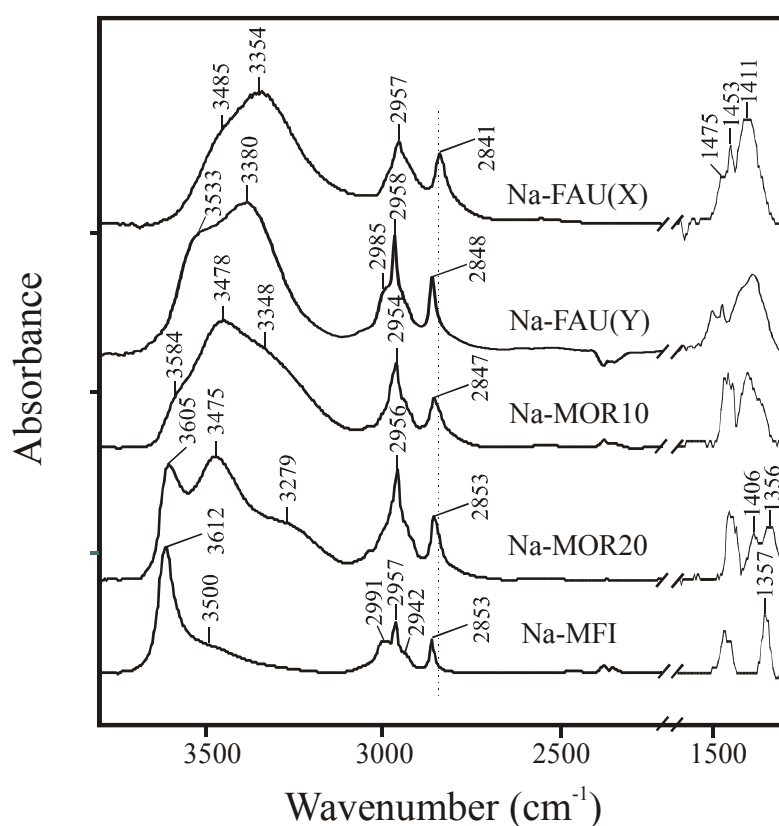


Figure 4.1: Difference *i.r.* spectra of MeOH adsorbed on Na-MFI ($\text{Si}/\text{Al} = 36$), Na-MOR20 ($\text{Si}/\text{Al} = 10$), Na-MOR10 ($\text{Si}/\text{Al} = 5$), Na-FAU(Y) ($\text{Si}/\text{Al} = 2.8$), Na-FAU(X) ($\text{Si}/\text{Al} = 1.3$). $T = 308\text{ K}$. $p = 10^{-3}\text{ mbar}$.

with decreasing electrostatic potential of the cation (see Table 4.2) which indicates that the strongest perturbation of the O-H band occurs with the metal cation of the highest Lewis acid strength (i.e., Li^+). The weak and broad band at approximately 3500 cm^{-1} is attributed to some additional methanol adsorption on the free hydroxy group of an already adsorbed methanol molecule [1]. This band

17. Serrallach, A.; Meyer, R.; Günthard, Hs.H., *J. Mol. Spectrosc.* **1974**, *52*, 94.

TABLE 4.1: Stretching vibration (ν_{O-H} , ν_{C-H}) and deformation bands (δ_{O-H} , δ_{C-H}) of MeOH after adsorption on Na⁺ exchanged zeolites, calculated intermediate Sanderson electronegativity (S_{int}^a), and calculated average charge on the oxygen of the lattice ($-\delta_O^b$).

Sample	ν_{O-H} (cm ⁻¹)	ν_{C-H} (cm ⁻¹)	δ_{O-H} (cm ⁻¹)	δ_{C-H} (cm ⁻¹)	S_{int}	$-\delta_O$
Methanol (g) ^c	3682	2999, 2970, 2920 2844	1340	1477, 1465, 1454		
Na-MFI	3612, 3500	2991, 2957, 2942 2853	1357, 1344	1473, 1463, 1454	3.011	0.162
Na-MOR20	3605, 3475, 3279	2984, 2956, 2940 2853, 2843	1406, 1356	1478, 1462, 1450	2.891	0.192
Na-MOR10	3584, 3478, 3348	2977, 2954, 2933 2847	1408, 1366	1474, 1461, 1450	2.762	0.224
Na-FAU(Y)	3533, 3380	2985, 2958, 2944 2848	1413, 1376	1475, 1464 (vw), 1454	2.564	0.274
Na-FAU(X)	3485, 3354	2984, 2957, 2929 2841	1411, 1362	1475, 1463 (vw), 1453	2.486	0.317
Methanol (l) ^d	3337	2934 2822	1420	1475, 1453		

^a Intermediate Sanderson electronegativity S_{int} calculated from $S_{int} = (S_p^p S_o^q S_r^r S_t^t)^{1/(p+q+r+t)}$ for a compound P_pQ_qR_rT_t [9]; for electronegativity S of atom P, see Sanderson [10].

^b Calculated average charge $-\delta_O$ on the oxygen of the lattice, using $(S_{int} - S_o)/2.08 S_o^{1/2}$ [9].

^c From reference [17].

^d From reference [20].

TABLE 4.2: Stretching vibration (ν_{O-H} , ν_{C-H}) and deformation bands (δ_{O-H} , δ_{C-H}) of MeOH on alkali cation exchanged MFI zeolites, calculated intermediate Sanderson electronegativity (S_{int}^a), calculated average charge on the oxygen of the lattice ($-\delta_o$), and the electrostatic potential of the cation (e/r).

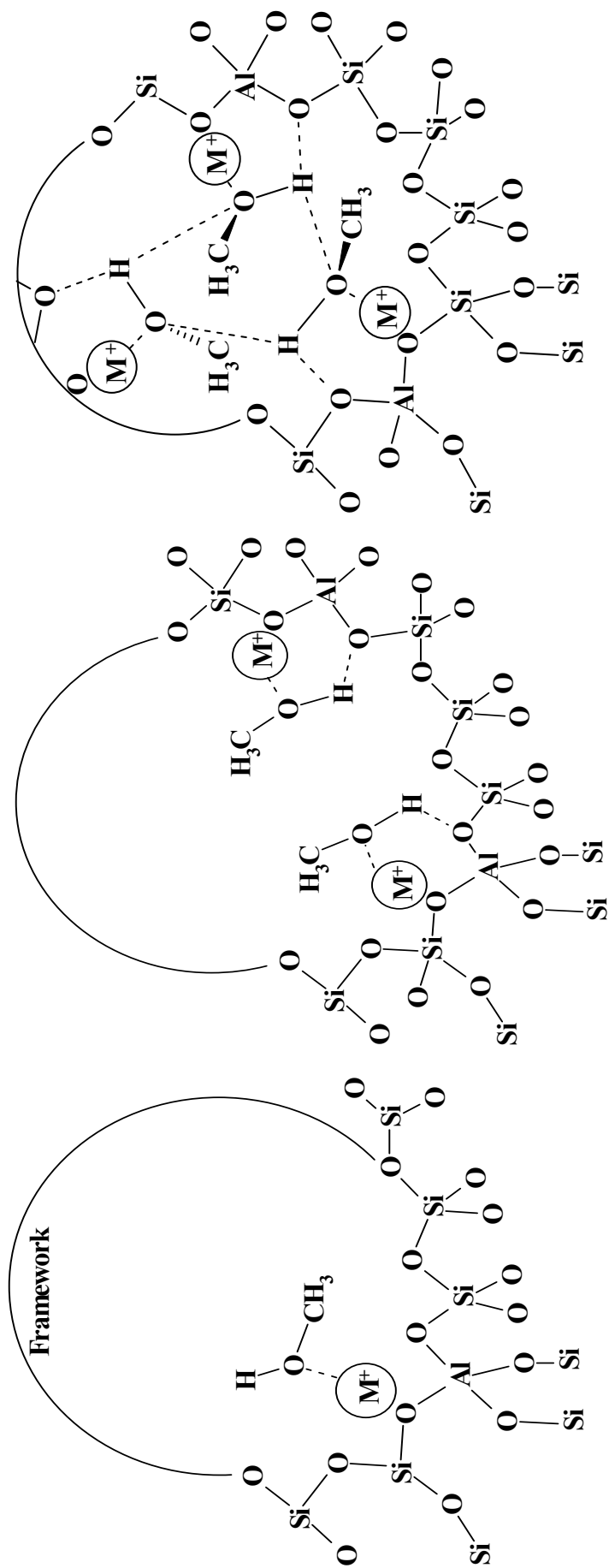
Sample	ν_{O-H} (cm^{-1})	ν_{C-H} (cm^{-1})	δ_{O-H} (cm^{-1})	δ_{C-H} (cm^{-1})	S_{int}	$-\delta_o$	e/r (\AA^{-1})
Li-MFI	3602	2958, 2854	1356	1473, 1461, 1452	3.012	0.161	1.67
Na-MFI	3612	2957, 2853	1357, 1344	1473, 1463, 1454	3.011	0.162	1.05
K-MFI	3614	2954, 2848	1356	1473, 1464, 1451	3.002	0.164	0.75
Cs-MFI	3620	2955, 2854			2.984	0.168	0.59

^a See Table 4.1 for the calculation of the intermediate Sanderson electronegativity (S_{int}) and the average charge ($-\delta_o$) on the oxygen of the zeolite lattice.

TABLE 4.3: Stretching vibration (ν_{O-H} , ν_{C-H}) and deformation bands (δ_{O-H} , δ_{C-H}) of MeOH on alkali cation exchanged FAU(X) zeolites, calculated intermediate Sanderson electronegativity (S_{int}^a), calculated average charge on the oxygen of the lattice ($-\delta_o$), and the electrostatic potential of the cation (e/r).

Sample	ν_{O-H} (cm^{-1})	ν_{C-H} (cm^{-1})	δ_{O-H} (cm^{-1})	δ_{C-H} (cm^{-1})	S_{int}	$-\delta_o$	e/r (\AA^{-1})
Na-FAU(X)	3485, 3354	2957, 2841	1411, 1362	1475, 1463(vw), 1453	2.486	0.317	1.05
K-FAU(X)	3413, 3235	2943, 2825	1423, 1392	1484, 1460, 1450	2.425	0.358	0.75
Rb-FAU(X)	3409, 3213	2934, 2820	1434, 1407	1483, 1461, 1450	2.385	0.378	0.67
Cs-FAU(X)	3244	2941, 2820	1428, 1389	1481, 1462, 1451	2.326	0.384	0.59

^a See Table 4.1 for the calculation of the intermediate Sanderson electronegativity (S_{int}) and the average charge ($-\delta_o$) on the oxygen of the zeolite lattice.



Structure 1

Structure 2

Structure 3

Figure 4.2: The different adsorption states of methanol in the used zeolites, related to the Si/Al ratio (see text): Structure 1, a freely vibrating OH group, as found for Na-MFI (3612 cm⁻¹; see text); Structure 2, hydrogen bonding between the methanol OH group and the lattice oxygen, as found for Na-MOR and Na-FAU(Y) (≈ 3500 cm⁻¹; see text); Structure 3, hydrogen bonding (see Structure 2) and additional lateral interaction between adsorbed methanol molecules, as found for Na-FAU(X) (3354 cm⁻¹; see text).

increased significantly with increasing equilibrium pressure and shifted to lower wavenumbers (3434 cm^{-1} at 10 mbar; see Chapter 6 (not shown here)).

Methanol adsorbed on two samples of Na-MOR showed three bands of hydroxy groups (see Figure 4.1). Their relative intensities and widths at half height changed with the framework composition. The most narrow band at 3605 cm^{-1} in Na-MOR20 (see Table 4.1) is attributed to a relatively freely vibrating OH group from methanol bound in a similar way as described in Figure 4.2 (Structure 1). Because of their larger half width, the other two bands (3478 and approx. 3300 cm^{-1}) are assigned to methanol molecules for which the hydroxy group is hydrogen bonded. The band with the higher wavenumber (3478 cm^{-1}) is attributed to methanol molecules that experience lateral hydrogen bonding of their OH group with lattice oxygen (see Fig. 4.2; Structure 2). The second band (approx. 3300 cm^{-1}) is attributed to methanol molecules that in addition to the interactions described above are hydrogen bonded to other sorbed methanol molecules (see Fig. 4.2; Structure 3). Note that this requires the proximity of sorption sites. The higher intensity of that band in samples of lower Si/Al ratios, i.e., with increasing cation concentrations (a higher density of sorption sites), fully supports the assignment.

These two latter OH bands are the only ones observed in aluminum-rich zeolites such as Na-FAU(X) and Na-FAU(Y) (Figure 4.1). Methanol adsorbed on Na-FAU(X) showed a broad asymmetric band with a maximum around 3354 cm^{-1} (see Fig. 4.1), which is attributed to the methanol hydroxy group. The asymmetric shape indicates that the band consists of two components with maxima at 3485 and 3354 cm^{-1} . Their wavenumbers are considerably lower and their widths are larger compared to the band of the methanol OH group in Na-MFI (3612 cm^{-1}). This indicates strong lateral interactions of MeOH adsorbed on Na-FAU(X), which are attributed to hydrogen bonding between the hydroxy group and the zeolite lattice oxygen (3485 cm^{-1} , see also Fig. 4.2; Structure 2) and hydrogen bonding between molecules sorbed on neighboring cations (3354 cm^{-1} , see also Fig. 4.2; Structure 3). The band attributed to hydrogen bonding of MeOH to the zeolite lattice oxygens of Na-FAU(X) (at 3485 cm^{-1}) is more pronounced on Na-FAU(Y) (3533 cm^{-1}). This indicates a much higher contribution of MeOH-lattice interactions on Na-FAU(Y) compared to MeOH-MeOH interactions as found for MeOH adsorption on Na-FAU(X). This observation strengthens our conclusion that with decreasing Si/Al ratio of the zeolites, interactions between adsorbed MeOH molecules become increasingly important. Lavalley *et al.* reported a spectrum of methanol adsorbed on Na-FAU(Y) [18], which is in perfect agreement with the spectrum reported here (see Fig. 4.1).

The data presented here agree well with the i.r. spectra of gas phase $\text{Na}^+(\text{CH}_3\text{OH})_n$ -clusters [19] and the spectrum of liquid (clustered) methanol (see, e.g., Falk and Whalley [20]). Note also that Bonn *et al.* [15] have observed two broad bands interpreting them, however, to clustering of methanol molecules. However, in our case the bands appear at such low coverages of methanol per alkali metal cation that the attribution to clusters of physisorbed methanol is highly unlikely. At higher loadings of

18. Ziolk, M.; Czyzniewska, J.; Lamotte, J.; Lavalley, J.C. *Catal. Lett.* **1996**, *37*, 223.

19. Weinheimer, C.J.; Lisy, J.M. *J. Phys. Chem.* **1996**, *100*, 15305.

20. Falk, M.; Whalley, E. *J. Chem. Phys.* **1961**, *34*, 1554.

methanol (10^{-1} mbar) on Na-FAU(X), the band appeared at 3278 cm^{-1} (not shown here). This shift of the OH stretching vibration to lower wavenumber upon increasing loadings is attributed to MeOH clustering in the zeolite pores.

These variations of the i.r. spectra of sorbed methanol show that in zeolites with more basic lattice oxygens (higher aluminum concentrations) strong hydrogen bonding of the methanol hydroxy groups with the lattice oxygens exists in addition to the coordinative bond between the alcohol oxygen and the cation. DFT calculations have shown that the frequency shift of the O-H stretching mode correlates with the strength of the hydrogen bond and the proton affinity of the corresponding zeolite oxygen center [16]. It is interesting to note that the wavenumbers of the two forms of strongly hydrogen bonded methanol (see Fig.4.1 and Table 4.1) are higher for the faujasite samples (structure 2: 3533 cm^{-1} (Na-FAU(Y)) and 3485 cm^{-1} (Na-FAU(X)); structure 3: 3380 cm^{-1} (Na-FAU(Y)) and 3354 cm^{-1} (Na-FAU(X))) than for the two mordenites (structure 2: 3475 cm^{-1} (Na-MOR20) and 3478 cm^{-1} (Na-MOR10); structure 2: 3279 cm^{-1} (Na-MOR20) and 3348 cm^{-1} (Na-MOR10)). This suggests that the shape of the pore/cavity subtly influences the potential interaction between the polar molecules and the framework oxygens. The higher wavenumber found with the faujasites indicates that the narrower environment of mordenite enhances intermolecular sorbate-sorbate and lattice-sorbate interactions.

For a given material, the strength of hydrogen bonding increases with the polarity of the lattice (see Table 4.3). This is concluded from the wavenumber of the methanol OH stretching band decreasing from Na-FAU(X) to Rb-FAU(X) (3354 and 3213 cm^{-1} , respectively). For methanol on Cs-FAU(X), this band is observed at a somewhat higher wavenumber, 3244 cm^{-1} (see Table 4.3), compared to methanol on Rb-FAU(X) (3213 cm^{-1}). We tentatively assign this smaller shift to the steric constraints that the large Cs^+ ion exerts upon the intermolecular hydrogen bonding between methanol molecules.

CH stretching vibrations

The asymmetric and symmetric CH stretching vibration bands of methanol adsorbed on Na-MFI are compiled in Table 4.1 and 4.2 (see also Fig. 4.1) and appeared at 2991 , 2957 (both asymmetric CH stretching vibration [21,22], the band at 2991 cm^{-1} is also related to a center rotational band [23]), 2942 (overtone or combinations of methyl deformation modes [21]) and 2853 cm^{-1} (symmetric CH stretching). These wavenumbers were identical for all alkali-exchanged MFI (see Table 4.2). Note that also methanol sorbed on silica, for which the methyl group is regarded to freely rotate with respect to the molecule axis [22] showed similar wavenumbers. This strongly suggests that for alkali exchanged MFI the interactions between the lattice oxygen and methyl group of methanol are minimal (see Table 4.2). The higher wavenumber of the symmetric stretching vibration (2853 cm^{-1}),

21. Natal-Santiago, M.A.; Dumesic, J.A. *J. Catal.* **1998**, *175*, 252.

22. Pelmenchikov, A.G.; Morosi, G.; Gamba, A.; Zecchina, A.; Bordiga, S.; Paukshtis, E.A. *J. Phys. Chem.* **1993**, *97*, 11979.

compared to that of gas phase methanol (2844 cm^{-1} [17]), is attributed to minor strengthening of the C-H bonds in response to the elongation of the C-O bond as a result of the interactions of methanol with the metal cation [24]. After adsorption of methanol at model clusters with sodium or potassium a shortening of the C-H bonds by 0.3-0.5 pm was calculated [16], concomitant with an elongation of the C-O bond by 0.3-2.6 pm. Both changes of bond lengths are stronger for methanol adsorbed by a coordination bond only from the center to the metal cation (as opposed to the situation with an additional hydrogen bond). This finding correlates well with the highest frequency shift of symmetric C-H vibrations on MFI samples (Table 4.1) where methanol is essentially coordinatively bound. The slight increase of the positive frequency shift in the order K^+ , Na^+ , Li^+ for MFI samples (Table 4.2) is also in line with theoretical predictions [16].

The bands attributed to the CH stretching vibrations of methanol sorbed on Na-FAU(X) were observed at 2984, 2957, 2929 and 2841 cm^{-1} . The assignment of the observed i.r. bands is similar as for Na-MFI (see above). The downward shift of 12 cm^{-1} of the symmetric stretching vibration band (2841 cm^{-1}) and the very low intensity of the rotation-vibration coupling at 2984 cm^{-1} compared to MeOH sorbed on Na-MFI suggests additional, strong interactions between the methyl group and the zeolite framework oxygens. Note that the symmetric CH stretching vibration shifted to lower wavenumbers as the size of the cation increased (see Table 4.3). Similar results were reported by Takezawa and Kobayashi [25] for metal oxides as sorbents and Palomares *et al.* [26] for alkali exchanged FAU(X) zeolites as well as Lavalley *et al.* [18] for alkali exchanged FAU(Y) zeolites. In parallel, all bands attributed to CH stretching vibrations broadened compared to the less basic Na-MFI indicating also a stronger interaction between the hydrogen atoms of the methyl group and the zeolite lattice oxygen. Note that this is not a new proposition. The possibility of intermolecular hydrogen bonds between methyl hydrogens and neighbouring oxygen atoms has been proposed in methanol solution by Yuhnevich and Tarakanova [27]. In this context we would like to point to the results of Huber and Knözinger [28], who suggest, however, that the interaction between methane and the lattice oxygens in CsNa-FAU(Y) is very weak. This indicates that the concerted action between the polar hydroxy group of methanol and the methyl group is necessary to induce the broadening. A similar degree of concerted action has been reported for hydrogen bonding between the framework oxygens and the adsorbate in an ethylene-Mn(II) sorption complex in cation exchanged zeolite FAU(X) [29]. These results indicate that the framework oxygens of zeolites become more reactive as the polarity of the framework increases.

At this point attention should be drawn to the fact that the intensity of the methyl rotation - vibration coupling (between 2991 cm^{-1} (Na-MFI) and 2984 cm^{-1} (Na-FAU(X))) was most intense with

23. Pelmenchikov, A.G.; Morosi, G.; Gamba, A. In *Proceedings of the 9th International Zeolite Conference, Montreal*; van Ballmoos, R., Higgins, J.B., Treacy, M.M.J., Eds.; Butterworth-Heinemann: Boston, 1992; Vol. 1; pp 537-544.

24. Gutmann, V. *The Donor Acceptor Approach to Molecular Interactions*; Plenum Press: New York, 1978.

25. Takezawa, N.; Kobayashi, H. *J. Catal.* **1973**, *28*, 335.

26. Palomares, A.E.; Eder-Mirth, G.; Lercher, J.A. *J. Catal.* **1997**, *168*, 442.

27. Yuhnevich, G.V.; Tarakanova, E.G. *J. Mol. Struct.* **1998**, *447*, 257

28. Huber, S.; Knözinger, H. *Chem. Phys. Lett.* **1995**, *244*, 111.

Na-MFI and showed a much smaller intensity with Na-FAU(X) than with Na-FAU(Y) in line with the stronger interaction of the methyl group in the more polar environment. It is interesting to note that with both Na-MOR samples this band was not observed due to the complex structure of the vibration band. Its absence due to overlap of the broad asymmetric vibration band indicates that the tighter pores of mordenite (compared to zeolites FAU(X) and FAU(Y)) enhance the interaction and hinder the rotation of the methanol CH₃ group.

OH deformation bands

As compiled in Fig. 4.1 and Table 4.1, the bands between 1300-1500 cm⁻¹ of sorbed methanol also depend on the nature and chemical composition of the sorbing zeolite. The bands between 1356 and 1420 cm⁻¹ observed for all Na⁺ exchanged zeolites (see Table 4.1) are hydroxy group deformation vibrations ($\delta(\text{OH})$), in accordance with Herzberg [30]. The upward shift compared to the OH deformation band of methanol in the gas phase (1340 cm⁻¹ [17]) is typical for coordinatively sorbed methanol.

For Na-MFI, one sharp band was observed at 1357 cm⁻¹ (with additionally a small shoulder at 1344 cm⁻¹) indicating a relatively freely vibrating OH group. For all other spectra shown in Fig. 4.1 two (broader) bands were observed at higher wavenumbers after spectral deconvolution. These two bands underwent similar variations with the nature of adsorbent as the OH stretching vibration (see Table 4.1). The band at 1408 cm⁻¹ of Na-MOR10 is more pronounced than its counterpart of Na-MOR20 (1406 cm⁻¹). This is related to the more intense sorbate-sorbate and lattice-sorbate interactions on Na-MOR10. Similar to the variations of the OH stretching bands, a higher intensity of the band at low wavenumber (1376 cm⁻¹) was observed for Na-FAU(Y) than for Na-MOR10. This is attributed to the enhancement of sorbate-sorbate and lattice-sorbate interactions by the narrower pores of mordenite. With Na-FAU(X), in addition to the strong band at 1411 cm⁻¹, this second band appeared at 1362 cm⁻¹ and was of lower intensity than with Na-FAU(Y). This suggests that the interaction of the OH group with lattice oxygens is primarily cause for the upward shift of the deformation band.

The deformation band of the hydroxy group of methanol showed little variation in wavenumber with the different alkali metal cation exchanged MFI zeolites (see Table 4.2). Thus, we conclude that the variation in the strength of the direct interaction of the metal cation with the methanol oxygen is insufficient to be reflected in the deformation vibration (free movement of the functional group is still possible). Note that hydrogen bonding between methanol and the lattice oxygens in MFI is concluded to be insignificant. However, when adsorbed on alkali metal cation exchanged FAU(X) zeolites (see Table 4.3) the cation significantly influences the position of the $\delta(\text{OH})$ band. In this case the hydrogen bonding of the OH group to lattice oxygens increases with increasing cation size up to Rb-FAU(X). With Cs-FAU(X), the $\delta(\text{OH})$ band of methanol did not follow this trend and appeared at

29. Jang, S.B.; Jeong, M.S.; Kim, Y.; Seff, K. *J. Phys. Chem. B* **1997**, *101*, 9041.

30. Herzberg, G. *Molecular Spectra and Molecular Structure. II. Infrared and Raman Spectra of Polyatomic Molecules*; D. van Nostrand Company, Inc.: Princeton, 1964; pp 334-335.

lower wavenumber (1428 cm^{-1}) than for methanol on Rb-FAU(X) (1434 cm^{-1}) suggesting weakened hydrogen bonding.

CH deformation bands

The bands observed between 1450 and 1480 cm^{-1} (see Fig. 4.1 and Table 4.1), after methanol adsorption on the Na^+ exchanged zeolites, are attributed to $\delta(\text{CH}_3)$ vibrations [30]. While the wavenumbers (1475 , 1464 and 1454 cm^{-1}) of these bands were identical for all Na^+ exchanged zeolites investigated, their intensity varied with the structure and the chemical composition. For gas phase methanol these bands are found at 1473 , 1464 and 1452 cm^{-1} [17], liquid methanol exhibits only two bands at 1475 and 1453 cm^{-1} [20]. With decreasing Si/Al ratio, i.e., zeolite MFI compared to FAU(X), the band at 1464 cm^{-1} decreased in intensity and that at 1454 cm^{-1} increased. Similar results were reported by Pelmenchikov *et al.* [22] for the adsorption of methanol on silica. The variations of the intensity of the two bands is explained by a clustering of methanol sorbed on neighboring cations, deduced from the fact that lateral hydrogen bonding observed for the aluminum-rich zeolites produces similar type hydrogen bonds as observed for methanol clusters.

Interestingly, the methyl deformation band at 1475 cm^{-1} shifted to higher wavenumbers (1482 cm^{-1}) with increasing atomic weight of the exchanged alkali metal for FAU(X) zeolites (see Table 4.3), but not for MFI zeolites (see Table 4.2). This shift is attributed to the increasing interaction between the methanol CH_3 group and the lattice oxygens for zeolite FAU(X), which is concluded to be absent for MFI.

Thermal desorption and strength of interaction

Although the i.r. spectra of adsorbed methanol clearly indicate that methanol is more perturbed after adsorption on the more basic zeolites, i.e., Rb- and Cs-FAU(X), t.p.d. shows that bonding of methanol is strongest for the Na^+ exchanged zeolites (see Figure 4.3) The asymmetric peak shape in the MeOH desorption spectrum from Na-FAU(X) shows a second desorption maximum at approximately 490 K , indicating stronger bonded methanol species. From this and the results obtained by Avgul *et al.* [31] (decreasing heat of adsorption with decreasing electrostatic potential of the cation) we conclude that the cation with the largest electrostatic potential produces the strongest interaction. This suggests that for all zeolites the main interaction occurs between the cation (the electron pair acceptor) and the oxygen of methanol (the electron pair donor) in line with the suggestions by Mirth *et al.* [1]. Indeed, the theoretical study reported by Vayssilov *et al.* [16] found that the interaction energy due to coordination bonds to Na^+ or K^+ cations is $40\text{-}55\text{ kJ.mol}^{-1}$, while the hydrogen bond contributes in addition only about $12\text{-}18\text{ kJ.mol}^{-1}$ to the binding energy of methanol. This was also confirmed by t.p.d. experiments of MeOH adsorbed on Na- and Cs-MFI (in which MeOH does not form hydrogen bonds to the framework oxygen centers) showing desorption maxima of only 10 and 35 K lower,

31. Avgul, N.N.; Bezus, A.G.; Dzhit, O.M. In *Adv. Chem. Ser.-Molecular Sieve Zeolites*; Flanigen, E.M., Sand, L.B., Eds.; American Chemical Society: Washington, DC, 1971; Vol 101; pp 184-192.

compared to Na- and Cs-FAU, respectively. The shape of the curves at low temperatures (not shown here) also indicated lower initial desorption temperatures for the MFI samples (for both MFI samples no difference in initial temperature was found, only a concentration difference (Cs-MFI retained much less)). Therefore, we conclude that the interactions between the framework and the hydrogens of methanol and the mutual hydrogen bonding between sorbed molecules do not seem to contribute significantly to the strength of adsorption and primarily opens new pathways for surface chemical reactions.

Evidence of methanol decomposition into surface methoxy groups (indicated by the formation of a band at 1635 cm^{-1} , assigned to the formation of water, resulting from methanol decomposition [18]) or formates (indicated by a band at 1610 cm^{-1} [26]) was not observed under the adsorption conditions used in the present study. This is in line with results from i.r. and NMR spectroscopic characterization [6,18,32,33]. Similarly, evidence for the abstraction of a proton by the (basic) zeolite lattice, and the formation of an alcoholate was not observed, in agreement with Lavalley *et al.* [7].

Adsorption capacity for methanol

The results of the gravimetric measurements of methanol adsorption on various alkali exchanged zeolites are compiled in Fig. 4.4 and Table 4.4. It is observed that the concentration of the alkali cations determined the overall uptake and the average stoichiometry of

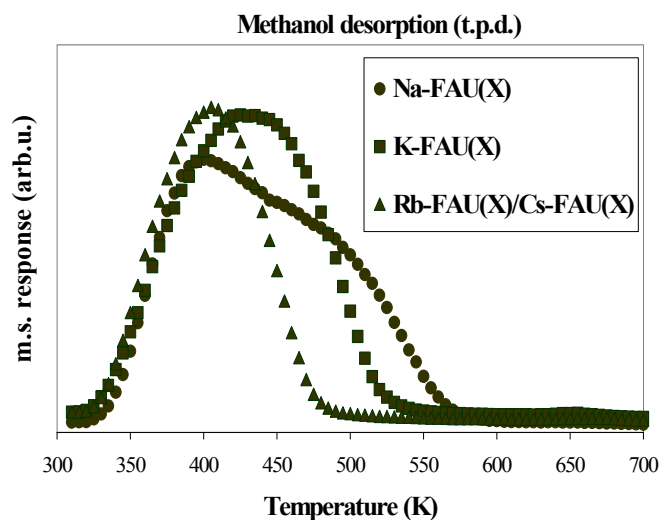


Figure 4.3: *T.p.d.* of MeOH adsorbed on alkali-exchanged FAU(X) zeolites (at temperatures $>700\text{ K}$ no methanol desorption is found). *T.p.d.* spectra are normalized to the weight of the catalysts employed during the *t.p.d.* experiment.

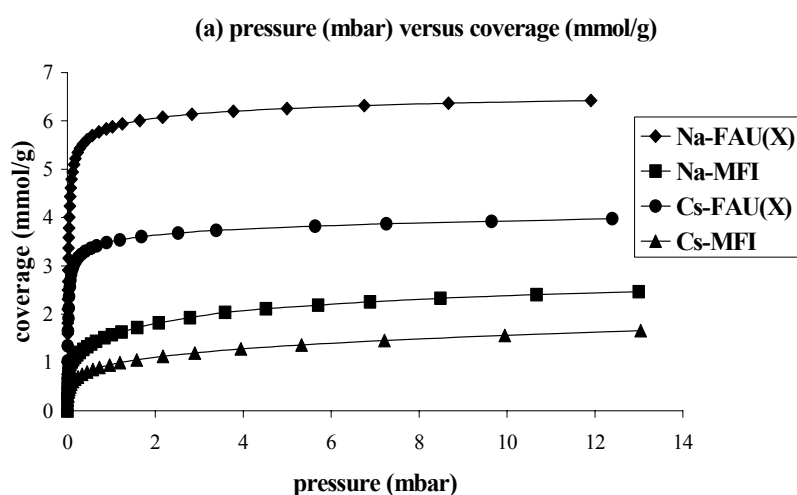


Figure 4.4(a): Adsorption isotherm: pressure vs mmol/g for the adsorption of methanol on alkali-exchanged FAU(X) and MFI. $T = 323\text{ K}$; $p = 10^{-3}$ - 13 mbar .

32. Forester, T.R.; Howe, R.F. *J. Am. Chem. Soc.* **1987**, *109*, 5076.

33. Philippou, A.; Anderson, M.W. *J. Am. Chem. Soc.* **1994**, *116*, 5774.

methanol adsorbed per alkali cation. This is best illustrated with the differences between Na-FAU(X) and Na-MFI with respect to the methanol uptake (see Fig. 4.4a and 4.4b). While Na-MFI could take up over five methanol molecules per Na^+ cation, this ratio decreased monotonously with increasing concentration of the alkali cations (increasing concentration of aluminum) to one methanol per Na^+ cation for Na-FAU(X). The higher value of methanol per Na^+ for Na-FAU(Y) than for Na-FAU(X) and the equal overall loading of both indicates that the variation is primarily related to the larger concentration of Na^+ in the pores. The influence of the size of the cation is well reflected in the lower maximum uptake of Cs^+ exchanged samples when compared to the Na^+ exchanged counterparts (see Table 4.4).

TABLE 4.4: Maximum loading achieved at about 13 mbar and Henry's constants (at 323 K) for methanol adsorption on the alkali metal cation exchanged zeolites, related to $-\delta_{\text{O}}$ of the lattice oxygens^a.

Sample	$-\delta_{\text{O}}$	Maximum loading			Henry's constant
		(mmol/g)	(molec./site)	(molec./u.c.) ^b	(mmol/g*atm)
Li-MFI	0.161		5.03	13.2	n.d. ^c
Na-MFI	0.162	2.47	5.32	14.4	$1.5 \cdot 10^5$
K-MFI	0.164	2.03	4.73	12.0	n.d.
Cs-MFI	0.168	1.66	3.92	10.1	$3.1 \cdot 10^4$
Na-MOR20	0.192	2.81 ^d	1.94 ^d	12.2 ^d	n.d.
Na-MOR10	0.224	3.99	1.51	12.2	$4.5 \cdot 10^5$
Na-FAU(Y)	0.274	6.32	1.58	79.8	$2.5 \cdot 10^5$
Na-FAU(X)	0.317	6.43	1.02	85.5	$3.6 \cdot 10^5$
Rb-FAU(X)	0.378	4.81	0.87	73.9	n.d.
Cs-FAU(X)	0.384	3.98	0.78	66.6	$5.7 \cdot 10^5$

^a For the calculation of $-\delta_{\text{O}}$ of the lattice oxygens, see Table 4.1; ^b u.c. = unit cell; ^c n.d. = not determined; ^d at 4.6 mbar.

As could be deduced from the adsorption isotherms (see Fig. 4.4b for the two limiting cases, i.e., Na-MFI and Na-FAU(X)), methanol adsorption on the molecular sieves used in this study has not yet reached 1 molecule per alkali cation, under the conditions used in the i.r. adsorption experiments. Methanol adsorption is suggested to occur solely on the cations and not on the pore walls caused by the different heats of adsorption for the alkali exchanged zeolites and silicalite, i.e., $90\text{-}100 \text{ kJ}\cdot\text{mol}^{-1}$ [14,31] and $65 \text{ kJ}\cdot\text{mol}^{-1}$ [34], respectively, as was shown also experimentally. It was found for a Na-A zeolite ($\text{Si}/\text{Al} = 1$) that all methanol molecules are bonded to Na^+ cations [35] (although increasing polarity of

34. Pope, C.G. *J. Chem. Soc., Faraday Trans.* **1993**, *89*, 1139.

35. Cheng, M.Y.; Lee, H.S.; Seff, K. *Zeolites* **1983**, *3*, 348.

the zeolite framework by decreasing the Si/Al ratio and/or increasing cation electropositivity might increase the probability of MeOH sorption on the wall instead of sorption on the extra framework alkali cations). Judging by the i.r. spectra and adsorption results of this study, we conclude that methanol does not cluster irregularly inside the zeolite pores under the conditions used in this study. Thus, irregular sorbate clustering can be excluded as the reason for the broadening of the methanol hydroxy and methyl bands with Na-FAU(X) and Cs-FAU(X).

The isotherm of Na-MFI showed a “plateau” around a coverage of two molecules / site (see Fig. 4.4(b)). We attribute this to the fact that the adsorption sites are well separated from each other, and direct interaction on the Na^+ cations prevails, as suggested by Mirth

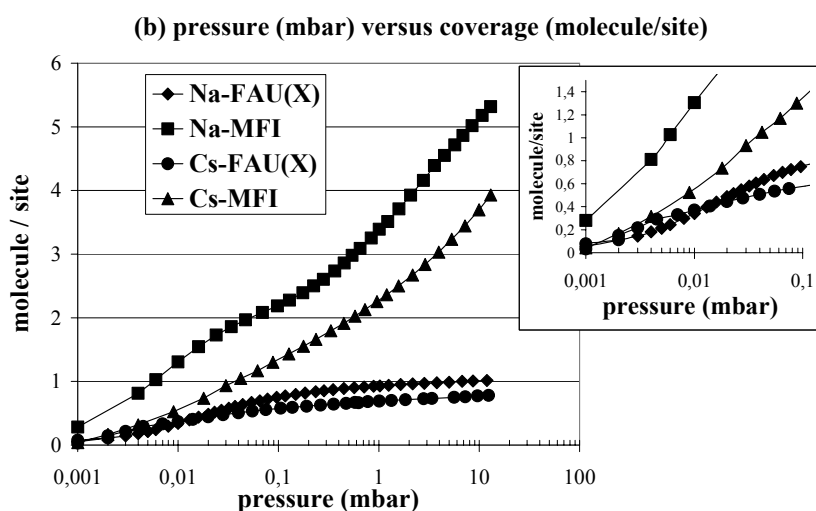


Figure 4.4(b): Adsorption isotherm: pressure vs molecule / site for the adsorption of methanol on alkali-exchanged FAU(X) and MFI. $T = 323 \text{ K}$; $p = 10^{-3}$ -13 mbar. For clarification, we show the adsorption isotherm (fractional coverage vs pressure) at low pressures ($p = 10^{-3}$ - 10^{-1} mbar) enlarged (see inset in (b)).

et al. [1], Boddenberg *et al.* [36] and Dubinin *et al.* [37]. This results in up to two methanol molecules directly interacting with one alkali cation without strong mutual interactions. Note in this context that gas phase clusters of Na^+ cations surrounded by 2-7 methanol have been reported by Weinheimer and Lisy [19]. At higher methanol partial pressures, the uptake increases again, which is indicative of the formation of chain like methanol clusters [1], probably caused by the limited space inside the pores of MFI, surrounding the cations. For Cs-MFI, increasing sorbate-sorbate interactions are observed at significant lower coverage as indicated by the absence of the plateau and the continuously slow increasing uptake (see Fig. 4.4b). This indicates that a weaker interaction between the cation and methanol facilitates the intermolecular interactions. A similar conclusion was drawn for $\text{Cs}^+(\text{CH}_3\text{OH})_n$ and $\text{Na}^+(\text{CH}_3\text{OH})_n$ clusters, whereby intermolecular interactions (hydrogen bonding) were observed for clusters as small as 3 MeOH molecules for Cs^+ (i.e., $\text{Cs}^+(\text{CH}_3\text{OH})_3$), while for $\text{Na}^+(\text{CH}_3\text{OH})_n$ this was with $n > 4$ [19].

As can be seen in the inset of Fig 4.4(b), the initial MeOH uptake on Cs-FAU(X) is larger at lower pressures than on Na-FAU(X) indicating a larger affinity of Cs-FAU(X). This is probably the result of the higher basicity of the Cs^+ exchanged zeolite and the smaller accessibility of the Na^+

36. Boddenberg, B.; Rakhmatkariev, G.U.; Greth, R. *J. Phys. Chem. B* **1997**, *101*, 1634.

cations, which are deeper embedded into the framework.

4.4 CONCLUSIONS

Methanol adsorbs on alkali cation exchanged zeolites in three types of local adsorption structures. The direct interaction between the alkali metal cation (electron pair acceptor) and the oxygen of methanol (electron pair donor) is important for all zeolites and in all three adsorption structures. With increasing polarity of the oxygen centers in the zeolite framework the interaction of the hydrogen atoms of methanol with the framework increases. This leads to a relatively isolated methanol molecule coordinatively bound to the alkali metal cation in MFI (Structure 1). The detailed analysis of the i.r. spectra suggests that the OH group and the methyl group of the adsorbate face little steric hinderance with respect to deformational and rotational movements. When the negative charge on the oxygen in the zeolite lattice is higher, additional hydrogen bonding between the hydrogen of the methanol hydroxy group and the oxygen of the zeolite lattice becomes more important (Structure 2). Furthermore, interaction between the hydrogens of the methyl group and the zeolite lattice is also observed. As the concentration of the alkali cations in the zeolites increases the higher density of the adsorption sites allow additional hydrogen bonding between sorbed methanol molecules (Structure 3). The i.r. spectra presented in this paper, in combination with gravimetric results, suggest that at low MeOH coverage the hydrogen bonding occurs primarily between coordinatively bound methanol molecules and not *via* clustering of several methanol molecules around an alkali metal cation (conditions chosen in the i.r. experiments were such that, as indicated by TG experiments, irregular MeOH clustering could be neglected). To elucidate the precise structure of these interactions, as proposed here, more detailed FAU(X)-ray diffraction measurements on large single crystals combined with i.r. spectroscopic analysis would be necessary. However, the analogy to a structural study with water [38] suggests that ring-like super-structures, as proposed here in Fig. 2 (Structure 3), are formed in the twelve-membered ring windows of faujasites.

Acknowledgment. Special thanks go to Dr. J.A.Z. Pieterse for helpful discussions concerning the gravimetric measurements.

37. Dubinin, M.M.; Rakhmatkariev, G.U.; Isirikyan, A.A. *Izv. AN SSSR, Ser. Khim.* **1989**, *11*, 2636.

38. Wiede, P., "Strukturchemische untersuchungen an zeolite Y/faujasite", PhD thesis, Technical University of Vienna, Vienna, Austria, 1997.

Chapter 5

Location of Methanol-Cation Adsorption Complexes in FAU, MOR and MFI

Abstract:

The previous chapter described the experimental results obtained during methanol adsorption over various alkali metal cation exchanged zeolites (MFI, MOR and FAU). It was concluded that lower Si/Al ratios (increasing the basicity of the zeolite lattice) increased the interaction between the methanol OH and CH₃ hydrogens and the oxygen of the zeolite lattice. The aim of this chapter is to describe the location of the methanol sorption complexes in the zeolite pores, based on theoretical considerations. It is concluded that only cations in the supercage (FAU), the main channel (MOR) or the channel intersections (MFI) interact with methanol. Small relocations of the cations to better accommodate the methanol cannot be excluded. Furthermore, ring like adsorption structures (might) occur in the supercage of FAU(X) zeolites.

5.1 INTRODUCTION

Chapter 4 described the adsorption of methanol in alkali metal cation exchanged zeolites

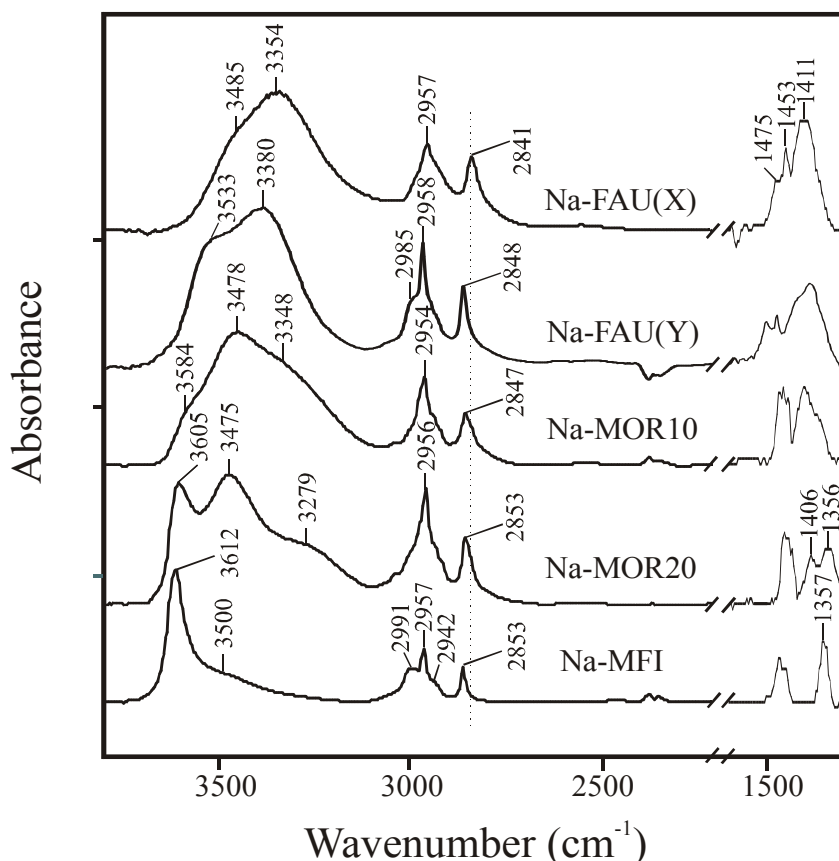


Figure 5.1: Difference i.r. spectra of MeOH on Na-MFI ($Si/Al = 36$), Na-MOR20 ($Si/Al = 10$), Na-MOR10 ($Si/Al = 5$), Na-FAU(Y) ($Si/Al = 2.8$), Na-FAU(X) ($Si/Al = 1.3$). $T = 308\text{ K}$, $p = 10^{-3}\text{ mbar}$.

based on experimental i.r. results. However, no attention was paid to the location of the adsorption complexes in these zeolites. This chapter, therefore, will describe the hypothetical location of methanol-cation sorption complexes in FAU (X and Y), MOR and MFI and is based on experimental results discussed in Chapter 4 and the location of the bare cations in dehydrated FAU, MOR and MFI zeolites as described in Chapter 2. For clarity of the following discussion, the infrared spectra of methanol adsorbed on Na-MFI (Na-ZSM5), Na-MOR, Na-FAU(Y) and Na-FAU(X) after equilibration at 1.10^{-3} mbar at 308 K are shown in Figure 5.1.

Methanol adsorption and location in alkali cation exchanged zeolites FAU(X) and FAU(Y)

As already outlined in Chapter 2, bare cations in dehydrated FAU(X) zeolites are found in the supercage (site II, III and III'), the sodalite cage (site I') and the hexagonal prism (site I). Na-FAU(Y) does not contain extra framework cations on site III and III' (extra framework cations are those cations which are balancing the negative charge on the framework and are easily exchangeable (they do not take part as T-atoms in the zeolite framework, as Si and Al do)). Extra framework cations in Na-FAU(Y) are found only in sites I, I' and II. Site II' is never found to be occupied by Na^+ cations; in dehydrated FAU zeolites this site is vacant, probably related to electrostatic repulsion induced by site

I'; in hydrated zeolites this site is occupied by H₂O [1]. Na-FAU(Y) does not hold cations on sites III and III', since calculations have shown a low binding energy for cations in this site (approximately 40 kJ.mol⁻¹ less than for cations in site II), which decreases with increasing Si/Al ratio (reducing the Al centers in the four-membered ring from 2 to 1 reduces the binding energy of sodium with 16 kJ.mol⁻¹ [2,3]). Because of the local geometry of the framework, a cation in site III has a lower number of nearest-neighbor oxygen centers and thus is coordinatively less saturated than cations in site II. This results in a lower binding energy for cations in site III.

Thus it is evident that sites III and III' become less occupied with increasing Si/Al ratios as was found experimentally with FAU(Y) zeolites compared to FAU(X) zeolites [1]. The locations of the different Na⁺ cations in the faujasite (X and Y) zeolite are shown in Figure 5.2. In the Na-FAU(X) sample methanol will first adsorb on the Na⁺ cations in site III and III', because these cations are the most accessible in the framework. Since Na-FAU(Y) does not contain extra framework cations on site III and III', methanol complexation occurs with the cations of site II.

For Na-FAU(X) the cations in site III and III' will be first occupied by MeOH, instead of cations in site II, because the framework oxygens of site III and III' have the lowest binding energy with the Na⁺ cations [2,3] (about 40 kJ.mol⁻¹ lower), compared to oxygens in site II. Because of the local geometry of the framework, a cation in site III and III' has a lower number of nearest-neighbor oxygen centers and thus is coordinatively less saturated than cations in site II, resulting in a lower binding energy. The low interaction energy between the cations and the framework oxygens of site III and III' results in a low charge delocalization between the cation and the framework oxygens and thus a higher electropositive charge on the cations compared to the cations in site II. A stronger adsorption of methanol is therefore expected as also found for CO adsorption on cations in site III compared to adsorption on cations in site II [3]. The interaction is mainly electrostatic. Secondly, the cations in site II of Na-FAU(X) will interact with methanol. However, bridging methanol molecules between adjacent cations in the supercage of Na-FAU(X) (site II and III') at loadings of less than 1 methanol molecule

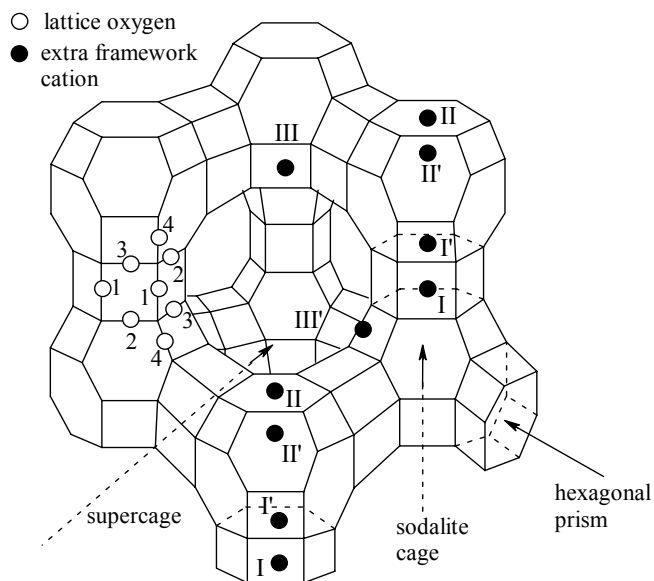


Figure 5.2: Framework structure of Na-FAU (X and Y). Cation locations are shown by Roman numerals I to III'. Methanol adsorption complexes are most likely only found at sites II and III' (see text). The different oxygen atoms, which are involved in the bonding of the extra framework cations are indicated by the numbers 1 to 4.

1. Mortier, W.J.; Van den Bossche, E.; Uytterhoeven, J.B. *Zeolites* **1984**, *4*, 41.

2. Buttefey, S.; Boutin, A.; Mellot-Draznieks, C.; Fuchs, A.H. *J. Phys. Chem. B* **2001**, *105*, 9569.

per cation can not be excluded as they were found for methanol sorption on Na-A [4]. (The distances between the Na^+ cations in the supercages of Na-A were found to be comparable to those in Na-FAU(X), 3.7-5.1Å [5] and 4.7-4.8Å [6], respectively.) Figure 5.3 shows a schematic representation of a bridging methanol molecule between two extra framework Na^+ cations of site II and III' in Na-FAU(X). Interaction of MeOH with two extra framework cations is only expected when there is no large difference in binding energy of the different cations to the framework oxygens (see below).

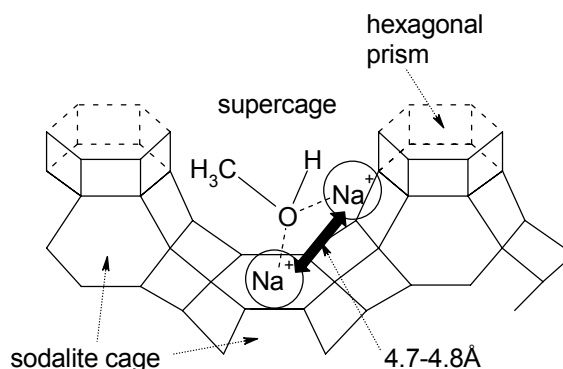


Figure 5.3: The interaction of two Na^+ cations associated with site II and site III', respectively, bridged by a MeOH molecule in Na-FAU(X) (see text).

As found for CO adsorption [3], cations in site II in Na-FAU(Y) will interact stronger with methanol than the corresponding cations in Na-FAU(X), because of their higher cation charge (despite their higher binding energy ($\approx 20 \text{ kJ}\cdot\text{mol}^{-1}$) to the framework oxygens), provided that Na-FAU(Y) contains 2 Al centers and not 3 Al centers per six ring as in Na-FAU(X) [3]. The higher cation charge of cations in site II in Na-FAU(Y) (with 2 Al centers per six ring), compared to cations located at a six ring with 3 Al centers per six ring in Na-FAU(X), is caused by the fact that the Na^+ cations in site II in Na-FAU(X) are much more shielded by the framework oxygen centers of the ring, compared to Na-FAU(Y).

Methanol diffusion into the sodalite- or β -cage to interact with cations in site I and I' is not expected as a result of the kinetic diameter of methanol. The kinetic diameter of methanol (comparable to that of methane: $\sigma_{\text{kinetic-methane}} = 4.4\text{\AA}$ [7]) is larger than the diameter of the D_6 window (which allows entrance to the sodalite cage from the supercage (only 2.4\AA)), and thus prohibits the diffusion of methanol into the sodalite cage. A similar conclusion was drawn by Narayana and Kevan using Electron Spin-Echo studies [8]. This is in sharp contrast with water and ammonia molecules, which have been shown to be able to penetrate the sodalite cage [9,10] and induce cation movement from sites I and I'.

On the other hand, penetration of only the methanol hydroxy group into the β -cage has been reported for H-FAU(Y) [11], but in Na-FAU(X) and Na-FAU(Y) this is expected to be hindered by the alkali metal cations of site II. However, if penetration of the methanol hydroxy group would occur then

3. Vayssilov, G.N.; Stauffer, M.; Belling, T.; Neyman, K.M.; Knözinger, H.; Rösch, N. *J. Phys. Chem. B* **1999**, *103*, 7920.

4. Cheng, M.Y.; Lee, H.S.; Seff, K. *Zeolites* **1983**, *3*, 348.

5. Subramanian, V.; Seff, K. *J. Phys. Chem.* **1977**, *81*, 2249.

6. Zhu, L.; Seff, K. *J. Phys. Chem. B* **1999**, *103*, 9512.

7. Csicsery, S.M. *Zeolites* **1984**, *4*, 202.

8. Narayana, M.; Kevan, L. *J. Am. Chem. Soc.* **1981**, *103*, 5729.

9. Dendooven, E.; Mortier, W.J.; Uytterhoeven, J.B. *J. Phys. Chem.* **1984**, *88*, 1916.

10. Kim, M.J.; Jeong, M.S.; Kim, Y.; Seff, K. *Microporous Mesoporous Mater.* **1999**, *30*, 233.

interaction is presumed to be very small, since the interaction energy decreases with $1/r^2$ (where r is the distance between the OH group and the cation in site I or I' and is approximately 5.75Å or 4.69Å to site I and I', respectively). Interaction of methanol with cations in site I and I' can, therefore, be ruled out.

Above discussion is in agreement with calorimetric measurements performed by Avgul *et al.* [12]. The heat of adsorption found for methanol on Na₇₇-FAU(X) (X zeolite containing 77 Na⁺ cations per unit cell) steadily decreases until 4 mmol methanol

per gram zeolite is adsorbed (corresponding to approximately 50 Na⁺ cations per unit cell). At zero loading a ΔH_{ads} of 82 kJ.mol⁻¹ was calculated (see Fig. 5.4); at 50 molec./u.c., $\Delta H_{\text{ads}} \approx 67$ kJ.mol⁻¹ [12]. This indicates that about 27 cations are not involved in the adsorption of methanol. These are the cations located in the sodalite cage and hexagonal prism, i.e., site I' and site I (see Fig. 5.2). By further increasing methanol loadings (> 4 mmol MeOH per gram zeolite) the heat of sorption increases again (up to 73 kJ.mol⁻¹) which can only be caused by molecule-molecule interactions, i.e., clustering of methanol *via* hydrogen bonding and/or dipole-dipole interactions (all cations in the supercage are now occupied). This effect has also been observed for the sorption of *n*-alkanes in FAU and EMT [13]. Another explanation might be the formation of Na⁺-(methanol)_n clusters (with $n > 1$). Increasing methanol cluster size around cations, i.e., cation solvation, was found to increase total binding energies [14]; mainly attributed to the cation-methanol and methanol-methanol interaction (hydrogen bonding). After 5.5 mmol methanol per gram zeolite, the heat of sorption decreases again. This decrease is related to steric effects imposed by the framework and the adsorbed molecules or methanol adsorption on the outside of the crystals.

Izmailova *et al.* [15], however, reported that the heat of adsorption initially decreased and remained constant (see Fig. 5.4) until all Na⁺ cations of a unit cell in zeolite FAU(X) (82 cations) were occupied (at zero loading: $\Delta H_{\text{ads}} = 98$ kJ.mol⁻¹; at 4.4 mmol_{MeOH}/g_{zeolite}: $\Delta H_{\text{ads}} \approx 77$ kJ.mol⁻¹). It was explained by a shift of all cations from the β -cage (site I') or hexagonal prism (site I) into the supercage upon adsorption. Since methanol adsorption has to overcome the framework-cation binding energy of site I and I', which was calculated to be approximately 490-520 kJ.mol⁻¹, this is hard to realize [3]. A

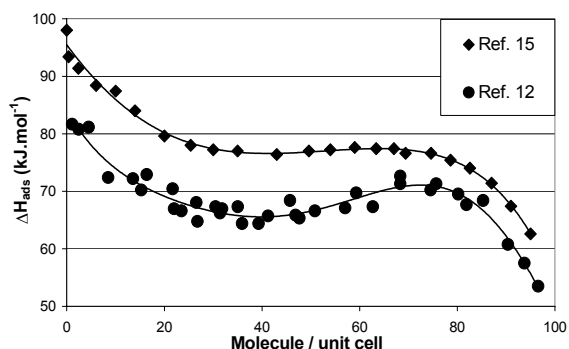


Figure 5.4: Heat of adsorption of methanol on Na-FAU(X) according to Ref. [12] (◆) and Ref. [15] (●) (see text).

11. Kogelbauer, A.; Goodwin, Jr., J.G.; Lercher, J.A. *J. Phys. Chem.* **1995**, *99*, 8777.
12. Avgul, N.N.; Bezus, A.G.; Dzhigit, O.M. In *Adv. Chem. Ser.-Molecular Sieve Zeolites*; Flanigen, E.M., Sand, L.B., Eds.; American Chemical Society: Washington, DC, 1971; Vol 101; pp 184-192.
13. Eder, F., "Thermodynamics and siting of alkane sorption in molecular sieves", PhD thesis, University of Twente, Enschede, The Netherlands, 1996.
14. a) Islam, M.S.; Pethrick, R.A.; Pugh, D. *J. Phys. Chem. A* **1998**, *102*, 2201; b) Glendening, E.D.; Feller, D. *J. Phys. Chem.* **1995**, *99*, 3060.
15. Izmailova, S.G.; Karetina, I.V.; Khvoshchev, S.S.; Shubaeva, M.A. *J. Colloid Interface Sci.* **1994**, *165*, 318.

very strong interaction can be excluded, since the diffusion of methanol into the sodalite cage is hindered and because of the long interatomic distance between the methanol hydroxy group (in the supercage) and cations in site I and I'. Therefore, we attribute this constant value of the heat of sorption found by Izmailova *et al.* to contamination with smaller molecules, e.g., water [12]. Water was shown to diffuse into the sodalite cage and remove all cations from site I and I' into the supercage [1,16]. The heat of adsorption of water on alkali cations [17] and alkali cation exchanged FAU(X) [12] is similar to that of MeOH on alkali cations [17] and alkali cation exchanged FAU(X) [12]; so there is no large preference of the zeolite cations for MeOH or H₂O. Closer examination of water adsorption as a function of coverage reported by Avgul *et al.* [12] shows the same trend for the ΔH_{ads} with coverage as found for MeOH adsorption by Izmailova *et al.* [15]. Thus the constant value of $\Delta H_{\text{ads,MeOH}}$, as reported in Ref. [15] for all 82 cations, is attributed to the contamination with water.

Increasing cation size from $\text{K}^+ \rightarrow \text{Cs}^+$ will decrease the binding energy differences between site II and III'. Because the radius of the cation is too large to make the cation fit in the plane of the six membered oxygen ring of site II, it is displaced to a great extent into the large supercage [18]. Simultaneous occupation of the cations in site II and III' by methanol is thus expected for Cs-FAU(X) as is also the case for H₂O adsorption on Cs-FAU(X) [12,19]. Because of the large Cs^+ cation radius (1.67Å) significant steric hindrance of the methanol sorption-complexes upon each other in Cs-FAU(X) is expected to occur and thus a slightly higher methanol hydroxy stretching vibration wavenumber compared to Rb-FAU(X) is found (see Table 4.4). At this point it is necessary to look more into detail at the cation locations in Cs-FAU(X). Our Cs-FAU(X) zeolite is a partially exchanged Na-FAU(X) zeolite. Literature reported that dehydrated Cs^+ cations are mainly found at positions I' and III' [16]. Site II is fully occupied by Na^+ cations (probably because of the steric repulsions of the Cs^+ cations, when equal occupation of site II and III occurs (interatomic distance between site II and III is approximately 4.7Å [6])) and therefore it is possible that the somewhat higher OH vibration band of methanol that we observe at 3244 cm^{-1} is in fact a combination of two bands at 3354 cm^{-1} (Na-FAU(X)) and 3213 cm^{-1} (Rb-FAU(X)).

An extra word may be said about the spatial structure of the sorption complexes in Na-FAU(X) (see Fig. 5.5). Complexes of 1 methanol molecule per cation are expected to have a trigonal pyramidal structure in FAU (site II), where the oxygen atom of methanol forms the top of the pyramid and three framework oxygens form the base [3,20]. The Na^+ cation is located in the interior of the trigonal pyramidal. Such conformation was also

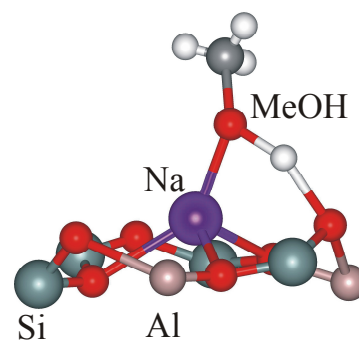


Figure 5.5: Spatial structure of a Na^+ -methanol sorption complex in Na-FAU(X) and Na-FAU(Y) (site II).

16. Shepelev, Yu.F.; Butikova, I.K.; Smolin, Yu.I. *Zeolites* **1991**, *11*, 287.

17. Smith, S.F.; Chandrasekhar, J.; Jorgensen, W.L. *J. Phys. Chem.* **1982**, *86*, 3308.

18. Huber, S.; Knözinger, H. *Appl. Catal. A: General* **1999**, *189*, 239.

19. Dzigit, O.M.; Kiselev, A.V.; Mikos, K.N.; Muttik, G.G.; Rakhmanova, T.A. *Trans. Faraday Soc.* **1971**, *67*, 458.

20. Vayssilov, G.N.; Rösch, N. *J. Catal.* **1999**, *186*, 423.

found for benzene sorption complexes of Ca-FAU(X) [21] and are known from organometallic chemistry. The methanol hydroxy hydrogen points towards the basic oxygen centers of the framework. In site III' the base is formed by two framework oxygens [20], resulting in a triangle in which the oxygen atom of MeOH forms the top. Upon adsorption, the distance of the Na⁺ cation in site II to the plane of the oxygens of the 6-ring remains unchanged [22]; for Na⁺ cations in site III' a displacement of the cation into the supercage upon methanol adsorption is expected to occur. The Na⁺-methanol oxygen distance was found to be approximately 2.38Å by experiment [4] and calculations [22] and is increasing with increasing cation radius. This value is in perfect agreement with the sum of the Na⁺ ionic radius (0.98Å) and the Van der Waals radius of oxygen (1.40Å).

Interaction of the methanol hydroxy group on Na-FAU(Y) and FAU(X)

So far nothing has been said about the interaction of the MeOH hydroxy group with the zeolite lattice in Na-FAU(Y) and with neighboring adsorbed methanol molecules in Na-FAU(X). As outlined in Chapter 4, the effect of increasing the Al content in the zeolite framework is two fold: 1) hydrogen bonding of the MeOH hydroxy group with the framework oxygens is enhanced, because the basicity of the framework is increased and 2) intermolecular hydrogen bonding between neighboring adsorbed methanol molecules is facilitated, since the concentration of extra framework cations in the zeolite pores is increased and thus the proximity of adsorption sites (from 7.69Å in Na-FAU(Y) [2] to 4.7Å in Na-FAU(X) [6]). In Chapter 4, it was concluded that upon MeOH sorption on Na-FAU(X), intermolecular hydrogen bonding was most important for the appearance of the band at 3354 cm⁻¹ (see Fig. 5.1), whereas on Na-FAU(Y) this was hydrogen bonding to the zeolite framework (band at 3533 cm⁻¹). In addition to the band at 3533 cm⁻¹ on Na-FAU(Y), also an intense i.r. band at lower wavenumbers (at 3380 cm⁻¹) was observed (see Fig. 5.1). In the case of Na-FAU(Y) intermolecular hydrogen bonding between adsorbed methanol molecules is more difficult to establish, since the interatomic distance between neighboring cations of site II is approximately 7.69 Å [2] (based on the Si/Al ratio (see Chapter 3) and X-ray crystal refinement of a similar Na-FAU(Y) sample (see Chapter 2), it is concluded that the used Na-FAU(Y) sample of Chapter 4 does not contain cations on site III or III'). The two different OH stretching vibration bands in the i.r. spectrum of the MeOH hydroxy group adsorbed on Na-FAU(Y) could, therefore, result from the interaction of the MeOH hydroxy group with framework oxygen centers in six rings containing different amounts of

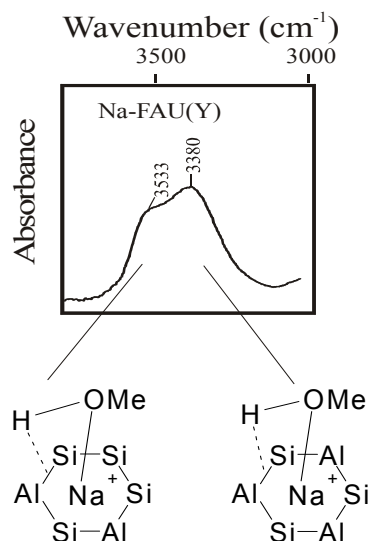


Figure 5.6: MeOH hydroxy i.r. bands as function of the local environment around Na⁺ cations in site II in Na-FAU(Y) (see text). Basic O centers are between T centers (Si and Al) and interact with MeOH hydroxy group.

21. Yeom, Y.H.; Kim, A.K.; Kim, Y.; Song, S.H.; Seff, K. *J. Phys. Chem. B* **1998**, *102*, 6071.

22. Vayssilov, G.N.; Lercher, J.A.; Rösch, N. *J. Phys. Chem. B* **2000**, *104*, 8614.

aluminum centers (see Fig. 5.6) [22]. Increasing Al concentration in the rings of site II increases the basicity of the ring and thus the strength of interaction, which is resembled by the red shift of the OH wavenumber to lower wavenumbers. This could account for the observed intense methanol OH band at 3380 cm^{-1} on Na-FAU(Y).

A similar conclusion was suggested for methanol adsorption on Na-FAU(X), since cations in site II are located in six rings with primarily 3 Al centers [22]. Since MeOH adsorption is expected to occur first on cations in site III', where the cation is surrounded by two Al centers (and the most basic framework O center (see Chapter 2)) explaining the lower OH wavenumbers at 3354 cm^{-1} (Na-FAU(X)) compared to 3380 cm^{-1} (Na-FAU(Y)). But as can be seen in the i.r. spectrum of fig. 5.1, the hydroxy band on Na-FAU(X) is broader than that on Na-FAU(Y). This indicates that cations of different surroundings are involved in MeOH adsorption. Therefore, we conclude that on Na-FAU(X), because of the small interatomic distance between cations in site III' and II (approximately $4.7\text{-}4.8\text{ \AA}$ [6]), it is possible that previously adsorbed MeOH molecules on site III' direct new MeOH molecules to adsorb on site II. Hydrogen bonding between MeOH molecules yields $12\text{-}18\text{ kJ.mol}^{-1}$ extra, which is approximately the difference in binding energy of the cation to the zeolite framework of site II and III' (cations in site II interact stronger with the framework than cations in site III' (approximately 40 kJ.mol^{-1}) [3]).

Sorption of methanol molecules on cations in site III' has also consequences for the observed reactivity. As the framework oxygen centers O1 and O4 (of site III') are the most basic [23], these oxygens mainly determine the reaction selectivity. MeOH reaction over basic Cs-FAU(X) yields formaldehyde, H_2 and CO, whereas reaction over Na-FAU(X) yields dimethyl ether (see Chapter 6).

Because of the small interatomic distances between the cations of site II and III in Na-FAU(X), hydrogen bonding between adsorbed methanol molecules is expected to occur as discussed above and in Chapter 4. In the case of Na^+ exchanged FAU(X) zeolites this leads to the formation of a ring like adsorption structure all around the wall of the supercage. Some relocation of Na^+ cations upon methanol adsorption might occur to better accommodate the methanol [4]. In the case of Na-FAU(Y) ring like adsorption structures are more difficult to establish, since the interatomic distance between neighboring cations of site II is approximately 7.69 \AA [2]. However, if methanol occupies locations in the 12-membered ring windows between adjacent supercages with increasing methanol loadings such ring like adsorption structures are feasible. Sorbate siting in the 12-membered ring windows of Na-FAU(Y) without interaction with nearby cations has also been reported for benzene [24] and ethylene [25]. Van der Waals forces (dipole-dipole interactions) are held responsible for such interactions. Ring like adsorption structures have been found for water adsorption in cation

23. Heidler, R.; Janssens, G.O.A.; Mortier, W.J.; Schoonheid, R.A. *J. Phys. Chem.* **1996**, *100*, 19728.

24. a) Fitch, A.N.; Jovic, H.; Renouprez, A. *J. Phys. Chem.* **1986**, *90*, 1311; b) Vitale, G.; Mellot, C.F.; Bull, L.M.; Cheetham *J. Phys. Chem B.* **1997**, *101*, 4559.

25. Henson, N.J.; Eckert, J.; Hay, P. J.; Redondo, A. *Chem. Phys.* **2000**, *261*, 111.

exchanged FAU(Y) zeolites [26] and for H₂S adsorption on Ca-FAU(X) [27].

Na⁺ exchanged MOR zeolites: location upon methanol adsorption

Figure 5.7 shows a schematic representation of the cation locations in alkali cation exchanged mordenite. As was shown in Chapter 2, extra framework cations in Na-MOR10 are located in site I and I' (designated as site I in Fig. 5.7; single crystal refinement revealed a small cation displacement of 0.53Å for site I' from its ideal position at site I (see Chapter 2)), site IV and site VI [28]. In Na-MOR20 most likely site VI is empty and the cations are located only in site I, I' and IV. Site VI in MOR zeolites is located at the wall of the main channel and cations in this site are poorly coordinated as found for cations in site III and III' in FAU(X) zeolites (cations in site VI in MOR have a much lower coordination number, compared to sites I, I' and IV and thus a low binding energy); increasing Si/Al ratio as in Na-MOR20, compared to Na-MOR10, results in a lowering of the binding energy (see also Chapter 2). Cation sites II and III were found empty for Na⁺ cations: site II is only occupied by cations with an ionic radius larger than 1.3Å, e.g., K⁺, Ba²⁺ etc. [28]; site III is only occupied by divalent cations, e.g., Ca²⁺, Ba²⁺ [28].

Sorption of methanol in Na-MOR10 and Na-MOR20 is expected to be similar to that outlined above for Na-FAU(X) and Na-FAU(Y). It is expected that in the case of Na-MOR10 mainly the sites in the main channel will be occupied (site IV and VI), of which site VI is first occupied. In Na-MOR20 only site IV is occupied. Diffusion of methanol into the side channel is most likely hindered by the methanol-Na⁺ sorption complex in site IV as also suggested by Sefchik *et al.* [29].

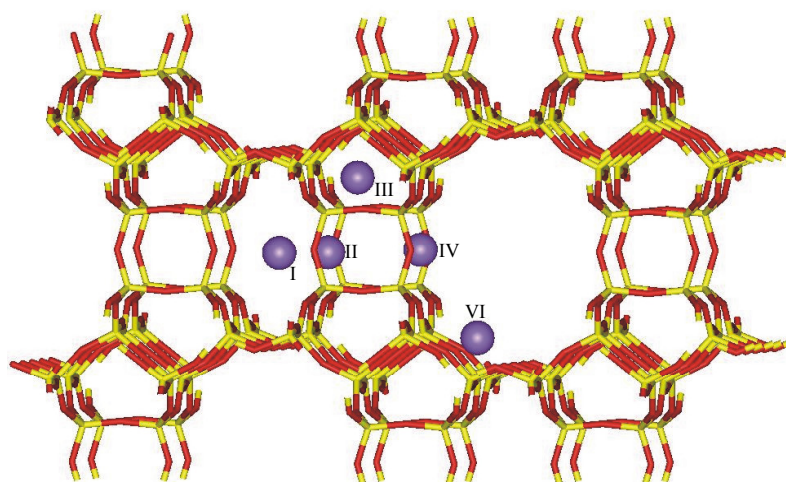


Figure 5.7: Framework structure of mordenite with the location of the cation sites (see Chapter 2 for details about locations). The methanol-cation complexes are probably only located in site IV and VI. Mordenite framework has been drawn, using the InsightII Program, courtesy of MSI.

Upon adsorption a large displacement into the supercage is expected for the Na⁺ cations in site IV of Na-MOR10 and Na-MOR20, since these cations have an unfavorable, one-sided, coordination with the framework oxygens (in bare dehydrated zeolites a large Na⁺-framework oxygen

26. Wiede, P., "Strukturchemische untersuchungen an zeolite Y/faujasite", PhD thesis, Technical University of Vienna, Vienna, Austria, 1997.

27. Jang, S.B.; Jeong, M.S.; Kim, Y.; Han, Y.W.; Seff, K. *Microporous Mesoporous Mater.* **1998**, *23*, 33.

28. Schlenker, J.L.; Pluth, J.J.; Smith, J.V. *Mat. Res. Bull.* **1979**, *14*, 751.

29. Sefchik, M.D.; Schaefer, J.; Stejskal, E.O. *ACS Symp. Ser.* **1977**, *40*, 344.

distance is observed and the Na⁺ cation is located at the fifth position in a 4 oxygen-Na⁺ five-ring [28] (usually the cation is located in the middle of the oxygen plane)). Figure 5.8 shows schematically the Na⁺-methanol complex in site IV of Na-MOR. In site VI (most likely only present in Na-MOR10), the Na⁺ cation binds to 4 oxygens [28] and is largely displaced into the main channel. Upon methanol adsorption a larger displacement into the supercage is assumed for the cations and the sorption complex is expected to have a square planar pyramidal structure. This large displacement is possible since the Na⁺ cations have an unfavorable coordination with the framework oxygens (large Na⁺ framework distance).

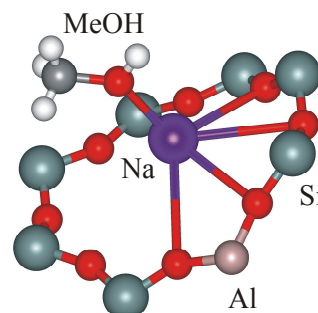


Figure 5.8: Spatial structure of a Na⁺-methanol sorption complex in site IV of Na-MOR.

If diffusion of methanol into the side channel would occur than diffusion through the small ellipsoidal aperture towards site I from the side channel is excluded since only H₂ was found to penetrate [30]. Some intermolecular interaction, however, is expected to occur, since ethanol sorption on H-MOR20 has shown that all acid sites are accessible [31] and protons in H-MOR occupy similar positions as Na⁺ cations in site I [32]. This implies that all the Na⁺ cations in side pockets as well as main channels are accessible to methanol. This interaction might move the Na⁺ cation in site I in the direction of the ellipsoidal window (site II). Note, however, the difference in binding energy of methanol to protons (proton affinity) and Na⁺ cations, 770-775 and 90-110 kJ.mol⁻¹, respectively [22,33], thus only a small interaction is expected.

Because of the large cation concentration in the main channel of Na-MOR10 and the small interatomic distance between neighboring cations in sites IV and VI (ranging from 4.4 to 5.8Å, between site IV and VI and site VI and VI, respectively [34]), intermolecular sorbate-sorbate interactions are likely to occur when these sites are simultaneously occupied by Na⁺ cations. This is evidenced by the presence of the broad band at 3348 cm⁻¹ (see Fig. 5.1). As for Na-MOR20 the cations are expected in the main channel as well (although only in site IV) the probability of hydrogen bonding between neighboring sorbed methanol molecules (in neighboring unit cells) also exists (cation distance is approximately 5.8Å). Such an interaction is evidenced by the presence of a shoulder at 3279 cm⁻¹ (see Fig. 5.1).

Alkali exchanged MFI zeolites: location of methanol adsorption complexes

Two distinct cation locations were observed for alkali cation exchanged MFI using powder XRD and i.r. (see Chapter 2); site I is at the intersections of the sinusoidal and straight channels at the

30. a) Kustov, L.M.; Kazansky, V.B. *J. Chem. Soc., Faraday Trans.* **1991**, *87*, 2675; b) Bordiga, S.; Garrone, E.; Lamberti, A.; Zecchina, A.; Otera Arean, C.; Kazansky, V.B.; Kustov, L.M. *J. Chem. Soc., Faraday Trans.* **1994**, *90*, 3367.

31. Veeffkind, V., "Shape selective synthesis of alkylamines over acid catalysts", PhD thesis, University of Twente, Enschede, The Netherlands, 1998.

32. Alberto, A. *Zeolites* **1997**, *19*, 411.

33. Zhang, X.; Castleman, Jr., A.W. *J. Am. Chem. Soc.* **1992**, *114*, 8607.

edge of a 4-membered ring and site II is in small cavities above the sinusoidal channel (see Fig. 5.9). MeOH adsorption at low loadings is, however, only expected for the cations which are situated at the intersection of the sinusoidal and the main channels (site I). Thus the band observed at 3612 and 1357 cm^{-1} (see Fig. 5.1) are assigned to cation-methanol adsorption complexes in these intersections. The methanol cation complexes are expected to extend largely into the channels (approximately 0.47Å), as was calculated for a Na^+ -methanol sorption complex in a cluster containing 1 Al [22]. Two framework oxygens in the 4 ring of site I form the base (see Figure 5.10).

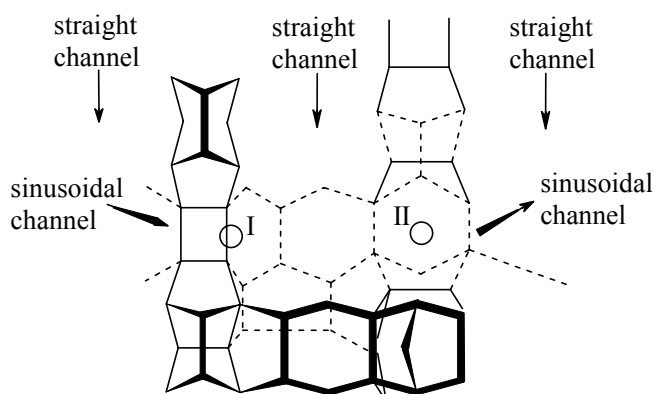


Figure 5.9: View of the [100] plane of MFI (ZSM5) with cation sites I and site II (see Chapter 2 for details). Methanol-cation complexes are found mostly in site I (see text).

I.r. spectroscopy of the methanol adsorption on Na-MFI also revealed a shoulder at the OH deformation band at lower wavenumbers (1344 cm^{-1}), compared to the most intense band at 1357 cm^{-1} (see Chapter 4 (Table 4.1)). This band can not be attributed to clustering of methanol, since then a shoulder at higher wavenumbers compared to the band at 1357 cm^{-1} should be observed [35], thus we tentatively assign this band to the presence of Na^+ cations in the cavities above the sinusoidal channels (site II). ^{23}Na -MAS-NMR of Na-MFI showed a very small occupancy of this location (10%) [36]. Such a shoulder at the OH deformation band at lower wavenumbers is not observed for Li^+ , K^+ and Cs^+ exchanged MFI zeolites. The larger cation radius of Na^+ compared to Li^+ probably displaces the Na^+ cation more into the sinusoidal channel of MFI, making its interaction with MeOH more stronger; the Li^+ cations which are situated in the small cavities (site II) above the sinusoidal channels are largely shielded by the framework [37]. The larger cations, K^+ and Cs^+ , are too big to fit in these confined spaces (see also Chapter 2) and occupy only sites at the channel intersections and thus giving rise to only one OH deformation band.

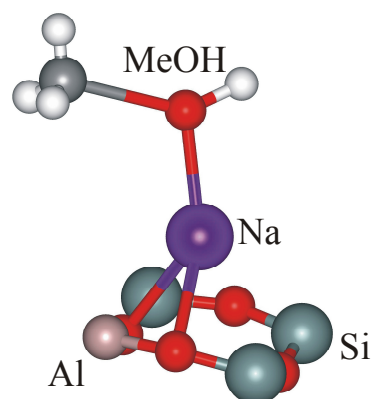


Figure 5.10: Spatial structure of Na^+ -methanol sorption complex in Site I in MFI zeolites.

34. Schlenker, J.L.; Pluth, J.J.; Smith, J.V. *Mat. Res. Bull.* **1978**, *13*, 77.

35. Pelmenschikov, A.G.; Morosi, G.; Gamba, A.; Zecchina, A.; Bordiga, S.; Paukshitis, E.A. *J. Phys. Chem.* **1993**, *97*, 11979.

36. Ohgushi, T.; Niwa, T.; Arakia, H.; Ichino, S. *Microporous Mater.* **1997**, *8*, 231.

37. Katoh, M.; Yamazaki, T.; Ozawa, S. *Bull. Chem. Soc. Jpn* **1994**, *67*, 1246.

5.2 CONCLUDING REMARKS

The intention of this chapter was to describe the theoretical location of the methanol cation sorption complexes in alkali cation exchanged FAU (X and Y), MOR and MFI zeolites. It is concluded that only cations in the supercage (FAU), the main channel (MOR) or the channel intersections (MFI (except in Na-MFI)) interact with methanol. In Na-MFI cations in the channel intersections and in the cavities above the sinusoidal channels also interact with methanol (based on the i.r. spectrum). Small relocations of the cations (in the supercage (FAU), the main channel (MOR) or the channel intersections (MFI)) to better accommodate the methanol can not be excluded. Cations, located in the sodalite cage and hexagonal prism in FAU (X and Y), are not occupied by methanol during adsorption, because of the hindered MeOH diffusion into the sodalite cage and the disability of the cations to move from the sodalite cage or hexagonal prism into the supercage.

Methanol hydroxy bands observed in the i.r. spectrum of MeOH sorption on Na-FAU(Y) indicate hydrogen bonding between the MeOH hydroxy group and the zeolite framework, containing different numbers of Al centers, resulting in different hydroxy i.r. wavenumbers. In Na-FAU(X) three possible methanol adsorption structures hydrogen bonded to the framework O centers at low MeOH partial pressures are possible: 1) MeOH molecules bridging between two cations (small interatomic distance between cations in site II and III'), 2) isolated MeOH molecules interacting with the framework oxygen centers of site III' and 3) intermolecular hydrogen bonding between adsorbed molecules on site III' and II (adsorption on site II being facilitated by the energy gain resulting from hydrogen bonding). This can not occur in Na-FAU(Y), since the cations in site II are too far separated.

Furthermore, ring like adsorption structures might occur in the supercage of FAU(X) and FAU(Y) zeolites. On Na-FAU(X) this probably already occurs at low partial pressures. On Na-FAU(Y) this is facilitated with increasing pressures.

Although small relocation of the cations upon MeOH sorption may occur, the apparent location of the cations at low MeOH loadings is similar to that observed for dehydrated zeolites.

Based on the here presented combination of i.r. spectra obtained during methanol adsorption on alkali cation exchanged zeolites and proposed adsorption structures (see Chapter 4), and the framework structure characterizations and cation locations from single crystal refinement and powder XRD studies, we were able to understand and explain in further detail the methanol-cation adsorption structure in the M^+ exchanged FAU, MOR and MFI zeolites ($M = \text{Li, Na, K, Rb, and Cs}$) and their location.

Recommendations for further research

As this Chapter is merely based on theoretical considerations, experiments of Na-FAU(X) at low MeOH partial pressures with increasing MeOH loadings is recommended to ascertain the adsorption structures in Na-FAU(X). For example, by using methanol ^{17}O -NMR experiments on Na-FAU(X), one can determine whether MeOH is adsorbed isolated (on site III') or interacts with two cations on neighboring sites (bridging between site II and III'). By using single crystal refinement

experiments locations of MeOH can also be determined. It was shown by Seff *et al.* that distinction can be made between bridging MeOH molecules and isolated molecules in Na-A [4]. However, this was done for a fully loaded Na-A zeolite.

Chapter 6

Methanol Reaction over Basic Zeolites

Abstract:

To understand the first reaction steps in the conversion of methanol over Na^+ and Cs^+ exchanged MFI (ZSM5) and FAU(X), methanol (MeOH) and dimethyl ether (DME) reaction was studied with combined infrared spectroscopy (FT-IR) and temperature programmed reaction (t.p.r.), and desorption (t.p.d.). All catalysts showed the formation of surface methoxy groups from either methanol or dimethyl ether. MeOH reaction over alkali exchanged FAU(X) molecular sieves yielded also the formation of surface formaldehyde and/or formate. Surface formaldehyde was found to decompose into CO and H_2 via surface formate. With DME reaction over alkali exchanged FAU(X) and MFI zeolites, no formate or formaldehyde was observed. Formaldehyde and formic acid adsorption – desorption was also studied. Based on these studies a reaction mechanism for the dehydration and dehydrogenation of methanol over alkali metal exchanged molecular sieves is proposed.

6.1 INTRODUCTION

Methanol as methylating agent has attracted significant attention over the past decades. The methylation of toluene to yield xylenes, (the most important product: *p*-xylene) [1], methylation of ammonia yielding methylamines (the most valuable: dimethyl amine) [2], and methylation of isobutene to methyl *tert*-butyl ether (MTBE) [3] as gasoline additive are just three examples that have been commercialized. Another very important reaction process that utilizes methanol is the Methanol to Gasoline (MTG) process, in which methanol is converted to higher hydrocarbons (alkenes, alkanes and aromatics) [4].

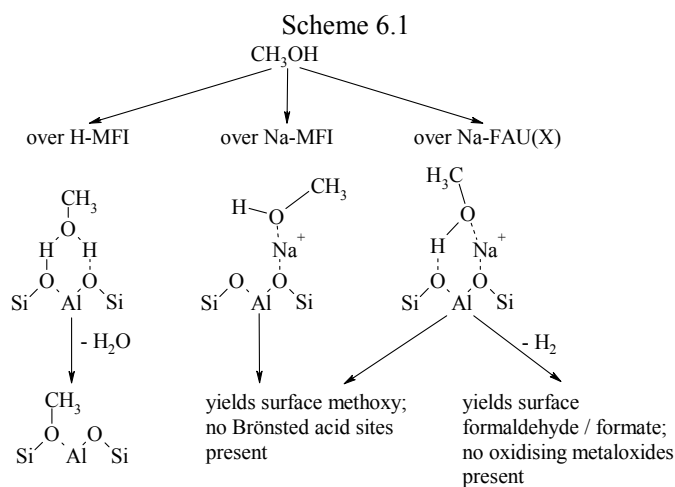
These reactions can be performed over acidic molecular sieves, such as H-MFI and H-MOR. Numerous mechanistic and/or sorption studies using, e.g., infrared spectroscopy, have been devoted to elucidate the reaction mechanism (see, e.g., Ref. [2,5]). The first step was shown to be the adsorption of methanol via hydrogen bonding to the surface oxygens and the Brønsted acid site, followed by the possible dehydration of methanol to surface methoxy groups and water. This surface methoxy group, subsequently, methylates other reagents, such as toluene or ammonia [6,7]. The suggested reaction pathways are in good agreement with theoretical calculations [8,9].

Methanol sorption on weakly acidic silica and amphoteric γ -alumina results also in the formation of surface methoxy groups. I.r. spectroscopy, kinetic studies and quantum chemical calculations, have shown that the reaction path to surface methoxy groups on silica proceeds via the dissociative adsorption of methanol on the (strained) siloxane bridge, in addition to the etherification of the terminal surface silanol groups [10,11]. During the dissociative adsorption of methanol, new surface hydroxy groups are formed (together with surface methoxy groups), which can recombine to water. The same reaction pathways, i.e., dissociative adsorption and etherification of surface hydroxy groups, were also proposed for γ -alumina, based on experimental techniques and modeling [12,13,14].

1. a) Mirth, G.; Lercher, J.A. *J. Catal.* **1991**, *132*, 244; b) Mirth, G.; Lercher, J.A. *J. Catal.* **1994**, *147*, 199.
2. Veefkind, V.A.; Grundling, Ch.; Lercher, J.A. *J. Mol. Catal. A: Chem.* **1998**, *134*, 111.
3. Kogelbauer, A.; Goodwin, Jr., J.G.; Lercher, J.A. *J. Phys. Chem.* **1995**, *99*, 8777.
4. Campbell, S.M.; Jiang, X.-Z.; Howe, R.F. *Microporous Mesoporous Mater.* **1999**, *29*, 91.
5. Smirniotis, P.G.; Ruckenstein, E. *Ind. Eng. Chem. Res.* **1995**, *34*, 1517.
6. Ivanova, I.I.; Corma, A. *J. Phys. Chem. B* **1997**, *101*, 547.
7. Veefkind, V.A.; Lercher, J.A. *Appl. Catal. A: General* **1999**, *181*, 245.
8. Blaszkowski, S.R.; Van Santen, R.A. *J. Phys. Chem. B* **1997**, *101*, 2292.
9. a) Corma, A.; Zicovich-Wilson, C.; Viruela, P.; *J. Phys. Org. Chem.* **1994**, *7*, 364; b) Corma, A.; Sastre, G.; Viruela, P.M. *J. Mol. Catal. A: Chem.* **1995**, *100*, 75.
10. a) Pelmenchikov, A.G.; Morosi, G.; Gamba, A. *J. Phys. Chem.* **1992**, *96*, 2241; b) Pelmenchikov, A.G.; Morosi, G.; Gamba, A.; Zecchina, A.; Bordiga, S.; Paukshtis, E.A. *J. Phys. Chem.* **1993**, *97*, 11979.
11. Natal-Santiago, M.A.; Dumesic, J.A. *J. Catal.* **1998**, *175*, 252.
12. a) Greenler, R.G. *J. Chem. Phys.* **1962**, *37*, 2094; b) Knözinger, H.; Stübner, B. *J. Phys. Chem.* **1978**, *82*, 1526; c) Busca, G.; Rossi, P.F.; Lorenzelli, V.; Benaissa, M.; Travert, J.; Lavalley, J.C. *J. Phys. Chem.* **1985**, *89*, 5433; d) Boiadjev, V.; Tysoe, W.T. *Chem. Mater.* **1998**, *10*, 334; e) Vigué, H.; Quintard, P.; Merle-Mejean, T.; Lorenzelli, V. *J. Eur. Ceram. Soc.* **1998**, *18*, 1753.
13. a) Schiffino, R.S.; Merrill, R.P. *J. Phys. Chem.* **1993**, *97*, 6425; b) Chen, B.; Falconer, J.L. *J. Catal.* **1993**, *144*, 214; c) Ebeid, F.M.; Amin, N.H.; Ali, L.I.; Ali, A.E.-G.A. *Egypt. J. Chem.* **1989**, *32*, 279.
14. a) Senchenya, I.N.; Frash, M.V.; Kazansky, V.B. *Kinet. Catal.* **1994**, *35*, 54; b) De Vito, D.A.; Gilardino, F.; Kiwi-Minsker, L.; Morgantini, P.-Y.; Porchet, S.; Renken, A.; Weber, J. *J. Mol. Struct.: THEOCHEM* **1999**, *469*, 7.

The conversion of methanol into formaldehyde over oxide catalysts or metallic catalysts on oxide supports which are able to change their oxidation state, such as V_2O_5 and Cu on silica, have been studied as well [15,16]. Here the reaction mechanism was shown to proceed via a methoxy group (resulting from the abstraction of the hydroxy proton by the lattice oxygens), with the subsequent abstraction of a proton from the surface methoxy group in the absence of gas phase oxygen by the surface metal cation [17]. This leads to an adsorbed hydride which recombines with the previously formed surface hydroxy group to form molecular hydrogen and surface dioxymethylene and/or formaldehyde [17].

Methanol reaction yielding formaldehyde (and surface formate) was also observed over γ -alumina [12a,d,18]. This step proceeds via the recombination of a surface γ -alumina hydroxy hydrogen and a methoxy hydrogen [13b,19] (facilitated by the simultaneous attack of the hydroxy oxygen on the carbon cation of the surface methoxy group) yielding H_2 and a surface dioxymethylene/adsorbed formaldehyde. This can then intermolecularly rearrange to form a surface methoxy and a surface formate via a *Cannizzaro* type disproportionation reaction [20]. Note that the formation of formaldehyde and/or surface formate does not require any redox properties of the catalysts. Also the reaction of dimethyl ether leads to surface methoxy groups (dissociative adsorption) and formate groups over partially dehydroxylated alumina [18a,21,22]. Heating of a methoxylated γ -alumina surface, where the surface hydroxy groups have been removed by reacting them with methyl chloride, did not show surface formate [23]; this indicates the necessity of surface hydroxyl groups for the abstraction of a methyl hydrogen to form adsorbed formaldehyde or dioxymethylene (as outlined above). The reaction of methanol over basic MgO yielded also surface methoxy and formate groups [24]; the mechanism assumed to be similar to that observed for



15. Feil, F.S.; Van Ommen, J.G.; Ross, J.R.H. *Langmuir* **1987**, *3*, 668.
16. Fisher, I.A.; Bell, A.T. *J. Catal.* **1999**, *184*, 357
17. Shinihara, Y., Nakajima, T., and Suzuki, S. *J. Mol. Struct.: THEOCHEM* **1999**, *460*, 231.
18. a) Matyshak, V.A.; Khomenko, T.I.; Lin, G.I.; Zavalishin, I.N.; Rozovskii, A.Ya. *Kinet. Catal.* **1999**, *40*, 269; b) Vigué, H.; Quintard, P.; Merle-Mejean, T.; Lorenzelli, V. *J. Eur. Ceram. Soc.* **1998**, *18*, 1753.
19. Busca, G. *Catal. Today* **1996**, *27*, 457.
20. Busca, G.; Lamotte, J.; Lavalley, J.C.; Lorenzelli, V. *J. Am. Chem. Soc.* **1987**, *109*, 5197.
21. a) Chen, J.G.; Basu, P.; Ballinger, T.H.; Yates, J.T. *Langmuir* **1989**, *5*, 352; b) Solymosi, F.; Cserenyi, J.; Ovari, L. *Catal. Lett.* **1997**, *44*, 89.
22. a) Yakerson, V.I.; Lafer, L.I.; Danyushevskii, V.Ya.; Rubinshtein, A.M.; *Izv. Akad. Nauk. SSSR, Ser. Khim.* **1967**, *10*, 2246; b) Li, P.; Ng, L.M.; Liang, J. *Surf. Sci.* **1997**, *380*, 530.
23. Beebe, Jr., T.P.; Crowell, J.E.; Yates, Jr., T. *J. Phys. Chem.* **1988**, *92*, 1296.

γ -alumina.

In contrast to these catalysts the conversion of methanol over basic zeolite catalysts, e.g., Na^+ and Cs^+ exchanged MFI, MOR and FAU, has received much less attention. It was shown in earlier studies (^{13}C -NMR [25], i.r. spectroscopy [26] and kinetics [27]) that methanol reaction over alkali exchanged MFI, MOR, and FAU(Y) led to surface methoxy, and dimethyl ether [26a,c,27a], while more basic Na- and Cs-FAU(X) yielded also formaldehyde, surface formate, H_2 and CO [25,26a,b,d,27b].

The purpose of the present paper is to determine the reaction mechanism for the dehydration and dehydrogenation of methanol over these zeolites, by relating i.r. spectroscopy to the catalyst performance. In Scheme 6.1, we have visualized the problem once more. Silica, silicalite-1 and γ -alumina were used as reference materials as these materials are known to dehydrate and dehydrogenate methanol.

6.2 EXPERIMENTAL

Materials

Materials used were Na^+ and Cs^+ exchanged MFI, Na^+ , Rb^+ and Cs^+ exchanged FAU(X) and Cs-FAU(X2). Cs-FAU(X) and Cs-FAU(X2) were prepared according to standard exchange procedures, after which Cs-FAU(X2) was thoroughly washed; Cs-FAU(X) and Cs-FAU(X2) differ mainly in the cation concentration. Cs-FAU(X2) has less charge balancing Na^+ and Cs^+ cations (total 72), whereas the Si/Al ratio of Cs-FAU(X) and Cs-FAU(X2) are similar (= 1.25) [28]. CO_2 desorption showed slightly higher basicity for Cs-FAU(X2). XRD showed an amorphous phase in both samples. See also Chapter 3 for a more detailed description of chemical composition, and characterization of these materials. γ -Alumina, silica and silicalite-1 (purely siliceous MFI) were used as reference materials. Activation procedures were as described in Chapter 3.

Infrared spectroscopy, temperature programmed desorption and catalytic testing

In Chapter 3 the equipment used for the infrared (i.r.) spectroscopy, catalytic testing and

24. Kagel, R.O.; Greenler, R.G. *J. Chem. Phys.* **1968**, *49*, 1638.

25. a) Sefcik, M.D. *J. Am. Chem. Soc.* **1979**, *101*, 2164; b) Philippou, A.; Anderson, M.W. *J. Am. Chem. Soc.* **1994**, *116*, 5774; c) Hunger, M.; Schenk, U.; Weitkamp, J. *J. Mol. Catal.* **1998**, *134*, 97.

26. a) Unland, M.L. *J. Phys. Chem.* **1978**, *82*, 580; b) King, S.T.; Garces, J.M.; *J. Catal.* **1987**, *104*, 59; c) Ziolk, M.; Czyzniewska, J.; Lamotte, J.; Lavalley, J.C. *Catal. Lett.* **1996**, *37*, 223; d) Palomares, A.E.; Eder-Mirth, G.; Rep, M.; Lercher, J.A. *J. Catal.* **1998**, *180*, 56.

27. a) Kogelbauer, A.; Gründling, Ch.; Lercher, J.A. *J. Phys. Chem.* **1996**, *100*, 1852; b) Archier, D.; Coudurier, G.; Naccache, C. In *Proceedings of the 9th International Zeolite Conference, Montreal*; Von Ballmoos, R., Higgins, J.B., and Treacy, M.M.J., Eds.; Butterworth-Heinemann: Boston, 1992; Vol. 2, pp 525-533.

28. A Si/Al ratio of 1.25 corresponds to about 87 basic framework oxygen centers per unit cell of Cs-FAU(X2). The presence of only 72 charge balancing Na^+ and Cs^+ cations implies that some (approximately 17%) of the oxygen centers in Cs-FAU(X2) are not compensated by a positive charge. However, no Brønsted acidity for charge compensation was observed in Cs-FAU(X2). Thus the actual state of the framework remains unclear (see also Chapter 3).

temperature programmed desorption (t.p.d.) studies has been described.

Reaction conditions in the reactor i.r. cell were as follows: 1) 10 mbar of methanol (MeOH) in flowing He (19 ml.min⁻¹) or 2) 10 mbar of dimethyl ether (DME) in He (47.5 ml.min⁻¹). Catalysts were heated in a continuous reactant stream during heating (5 K.min⁻¹) up to 773 K and kept there for 10 minutes before stopping the reaction. Heating was only started when the i.r. signals belonging to methanol were stable in time (adsorption - desorption equilibrium reached). The gas phase was analysed using mass spectrometry. As a result of the short path length in the i.r. reactor (~5 mm) no contribution of gaseous MeOH or DME to the recorded i.r. spectra was observed.

I.r. adsorption studies with formaldehyde (CH₂O) and formic acid (HCOOH) were performed as follows: the activated wafer was contacted with the appropriate partial pressure of formaldehyde or formic acid (10⁻² mbar) at 323 K. After adsorption - desorption equilibrium was reached, t.p.d. experiments were started (10 K.min⁻¹ to 773 K).

T.p.d. studies of MeOH, DME, CH₂O and formic acid (HCOOH) were performed as described in Chapter 3. After activation 40-55 mg of alkali cation exchanged MFI and FAU(X) zeolites were contacted with 7 mbar (MeOH, DME and formic acid) or 1.9 mbar (CH₂O) of the appropriate adsorbate at 323 K, respectively. During t.p.d. the gas stream was scanned for the following masses simultaneously: MeOH: (m/z) 46, 45, 31, 30, 29, 28, 15; DME: (m/z) 46, 45, 15; HCOOH: (m/z) 46, 45, 44, 29, 28, 18, 2; CH₂O: (m/z) 31, 30, 29, 28, 15.

Reaction conditions in the fixed bed flow reactor were: 10 mbar of methanol, continuously, in flowing Ar. Catalysts at 323 K (approximately 50 mg (particle size: 0.3-0.6 mm)) were allowed to equilibrate in MeOH (about 80 minutes) before heating in MeOH flow (linear heating rate: 5 K.min⁻¹) to 773 K was started. The overall flow was 19 ml.min⁻¹. This corresponds to a W/F ratio of 0.96 g of catalyst.h.mol⁻¹ of methanol (WHSV: 0.331 h⁻¹). Gas phase analysis was performed using a mass spectrometer (online continuously) and gas chromatograph (samples taken at 323, 653 and 773 K, respectively). MeOH conversion, product yield and selectivity were calculated using Equation 6.1-6.3 (see also Chapter 3):

$$X_{MeOH} = ((N_{MeOH,in} - N_{MeOH,out}) / N_{MeOH,in}) \times 100\% \quad (\text{Eq. 6.1})$$

$$Y_{product} = N_{product} / N_{MeOH,in} \times 100\% \quad (\text{Eq. 6.2})$$

$$S_{product} = Y_{product} / X_{MeOH} \times 100\% \quad (\text{Eq. 6.3})$$

Due to the limiting properties of the setup (Ar as carrier gas, chosen GC columns, and capillary column (limited heating range)) accurate gas chromatographic measurements of H₂O, CO and CO₂ could not be done (see also Chapter 3).

6.3 RESULTS

I.r. spectroscopy

Activated materials

In the i.r. spectra of the activated alkali exchanged MFI, FAU(X) and Cs-FAU(X2) molecular sieve catalysts (not shown) only bands were observed attributed to SiOH groups at the outside of the crystallites and at lattice defects [29]. No indication of extra framework alumina (AlOH), assigned to an i.r. band at 3664 cm^{-1} [29], or Brönsted acid sites, assigned to i.r. bands between $3610\text{--}3590\text{ cm}^{-1}$, are observed. This indicates that the ion exchange has been complete and the protons at Brönsted acid sites have been exchanged for Na^+ and Cs^+ . With Na-FAU(X) small residual bands at 1480 and 1430 cm^{-1}

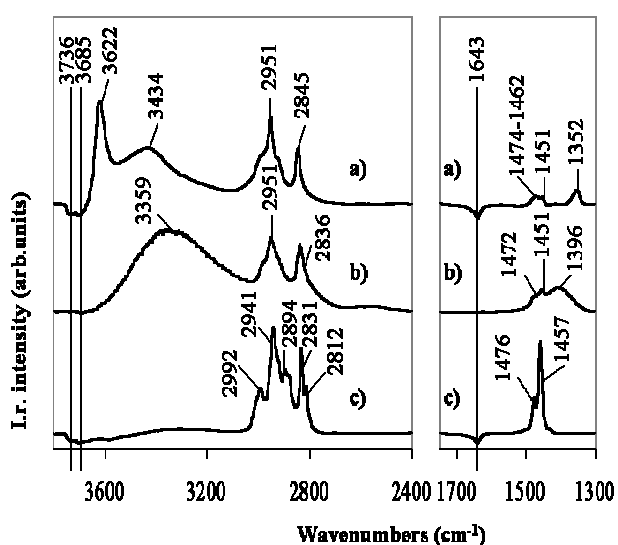


Figure 6.1: MeOH and DME adsorption on Na-MFI and Na-FAU(X). Top: MeOH adsorption on Na-MFI (4x enlarged) (a); middle: MeOH adsorption on Na-FAU(X) (b); bottom: DME adsorption on Na-MFI (4x enlarged) (c).

were observed attributed to surface carbonates. With Cs-FAU(X2) a sharp band at 3585 cm^{-1} is observed, indicating the presence of freely vibrating OH groups associated with an alkali cation. A similar band was reported by Karge *et al.* for a Cs^+ exchanged FAU(X) zeolite [30]; no explanation for this band was given.

I.r. results obtained in present study for the MeOH and DME reaction over basic zeolites are compared to results obtained for silica, silicalite-1 and γ -alumina (see Appendix 1). The results with silica, silicalite-1, and γ -alumina agree well with literature.

MFI and FAU(X) based materials: Methanol and dimethyl ether adsorption and reaction

a) Adsorbate physisorption on MFI and FAU(X) materials

Fig. 6.1 shows the i.r. spectra obtained during methanol adsorption on Na-MFI (a) and Na-FAU(X) (b). In Table 6.1 the observed i.r. bands upon methanol (MeOH) adsorption are listed together with reported i.r. wavenumbers of gaseous [31] and liquid phase MeOH [32]. Also the i.r. absorption results obtained during MeOH adsorption on the Cs^+ analogues are listed in Table 6.1. Fig. 6.1c shows the i.r. spectrum of dimethyl ether (DME) adsorbed on Na-MFI. Note that no bands

29. Kubelková, L.; Nováková, J.; Nedomová, K. *J. Catal.* **1990**, *124*, 441.

30. Concepción-Heydorn, P.; Jia, C.; Herein, D.; Pfänder, N.; Karge, H.G.; Jentoft, F.C. *J. Mol. Catal. A: Chem.* **2000**, *163*, 227.

31. Serrallach, A.; Meyer, R.; Günthard, Hs.H. *J. Mol. Spectrosc.* **1974**, *52*, 94.

between 3700-3100 cm^{-1} were observed during DME adsorption on Na-MFI and Na-FAU(X) at 323 K attributable to hydroxy groups. This is related to the fact that DME does not have this functional group. Since only small differences were observed during DME adsorption on Na-MFI and Na-FAU(X), only the i.r. spectrum of DME adsorbed on Na-MFI is shown. In Table 6.2 the observed i.r. bands upon DME adsorption on Na-MFI and Na-FAU(X) are compiled. Table 6.2 also lists observed i.r. bands of gaseous [33] and solid state DME [34], and in CCl_4 solution [35]. In agreement with earlier assignments [36,37] the observed bands are attributed to methanol hydroxy group vibrations (3622-3100 cm^{-1}), stretching vibrations of the methyl group of adsorbed methanol or dimethyl ether (3000-2840 cm^{-1}), OH deformation vibrations or COH bending vibrations (1400-1350 cm^{-1}) and CH deformation vibrations of the methyl group of adsorbed methanol or dimethyl ether (1480-1450 cm^{-1}) (see also Ref. [38,39,40]). The negative band observed at 3685 and 1643 cm^{-1} in the spectra of Na-MFI is attributed to desorbing water ($\nu_{\text{OH}}(\text{H}_2\text{O})$ and $\delta_{\text{OH}}(\text{H}_2\text{O})$, respectively) [41], which had been readsorbed after activation. The negative band at 3736 cm^{-1} is attributed to surface silanol interacting with the adsorbate.

b) Reaction in the presence of methanol:

In Fig. 6.2 the i.r. spectra obtained during methanol temperature programmed reaction are shown. In Fig. 6.3 the region of the methyl stretching vibration is shown enlarged. At 388 K (see Fig. 6.2), methanol adsorption on Na^+ exchanged MFI showed no other distinct differences, compared to the spectra obtained at 323 K (see Fig. 6.2), than the lower intensities of all bands and that the band at 3434 cm^{-1} almost disappeared. This decrease is caused by desorption of physisorbed methanol from the zeolite pores. At increasing temperatures ($T > 560$ K), the evolution of new bands at 2957 and 2855 cm^{-1} was observed for Na-MFI as evidenced by a shift of the CH stretching vibrations to higher wavenumbers (see Fig. 6.3) and the concomitant loss of the MeOH hydroxy stretching vibration (3622-3614 cm^{-1}) (see Fig. 6.2). At 616 K the CH stretching vibrational bands were the only visible, i.e., the MeOH OH stretching vibration was no longer observed. In Fig. 6.3 these newly formed bands are shown more clearly. These new bands were stable up to 773 K in a methanol flow; in absence of

32. Falk, M.; Whalley, E.; *J. Chem. Phys.* **1961**, *134*, 1554.

33. a) Shimanouchi, T. *Tables of Molecular Vibrational Frequencies Consolidated*, Vol. 1, Nat. Bureau Stand., 1972; b) Blom, C.E.; Altona, C.; Oskam, A. *Mol. Phys.* **1977**, *34*, 557; c) Labarre, P.; Forel, M.T.; Bessis, G. *Spectrochim. Acta* **1968**, *24A*, 2165.

34. a) Snyder, R.G.; Zerbi, G. *Spectrochim. Acta* **1967**, *23A*, 391; b) Allan, A.; McKean, D.C.; Perchard, J.-P.; Josien, M.-L. *Spectrochim. Acta* **1971**, *27A*, 1409.

35. Kanazawa, Y.; Nukada, K. *Bull. Chem. Soc. Jpn.* **1962**, *35*, 612.

36. a) Chapter 4 of this thesis; b) Rep, M.; Palomares, A.E.; Eder-Mirth, G.; Van Ommen, J.G.; Rösch, N.; Lercher, J.A. *J. Phys. Chem. B* **2000**, *104*, 8624.

37. Mirth, G.; Lercher, J.A.; Anderson, M.W.; Klinowski, J. *J. Chem. Soc., Faraday Trans.* **1990**, *86*, 3039.

38. Socrates, G. *Infrared Characteristic Group Frequencies*, 2nd Edition; John Wiley and Sons: Chichester, 1994.

39. Colthup, N.B.; Daly, L.H.; Wiberley, S.E. *Introduction to Infrared and Raman Spectroscopy*, 3rd Edition; Academic Press: San Diego, 1990.

40. Herzberg, G. *Molecular Spectra and Molecular Structure. II. Infrared and Raman Spectra of Polyatomic Molecules*, 10th Edition; D. van Nostrand Company, Inc.: Princeton, 1962.

41. Jentys, A.; Warecka, G.; Derewinski, M.; Lercher, J.A. *J. Phys. Chem.* **1989**, *93*, 4837.

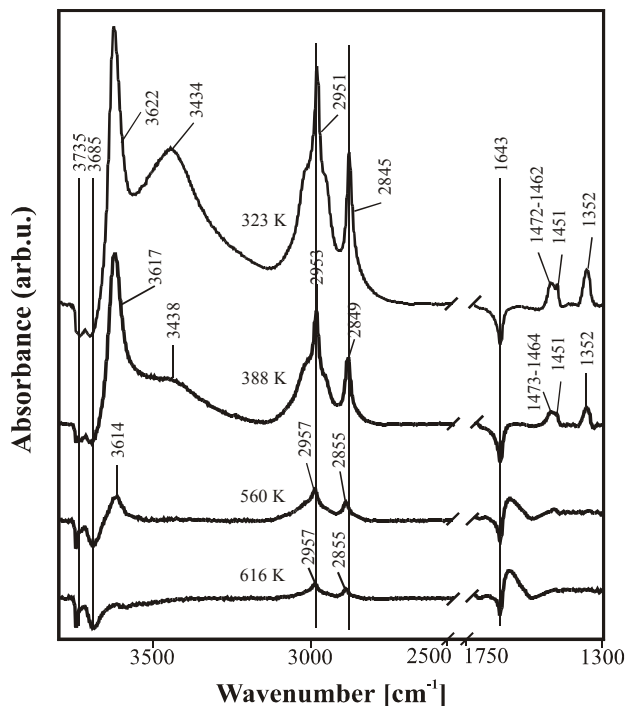


Figure 6.2: Adsorption and reaction of methanol over Na-MFI (reaction conditions: 10 mbar MeOH in 19 ml.min⁻¹ He: 323-773 K, T_r = 5 K.min⁻¹).

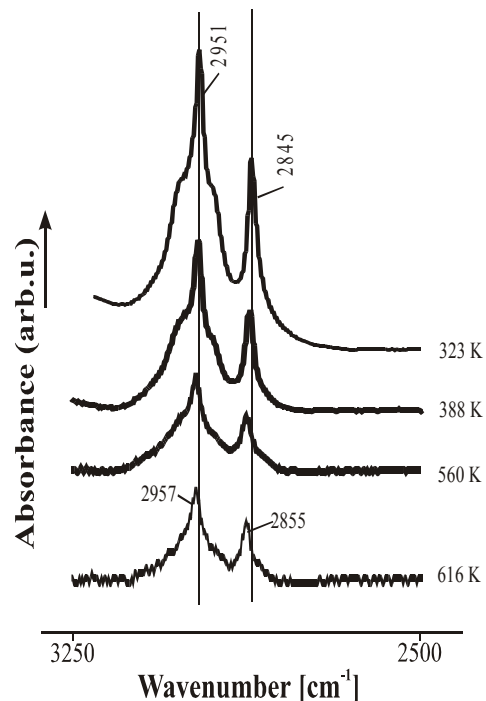


Figure 6.3: Methyl group stretching vibration at different temperatures on Na-MFI (for reaction conditions see Fig. 6.2).

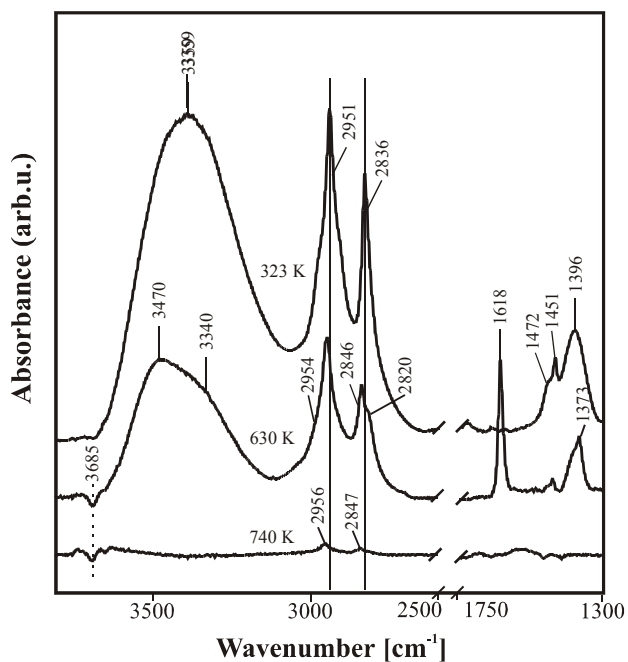


Figure 6.4: Adsorption and reaction of methanol over Na-FAU(X) (for reaction conditions see Fig. 6.2).

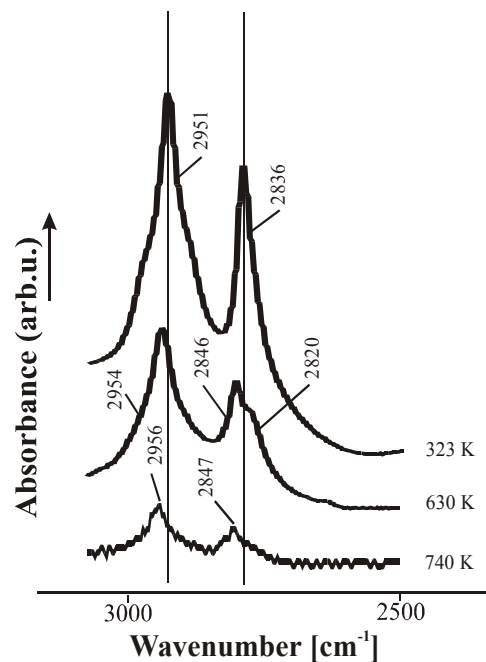


Figure 6.5: Methyl group stretching vibration at different temperatures on Na-FAU(X) (for reaction conditions see Fig. 6.2).

TABLE 6.1: Vibrational frequencies (cm^{-1}) of methanol (gas and liquid phase) compared with adsorbed methanol^a.

Adsorbate	Reference	Vibrational frequencies of molecular methanol
Methanol (g)	31	3682 ^b , 2999 ^c , 2970 ^c , 2920 ^d , 2844 ^e , 1477 ^f , 1465 ^f , 1454 ^f , 1340 ^g
Methanol (l)	32	3337 ^b , 2934 ^c , 2822 ^c , 1475 ^f , 1453 ^f , 1420 ^g
Materials used	Vibrational frequencies of surface species derived after methanol adsorption	
Silica (ref. F5)		3700-2700 ^b (br) ^b , 3003 ^c , 2997 ^c , 2970 ^c , 2954 ^c , 2920 ^d , 2847 ^e , 1472 ^f , 1463 ^f , 1452 ^f , 1380 ^g
Silicalite-1		3700-3233 ^b (br) ^b , 2946 ^c , 2840 ^e , 1470 ^f , 1450 ^f , 1347 ^g
Na-MFI		3622 ^b , 3434 ^b , 2995 ^c , 2951 ^c , 2923 ^d , 2845 ^e , 1474 ^f , 1462 ^f , 1451 ^f , 1352 ^g
Cs-MFI		3621 ^b , 3495 ^b , 2989 ^c , 2949 ^c , 2921 ^d , 2843 ^e , 1474 ^f , 1466 ^f , 1451 ^f , 1350 ^g
Na-FAU(X)		3359 ^b , 2951 ^c , 2836 ^e , 1472 ^f , 1451 ^f , 1396 ^g
Cs-FAU(X)		3242 ^b , 2979 ^c , 2946 ^c , 2914 ^d , 2833 ^e , 1478 ^f , 1453 ^f , 1408 ^g
Cs-FAU(X2)		3250 ^b , 2979 ^c , 2943 ^c , 2913 ^d , 2831 ^e , 1476 ^f , 1451 ^f , 1418 ^g
γ -Alumina (ref. 000-1.5E)		3700-2500 (br) ^j , 2994 ^c , 2964 ^c , 2945 ^c , 2903 ^d , 2844 ^e , 2823 ^e , 1490-1350 ^{f,g}

^a At 323 K (10 mbar in 19 ml/min He); presented i.r. absorption maxima were obtained when methanol adsorption-desorption is reached.

^b Methanol OH stretching vibration, $\nu(\text{OH})$; ^c asymmetric CH_3 stretching vibration, $\nu_{\text{as}}(\text{CH})$; ^d overtones or combination of methyl deformation modes; ^e symmetric CH_3 stretching vibration, $\nu_s(\text{CH})$; ^f CH_3 deformations $\delta(\text{CH})$; ^g OH deformations $\delta(\text{OH})$ (see also Ref. [38-40]).

^h Weak hydrogen bonding of the silica surface hydroxy groups with the hydroxy group of methanol (very broad): maxima at approximately 3620, 3496, and 3350 cm^{-1} ; negative band is observed at 3744 cm^{-1} .

ⁱ Weak hydrogen bonding between MeOH molecules adsorbed on the walls of silicalite-1 (very broad): maxima at approximately 3496 cm^{-1} ; weakly perturbed, freely vibrating MeOH hydroxy group at 3627 cm^{-1} .

^j Weak hydrogen bonding of the γ -alumina surface hydroxy groups with the hydroxy group of methanol (very broad): maximum at approximately 3298 cm^{-1} ; negative band is observed at 3734 and 3687 cm^{-1} .

TABLE 6.2: Vibrational frequencies (cm^{-1}) of dimethyl ether (gas, liquid and solid phase) compared with adsorbed dimethyl ether^a.

Adsorbate	Reference	Vibrational frequencies of molecular dimethyl ether
Dimethyl ether (g)	33	2996 ^b , 2952 ^b , 2925 ^b , 2817 ^c , 1470-1456 ^d , 1248 ^e , 1179 ^e , 1102 ^f
Dimethyl ether (CCl ₄ sol.)	35	2985 ^b , 2918 ^g , 2880 ^g , 2864 ^g , 2813 ^c , 1470 ^d , 1464 ^d , 1454 ^d , 1240 ^e , 1167 ^e , 1094 ^f
Dimethyl ether (solid)	34	2993 ^b , 2989 ^b , 2953 ^b , 2923 ^b , 2893 ^g , 2877 ^g , 2826 ^c , 2819 ^c , 1484 ^d , 1470 ^d , 1463 ^d , 1450 ^d , 1432 ^d , 1250 ^e , 1165 ^e , 1092 ^f
Materials used		
Vibrational frequencies of surface species derived after dimethyl ether adsorption		
Silica (ref. F5)		3700-2900 (br) ^h , 3005 ^b , 2997 ^b , 2982 ^b , 2939 ^b , 2928 ^b , 2894 ^g , 2877 ^g , 2831 ^c , 2813 ^c , 2805 ^c , 1476 ^d , 1459 ^d
Na-MFI		2992 ^b , 2941 ^b , 2929 ^b , 2918 ^b , 2894 ^g , 2880 ^g , 2831 ^c , 2812 ^c , 1476 ^d , 1457 ^d
Na-FAU(X)		2993 ^b , 2937 ^b , 2924 ^b , 2918 ^b , 2894 ^g , 2876 ^g , 2825 ^c , 1475 ^d , 1457 ^d
γ -Alumina (ref. 000-1.5E)		3750-2630 (br) ⁱ , 2994 ^b , 2957 ^b , 2942 ^b , 2926 ^b , 2897 ^g , 2877 ^g , 2830 ^c , 2803 ^c , 1475 ^d , 1459 ^d , 1249 ^e , 1162 ^e

^a At 323 K (10 mbar in 45 ml/min He); presented i.r. absorption maxima were obtained when dimethyl ether adsorption-desorption is reached.

^b Asymmetric CH₃ stretching vibration, $\nu_{\text{as}}(\text{CH})$; ^c symmetric CH₃ stretching vibration, $\nu_{\text{s}}(\text{CH})$; ^d CH₃ deformations, $\delta(\text{CH})$; ^e CH₃ rocking vibrations, $\gamma(\text{CH})$; ^f asymmetric C-O stretching vibration, $\nu_{\text{as}}(\text{CO})$; ^g overtones or combination of methyl deformation modes (see also Ref. [38-40]).

^h Weak hydrogen bonding of the silica hydroxy groups with the oxygen of DME (very broad): maximum at approximately 3298 cm^{-1} ; negative bands are observed at 3745 cm^{-1} .

ⁱ Hydrogen bonded γ -alumina surface hydroxy groups with the oxygen of DME (very broad): maximum at approximately 3362 cm^{-1} ; negative bands are observed at 3734 and 3692 cm^{-1} .

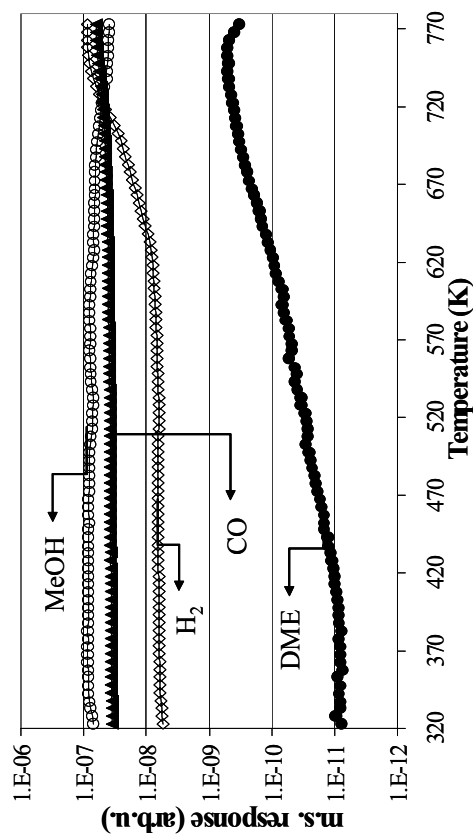


Figure 6.6: Gas phase composition as function of temperature over Na-MFI (for reaction conditions see Fig. 6.5).

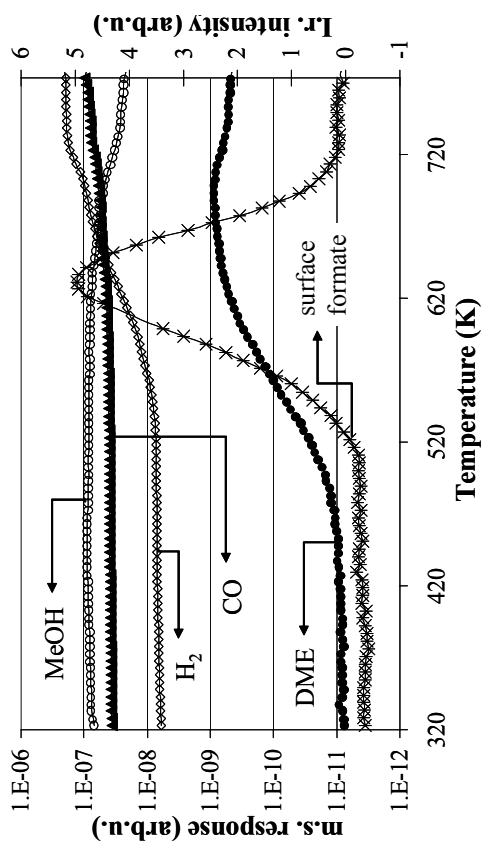


Figure 6.7: Gas phase composition as function of temperature over Na-FAU(X) (for reaction conditions see Fig. 6.5).

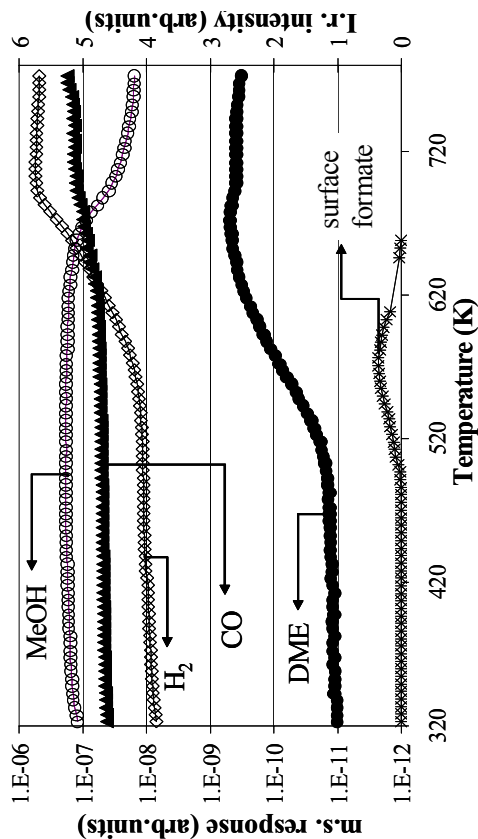


Figure 6.8: Gas phase composition as function of temperature over Cs-FAU(X) (for reaction conditions see Fig. 6.5).

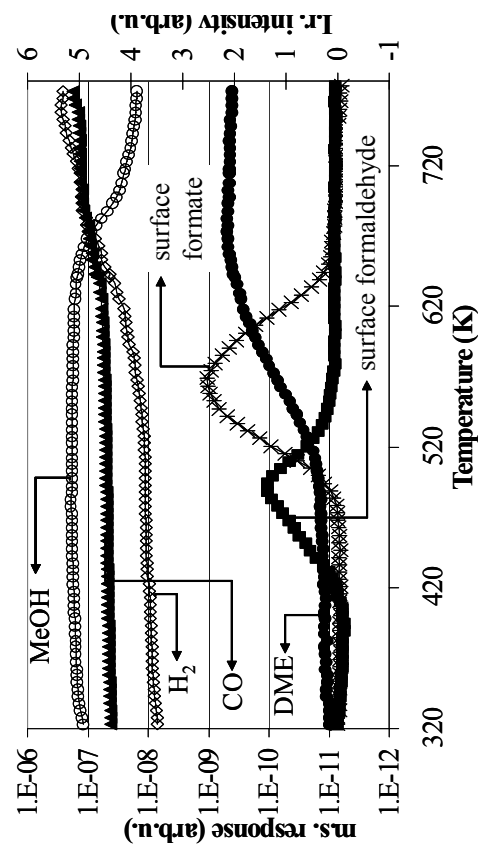


Figure 6.9: Gas phase composition as function of temperature over Cs-FAU(X2) (for reaction conditions see Fig. 6.5).

methanol these groups immediately disappeared. No other surface species, such as surface hydroxy groups resulting from the abstraction of a proton from methanol were observed. For Cs-MFI, the bands corresponding to surface methoxy were found at 2956 and 2853 cm^{-1} (not shown here).

During the temperature programmed reaction of methanol over both alkali exchanged FAU(X) catalysts, we also observed the evolution of surface methoxy groups at 2820 (Na-FAU(X)) (see Fig. 6.4 and 6.5 at 630 K) and 2804 cm^{-1} (Cs-FAU(X)) (not shown here) at approximately 570 K. With Cs-FAU(X2) the band assigned to surface methoxy groups was found at 2807 cm^{-1} (not shown here). Only the symmetric stretching vibration bands of the surface methoxy groups were observed, since these were clearly present as a shoulder on the large methanol methyl i.r. peak of molecularly sorbed methanol (see Fig. 6.4 and 6.5). The asymmetric stretching vibration bands of the surface methoxy groups (at approximately 2961 cm^{-1}) are hidden under the large methanol methyl i.r. band of molecularly adsorbed methanol. At 773 K vibrational i.r. bands at 2956 and 2847 cm^{-1} also assigned to surface methoxy groups were the only visible (see Fig. 6.5, where we show these bands at 740 K). The negative band observed at 3685 cm^{-1} in the spectra of Na-FAU(X) (Fig. 6.4) is attributed to desorbing water ($\nu_{\text{OH}}(\text{H}_2\text{O})$) [42], which had been readsorbed after activation. The newly observed methoxy bands at 2820-2804 cm^{-1} on Na-FAU(X), Cs-FAU(X), and Cs-FAU(X2) coincide very closely with those observed during methanol dehydrogenation over γ -alumina (see Appendix 1).

Gas phase analysis showed the presence of dimethyl ether starting at 404 K over Na-MFI (see Fig. 6.6). DME production over Cs-MFI was observed at 463 K (not shown here). With Na- and Cs-FAU(X), the presence of DME was found at 453 (see Fig. 6.7) and 498 K (see Fig. 6.8), respectively. Also with Cs-FAU(X2) was gaseous DME found starting at 498 K (see Fig. 6.9), while a small i.r. band appeared at 2863 cm^{-1} that is assigned to adsorbed DME at 570 K (not shown here). The production of dimethyl ether is observed at lower temperatures compared to the observation of surface methoxy groups. This is related to the fact that the i.r. vibrational bands of surface methoxy groups are hidden under the large methanol methyl i.r. band of molecularly adsorbed methanol. In the absence of MeOH the DME production stopped.

At around 510 K new i.r. bands were observed at 1618 (Na-FAU(X)), 1611 (Cs-FAU(X)) and 1614 (Cs-FAU(X2)) cm^{-1} , which increased with increasing temperatures. Figure 6.4 shows the new i.r. vibration band at 1618 cm^{-1} in the spectrum recorded at 630 K (maximum i.r. intensity) during MeOH reaction over Na-FAU(X). These new bands were assigned to the formation of surface formate (the asymmetric stretching vibration), in accordance with literature [26a]. (The symmetric stretching vibration of surface formate was observed as a shoulder on the MeOH deformation band at 1371-1345 cm^{-1} .) In Fig. 6.7 the i.r. intensity of surface formate (band at 1618 cm^{-1}) as function of temperature is shown. The i.r. intensity of the respective symmetric stretching vibration of formate on Cs-FAU(X) and Cs-FAU(X2) as function of temperature is shown in Fig. 6.8 and 6.9 (maximum intensities at 570-576

42. Bertsch, L.; Habgood, H.W. *J.Phys. Chem.* **1963**, *67*, 1621.

K for both Cs⁺ exchanged zeolites). The formate band was much more intensive for Na-FAU(X) and smallest with Cs-FAU(X). The appearance of surface formate on these catalysts is indicative of MeOH dehydrogenation, yielding formaldehyde [26d]. In the case of Cs-FAU(X2), we did also observe the formation of a carbonyl group at 1716 cm⁻¹ (see Fig. 6.10) (between 423 and 583 K; maximum surface concentration at 490 K), which only decreased in intensity when the formation of surface formate (band at 1614 cm⁻¹) is observed (see Fig. 6.9 and 6.10). Note that other forms of adsorbed formaldehyde during MeOH reaction over Na- and Cs-FAU(X) and Cs-FAU(X2), i.e., polymerised formaldehyde, characterized by bands between 1486 and 1377 cm⁻¹ [16], were not observed. In contrast to other studies (see Chapter 8 and Ref. [26d]), formaldehyde was not observed in the gas phase over Na- and Cs-FAU(X), and Cs-FAU(X2) and could be related to the fast surface decomposition to formate and, subsequently, to CO and H₂. On alkali exchanged MFI zeolites bands attributed to surface formaldehyde and/or surface formate were not observed.

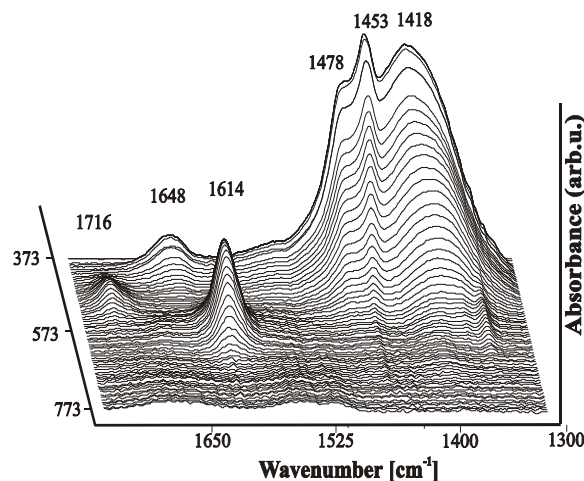


Figure 6.10: I.r. spectra obtained during the reaction of MeOH over Cs-FAU(X2). $T = 373\text{--}673\text{ K}$; $T_r = 5\text{ K}\cdot\text{min}^{-1}$.

Figures 6.7 to 6.9 show the gas phase composition of the effluent gas after MeOH reaction over Na- and Cs-FAU(X) and Cs-FAU(X2). Gas phase H₂ production started at 543 K over Na-FAU(X), at 538 K over Cs-FAU(X), and at 538 K over Cs-FAU(X2), respectively, and coincides closely with the formation of surface formate. During MeOH reaction over Na-FAU(X), gaseous CO was observed from 633 K and increases with decreasing surface formate i.r. intensity (see Fig. 6.7). Gaseous CO was observed starting from 620 K with Cs-FAU(X) (see Fig. 6.8) and Cs-FAU(X2) (see Fig. 6.9). These temperatures are slightly higher, compared to the temperature where the maximum formate i.r. intensity is observed. This probably is due to the low surface formate concentration, making detection of CO difficult. Also with Na-MFI, H₂ production was observed starting at 620 K (see Fig. 6.6). This is related to the formation of coke deposits. Gas phase analysis showed that methanol reaction over Cs-FAU(X) yielded CO and H₂ at lower reaction temperatures and larger concentrations than over Na-FAU(X), this in contrast to DME production over these materials.

MeOH reaction over Na⁺ and Cs⁺ exchanged MFI and FAU(X) zeolites were performed in a fixed bed flow reactor to quantify the gas phase composition of the product stream. Note that this can be different from what we find in the i.r. reactor, which is supposed to be a CSTR reactor. In Table 6.3 the results from the temperature programmed reaction in the fixed bed reactor are compiled.

From Table 6.3 it becomes clear that basic MFI catalysts produce more DME, while basic FAU(X) catalysts produce more CO and H₂. The large production of H₂ with Na-MFI is related with the formation of coke deposits.

TABLE 6.3: MeOH conversion (%), and DME and H₂ yield (mol%) and selectivity (mol%) over alkali exchanged MFI, FAU(X) and Cs-FAU(X2) (between brackets is listed the selectivity) in the fixed bed reactor compared to the electrostatic potential of the alkali cation (e/r) and the calculated average charge on the zeolite framework oxygen ($-\delta_O$).

	Zeolite				
	Na-MFI	Cs-MFI	Na-FAU(X)	Cs-FAU(X)	Cs-FAU(X2)
Gas phase composition at 653 K^a					
MeOH conv.	75	55	40	12	6.6
DME yield	8.9 (12)	5.6 (10.4)	4.8 (12)	0.4 (3.7)	0.3 (6)
H ₂ yield	5.6 (7.4)	0.9 (1.7)	9 (23)	8.2 (70.1)	1.4 (25)
e/r (\AA^{-1})	1.05	0.59	1.05	0.59	0.59
$-\delta_O^b$	0.162	0.168	0.317	0.384	0.33

^a: Reaction conditions: W/F = 96.7 g.h.mol⁻¹; WHSV = 0.331 h⁻¹.

^b: $-\delta_O$ is average negative charge calculated using Equations 2.1 and 2.2 shown in Chapter 2.

In Appendix 1, methanol reaction over acidic silica, neutral silicalite-1, and amphoteric γ -alumina is described. Results obtained with these materials are similar as in literature. MeOH reaction over silica yielded surface methoxy groups, whereas reaction over γ -alumina yielded besides surface methoxy groups also surface formate in analogy with basic FAU(X). Similar low wavenumbers for the methoxy groups were found on γ -alumina as on basic FAU(X) and these were found to decrease with increasing surface formate concentration. A clear relation between the disappearance of surface methoxy and appearance of surface formate was established (see Appendix 1).

c) Reaction in the presence of dimethyl ether:

In Fig. 6.1c the i.r. spectrum of adsorbed dimethyl ether on Na-MFI is shown (10 mbar at 323 K). By increasing the temperature in the presence of dimethyl ether over Na-MFI, bands at 2995 (partially), 2894 and 2813 cm⁻¹ disappeared, indicating that these bands partially correspond to a weaker form of adsorption. The disappearance of the remaining bands, at higher temperatures (723 K), revealed the presence of a broad band with maxima at 2957, 2903, and 2847 cm⁻¹ (see Fig. 6.11, where we show the i.r. spectrum (3100-2700 cm⁻¹)) of MeOH and DME on Na-MFI at 773 K). The shape and width at half height of this band is almost similar to those observed at the same temperature for methanol reaction over Na-MFI molecular sieves although the bands are more intense (the area under the broad band was 2x larger) (see Fig. 6.11); this agrees well with the presence of two methyl groups in DME. These new bands are stable up to 773 K (in the presence of DME). The additional absorption maximum around 2903 cm⁻¹ during DME reaction, compared to MeOH reaction, indicates surface methoxy groups on different (extra) lattice atoms. During reaction no hydroxy groups are observed.

Upon heating Na-FAU(X) in the presence of dimethyl ether (not shown here), similar features are observed as described for dimethyl ether reaction over Na-MFI. At approximately 673 K, a broad band between 3060-2760 cm^{-1} was observed without fine structure (a shoulder could be observed at 2820 cm^{-1}). No other surface species, such as surface formaldehyde or formate, were observed. During reaction no hydroxy groups are observed. Most interestingly, with DME reaction over Na-FAU(X) no bands at 1618-1611 cm^{-1} are observed, this in contrast to MeOH reaction over Na-FAU(X).

Dimethyl ether reaction over silica (as described in Appendix 1) yielded also surface methoxy groups, whereas reaction over γ -alumina yielded surface methoxy groups and surface formate, this in contrast to DME reaction over basic FAU(X). Apparently, basic "surface" hydroxyl groups are needed for the abstraction of methyl hydrogen (see Appendix 1).

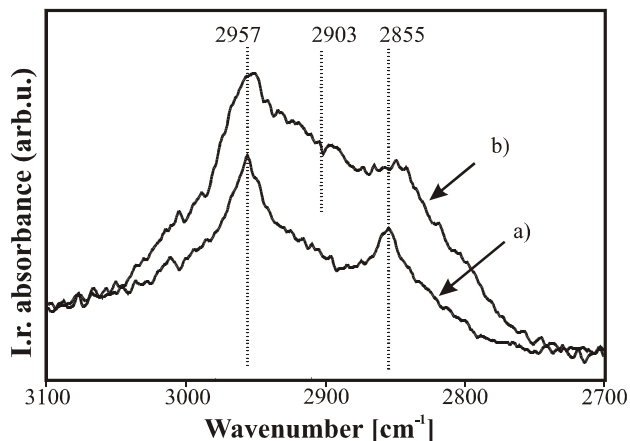


Figure 6.11: *I.r. spectra of the surface species during a) methanol and b) dimethyl ether reaction over Na-MFI at 773 K. Note the similarity in band shape indicating the formation of surface methoxy groups.*

Formaldehyde adsorption on alkali exchanged FAU(X) and MFI zeolites

To further aid the identification of surface species formed during methanol reaction over alkali exchanged FAU(X) zeolites formaldehyde (CH_2O) adsorption was performed. CH_2O adsorption on Cs-FAU(X) at 323 K (see Fig. 6.12) shows clearly bands at 1711, and 1613 and 1345 cm^{-1} , which are attributed to adsorbed formaldehyde and surface formate, respectively [26a]. These bands were also observed during methanol decomposition over Na- and Cs-FAU(X), and Cs-FAU(X2); thus the observed carbonyl stretching vibration band observed at 1716 cm^{-1} with Cs-FAU(X2) is attributed to adsorbed formaldehyde and the bands observed between 1618 and 1611 cm^{-1} for the alkali exchanged FAU(X) and Cs-FAU(X2) are attributed to surface formate (see also Ref. [26a]).

Bands at 2961 and 2816 cm^{-1} were observed, simultaneously, with the observation of surface formate (bands at 1613 and 1345 cm^{-1}) and are assigned to surface methoxy groups. Those surface methoxy i.r. bands were quite weak and are, therefore, not shown. Additional bands on Cs-FAU(X) were observed at 2825 and 1504 cm^{-1} , which are assigned to stretching and deformation bands of the formaldehyde

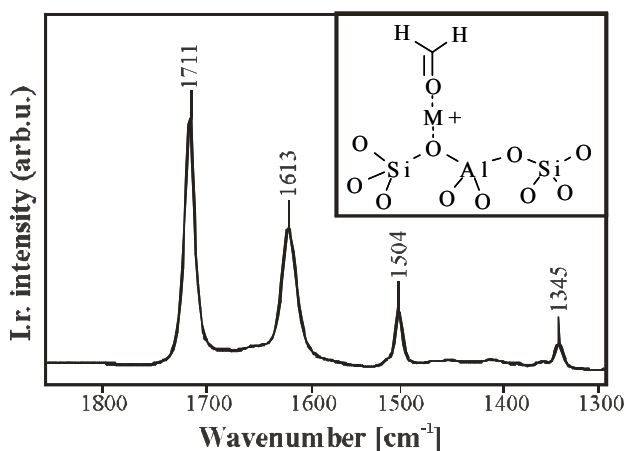


Figure 6.12: *Difference i.r. spectrum (1850-1300 cm^{-1}) of formaldehyde adsorption on Cs-FAU(X). Note the direct formation of formate (1613 cm^{-1}). $T=323$ K, $p=10^{-2}$ mbar. Inset: representation of the adsorbed species.*

CH₂ group, respectively. (Those bands are not listed in Table 6.4.)

Formaldehyde adsorption on K- and Rb-FAU(X) showed similar results as found for Cs-FAU(X). The results are compiled in Table 6.4 and are compared with the i.r. bands of free formaldehyde [43]. It can be seen from Table 6.4 that the shift of the carbonyl stretching vibration (ν_{CO}), compared to free formaldehyde, decreases with decreasing electrostatic potential of the alkali cation (see also Appendix 2). With Na-FAU(X) a much smaller shift of the formaldehyde carbonyl stretching vibration, compared to free formaldehyde and the other alkali exchanged FAU(X) zeolites was observed, indicating different interaction with the zeolite (see Appendix 2). Results presented here are in agreement with results reported by others [26a]. Additional bands on Na-FAU(X) were observed at 2903, 2843 and 1501 cm⁻¹. Surface methoxy groups were observed, simultaneously with the formation of surface formate, at 2961 and 2820 cm⁻¹.

TABLE 6.4: Wavenumbers (in cm⁻¹) of adsorbed formaldehyde and formate on M⁺ exchanged FAU(X) and MFI zeolites, compared to gas phase formaldehyde^a and free formate anion^b.

Zeolites	$-\delta_{\text{O}}^{\text{c}}$	e/r^{d} (Å ⁻¹)	Carbonyl stretch (ν_{CO}) formaldehyde	$\nu_{\text{as,CO}}$ formate	$\nu_{\text{s,CO}}$ formate	$\Delta\nu_{\text{formate}} =$ $\nu_{\text{as,CO}} - \nu_{\text{s,CO}}$
Formaldehyde	-	-	1743	-	-	-
Na-FAU(X)	0.317	1.05	1724	1613	1371	242
K-FAU(X)	0.358	0.75	1702	1600	1349	251
Rb-FAU(X)	0.378	0.67	1708	1611	1345	266
Cs-FAU(X)	0.384	0.59	1711	1613	1345	268
Na-MFI	0.162	1.05	1730,1709	n.o. ^e	n.o.	n.o.
Cs-MFI	0.168	0.59	1741,1726,1713	n.o.	n.o.	n.o.
Formate anion	-	-	-	1585	1351	234

^a From Ref. [43]. ^b From Ref. [44].

^c $-\delta_{\text{O}}$ is the calculated average charge on the zeolite framework oxygen.

^d e/r is the electrostatic potential (in Å⁻¹) of the cation.

^e Not observed.

I.r. signals during CH₂O adsorption on Na-MFI were observed at 1730 (most intensive) and 1709 cm⁻¹ and on Cs-MFI at 1741, 1726 (most intensive) and 1712 cm⁻¹ (see also Table 6.4) and are assigned to ν_{CO} of molecular, non-dissociated formaldehyde interacting with cations. The band at 1741 cm⁻¹ (observed for CH₂O adsorption on Cs-MFI) is attributed to formaldehyde interacting with the walls of the zeolite pores, since no difference is observed compared to gaseous CH₂O. I.r. bands that are

43. Glisenti, A. *J. Mol. Catal. A: General* **2000**, 153, 169.

assigned to the (a)symmetric stretching (ν_{CH}) and deformation (δ_{CH}) bands of the formaldehyde CH_2 group were observed at 2814 ($\nu_{\text{s,CH}}$) and 1503 (δ_{CH}) cm^{-1} (Cs-MFI) and at 2906 ($\nu_{\text{as,CH}}$), 2835 ($\nu_{\text{s,CH}}$) and 1506 (δ_{CH}) cm^{-1} (Na-MFI).

Table 6.4 also lists the wavenumbers observed for the asymmetric and symmetric C=O stretching vibration of the surface formate observed on basic FAU(X) zeolites. No systematic correlation of the i.r. bands of surface formate with the basicity of the zeolite framework or with the electrostatic potential of the extra framework alkali metal cation is apparent. This is tentatively affiliated with the surface formate structure (see also Ref. [26a]) and will be discussed more in detail in Appendix 3. In contrast to FAU(X) zeolites, where formaldehyde sorption immediately yielded surface formate and surface methoxy as observed with i.r. spectroscopy, no such surface species were observed upon CH_2O sorption on basic MFI zeolites. Also increasing temperatures did not show any formation of surface formate.

Catalytic testing: The influence of different MeOH concentrations

In a fixed bed flow reactor, the influence of different methanol concentrations was examined over Rb-FAU(X) at 698 K to establish the effect of different MeOH concentrations on the production of dimethyl ether and dihydrogen. As will be discussed later, two MeOH molecules are needed to react towards DME, while only one MeOH molecule is needed to dehydrogenate to formaldehyde. Thus DME production would be favored with increasing MeOH pressures, while MeOH dehydrogenation would be favored with decreasing MeOH pressures. Indeed it was found that selectivity towards DME increased with increasing methanol partial pressures: a 4 fold increase of MeOH feed resulted only in a 2 fold increase of H_2 production, whereas it resulted in a ~ 4 fold increase in DME production (in both cases approximately 20% MeOH is converted). This indicates a higher order in methanol in the rate of production of DME, compared to the rate of production of H_2 , as expected. Note that exact orders can not be determined since the catalyst was deactivating. This indicates that the same active surface groups are responsible for the dehydration and dehydrogenation of methanol, favoring dehydrogenation when only one methanol molecule is present. In Fig. 6.13 the effect of increasing MeOH is shown.

From a practical point of view, it needs to be said that all samples used showed severe coking of the catalysts; a very unfavourable carbon balance was found, meaning that less than 50% of the reacted MeOH was found back as H_2 (dehydrogenation) and DME (dehydration) as can be seen in

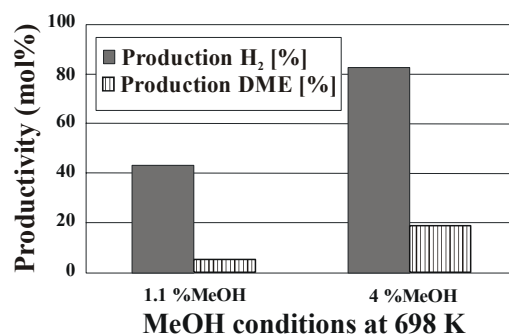


Figure 6.13: The effect of increasing MeOH partial pressures on the reaction selectivity over Rb-FAU(X) at 698 K.

Table 6.3. Results obtained during MeOH reaction over Cs-FAU(X) at 673 K (reaction time 4 hrs) in the i.r. flow reactor revealed the formation of a broad band between 1610-1570 and 1442-1334 cm^{-1} which are assigned to coke. The nature of the coke, i.e. aliphatic, aromatic and/or carbonylic, was not determined. The increased production of H_2 over Na- and Cs-MFI (with a decreasing DME production over Na-MFI) is attributed to the formation of coke on these samples.

Temperature programmed desorption of reactants and possible products

Here we discuss the t.p.d. spectra of methanol, dimethyl ether, formic acid, and formaldehyde desorption from Na^+ and Cs^+ exchanged FAU(X) and MFI zeolites. T.p.d. experiments were performed to examine adsorption strength of the different adsorbates, desorbing amounts, and decomposition products.

It was observed that the amount of MeOH desorbing from Na^+ exchanged zeolites was higher and MeOH desorption was still found to occur at higher temperatures ($T > 520$ K), compared to the Cs^+ exchanged zeolites, indicating higher adsorption capacity and some stronger adsorption sites compared to the Cs^+ homologues (see Fig. 6.14), in agreement with Chapter 4 (see also Ref. [36]). This is related to the higher electrostatic field in the Na^+ exchanged zeolites (see also Chapter 4 and Ref. [45]). The second maximum at approximately 570 K observed with Na-FAU(X), is slightly higher compared to Na-MFI, is related to the small positive contribution of the additional hydrogen bonding between the methanol hydroxy group and the zeolite framework oxygens of FAU(X) to the adsorption strength [45]. No other desorbing species are detected.

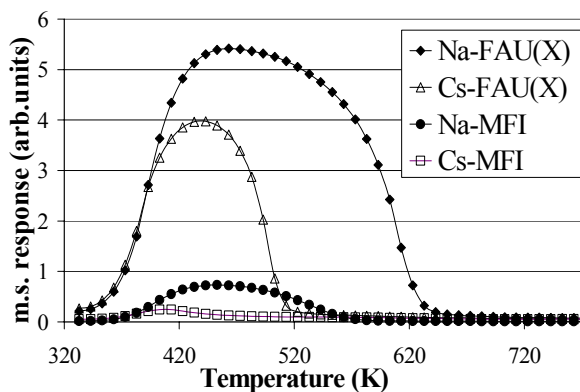


Figure 6.14: *T.p.d. of methanol adsorbed on Na-FAU(X), Cs-FAU(X), Na-MFI and Cs-MFI. All t.p.d. curves shown are normalised to the weight of the catalyst used.*

T.p.d. of dimethyl ether adsorbed on Cs-FAU(X) was observed at highest temperature and decreased in the order Cs-FAU(X) > Na-MFI > Cs-MFI indicating that some sites in Cs-FAU(X) interact strongest with dimethyl ether. This is shown in Fig. 6.15. Furthermore, the adsorption capacity of Cs-MFI, compared to Na-MFI, was much lower (this was also observed for MeOH desorption). The desorbing amount of DME from Cs-FAU(X) is much smaller, compared to MeOH, however, DME is much stronger bound as is indicated by the much higher desorption temperatures ($T_{\text{MeOH}} < 520$ K; $T_{\text{DME}} > 520$ K). The higher desorption temperature for DME compared to MeOH in Cs-FAU(X) is explained by the fact that in general an increase in interaction energy (of ~ 10 $\text{kJ}\cdot\text{mol}^{-1}$) and thus a higher

45. Vayssilov, G.; Lercher, J.A.; Rösch, N. *J. Phys. Chem. B* **2000**, *104*, 8614.

desorption energy is observed with increasing carbon number [46]. Comparison of DME and MeOH desorption from Na- and Cs-MFI showed slightly higher desorption temperatures for MeOH. The reason for this is not clear; maybe this is related to steric hindrance by the wall of the MFI pore (pore size approximately 5.1-5.6Å) and therefore has a low interaction energy with the alkali cation.

Formaldehyde desorption (t.p.d.) from Cs-FAU(X) yielded formaldehyde (483 K), as well as MeOH (603 K), CO (maxima: 533 and 613 K) and H₂ (633 K) (see Fig. 6.16). The maximum intensity of H₂ desorption was

observed later than the corresponding CO desorption and might indicate a surface migration of hydroxy groups. This cannot be observed during MeOH reaction (since MeOH dehydrogenation yields H₂).

T.p.d. of adsorbed CH₂O on Na-FAU(X) yielded mainly methanol (458 K) and CO (560 K). No H₂ or DME was observed. The production of MeOH and CO is clear evidence of the bimolecular *Cannizzaro* disproportioning [20,25b]. Temperature programmed desorption (t.p.d.) of formaldehyde adsorbed on Na-FAU(X) showed also the formation of methyl formate between 378 and 539 K (maximum at 454 K) (not shown here).

On Cs-FAU(X) this product species was not analyzed. The production of methyl formate will be discussed in Chapter 7.

Formic acid adsorption on Cs-FAU(X) monitored by i.r. spectroscopy yielded bands at 1612 and 1343 cm⁻¹ (together with a broad hydroxy band between 3700-3200 cm⁻¹), in good agreement with surface formate observed during the methanol decomposition over Cs-FAU(X). Thus we used formic acid (HCOOH) as a model compound for the surface formate obtained during MeOH reaction and performed formic acid t.p.d. experiments.

Temperature programmed desorption (t.p.d.) of formic acid adsorbed on Cs-FAU(X) yielded non-dissociated formic acid between 373 and 573 K (maximum at 433 K). In Fig. 6.17 (top spectrum)

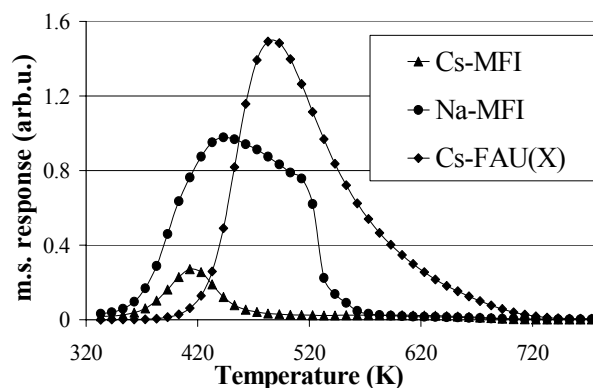


Figure 6.15: T.p.d. of DME adsorbed on Cs-FAU(X), Cs-MFI and Na-MFI. All t.p.d. curves shown are normalised to the weight of the catalyst used.

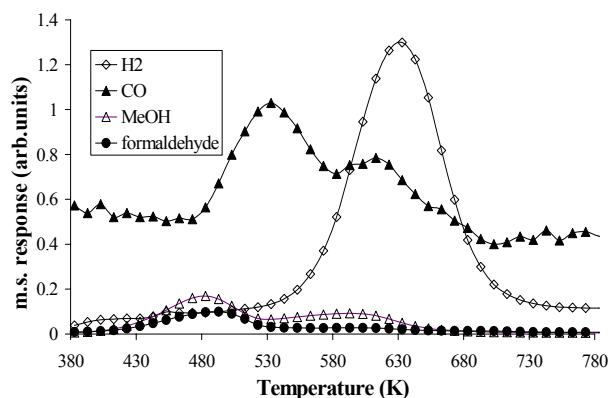


Figure 6.16: T.p.d. of formaldehyde adsorbed on Cs-FAU(X). Formaldehyde: m/z 29. MeOH: m/z 31. The higher starting response of CO is attributed to a background of N₂.

46. Avgul, N.N.; Bezus, A.G.; Dzhigit, O.M. In *Adv. Chem. Ser.-Molecular Sieve Zeolites*; Flanigen, E.M., Sand,

the evolution of the decomposition products H_2O , CO_2 , CO and H_2 during t.p.d. of HCOOH adsorbed on Cs-FAU(X) is shown. Production of CO_2 and H_2 was observed starting at 493 K and increased with increasing temperatures (maximum rate of formation at 610 K). The simultaneous production of CO_2 and H_2 indicates dehydrogenation of formic acid [47]. H_2O desorption is observed over the full range ($T = 323\text{-}973$ K), while CO production shows maxima at 543 and 663 K (starting at 420 K). H_2O and CO are the products of formic acid dehydration [47].

Desorption of formic acid from Na-FAU(X) shows the production of CO_2 and H_2 (maximum rate of formation at 633K) (see Fig. 6.17 (bottom spectrum)). Increasing CO_2 and H_2 concentration is already observed at 543 K. H_2O desorption is observed over the full range

($T = 323\text{-}973$ K). CO is observed as a broad band between 443 and 723 K with desorption rate maxima at 593 and 653 K. Non-dissociated formic acid is observed between 353 and 623 K (maximum at 423 K). Comparison of the t.p.d. spectra of formic acid adsorbed on Na- and Cs-FAU(X) (see Fig. 6.17) indicates a higher activity for HCOOH dehydrogenation (production of CO_2 and H_2) of Cs-FAU(X), compared to Na-FAU(X), indicated by the lower starting temperatures and higher concentrations (at lower temperatures). For dehydration of formic acid a higher activity was found for Na-FAU(X).

6.4 DISCUSSION

Adsorbate adsorption on MFI and FAU(X) materials

The i.r. spectra obtained during the adsorption of methanol (Fig. 6.1a and b) and dimethyl ether (Fig. 6.1c) at 323 K suggest clustering of the adsorbate inside the Na-MFI and Na-FAU(X) pores as expected for the high partial pressure (10 mbar). This is indicated by the presence of the broad

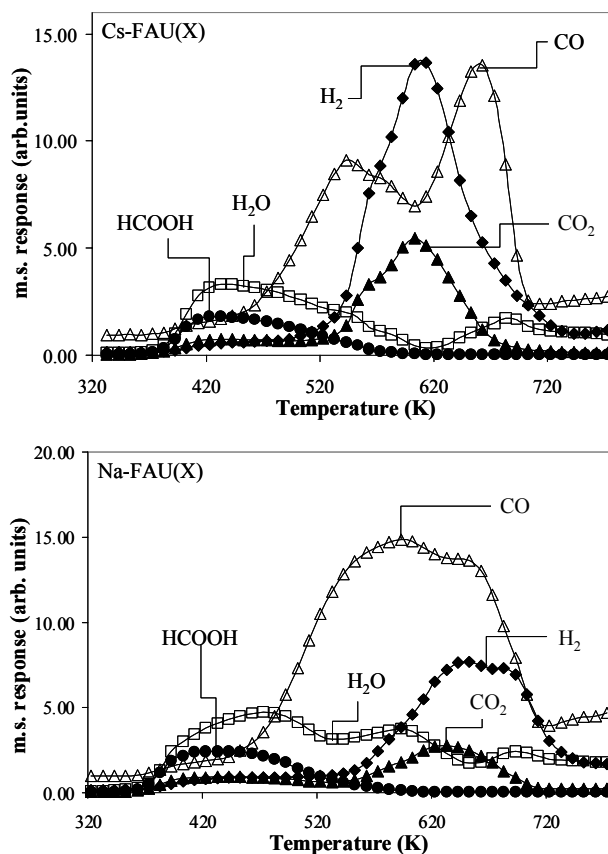


Figure 6.17: Temperature programmed desorption and decomposition of formic acid; comparison of the peak intensities of CO and H_2O (HCOOH dehydration) and CO_2 and H_2 (HCOOH dehydrogenation) from Cs-FAU(X) (Top), and Na-FAU(X) (Middle).

MeOH OH band at 3434 and 3495 cm^{-1} with Na- and Cs-MFI and a shift of approximately 10 cm^{-1} was observed for the weakly perturbed hydroxyl bands and CH_3 stretching vibrations of MeOH on Na- and Cs-MFI, and on Na- and Cs-FAU(X) and agrees well with the adsorption study reported in Chapter 4. Mirth *et al.* reported similar results [37].

Adsorption and/or reaction studies of dimethyl ether over alkali cation exchanged zeolites [48] are rare. Since increasing temperatures in the presence of dimethyl ether over Na-MFI and Na-FAU(X) to 420 K, led to the disappearance of bands at 2995 (partially), 2894 and 2813 cm^{-1} (while others remained), it was concluded that these bands partially also correspond to a weaker form of adsorption (probably to clustered dimethyl ether (in agreement with the i.r. spectrum of solid DME and DME/ CCl_4 -solution [34,35])) inside the pores. The multiplicity of DME vibrational i.r. bands in the i.r. spectrum compared to MeOH adsorption corresponds to a larger number of overtones or combinations of deformation methyl modes in the i.r. spectrum.

MeOH and DME are adsorbed via their oxygen lone pairs on the alkali cations (see also Ref. [36,37,45,48]). T.p.d. experiments show a dominant role of the cation in the adsorption strength, in spite of the increased surface basicity (see Fig. 6.14 and 6.15). The features observed in the hydroxy stretching vibration region of methanol (3700-3100 cm^{-1} ; see Fig. 6.1 and Table 6.1) can be explained as follows. (1) The sharp band and small downward shift of the methanol OH group on Na-MFI, at 3622 cm^{-1} (see Fig. 6.1a and Table 6.1), compared to gas phase methanol [31], indicate no hydrogen bonding with the zeolite framework and is assigned to the terminal OH group of chain-like methanol clusters [36]. (2) The broad band, observed with maxima at 3434 and 3495 cm^{-1} for methanol on Na- and Cs-MFI (see Table 6.1), respectively, is attributed to chain-like methanol clusters inside the zeolite pores [36]; the large difference between the observed maxima in Na- and Cs-MFI is attributed to the lower methanol adsorption capacity at 10 mbar of Cs-MFI (2.47 or 1.66 mmol MeOH per gram Na- or Cs-MFI zeolite, respectively) [36]. This was also observed during MeOH desorption experiments. Similar observations were done for MeOH clusters surrounding bare Na^+ and Cs^+ cations [49]. (3) The large half width and downward shift of the stretching vibration of the methanol OH group in the Na-FAU(X), Cs-FAU(X) and Cs-FAU(X2) samples (see Fig. 6.1b and Table 6.1) indicate hydrogen bonding of the methanol hydroxy group with the pore walls and neighboring adsorbed methanol molecules (see also Chapter 4).

The increased broadening of the methanol CH_3 (a)symmetric stretching vibration (between 3000-2800 cm^{-1}) on Na- and Cs-FAU(X) and Cs-FAU(X2), compared to those observed on Na- and Cs-MFI, can be caused by steric hindrance of the CH group at these high methanol loadings. Similar trends were observed for the CH deformation bands of adsorbed methanol. It is supposed, however, that the observed broadening of the CH stretching vibration is attributed to hydrogen bonding of the methyl

47. Borowiak, M.A.; Jamróz, M.H.; Larsson, R. *J. Mol. Catal. A: Chem.* **1999**, *139*, 97.

48. Forester, T.R.; Howe, R.F. *J. Am. Chem.Soc.* **1987**, *109*, 5076.

hydrogens with the basic oxygen centers of the zeolite framework. This is induced by the higher negative charge ($-\delta_{\text{O}}$) on the zeolite oxygens of FAU(X) and FAU(X2) compared to MFI [36] (see Table 6.3). It was shown that methyl hydrogens of MeOH are reactive enough to form intermolecular hydrogen bonds with the hydroxy oxygen of other methanol molecules in liquid methanol [50] illustrating that such interactions are most likely to occur in zeolites as well. Hydrogen bonding with the framework oxygens was also observed for a Mn(II)-ethylene adsorption complex in a Mn^{2+} exchanged FAU(X) zeolite [51]. This hydrogen bonding with alkali exchanged FAU(X) is likely the origin of the different catalytic activities of these samples.

Also formaldehyde adsorbs via its oxygen lone pair on alkali exchanged MFI and FAU(X) zeolites (bands observed between 1730 and 1702 cm^{-1}): from K^+ to Cs^+ a decreasing shift of the carbonyl stretching vibration (ν_{CO}) is observed (with decreasing electrostatic potential of the cation) (see Table 6.4). This indicates an adsorbed aldehyde species which interacts solely via its oxygen atom with the extra framework cations (*end-on* CH_2O adsorption) (see Fig. 6.12 (inset)). However, the shift of the formaldehyde ν_{CO} adsorbed on Na-FAU(X) did not follow that trend. This is attributed to a different interaction with the zeolite. In Appendix 2 a more detailed description of the features observed is given, but it is speculated that this is either the result of two CH_2O molecules adsorbed per sodium cation (*end-on* CH_2O adsorption) (see Fig. 6.18a) or simultaneous interaction of the carbonyl group with the Na^+ cation and the basic framework oxygen centers (*side-on* CH_2O adsorption) (see Fig. 6.18b).

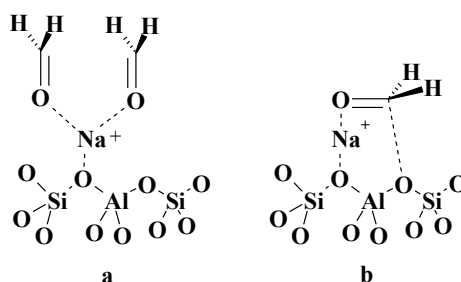


Figure 6.18: End-on adsorption of two molecules CH_2O (a) and side-on adsorption of one molecule CH_2O (b) on Na-FAU(X) (see text).

CH_2O sorption on basic FAU(X) zeolites yielded also surface formate (bands at 1618-1611 cm^{-1} together with bands at 1371-1345 cm^{-1}) and methoxy at 323 K (see also Ref. [26a]). As can be seen in Table 6.4 no systematic correlation for the asymmetric and symmetric $\text{C}=\text{O}$ stretching vibration of the surface formate with the basicity of the zeolite framework or with the electrostatic potential of the extra framework alkali metal cation is apparent. This is tentatively affiliated with the surface formate structure [26a]; in the case of Na-FAU(X) a bidentate formate to the extra framework Na^+ cations in the zeolite pores is formed (see Fig. 6.19a) [25c,26a], while in the case of K-, Rb- and Cs-FAU(X) zeolites monodentate

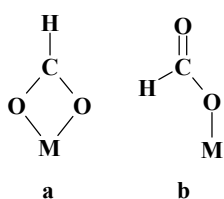


Figure 6.19: Bidentate (a) and monodentate (b) coordination of surface formate on M-FAU(X) (M = extra framework alkali cation)

49 a) Weinheimer, C.J.; Lisy, J.M. *J. Phys. Chem.* **1996**, *100*, 15305; b) Weinheimer, C.J.; Lisy, J.M. *Int. J. Mass Spectrom. Ion Process.* **1996**, *159*, 197.

50. Yuhnevich, G.V.; Tarakanova, E.G. *J. Mol. Struct.* **1998**, *447*, 257.

51. Yang, S.B.; Jeong, M.S.; Kim, Y.; Seff, K. *J. Phys. Chem. B* **1997**, *101*, 9041.

surface formate is expected to form (see Fig. 6.19b) [26a]. This will be discussed more in detail in Appendix 3.

Formaldehyde desorption from Cs-FAU(X) yielded formaldehyde (483 K), MeOH (603 K), CO (maxima: 533 and 613 K) and H₂ (633 K), while a decrease in the i.r. intensity of the formaldehyde and an increase in the intensity of the formate and methoxy groups during t.p.d. was observed (not shown here) indicating the decomposition of formaldehyde into the more stable surface formate and surface methoxy. CH₂O t.p.d. adsorbed on Na-FAU(X) yielded mainly methanol (458 K) and CO (560 K). No H₂ or DME was observed. The high reactivity of Na- and Cs-FAU(X) towards formaldehyde decomposition yielding formate and methanol observed during CH₂O adsorption and desorption is illustrative of the low formaldehyde stability during MeOH reaction and poor methanol selectivity in the methanol side chain alkylation of toluene observed over basic materials [26d].

The simultaneous formation of surface methoxy groups and formate and the observation of MeOH during CH₂O t.p.d. on basic FAU(X) molecular sieves is in agreement with Sefcik [25a] and is evidence for a *Cannizzaro* type disproportionation (see also Ref. [20,25b,52]). This involves most likely a surface dioxymethylene species. Dioxymethylene itself was not observed, probably because of its low surface stability [20].

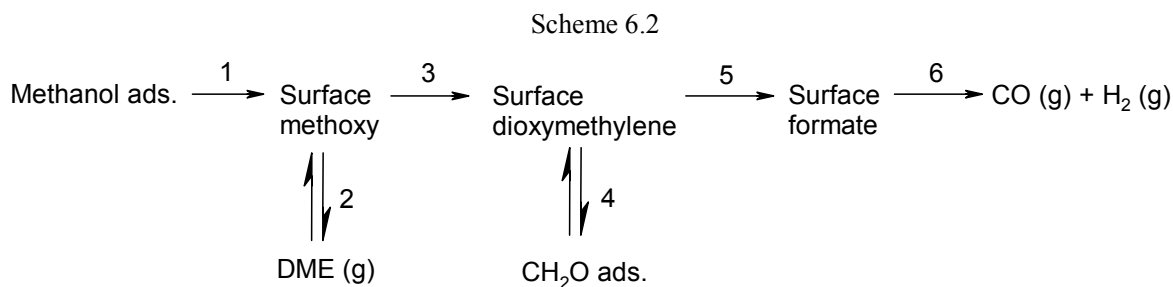
In contrast to FAU(X) zeolites, where formaldehyde sorption immediately yielded surface formate as observed with i.r. spectroscopy, no surface species were observed upon CH₂O adsorption on basic MFI molecular sieves. Also increasing temperatures did not show any formation of surface formate. This is related to the fact that 1) the framework oxygens of alkali cation exchanged MFI are not basic enough (to yield dioxymethylene) and 2) the sites are too far separated for hydride transfer between neighboring adsorbed formaldehyde molecules, thus prohibiting a *Cannizzaro* type disproportionation as outlined above for basic FAU(X) and FAU(X2). A similar observation was made by Wieland *et al.* [53].

Reaction of methanol and dimethyl ether: Elucidation of the reaction mechanism

Due to the observed similarities between MeOH and DME reaction yielding dimethyl ether and surface formate over γ -alumina and basic zeolites, we propose a similar reaction pathway for these materials (see Scheme 6.2) as proposed by Busca [19] for γ -alumina. In the remaining part of this Chapter spectroscopic evidence will be discussed in the light of our proposal.

52. Venuto, P.B.; Landis, P.S. *Adv. Catal.* **1968**, *19*, 259.

53. Wieland, W.S.; Davis, R.J.; Garces, J.M. *J. Catal.* **1998**, *173*, 490.



Reaction 1 and 2: ADSORBED METHANOL \rightarrow SURFACE METHOXY \rightarrow DME

During the temperature increase of the catalysts in the presence of MeOH and DME some new bands were observed on the catalysts surface with i.r. spectroscopy; on Na-MFI at 2957 and 2855 cm^{-1} , Cs-MFI at 2956 and 2853 cm^{-1} , on Na-FAU(X) at 2820 cm^{-1} , on Cs-FAU(X2) at 2807 cm^{-1} , and on Cs-FAU(X) at 2804 cm^{-1} (species B in Scheme 6.2). DME reaction over Na-MFI and FAU(X) yielded similar surface bands at $T > 723$ K as observed for MeOH reaction (this is shown in Fig. 6.11 for Na-MFI). As the i.r. wavenumbers of these new bands observed at 2957 and 2855 cm^{-1} on Na-MFI closely resemble those observed at low MeOH loadings (see Chapter 4 and Ref. [37]) they could also be attributed to chemisorbed MeOH. However, the observed MeOH OH stretching vibration at 560 K had lost significantly in intensity (see Fig. 6.2), compared to the methyl stretching vibrational bands (and to the bands observed at low loadings (see Chapter 4)), and with further increasing temperatures the OH stretching vibration had completely disappeared; at $T > 616$ K the bands observed at 2957 and 2855 cm^{-1} were the only visible (see Fig. 6.2). In Fig. 6.3 these newly observed bands are shown more clearly. Similar observations were done for Cs-MFI. In the case of Na- and Cs-FAU(X) and Cs-FAU(X2), the newly visible i.r. bands also can not be attributed to: 1) molecularly adsorbed methanol at low loadings, since the bands 2820-2804 cm^{-1} are not observed at low methanol loadings at 323 K (see Ref. [36]) or 2) to temperature effects, since this results in a weaker interaction and thus a shift to higher wavenumbers. DME reaction yielded similar bands observed for MeOH reaction over basic zeolites, together with an additional absorption maximum around 2903 cm^{-1} (see Fig. 6.11) indicating surface methoxy groups on different (extra) lattice atoms. From the above it is clear that a surface reaction has taken place and we attribute the new bands to surface methoxy groups; i.r. results of Na-methylate show similar wavenumbers [54] as those observed for Na-MFI. On Na-FAU(X) at 773 K a second set of i.r. vibrational CH bands at 2956 and 2847 cm^{-1} was observed that are also assigned to surface methoxy groups (see Fig. 6.5). A similar observation was made for γ -alumina (see Appendix 1), and were attributed to spectator species. At this moment the precise surface structure and/or location of this second surface methoxy group is not clear.

Because of the overlap of the CH_3 stretching vibrational bands of molecularly adsorbed methanol and surface methoxy groups, it is difficult to point out the exact starting temperature of the

decomposition of methanol; the i.r. signal of surface methoxy groups becomes visible only after desorption of molecularly adsorbed methanol. Formation of methoxy may well take place at low temperature (as indicated by the formation of DME). The production of gas phase DME is in agreement with the observation of surface methoxy groups (at $T > 560$ K), which are known intermediates [55]. At the temperatures where we observe surface methoxy groups, the formation of surface hydroxy groups was not observed (i.e., a proton transfer to the zeolite framework) [56].

Gas phase analysis showed that DME production over Na^+ exchanged zeolites started at lower reaction temperatures (compare Fig. 6.6-6.9), and also a higher DME yield was obtained at 653 K (see Table 6.3), compared to the corresponding Cs^+ exchanged homologues; apparently, a correlation between electrostatic potential of the metal cation ($e/r_{\text{Na}} = 1.05 \text{ \AA}^{-1}$ and $e/r_{\text{Cs}} = 0.59 \text{ \AA}^{-1}$) and activity exists. Such a simple correlation was also found by Lavalley *et al.* [26c]. Also differences in DME production are observed between the different zeolites. DME production over MFI based catalysts starts at lower reaction temperatures than over FAU(X) based catalysts. This is caused by the higher positive charge of the extra framework cations in MFI, compared to those in FAU(X) [57]. Thus the formation of DME and most likely the production of surface methoxy appear to be a function of the Lewis acidity of the cation, the reaction to DME being favored with higher MeOH partial pressures as expected.

This fine correlation between DME production and cation acidity indicates that surface silanol groups located at framework defects or at the outside of the crystallites do not participate in the reaction. This agrees well with the result obtained by MeOH reaction over silicalite-1 (see Appendix 1). Furthermore, dimethyl ether production over basic zeolites agrees well with earlier studies [26c,d,27,58] and also gas phase alkali cation-(MeOH)_n clusters yielded dimethyl ether (via intermolecular methanol reaction) [59]. This does not require the presence of Brønsted acid sites as was shown by Lercher and Rumlmayr [58] and also in the present study the existence of such surface groups was not observed. No extra framework alumina is present in our samples, but if a very small amount would be present the Lewis acid centers assigned to (extra) framework alumina would not participate in the production of DME [58].

54. D'Hondt, P. *Acros Organics*, www.acros.be.

55. However, DME production can not be used as an indication for the formation of surface methoxy groups, since at low temperatures an associative mechanism might prevail [8]: this involves the simultaneous adsorption and reaction of two methanol molecules (intermolecular dehydration). Blaszkowski and Van Santen [8] reported that the activation barrier for this process (over acid sites) is rather low.

56. This in sharp contrast to Lavalley *et al.* [26c], who reported surface hydroxy groups on alkali cation exchanged FAU zeolites. See also a) Ziolk, M.; Czyniewska, J.; Lamotte, J.; Lavalley, J.C. *React. Kinet. Catal. Lett.* **1994**, *53*, 339; b) *Idem*, *Zeolites* **1996**, *16*, 42. Most likely this results from subsequent reactions yielding gas phase products, i.e., DME, H_2O , and H_2 and the overlap with the MeOH OH group at low reaction temperatures.

57. a) Limtrakul, J.; Khongpracha, P.; Jungsuttiwong, S.; Truong, T.N. *J. Mol. Catal. A: General* **2000**, *153*, 155; b) Limtrakul, J.; Jungsuttiwong, S.; Khongpracha, P. *J. Mol. Struct.* **2000**, *525*, 153.

58. Lercher, J.A.; Rumlmayr, G. *Z. Phys. Chem. NF* **1985**, *Bd. 146*, 113.

59. Zhang, X.; Castleman, Jr., A.W. *J. Am. Chem. Soc.* **1992**, *114*, 8607.

Reaction 3 and 4: SURFACE METHOXY → SURFACE DIOXYMETHYLENE → ADSORBED FORMALDEHYDE and SURFACE FORMATE

The lower wavenumbers of the symmetric methoxy CH_3 vibration on alkali cation exchanged FAU(X) (at 2820 (Na^+), 2804 cm^{-1} (Cs^+)) and 2807 cm^{-1} on Cs-FAU(X2) compared to MFI (2855 (Na^+) and 2853 cm^{-1} (Cs^+)), are attributed to the higher surface basicity of FAU(X). Using Sanderson's electronegativity equalization principle one can approximate the mean negative charge of the framework oxygens (see Ref. [36] and references cited therein). As the mean negative charge of the framework oxygens of the FAU(X) samples is higher than that of the MFI samples (approximately 0.350 and 0.164, respectively [36]), this, in turn, leads to a more polar surface CH_3 group on the FAU(X) and FAU(X2) zeolites in which the C-H bond can be lengthened [60,61]. This is manifested by the relatively low wavenumbers of the C-H stretching vibration on alkali exchanged FAU(X) and FAU(X2), compared to MFI. DME reaction over Na-FAU(X) yielded similar low wavenumbers for the surface methoxy group.

Due to the lengthening of the C-H bond of the surface methoxy group and the hydrogen bonding of the methyl hydrogens with the framework oxygen centers on alkali exchanged FAU(X) and FAU(X2) zeolites, hydrogen abstraction of the methoxy group becomes possible. This is further facilitated by interaction of neighboring basic framework oxygen centers with the carbon atom of the methoxy group, resulting in a further activated C-H bond. The lengthened or broken methanol OH group (due to hydrogen bonding with the basic framework oxygen centers) then reacts with the activated C-H group and yields H_2 and dioxymethylene ($\text{O}-\text{CH}_2-\text{O}$), the precursor to surface formaldehyde and formate [19,20]. (This is schematically shown in Fig. 6.20.) The intermediate dioxymethylene is, due to its low stability, not observed, however, in the case of MeOH reaction over Cs-FAU(X2), both products resulting from dioxymethylene, i.e., surface formaldehyde (reversibly) and formate [19,20], were observed.

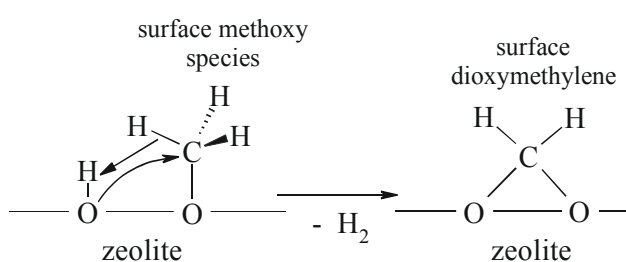


Figure 6.20: Schematic representation of the reaction of surface methoxy with hydroxy yielding dioxymethylene and H_2 .

formate [19,20], were observed.

A similar mechanism has been proposed for γ -alumina [19]. Also during MeOH and DME reaction over γ -alumina (see Appendix 1) low i.r. wavenumbers (at 2823 cm^{-1}) were observed for the surface methoxy group. This is evidence of the lengthening of the C-H bond, as supposed

for the methoxy groups on the basic FAU(X) and FAU(X2) zeolites. Furthermore, the i.r. band of these surface methoxy groups disappeared with the appearance of the surface formate (indicative of MeOH dehydrogenation yielding surface formaldehyde that, subsequently, decomposes to surface formate).

60. a) Takezawa, N.; Kobayashi, H. *J. Catal.* **1972**, *25*, 179; b) Takezawa, N.; Kobayashi, H. *J. Catal.* **1973**, *28*, 335.

Thus a clear correlation between surface formate and surface methoxy is apparent for γ -alumina. Although such correlation was not so clearly apparent for the Na- and Cs-FAU(X) and Cs-FAU(X2) samples the appearance of surface formaldehyde (band at 1716 cm^{-1}) and formate (band at $1618\text{--}1611\text{ cm}^{-1}$) during MeOH reaction over basic FAU(X) and FAU(X2) zeolites (see Fig. 6.4 and 6.7-6.10) indicates a correlation with the appearance of the surface methoxy i.r. bands at these low wavenumbers (at $2820\text{--}2804\text{ cm}^{-1}$).

Furthermore, the absence of surface formaldehyde and formate during the reaction of DME over Na-FAU(X) indicates the necessity of the hydroxy hydrogen. This is emphasized by the reaction of DME over γ -alumina yielding surface formate. The presence of basic surface hydroxy groups (absent in alkali cation exchanged FAU(X) and FAU(X2) zeolites) leads to the production of formate (see also Appendix 1).

**Reaction 4, 5 and 6: ADSORBED FORMALDEHYDE \rightarrow SURFACE DIOXYMETHYLENE
SURFACE FORMATE \rightarrow CO + H₂**

As said before, MeOH reaction over Cs-FAU(X2) yielded surface formaldehyde and formate, with the i.r. intensity of adsorbed formaldehyde decreasing with the simultaneous increase of the surface formate bands. This is shown in Fig. 6.21. Admission of formaldehyde to alkali exchanged FAU(X) zeolites at 323 K yielded surface formate and methoxy groups and the simultaneous decrease of the i.r. bands of the formaldehyde C=O and the increase of the formate C=O stretching vibrations during CH₂O t.p.d., also indicates a correlation between the production of formaldehyde and formate (see also Ref. [25,26a,b,d]). As already discussed, this proceeds via a *Cannizzaro* type disproportionation. From this we conclude that the formation of surface formate on Na- and Cs-FAU(X) is indicative for the formation of formaldehyde [26d].

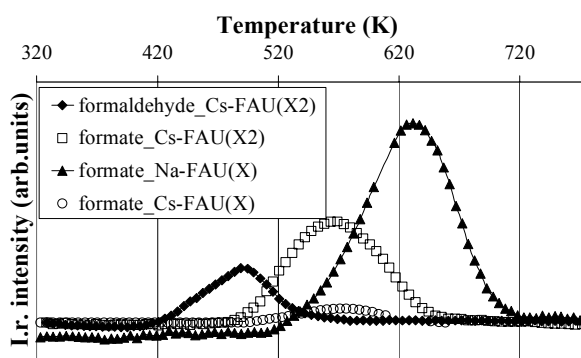


Figure 6.21: Formaldehyde and formate intensity as function of temperature ($323\text{--}773\text{ K}$, $T_r = 5\text{ K}\cdot\text{min}^{-1}$) over (a) Na- and (b) Cs-FAU(X) and (c) Cs-FAU(X2) during MeOH reaction.

The absence of the bands attributed to surface formaldehyde over Na- and Cs-FAU(X), compared to Cs-FAU(X2), during MeOH reaction is explained as follows: 1) the lower overall basicity of the framework oxygens of Na-FAU(X) results in a lower reactivity towards dehydrogenation: this implies that higher reaction temperatures are needed and thus a higher probability for formaldehyde decomposition. The formaldehyde carbonyl group is very polarized via its oxygen by the large electrostatic potential of the Na⁺ cation, making its carbon atom very reactive towards framework

oxygens, i.e., surface formate is formed (see Appendix 2). In the case of Cs-FAU(X), formaldehyde most likely rapidly decomposes to surface formate, because of the high basicity of the framework oxygens associated with the Si-O-Al bridges and the high concentration of cations (and hence short distances) facilitating CH₂O disproportionation (via attack of the framework oxygens on the carbon atom of formaldehyde yielding dioxymethylene species) and, subsequently, decomposition to formate.

The ability of Cs-FAU(X2) for the production of surface formaldehyde can also be attributed to the presence of basic oxide clusters within the pores as shown by Hunger *et al.* [25c] (an amorphous phase is detected in this zeolite with XRD); however, CO₂ adsorption did not indicate any Cs₂O clusters. In contrast to other studies [26d] formaldehyde was not observed in the gas phase over Na- and Cs-FAU(X) and Cs-FAU(X2). This could also be related to the fast surface decomposition to formate and, subsequently, to CO and H₂. Thus it is concluded that formaldehyde is only a surface species, in agreement with Hunger *et al.* [25c].

Interesting result is that the zeolite topology is not very important for the formation of surface formaldehyde and formate (microporous *vs* mesoporous, crystalline *vs* amorphous), as long as the surface oxygens are able to form strong enough basic hydroxy groups and activated methoxy CH groups for the abstraction of a methoxy hydride (surface methoxy groups on γ -alumina were found at almost similar wavenumbers as for basic FAU(X) and FAU(X2)).

The production of H₂ coincides well with the formation of surface formate (see Fig. 6.7-6.9) and results from the catalytic methanol dehydrogenation by the zeolite Lewis acid-base sites of alkali exchanged FAU(X) and FAU(X2) zeolites [27b] yielding adsorbed formaldehyde. Adsorbed CH₂O decomposes over Lewis base sites yielding formate, and, subsequently, H₂ and CO [27b,62]. CO production is found at higher temperature with the simultaneous decrease in surface formate i.r. intensity. Similar decomposition products were found during formaldehyde decomposition. H₂ production at lower reaction temperatures without the simultaneous CO production indicates that intermediately formed formaldehyde, resulting from methanol dehydrogenation, is stable until temperatures close to 633 K (as formaldehyde or formate). H₂ and CO are produced at lower temperatures and in larger H₂ selectivity over Cs-FAU(X) (see Table 6.3), compared to Na-FAU(X). This is related to the higher surface basicity of Cs-FAU(X), compared to Na-FAU(X) ($-\delta_{\text{O}} = 0.384$ and 0.317 , respectively (see Table 6.3)) [36] and agrees well with those reported by others (see e.g., Ref. [26a]). The similar off set temperatures for H₂ (see Fig. 6.8 and 6.9) and formate (see Fig. 6.21) production over Cs-FAU(X) and Cs-FAU(X2) indicates similar active sites; the lower production of H₂ over Cs-FAU(X2) can thus be explained by a lower site concentration. Most probably the oxygens O1 and O4 in the FAU(X) supercage (related to the Lewis acid site in site III') are responsible for this reaction, since these are the most basic and the only accessible (together with oxygen O2 (related to the

62. Hathaway, P.E.; Davis, M.E. *J. Catal.* **1989**, *119*, 497.

Lewis acid site in site II, which is less basic)) [63]. MeOH dehydrogenation over basic FAU(X) is facilitated with low MeOH partial pressures, indicating that most likely the same intermediates are responsible for the intramolecular dehydrogenation (to CH₂O) and intermolecular dehydration (to DME), i.e., methoxy, and thus similar active sites.

Formic acid decomposition over basic FAU(X) led to CO₂ production (resulting from formic acid dehydrogenation) above 493 K (see Fig. 6.17). However, no CO₂ was observed during the decomposition of surface formate. This indicates that the surface formate formed during methanol decomposition over alkali exchanged FAU(X) and FAU(X2) zeolites and during formic acid adsorption are not similar, although the i.r. wavenumbers of the (a)symmetric stretching vibrations are similar. (In Appendix 3 a more detailed discussion is given regarding formic acid adsorption and t.p.d.)

Na- and Cs-MFI molecular sieves are inactive for the production of surface formaldehyde and formate (in agreement with literature [26a,c,27a]), despite the fact that MeOH reaction yielded surface methoxy groups. This is explained by the fact that the framework oxygen centers are not basic enough for the abstraction of the methyl hydrogen and subsequent production of surface formate (see also CH₂O adsorption, where it was concluded that the framework oxygen centers of MFI were not basic enough to yield intermediate dioxymethylene). The H₂ production (see Table 6.1) results from the formation of coke on these samples.

Above results thus indicate a strong influence of the zeolite composition on the reactivity of methanol towards surface methoxy and, subsequently to either DME or adsorbed CH₂O, CO and H₂. The dominant role of the coordination bond to the Lewis acidic cation influences the chemical reactivity of the adsorbed methanol species on alkali exchanged zeolites, by activating the methanol O-H bond, which leads to the formation of surface methoxy groups yielding DME; increasing hydrogen bonding between MeOH and the framework oxygen centers results in the abstraction of the hydroxy and methyl hydrogens yielding surface formaldehyde and formate. Also the rupture of the C-O bond in dimethyl ether, yielding two surface methoxy groups, is caused by the high electrostatic potential of the Na⁺ cation. The absence of hydroxy hydrogen on DME prohibits the formation of surface formate on basic FAU(X) due to the fact that although the C-H bond is lengthened it can not react with a basic OH group since these are not present.

6.5 CONCLUSIONS

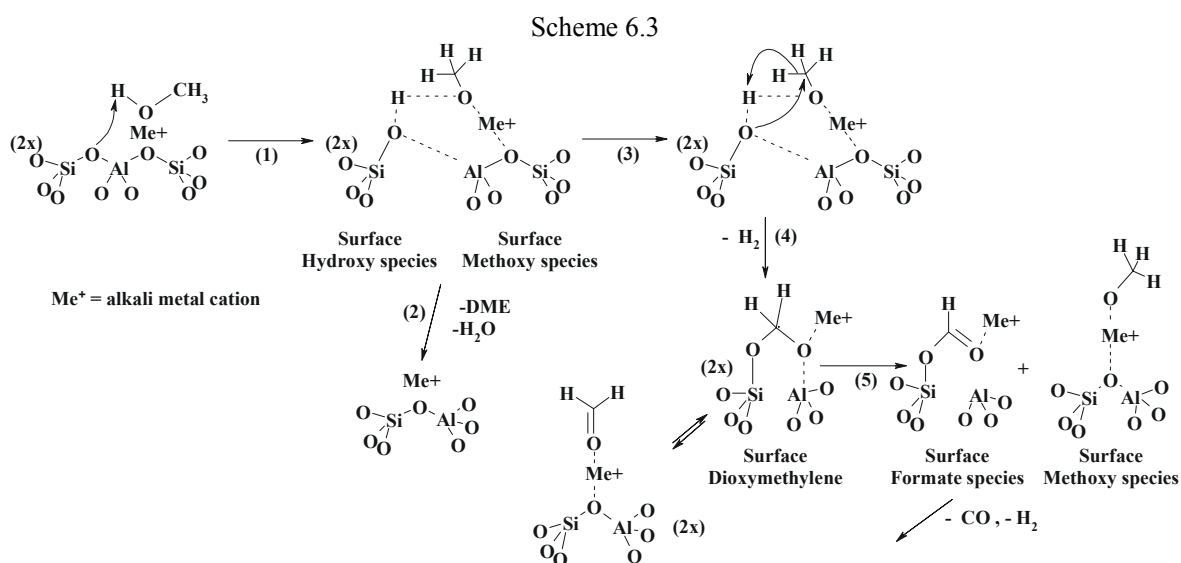
MeOH and DME reaction over basic zeolites was studied using i.r. spectroscopy, temperature programmed reaction and temperature desorption techniques. In contrast to others we were able to observe the intermediate formaldehyde and show that its decomposition leads to the formation of surface formate. From the results presented here (and literature), we can summarize that:

63. Heidler, R.; Janssens, G.O.A.; Mortier, W.J.; Schoonheydt, R.A. *J. Phys. Chem.* **1996**, *100*, 19728.

- 1) intermolecular MeOH dehydration yielding DME proceeds over the Lewis acid sites, i.e., the alkali cation, and results most likely from surface “methoxy” groups,
- 2) on the most basic catalysts, i.r. results indicate a large polarization of the methanol hydroxy group and a large influence of the zeolite framework oxygen center on the methyl group. Surface methoxy groups (at low wavenumbers) and surface formaldehyde and/or formate are found. MeOH dehydrogenation needs the concerted action of both the alkali cation and the basic framework oxygen centers,
- 3) reaction of DME yields only surface methoxy groups; no formaldehyde or formate is observed: this is attributed to the absence of the hydroxy hydrogen (and thus to the absence of OH groups of DME), thus the presence of OH groups is indispensable,
- 4) the zeolite topology is not very important for the formation of surface formaldehyde and formate (microporous vs mesoporous, crystalline vs amorphous), as long as the surface oxygens are able to form strong enough basic hydroxy groups and activated C-H bonds for the abstraction of a methoxy hydride, and
- 5) it was observed that formaldehyde decomposes into surface methoxy and formate, yielding MeOH, CO, and H₂. This illustrates the low MeOH selectivity during side chain alkylation. The formation of formate from formaldehyde proceeds via a *Cannizzaro* type disproportionation.

Based on the results reported here we suggest that the mechanism for methanol intermolecular dehydration, yielding DME, and intramolecular dehydrogenation, yielding formaldehyde, proceeds as previously has been reported for γ -alumina [13,19,20]. In Scheme 6.3 the proposed mechanism for methanol dehydration and dehydrogenation is shown.

Methanol adsorbs “dissociatively” on the alkali cation yielding surface methoxy and hydroxy (Scheme 6.3: step 1). Whereas the resulting methoxy can dimerize yielding water and DME over alkali exchanged MFI (Scheme 6.3: step 2), the resulting surface hydroxy groups on alkali exchanged



FAU(X) and FAU(X2) possesses enough acid-base properties to abstract a hydride from the surface methoxy group (Scheme 6.3: step 3) to form formaldehyde (as observed with Cs-FAU(X2)) and molecular hydrogen (Scheme 6.3: step 4), which can rearrange to surface formate and methoxy groups via a *Cannizzaro* type disproportionation reaction (Scheme 6.3: step 5). The abstraction of the methyl hydride is facilitated by the interaction of a framework oxygen center with the methyl carbon yielding negatively charged hydrogen that reacts with a surface hydroxyl group, yielding hydrogen and adsorbed dioxymethylene/formaldehyde (Scheme 6.3: step 4).

Although the i.r. spectra of methanol and dimethyl ether decomposition do not show intermediates, like surface hydroxy and dioxomethylene, we suggest that this mechanism can also be applied to alkali exchanged zeolites. Indirect evidence for this can be found in literature [26c].

It has to be said that surface formaldehyde and formate are observed at lower reaction temperatures compared to temperatures necessary for the side chain alkylation reaction of toluene over basic zeolites with methanol. This does not imply that the reaction in the presence of toluene would be different. Second, the observation of formaldehyde at low temperature in the present study implies that this could be the alkylating species in the side chain alkylation of toluene. Low temperature activation of methanol means that at high reaction temperatures during alkylation, the rate of decomposition into surface formate and, subsequently CO and H₂, will be high and only a low surface concentration will be present, as is indicated by the low yields during toluene alkylation.

Based on these last statements it is clear that in order to improve MeOH selectivity the activity for side chain alkylation has to increase and best at lower reaction temperatures. This can only be done by improving the activation of toluene.

ADDED NOTE:

During our experiments a large influence of the reaction conditions on the formaldehyde selectivity was observed. The contamination of the feed with molecular oxygen yielded formaldehyde in all used basic zeolites. This resulted also in the formation of surface formate in the case of alkali cation exchanged FAU(X) zeolites (not in the case of M⁺-MFI zeolites). In the next Chapter O₂ is added on purpose to the reactor to induce formaldehyde production.

Appendix 1 - Silica(lite-1) and γ -Alumina: Methanol and dimethyl ether sorption and reaction

To understand the reactive surface groups of the basic zeolites also MeOH and DME reaction over silica, silicalite-1, and γ -alumina from 323-773 K was studied. I.r. spectra of the activated silica, silicalite-1 and γ -alumina samples correspond well with literature data [10,64] and show that the samples are not completely dehydroxylated after the activation procedure.

64. Morterra, C.; Magnacca, G. *Catal. Today* **1996**, *27*, 497.

The i.r. spectra obtained after methanol and dimethyl ether sorption and reaction on silica, and γ -alumina at 323-773 K are in good agreement with earlier reports (silica [10,11], and γ -alumina [12a-c,e,21a]). Therefore, no detailed description of the bands observed will be given (bands are assigned according to Ref. [38,39,40]). No literature data reports were found related to DME sorption and reaction over silica. Methanol and dimethyl ether i.r. absorption bands observed in the spectra at 323 K are listed in Table 6.2 and 6.3.

The multiplicity of CH_3 stretching vibration bands observed for DME adsorption on γ -alumina and silica is attributed to clustering of DME on the mesoporous catalyst surface (see also before). The higher CH stretching vibration at 3005 cm^{-1} observed for DME adsorption on silica is attributed to DME adsorption on the acidic surface Si-OH groups [48]. This high CH stretching band is not observed on γ -alumina, indicating the absence of (strong) acidic surface hydroxy groups.

Upon heating, the same phenomena were observed as reported in literature, i.e., the production of surface methoxy groups (on silica and γ -alumina) and formate (only on γ -alumina). Surface methoxy groups were observed at 2959 and 2857 cm^{-1} on silica during methanol reaction. After reaction approximately 17% of silica silanol surface groups were permanently methoxylated (reactivation in inert gas at 773 K did not remove those surface methoxyl groups). Heating of silica in the presence of dimethyl ether also yielded surface methoxy groups at 2960 and 2855 cm^{-1} . No surface formate is observed over silica.

On γ -alumina, surface methoxy groups were observed at 2823 cm^{-1} before and during heating in methanol. This is at slightly lower wavenumbers than previously reported [12a-c], but was explained by the presence of residual cations inside the γ -alumina framework [65]. Upon further heating (above 423 K), we observed the appearance of surface formate (bands at 1592 cm^{-1} (with a shoulder at 1604, both $\nu_{\text{as}}(\text{C}=\text{O})$), 1393 ($\delta_{\text{as}}(\text{CH})$) and 1377 cm^{-1} ($\nu_{\text{s}}(\text{C}=\text{O})$)) and is in perfect agreement with that observed by Greenler [12a] and Matyshak *et al.* [18a]), while the band assigned to surface methoxy groups at 2823 cm^{-1} decreased in intensity. The formed surface formate species were stable up to 773 K. The bands observed at 2960 and 2850 cm^{-1} , assigned to methoxy groups as well, appear to be stable spectator species (up to 773 K) which are not involved in the formation of surface formate. Most likely these are formed by the disproportionation reaction yielding formate. Similar observations were made for dimethyl ether reaction over γ -alumina (here the formation of surface formate started at 463 K, with the simultaneous decrease of the band assigned to surface methoxy groups).

The concentration of adsorbed methanol on silicalite-1 was found to be very low, compared to silica and γ -alumina. This is expected since silicalite-1 is highly hydrophobic and hence it adsorbs

65. The lower wavenumbers, observed for surface methoxy groups on γ -alumina, compared to ref. [12a,c], are explained as follows: the $\nu_{\text{s}}(\text{CH}_3)$ wavenumbers are sensitive towards residual cations inside the framework, inducing charge effects on the γ -alumina framework and thus shifting its wavenumber to lower positions [12e]. Here, XRF has also shown the presence of Na^+ and Ca^{2+} cations (total 0.25 wt%).

organic molecules over water [66]; at higher temperatures it has little or no catalytic activity [66]. In agreement, no surface methoxy groups were observed during heating.

Formation of surface methoxy and formate groups over silica and γ -alumina proceeds as outlined in the Introduction. Surface formate is not formed over silica as a result of its acidic surface character. Basic surface hydroxy groups on γ -alumina are responsible for the methoxy hydride abstraction, yielding formaldehyde and, subsequently, formate.

From these results we can conclude that 1) surface silanol groups located at framework defects or at the outside of the crystallites of zeolites do not participate in the reaction in contrast to silica and 2) the zeolite topology is not very important for the formation of surface formaldehyde and formate (microporous vs mesoporous, crystalline vs amorphous), as long as the surface oxygens are able to form strong enough basic hydroxy and methoxy groups for the abstraction of a methoxy hydride.

Appendix 2 - Formaldehyde adsorbed on alkali exchanged FAU(X) and MFI zeolites

The lowering of the formaldehyde carbonyl stretching vibration compared to gas phase formaldehyde [43] after sorption on Cs-FAU(X) ($\Delta\nu = 34 \text{ cm}^{-1}$) is attributed to an adsorbed aldehyde species which interacts solely via its oxygen atom with the extra framework Cs^+ cations (*end-on* CH_2O adsorption) (see Fig. 6.12 (inset)), in accordance with Lercher [67]. This is further emphasized by the fact that adsorption of CH_2O on alkali cations had no effect on the CH_2 deformation band at 1504 cm^{-1} (in gaseous CH_2O this band is found at 1503 cm^{-1} [43]).

As can be seen from Table 6.4 a fair agreement between the decreasing electrostatic potential of the alkali cation and the $\text{C}=\text{O}$ stretching vibration (ν_{CO}) of adsorbed formaldehyde exists (see also Fig. 6.22), but no correlation with the framework basicity (given as the average charge on the zeolite framework oxygen ($-\delta_{\text{O}}$)). The increasing $\Delta\nu_{\text{CO}}$ with increasing electrostatic potential compared to gas phase CH_2O strengthens our conclusion that CH_2O is primarily adsorbed via its oxygen atom on the alkali metal cation, without significant additional interaction of the carbon atom with the negative framework oxygens (*end-on* CH_2O adsorption) (see Fig. 6.12 (inset)). Furthermore, on Cs-FAU(X), CH_2O appears to be more stabilized, than on K-FAU(X), as follows from its higher $\text{C}=\text{O}$ stretching vibration.

No such correlation between the electrostatic potential of the alkali cation or framework basicity and the $\text{C}=\text{O}$ stretching vibration of adsorbed formaldehyde was found for CH_2O adsorption on Na-FAU(X) (see Table 6.4 and Fig. 6.22); formaldehyde interaction with Na-FAU(X) led to a much smaller shift of the carbonyl stretching vibration, compared to free formaldehyde. As the CH_2 deformation band was found at 1501 cm^{-1} , in perfect agreement with that found for gaseous CH_2O [43] and that observed for K-, Rb- and Cs-FAU(X) (see above), this indicates no interaction of the

66. Choudhary, V.S.; Mayadevi, S. *Zeolites* **1996**, *17*, 501.

framework oxygen centers with formaldehyde. It can be speculated that the most likely suggestion for the small perturbation of the C=O stretching vibration of adsorbed formaldehyde observed with Na⁺ cation is that, as a result of the large electrostatic potential of Na⁺, two formaldehyde molecules simultaneously adsorb *end-on* (see Fig. 6.18a), resulting in a weak interaction and thus a small shift. Integration of the CH₂ deformation band at ~1500 cm⁻¹ indicated 1.5x as much CH₂O on Na-FAU(X), compared to Cs-FAU(X). However, it should be noted that the same ratio was found for MeOH adsorption on Na- and Cs-FAU(X) (see also Chapter 4) and thus the observed CH₂O ratio might only indicate more available adsorption sites on Na-FAU(X).

However, the strong electrostatic field induced by the Na⁺ cation might result in a large polarization of the CH₂O carbonyl group (upon formaldehyde sorption) yielding a highly positively charged carbonyl carbon atom, which promotes interaction of the C-atom with the basic zeolite oxygens (*side-on* CH₂O adsorption) (see Fig. 6.18b). This mode of interaction on Na-FAU(X) would be more reactive, in agreement with the observation that methanol reaction over Na-FAU(X) showed no adsorbed formaldehyde in contrast to Cs-FAU(X2). Although both explanations for the CH₂O shift on Na-FAU(X) are attractive, they remain unproven.

Also on Na-MFI the formaldehyde C=O stretching wavenumber (1730 cm⁻¹) is observed at slightly higher wavenumber than the corresponding one on Cs-MFI (1726 cm⁻¹). Since the reactivity of the framework oxygens of MFI is much less (they are much less basic), compared to FAU(X) zeolites, we do not expect interaction of the MFI framework oxygens with the formaldehyde carbon atom in a similar way as outlined above for Na-FAU(X). Thus we attribute this shift to the simultaneous adsorption of two formaldehyde molecules on Na-MFI, as a result of the large electrostatic potential of Na⁺. Integration of the CH₂ deformation band at ~1500 cm⁻¹ indicated 4x more CH₂O sorbed on Na-MFI, compared to Cs-MFI.

Appendix 3 - Surface formate on Na-FAU(X): Really bidentate bound?

No systematic correlation for the asymmetric and symmetric C=O stretching vibration of the surface formate with the basicity of the zeolite framework or with the electrostatic potential of the extra framework alkali metal cation is apparent. Both the $\nu_{as}(C=O)$ and $\nu_s(C=O)$ wavenumbers of formate on Na-FAU(X) increase compared to those of free formate, as is shown in Table 6.4. For the FAU(X) group, K⁺ to Cs⁺, the trend is opposite for the $\nu_{as}(C=O)$ and $\nu_s(C=O)$. This is tentatively affiliated with

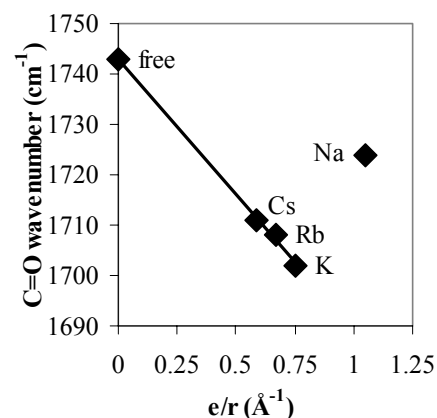


Figure 6.22: Representation of the free formaldehyde stretching C=O vibration [43] and on alkali exchanged FAU(X) zeolites as a function of the electrostatic potential of the cation, denoted as e/r .

the surface formate structure (see also Ref. [26a]). The simultaneous increase of the CO symmetrical and asymmetrical stretching vibrations of the surface formate compared to those of free formate as observed on Na-FAU(X) was explained by a bidentate coordination of the formed formate to the extra framework Na^+ cations in the zeolite pores (see Fig. 6.19a) [25c,26a], as similar features were observed for the CO stretching vibrations in Na-formate crystals. The O-C-O bond angle in the Na-formate crystal is approximately 126° and the Na-O bond length to both formate oxygens is approximately 2.40 \AA [68]. This conclusion indicates a migration of surface oxygen to the alkali formate complex, leaving unsaturated surface Si. However, no evidence of migration of surface oxygen out of the framework at room temperature was found in literature (oxygen isotope exchange experiments, to examine framework oxygen mobility, showed that oxygen exchange only proceeds at high temperatures (873-973 K) [69]; much higher than the temperature range studied here). In the case of K^+ to Cs^+ exchanged zeolites monodentate surface formate is expected to form (see Fig. 6.19b) [26a]. This will also be further discussed below. However, when the difference between the symmetrical and asymmetrical C=O stretching vibration is plotted as a function of the average negative charge of the framework, a clear correlation is observed (see Fig. 6.23 and Table 6.4); the difference increasing with increasing surface basicity (highest for Cs-FAU(X) (see Table 6.4)). This indicates increasing electron density on the formate O-C-O group and thus points to a surface bound formate. A similar correlation is found for organic nitrates and nitrate anion; with increasing negative charge on the NO_3 moiety, a larger difference is observed for the symmetric and asymmetric N=O stretching vibration [70]. The effect of the cation is not yet understood. Most likely it interacts with the carboxyl oxygen of the surface formate, however, this does not explain the difference in trend observed for the symmetric and asymmetric C=O stretching vibration.

As already discussed before, the nature of the surface formate species, i.e., mono- or bidentate coordination, observed during methanol reaction and formaldehyde adsorption over alkali exchanged FAU(X) zeolites is still debated. Mainly the migration of surface oxygen (at 323 K) to form a bidentate formate species as claimed for Na-FAU(X) remains uncertain, although the i.r. bands attributed to surface formate on Na-FAU(X) agree well with those of solid Na-formate [68].

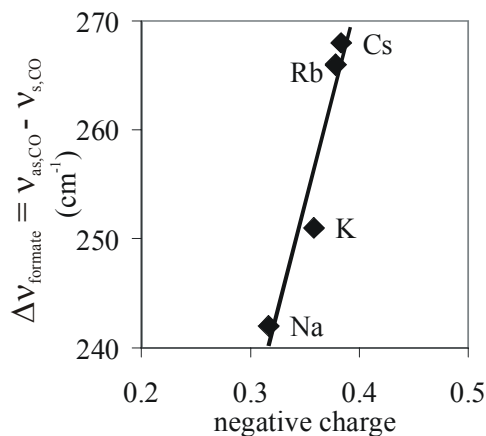


Figure 6.23: Representation of $\Delta V_{\text{formate}}$ ($= \nu_{\text{as,CO}} - \nu_{\text{s,CO}}$) of surface formate on alkali cation exchanged FAU(X) zeolites as a function of the framework oxygen charge ($-\delta_o$).

68. Markila, P.L.; Rettig, S.J.; Trotter, J. *Acta Crystallogr.* **1975**, *B31*, 2927.

69. Zulfugarova, S. In *Proceedings of the 13th International Zeolite Conference, Montpellier*; Galarneau, A., Di Renzo, F., Fajula, F., and Vedrine, J., Eds.; Elsevier: Amsterdam, 2001; Vol. 135, p 367.

70. Williams, D.H.; Fleming, I. *Spectroscopic Methods in Organic Chemistry*, 4th Edition; McGraw-Hill: London, 1989; p 54.

Previously it was shown by NMR that surface formate resulting from the adsorption of HCOOH on Na-FAU(X) at 171 ppm [71] was in good agreement with surface formate observed during the methanol decomposition over Na-FAU(X) (167-171 ppm) [25b]; formic acid adsorption on alkali cation exchanged zeolites yielded surface formate anion bonded to the alkali cation (and yielded also Brønsted acid sites). Formic acid adsorption on Cs-FAU(X) monitored by i.r. spectroscopy in our own lab yielded bands at 1612 and 1343 cm^{-1} (together with a broad hydroxy band between 3700-3200 cm^{-1}), in good agreement with surface formate observed during the methanol decomposition over Cs-FAU(X). Thus we used formic acid (HCOOH) as a model compound for the surface formate obtained during MeOH reaction and performed HCOOH t.p.d. experiments.

Before we discuss the results obtained during formic acid desorption, it needs to be said that the decomposition products of formic acid over oxide catalysts can be related to the surface structure of its anion, i.e., mono- or bidentate coordination of the surface formate anion (HCOO^-) to the extra framework cation (see also Fig. 6.19) [72]. Monodentate formate leads to dehydration, i.e., the formation of H_2O and CO , while bidentate formate prefers dehydrogenation, i.e., the formation of CO_2 and H_2 [72]. For the dehydrogenation reaction of surface formate, it was concluded that the formation of acidic hydroxyl groups is indispensable [71]; this was explained by a tilting of the bidentate formate, whereby the C-H bond approaches the acidic surface hydroxy and is weakened, leading to CO_2 and H_2 [73]. Others have claimed that a relation exists between the linearity of the formate OCO group and the formation of CO_2 : the more linear the OCO moiety the higher the probability to the formation of molecular CO_2 [74]. For the dehydration reaction a simultaneous contraction / expansion is needed of the surface formate O-C-O moiety to facilitate CO and H_2O desorption [74].

Formic acid desorption from all zeolites studied yielded non-dissociated formic acid with desorption maxima at 408 K for Cs-MFI (sharp), at 433 K for Na-MFI (sharp) and Cs-FAU(X) (broad) and at 423 K for Na-FAU(X) (broad). Furthermore, HCOOH desorption from Na- and Cs-FAU(X) yielded besides H_2O and CO (dehydration) also CO_2 and H_2 (dehydrogenation); with Cs-FAU(X), H_2 (thus dehydrogenation) was most intense, with Na-FAU(X), CO (thus dehydration) was most intense. In Fig. 6.17 the evolution of HCOOH decomposition products, i.e., CO , H_2O , CO_2 and H_2 is shown from Na- and Cs-FAU(X) during t.p.d. of adsorbed formic acid. In Fig. 6.24, the t.p.d. spectrum of formic acid adsorbed on Na-MFI and its decomposition products is shown.

Formic acid decomposition from Na-MFI (see Fig. 6.24) yielded, at higher temperatures, only CO and H_2O (starting at 378 K; maximum at 513 K) resulting from formic acid dehydration. HCOOH decomposition from Cs-MFI (not shown here) yielded mainly non-dissociated formic acid (only a small amount of CO_2 and H_2 at 588 K was found (formic acid dehydrogenation)). Overall, the total concentration of formic acid desorbed and decomposed from Cs-MFI was much smaller, compared to

71. Fraissard, J.; Rouabah, D.; Gruia, M. *J. Chim. Phys. Phys.-Chim. Biol.* **1986**, *83*, 681.

72. Borowiak, M.A.; Jamróz, M.H.; Larsson, R. *J. Mol. Catal. A: Chem.* **1999**, *139*, 97.

73. Jang, Y.H.; Hwang, S.; Kim, H. *Surf. Sci* **1995**, *340*, 245.

that found with the other catalysts. From the above it is clear that Na^+ exchanged zeolites are active catalysts for the dehydration of formic acid, whereas Cs^+ exchanged zeolites are active catalysts for the dehydrogenation of formic acid.

In Na-MFI and Na-FAU(X), the formed surface formate was concluded to be bidentate coordinated to the extra framework Na^+ cations in the zeolite pores [25c,26a,71]. Therefore, decomposition of bidentate formate should lead to dehydrogenation products (only observed for Na-FAU(X): minor reaction product). In Cs-MFI and Cs-FAU(X), the surface formate most likely is monodentate coordinated to the Cs^+ cation [26a]. Decomposition of monodentate formate should lead to dehydration products (only observed for Cs-FAU(X): minor reaction product). Apparently the zeolite framework has a large influence on the formic acid decomposition. As the decomposition of formic acid over basic zeolites showed almost no correlation with the observed surface structures (bi- vs monodentate with dehydration vs dehydrogenation), it is thus concluded that formic acid decomposition over alkali cation exchanged MFI and FAU(X) does not lead to a better understanding of the surface structure of the alkali-formate formed during MeOH decomposition these same materials.

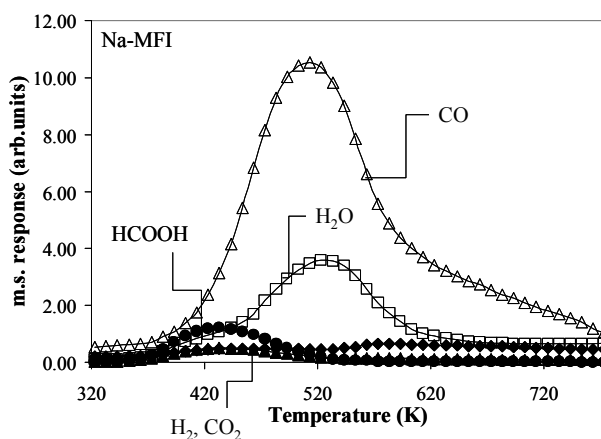


Figure 6.24: Temperature programmed desorption and decomposition of formic acid; comparison of the peak intensities of CO and H_2O (HCOOH dehydration) and CO_2 and H_2 (HCOOH dehydrogenation) from Na-MFI (Bottom).

Chapter 7

Oxydehydrogenation of Methanol over Basic Zeolites

Abstract:

In the previous Chapter we reported on the reaction of methanol and proposed a reaction mechanism for its decomposition over alkali cation exchanged MFI and FAU(X). Here we report on the conversion of methanol to surface formaldehyde in the presence of molecular oxygen over these same type of materials. Methanol is readily converted into surface formaldehyde at low temperatures over M-FAU(X) and M-MFI (whereby M = Na or Cs). The use of O₂ led also to the production of methyl formate, H₂, CO, CO₂, H₂O and DME. These products are explained by formaldehyde oxidation, decomposition, condensation and/or coupling.

Based on the product distribution, temperature windows for formaldehyde and methyl formate production, and catalyst activity it is concluded that Cs-MFI is the most active and selective surface formaldehyde production catalyst in the methanol oxydehydrogenation reaction.

7.1 INTRODUCTION

In large-scale synthesis, the use of O₂ as an oxidant is very beneficial from an economic point of view. Oxidative dehydrogenation (ODH, oxydehydrogenation etc.) of paraffins to the corresponding olefins and alcohols to aldehydes or ketones over, for example, mixed oxides like lithium-magnesium oxide [1] or iron-molybdate [2], respectively, in order to upgrade cheaper feedstocks, are examples under study.

Recently also basic zeolites are increasingly investigated as ODH catalysts. Chang *et al.* [3] investigated the oxidative dehydrogenation of ethane over Na-MFI catalyst exchanged with transition metal cations, like Ga, Pt and Ni, while Kubacka *et al.* [4] examined propane ODH over Na-FAU(Y), stabilized Y (USY) and MFI catalyst exchanged with metal cations, like Mg, Ca, Sn and Sb, respectively. It was found by both research groups [3,4] that MFI catalysts exhibit the highest alkane conversion activity and alkene selectivity. Furthermore, it was concluded that the presence of reducible and non-reducible cations inside zeolite pores did not increase the activity and or selectivity of the used catalysts [4]; Si/Al ratio of the zeolite structure played a more decisive role.

Oxidative dehydrogenation of oxygen atom containing compounds, i.e., alcohols, over metal cation exchanged zeolites is known to proceed much more easily, as it does for, e.g., propane and 2-propanol over MgO (773 and 433 K, respectively [1,5]). In the mid 80's Gryaznova *et al.* [6] reported on the ODH of methanol over Na-FAU (X and Y), Na/K-LTL, Na-MOR, and Na-MFI; Na-FAU(Y) showed the highest CH₂O activity, although zeolite framework structure and Si/Al ratio were concluded not to be very important. Chemical nature and concentration of the extra framework cations have a much stronger influence on the ODH activity and selectivity. Transition metal (Cu, Co and Ni) exchanged Na-FAU(Y), Na/K-LTL, Na-MOR, and Na-MFI increased ODH activity. It was found that Co²⁺ exchanged zeolites have a high selectivity towards CO₂, whereas Ni²⁺ exchanged zeolites have a high selectivity towards formaldehyde (CH₂O). Increasing reaction temperature resulted in increasing CO₂ selectivity.

Different types of oxygen have been detected on the surface of oxidation catalysts, e.g., O⁻, O₂⁻ etc. [7]. The nature of these active oxygen species found on the catalyst surface depends strongly on the counter metal cation and structural conditions.

In alkali and alkaline earth cation exchanged zeolites two types of oxygen have been suggested. Russian scientists have reported only recently on the thermal generation of "singlet oxygen" (known as ¹Δ_gO₂, O₂(¹Δ_g) or ¹O₂) on Cs⁺ and Ca²⁺/Cs⁺ exchanged MFI (ZSM5) [8]. Singlet oxygen

-
1. Fuchs, S.; Leveles, L.; Seshan, K.; Lefferts, L.; Leminodou, A.; Lercher, J.A. *Topics Catal.* **2001**, *15*, 169.
 2. Faliks, A.; Yetter, R.A.; Floudas, C.A.; Bernasek, S.L.; Fransson, M.; Rabitz, H. *J. Phys. Chem. A* **2001**, *105*, 2099.
 3. Chang, Y.-F.; Somorjai, G.A.; Heinemann, H. *Appl. Catal. A: General* **1993**, *96*, 305.
 4. Kubacka, A.; Wloch, E.; Sulikowski, B.; Valenzuela, R.X.; Cortés Corberán, V. *Catal. Today* **2000**, *61*, 343.
 5. Miyata, H.; Wakamiya, M.; Kukokawa, Y. *J. Catal.* **1974**, *34*, 117.
 6. Gryaznova, Z.V.; Nefjodova, A.R.; Sidamonidze, Sh.I.; Akhalbedashvili, L.G. *Zeolites* **1987**, *7*, 123.
 7. a) Lunsford, J.H. *Catal. Rev.* **1973**, *8*, 135; b) Moro-oka, Y. *Catal. Today* **1998**, *45*, 3.
 8. Romanov, A.N.; Bykhovskii, M.Ya.; Ruffov, Yu.N.; Korchak, V.N. *Kinet. Catal.* **2000**, *41*, 782.

molecules are used as oxidizing agent of alkenes, yielding peroxides, which, subsequently, rearrange to hydroperoxides [9,10]. Others have claimed an O₂-hydrocarbon charge-transfer complex, which leads to the formation of superoxide anions (O₂⁻) and hydrocarbon radical cations (of alkanes [11], alkenes [12] and aromatics [13]) by the transfer of electrons, followed by proton transfer from the hydrocarbon radical to O₂⁻ to yield peroxides and, subsequently, decompose into the corresponding carbonyl species and water over basic alkali and alkaline earth exchanged zeolites [14]. However, these type of oxygens (singlet and superoxide anions) were found to add to the organic substrate (resulting in oxygenates; see Ref. [9-14]), rather than to dehydrogenate. Dehydrogenation abilities of the gaseous oxygen molecule over basic zeolites were only reported by Kovacheva and coworkers for the oxidative coupling of methane at reaction temperatures higher than 973 K [15]. However, the mechanism for the abstraction of hydrogens from methane over basic zeolites is not yet understood, since it most likely involves removal of framework oxygen as was found for, e.g., Li/MgO [16,17] (see also Chapter 1). The dehydrogenation of higher alkanes was found to occur already at lower temperatures [4]. Probably the framework oxygen centers abstract the hydrogens of the alkane, which then are removed with gaseous oxygen as was found for Li modified magnesia [18]. So far no study has been undertaken to analyze the active oxygen species in alcohol dehydrogenation as reported in Ref. [6].

It was shown recently that methanol reaction over too basic material like Rb- and Cs-FAU(X) and hydrotalcites yielded mainly CO (see Ref. [19] and Chapter 6). The unselective MeOH decomposition to CO is also one of the major problems in the side chain alkylation of toluene with methanol over Rb- and Cs-FAU(X) and proceeds via the intermediates, surface formaldehyde and formate (see Chapter 6 of this thesis). By using alkali exchanged MFI zeolites in the toluene alkylation, higher methanol selectivity could be obtained; MFI zeolites are much less basic [20] and thereby less active in the decomposition of methanol and the alkylation intermediate formaldehyde into CO and H₂ (as shown in Chapter 6 of this thesis).

-
9. a) Clennan, E.L.; Sram, J.P. *Tetrahedron* **2000**, *56*, 6945; b) Clennan, E.L. *Tetrahedron* **2000**, *56*, 9151.
 10. Shailaja, J.; Sivaguru, J.; Robbins, R.J.; Ramamurthy, V.; Sunoj, R.B.; Chandrasekhar, J. *Tetrahedron* **2000**, *56*, 6927.
 11. a) Sun, H.; Blatter, F.; Frei, H. *J. Am. Chem. Soc.* **1996**, *118*, 6873; b) Sun, H.; Blatter, F.; Frei, H. *Catal. Lett.* **1997**, *44*, 247; c) Vanoppen, D.L.; De Vos, D.E.; Jacobs, P.A. *J. Catal.* **1998**, *177*, 22.
 12. a) Blatter, F.; Frei, H. *J. Am. Chem. Soc.* **1994**, *116*, 1812; b) Blatter, F.; Moreau, F.; Frei, H. *J. Phys. Chem.* **1994**, *98*, 13403; c) Xiang, Y.; Larsen, S.C.; Grassian, V.H. *J. Am. Chem. Soc.* **1999**, *121*, 5063.
 13. a) Sun, H.; Blatter, F.; Frei, H. *J. Am. Chem. Soc.* **1994**, *116*, 7951; b) Panov, A.G.; Larsen, R.G.; Totah, N.I.; Larsen, S.C.; Grassian, V.H. *J. Phys. Chem. B* **2000**, *104*, 5706.
 14. a) Frei, H. In *3rd World Congress on Oxidation Catalysis, San Diego*; Grasselli, R.K., Oyama, S.T., Gaffney, A.M., and Lyons, J.E., Eds.; Elsevier: Amsterdam, 1997; Vol. 110, pp 1041-1050; b) Blatter, F.; Sun, H.; Vasenkov, S.; Frei, H. *Catal. Today* **1998**, *41*, 297; c) Frei, H.; Blatter, F.; Sun, H. *U.S. Pat. 6,329,553*, 2001, assigned to University of California, USA.
 15. Kovacheva, P.; Arishtirova, K.; Davidova, N. *Appl. Catal. A: General* **1997**, *149*, 277.
 16. Kim, H.; Suh, H.; Paik, H. *Appl. Catal. A: General* **1992**, *87*, 115.
 17. a) Ito, T.; Wang, J.-X.; Lin, C.-H.; Lunsford, J.H. *J. Am. Chem. Soc.* **1985**, *107*, 5062; b) Lin, C.-H.; Wang, J.-X.; Lunsford, J.H. *J. Catal.* **1988**, *111*, 302.
 18. Leveles, L., "Oxidative conversion of lower alkanes to olefins", PhD thesis, University of Twente, Enschede, The Netherlands, 2002.
 19. a) Chapter 6 of this thesis; b) Palomares, A.E.; Eder-Mirth, G.; Rep, M.; Lercher, J.A. *J. Catal.* **1998**, *180*, 56.
 20. a) Chapter 4 of this thesis; b) Rep, M.; Palomares, A.E.; Eder-Mirth, G.; Van Ommen, J.G.; Rösch, N.; Lercher, J.A. *J. Phys. Chem. B* **2000**, *104*, 8624.

However, the surface oxygen centers of basic MFI catalysts are not basic enough for abstracting the methyl hydrogen of methanol yielding the necessary formaldehyde intermediate for the side chain alkylation reaction of toluene. With basic MFI zeolites only surface methoxy groups were found (see Chapter 6), which are highly active for the methylation of the toluene ring (see Chapter 9).

Based on the report by Ref. [6] where O₂ was used to dehydrogenate alcohols over basic MFI zeolites yielding the corresponding carbonyl compounds we decided to study the reaction of methanol with oxygen over different basic molecular sieves. Here we report a study on the influence of the zeolite composition, i.e., the morphology, exchanged alkali cation and Si/Al ratio, on the reaction of methanol in the presence of molecular oxygen. Alkali exchanged MFI (ZSM5), MOR and FAU (X and Y) zeolites were used. The aim of present study was to probe whether the presence of oxygen could be used to get higher yields of formaldehyde from methanol over basic FAU(X) and MFI zeolites, and if so, could the higher concentration of formaldehyde then be used for increasing the yield of side chain alkylation of toluene. Our main concern here was to determine the reaction conditions where MeOH oxidation yielded selectively formaldehyde without the concomitant loss of selectivity due to byproduct (e.g., CO_x) formation. In Chapter 9 of this thesis results obtained during the methanol side chain alkylation of toluene in the presence of O₂ are reported.

7.2 EXPERIMENTAL

Zeolites (Na- and Cs-FAU(X), Na- and Cs-MFI, Na-FAU(Y), Na-MOR10 and Na-MOR20) were pressed into self-supporting wafers and loaded into the i.r. spectrophotometer, where they were analysed *in situ* during all treatments. Activation procedures were as reported in Chapter 3 in Helium. The infrared reactor equipment is described in Chapter 3. After activation the zeolites were brought into contact with a methanol/oxygen mixture (10 mbar MeOH / 3 mbar O₂ in 19 ml.min⁻¹ He) and were allowed to equilibrate. Experiments where the catalyst was first equilibrated with methanol at a partial pressure of 10 mbar and, subsequently, was exposed to 3 mbar of oxygen until adsorption - desorption equilibrium was reached (while keeping the partial pressure of the first reactant constant) yielded equal results. Then the samples were heated under continuous methanol and oxygen flow (heating rate: 5 K.min⁻¹). Gas phase analysis was performed using a Balzers OMNISTAR GSD 300 O₂ mass spectrometer. Also the reaction in 0.231 and 0.723 mbar O₂ with MeOH on Cs-FAU(X) was studied.

Blank experiments in an empty (no catalyst) i.r. reactor were carried out ($p_{\text{MeOH}} = 10$ mbar; $p_{\text{O}_2} = 3$ mbar) in order to examine the contribution of the thermal gas phase oxidation reactions to the catalytic one. The presence of the heating wires in the i.r. reactor cell was found to catalyze MeOH oxidation into H₂O, DME and CO₂ at temperatures above 350 K (see Fig 7.1). Increasing MeOH conversion was observed above 400 K. H₂ production was found above 500 K. The effect was not quantified. In the measured temperature range (323-773 K) no formaldehyde, CO or methyl formate was observed in the gas phase (see Fig 7.1).

The presence of a zeolite wafer in the i.r. reactor during the catalytic runs ($p_{\text{MeOH}} = 10$ mbar; $p_{\text{O}_2} = 3$ mbar) influenced the composition of the measured effluent streams. Differences in conversion caused by the presence of the “heating wires” and “heating wires+catalyst” were measured. MeOH conversion was smaller until approximately 500 K when a zeolite wafer (Cs-MFI) was present in the i.r. reactor (catalytic activity was measured above 440 K). The temperature range differed per catalyst present (start MeOH conversion Na-MFI = Na-FAU(X): 440 K (similar conversion as empty i.r. reactor at $T > 650$ K); Cs-FAU(X): 500 K (much lower conversion as the empty i.r. reactor in temperature range 323-773 K)). This indicates a large influence of the catalyst on the methanol oxidation reaction catalyzed by the heating wires and most likely caused by a better heat transfer of the heating wires when a wafer is present. Therefore, gas phase data obtained during reaction in the i.r. reactor will be used only below $T < 350$ K for H_2O , CO_2 and DME, below $T < 500$ K for H_2 , and the whole temperature range (323-773 K) for the production of formaldehyde, methyl formate and CO. Gas phase data (above $T > 350$ K) will only be treated qualitatively due to the fact that the gas phase MeOH concentration is very much influenced by the heating wires of the i.r. reactor (that could not be quantified). Blank MeOH oxidation experiments using 0.231 and 0.723 mbar O_2 were not performed; however, due to the reactivity of the i.r. reactor cell gas phase data above 350 K will be treated only qualitatively.

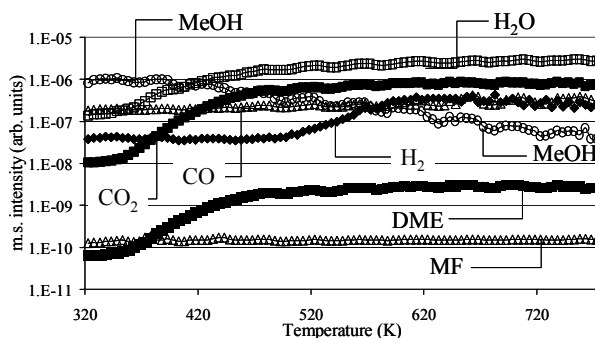


Figure 7.1: Gas phase analysis of the effluent stream after methanol oxidation ($p_{\text{MeOH}} = 10$ mbar; $p_{\text{O}_2} = 3$ mbar) in the empty i.r. reactor as function of temperature (323-773 K, $T_r = 5 \text{ K}\cdot\text{min}^{-1}$). (DME = dimethyl ether; MF = methyl formate)

Reaction conditions in the fixed bed flow reactor were: 15 mbar of methanol and 5 mbar of molecular oxygen, continuously, in flowing Ar ($16 \text{ ml}\cdot\text{min}^{-1}$). Catalysts at 323 K (approximately 50 mg) were allowed to equilibrate in MeOH and O_2 (about 80 minutes) before heating in MeOH/ O_2 flow was started (heating rate: $5 \text{ K}\cdot\text{min}^{-1}$). Gas phase analysis was performed using a mass spectrometer (online continuously for the gas phase analysis of water, CO and CO_2) and gas chromatograph (samples taken at 323, 673, and 773 K, respectively). The reaction equipment is described in Chapter 3. MeOH conversion was calculated using Equation 7.1 at a fixed temperature (773 K) during an isothermal experiment (see also Chapter 3):

$$X_{\text{MeOH}} = ((N_{\text{MeOH},in} - N_{\text{MeOH},out}) / N_{\text{MeOH},in}) \times 100\% \quad (\text{Eq. 7.1})$$

Blank experiments in an empty fixed bed reactor were performed to show the contribution of non-catalytic (thermal gas phase) reactions to the catalytic reaction. A small contribution of thermal non-catalytic oxidation reactions to the catalytic performances above 673 (H_2 and DME), 743 (H_2O) and 773 (CO_2) K was observed. No gaseous formaldehyde, CO or methyl formate was found in the temperature range 323-773 K.

7.3 RESULTS

Methanol reaction over alkali exchanged FAU, MOR and MFI zeolites in the presence of oxygen

MeOH oxydehydrogenation over alkali exchanged FAU(X) catalysts

In Figure 7.2 i.r. spectra obtained after methanol adsorption on Na-FAU(X) in the absence (Fig. 7.2a) and presence of oxygen (Fig. 7.2b) are shown. The coadsorption of methanol and oxygen on alkali cation exchanged FAU(X) catalysts (conditions: $T = 323$ K, $p_{\text{MeOH}} = 10$ mbar; $p_{\text{O}_2} = 3$ mbar) did not result in a marked difference in the i.r. wavenumbers of adsorbed methanol over FAU(X) catalysts with those reported in Chapter 6 (adsorption of methanol ($p_{\text{MeOH}} = 10$ mbar) in the absence of O_2). The same observation was made for the deformation i.r. band of the OH group (δ_{OH}) at approximately 1400-1390 cm^{-1} and CH group at approximately 1480-1450 cm^{-1} (δ_{CH}) of molecularly adsorbed methanol on Na- (see Fig. 7.2a and b) and Cs-FAU(X) (not shown here). However, we did observe additional new bands at 1721 (Na-FAU(X))-1717 (Cs-FAU(X)) and 1651 cm^{-1} in the i.r. spectrum at 323 K (see below for assignment). These bands are absent in the spectrum of MeOH adsorbed on Na-FAU(X) in the absence of O_2 (compare Fig. 7.2a and b). In summary, the stretching vibration of the methanol hydroxyl and methyl group adsorbed on Na-FAU(X) at 323 K are found at 3369 ($\nu(\text{OH})$), and 2946 and 2838 ($\nu(\text{CH}_3)$) cm^{-1} (see Fig. 7.2b), while on Cs-FAU(X) these are found at 3260 ($\nu(\text{OH})$), and 2946 and 2831 ($\nu(\text{CH}_3)$) cm^{-1} (not shown here) at 323 K.

The new i.r. bands observed after admission of methanol (10 mbar) and O_2 (3 mbar = 23 mol% (based on total $[\text{MeOH}+\text{O}_2]$ concentration)) on Na-FAU(X) at 323 K at 1721 and 1651 cm^{-1} (see Fig.7.2b) are assigned to adsorbed formaldehyde (1721 cm^{-1} : $\nu_{\text{C=O}}(\text{CH}_2\text{O})$) [21] and water (1651 cm^{-1} $\delta_{\text{OH}}(\text{H}_2\text{O})$) [22], respectively. Water is produced during the oxidation of MeOH yielding formaldehyde. At higher temperatures also the freely vibrating OH stretching vibration of adsorbed water (3687 cm^{-1} (isolated $\nu_{\text{O-H}}(\text{H}_2\text{O})$) [22]) was observed (see Fig. 7.3, where the i.r. spectrum recorded during MeOH t.p.o. over Na-FAU(X) at 516 K is shown) and the OH deformation band ($\delta_{\text{O-H}}(\text{H}_2\text{O})$) shifted to higher wavenumbers (compare Fig. 7.2b (1646 cm^{-1}) at 323 K and Fig. 7.3a (1651 cm^{-1}) at 516 K). The bands at 3455 cm^{-1} in Fig. 7.3 is assigned to chemisorbed methanol on Na^+ cations in Na-FAU(X).

During the temperature programmed methanol oxidation over Na-FAU(X) ($T = 323$ -773 K) in the i.r. reactor the intensity of the band assigned to surface formaldehyde increased till 424 K after which it decreased again (surface CH_2O observed between 323 and 516 K) with the simultaneous increase of new bands at 1615 ($\nu_{\text{as,C=O}}(\text{HCOO})$), 1371 ($\nu_{\text{s,C=O}}(\text{HCOO})$), and 2714 ($\nu_{\text{C-H}}(\text{CH})$) cm^{-1} assigned to surface formate [19,21], and surface methoxy (2814 ($\nu_{\text{s}}(\text{CH}_3)$)). Clearly the bands assigned to surface formate (1615 and 1371 cm^{-1}) can be seen in Fig. 7.3a at 516 K. In Fig.7.4 (bottom) the intensity of the i.r. bands assigned to surface formaldehyde (1721 cm^{-1}) and formate (1615 cm^{-1}) as a

21. Unland, M.L. *J. Phys. Chem.* **1978**, 82, 580.

22. Bertsch, L.; Habgood, H.W. *J. Phys. Chem.* **1963**, 67 1621.

function of temperature are shown. Surface formate (band at 1615 cm^{-1}) was observed between 398 and 645 K (maximum i.r. intensity at 523 K). The bands assigned to surface formaldehyde and formate are in perfect agreement with those observed during formaldehyde adsorption on Na-FAU(X) (see Chapter 6). No surface species were detected above 680 K. This in sharp contrast to MeOH decomposition over Na-FAU(X) where surface methoxy groups (i.r. bands at 2956 and 2847 cm^{-1}) were still observed at 773 K (see Chapter 6).

Simultaneously with the monitoring of the surface species by i.r. spectroscopy during MeOH t.p.o. over Na-FAU(X) the gas phase composition of the effluent stream was analyzed; Fig. 7.4 shows the gas phase composition as a function of temperature. However, as said in the Experimental section,

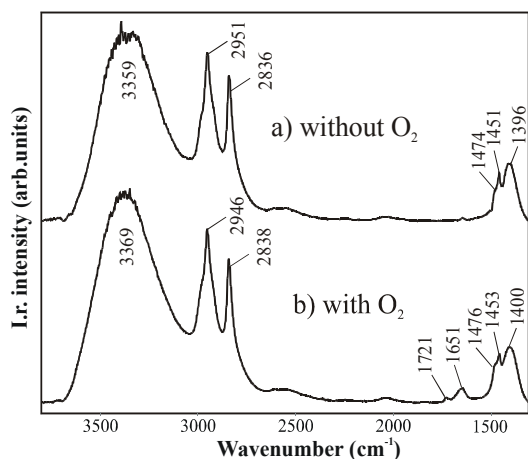


Figure 7.2: Difference i.r. spectra at 323 K during MeOH adsorption over Na-FAU(X) in the a) absence and b) presence of O_2 . Note the appearance of bands at 1721 and at 1651 cm^{-1} in spectrum b. (See text for assignment of the shown i.r. bands.)

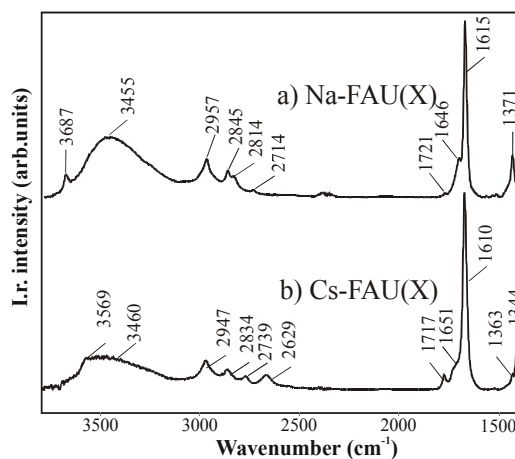


Figure 7.3: Difference i.r. spectrum during MeOH oxidation ($p_{\text{MeOH}} = 10\text{ mbar}$; $p_{\text{O}_2} = 3\text{ mbar}$) over a) Na- and b) Cs-FAU(X) at 516 K yielding surface formaldehyde (band at $1721\text{--}1717\text{ cm}^{-1}$) and surface formate (band at $1615\text{--}1610\text{ cm}^{-1}$).

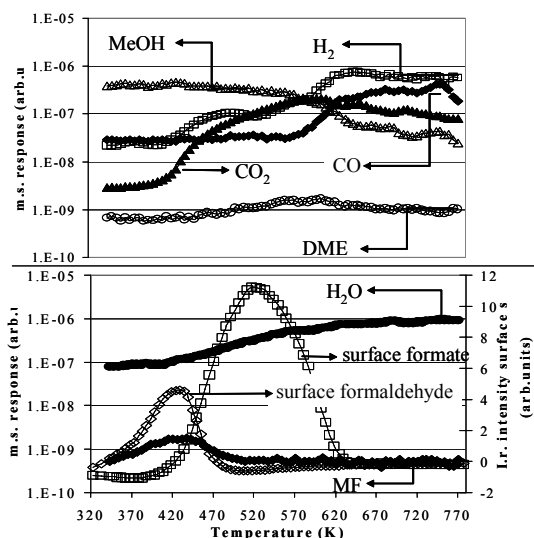


Figure 7.4: Gas phase analysis of the effluent stream after methanol oxidation (in the i.r. reactor) and evolution of the i.r. intensity of surface formaldehyde and formate over the same Na-FAU(X) (bottom) as function of temperature. Reaction conditions as in Fig. 7.1. (DME = dimethyl ether; MF = methyl formate)

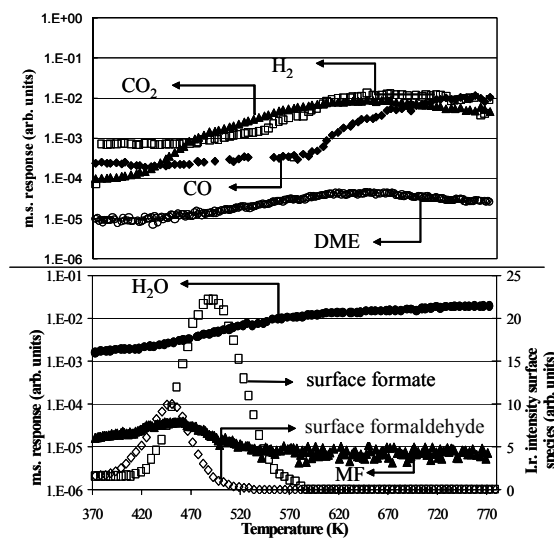


Figure 7.5: Gas phase analysis of the effluent stream after methanol oxidation (in the i.r. reactor) and evolution of the i.r. intensity of surface formaldehyde and formate over the same Cs-FAU(X) (bottom) as function of temperature. Reaction conditions as in Fig. 7.1. (DME = dimethyl ether; MF = methyl formate)

the gas phase composition shown in Fig. 7.4 is produced by the heating wires and the catalyst, simultaneously (it can not be decided how large each contribution is). The effect of the heating wires on the production of DME, CO₂, H₂, and H₂O above 350 K can not be neglected, although there appears to be hardly any MeOH conversion below 440 K over Na-FAU(X) (see Experimental section). Almost similar gas phase concentrations of DME, CO₂, H₂, and H₂O above 350 K were found in the empty i.r. reactor as with the catalyst present (compare Fig. 7.1 and 7.4)). Thus only a qualitative analysis of the gas phase composition is possible above 350 K (see also Experimental section). It was noticed, however, that even above 350 K small differences did occur. These differences will be treated only qualitative.

Gas phase analysis of the effluent stream after MeOH oxidation over Na-FAU(X) showed no gaseous formaldehyde between 323 and 773 K. This indicates that adsorbed formaldehyde is produced by methanol oxydehydrogenation over the Na⁺ exchanged FAU(X) zeolite solely and not over the heating wires and thus it is safe to show results from the i.r. spectra with respect to adsorbed formaldehyde and/or formate. Methyl formate (MF) was observed between 343 and 465 K (maximum intensity at 443 K). This product was not observed during the reaction catalyzed by the heating wires. The temperature range (and maximum) of methyl formate coincides closely with the temperature range (and maximum) of adsorbed formaldehyde, and is likely formed during the desorption of CH₂O. Also during temperature programmed desorption (t.p.d.) of formaldehyde adsorbed on Na-FAU(X) was the evolution of methyl formate between 378 and 539 K (maximum at 454 K) observed (see Chapter 6).

Also a small increase in the H₂O content in the gas phase was detected during methanol oxidation till 380 K (see Fig. 7.4), which is attributed to the oxydehydrogenation of methanol yielding water and surface formaldehyde. Above 380 K a fast increase in H₂O production was observed which can be attributed to the heating wires.

The gas phase concentration of CO₂ was found to exhibit two differences compared to the reaction in the empty i.r. reactor; a shoulder was observed at 460 K and a maximum in the CO₂ concentration at 593 K, after which the CO₂ concentration dropped slightly (these features were not observed in the empty i.r. reactor) and are attributed to the catalyst. No indication of adsorbed CO₂ (bands at, e.g., 1660, 1480 and 1425 cm⁻¹ (on Na-FAU(X)) [21]) was found during MeOH oxidation over Na-FAU(X).

H₂ was detected starting at 410 K, and showed two maxima (at 493 and 615 K). This is at a much lower temperature than observed with the empty i.r. reactor (and also the two maxima are not observed with reaction in the empty i.r. reactor) and is thus attributed to the presence of the catalyst. The shape of the CO₂ production curve is almost similar as for the H₂ production curve (see Fig. 7.8) until 480 K. The simultaneous fast increase of H₂ and CO₂ during methanol oxidation at approximately 410 K and the shoulder at approximately 480 K could indicate oxidation of formaldehyde.

At higher temperatures also the formation of CO was observed (T > 570 K) that increased till 773 K (this product of MeOH oxidation is not observed during the blank experiments in an empty i.r. reactor and is thus solely attributed to the catalysts activity). The production of gaseous CO is 60 K

lower compared to the MeOH reaction in the absence of O₂ (see Chapter 6). Almost no DME was observed in the gas phase, in sharp contrast to the reaction of MeOH in the absence of O₂ where the production of DME is observed (see Chapter 6).

As with Na-FAU(X), MeOH oxidation with O₂ (3 mbar = 23 mol% (based on total [MeOH+O₂] concentration)) over Cs-FAU(X) (T = 323-773 K) yielded also adsorbed formaldehyde (band at 1717 cm⁻¹: $\nu_{C=O}(\text{CH}_2\text{O})$) and surface formate (bands at 1610 ($\nu_{\text{as},C=O}(\text{HCOO})$), 1344 ($\nu_{\text{s},C=O}(\text{HCOO})$), 1363 ($\delta_{C-H}(\text{HCOO})$), and 2739 (CH) cm⁻¹). These bands are similar to those observed during formaldehyde adsorption on Cs-FAU(X) (see Chapter 6). The i.r. intensity of formaldehyde only decreased in intensity upon the formation of surface formate and methoxy (at 2947 ($\nu_{\text{as}}(\text{CH}_3)$), and 2810 ($\nu_{\text{s}}(\text{CH}_3)$) cm⁻¹ (not shown)). In Fig. 7.3b the i.r. spectrum recorded during MeOH oxidation over Cs-FAU(X) at 516 K is shown. During the production of surface formaldehyde also the evolution of adsorbed water (1651 cm⁻¹ ($\delta_{\text{OH}}(\text{H}_2\text{O})$) [22]) was observed; the other product of methanol oxidative dehydrogenation to formaldehyde.

In Figure 7.5 (bottom) the evolution of surface formaldehyde and formate during MeOH oxydehydrogenation over Cs-FAU(X) is plotted as function of temperature. Surface formaldehyde was observed between 323 and 521 K (maximum i.r. intensity at 448 K), thus the temperature range was almost similar as with Na-FAU(X); maximum i.r. intensity was found at slightly higher temperature (24 K). Apparently the nature of the cation does not influence the reaction much. However, the surface formaldehyde concentration at the top of the formaldehyde curve was found to be two times higher on Cs-FAU(X), compared to Na-FAU(X). The same result was obtained for the surface formate species on Cs-FAU(X), i.e., a three times higher surface concentration (at the temperature with the maximum i.r. intensity). Surface formate was observed between 383 and 585 K (maximum i.r. intensity at 495 K); the temperature of the maximum i.r. intensity and the maximum temperature where surface formate still could be observed on Cs-FAU(X) were 60 K and 30 K lower, respectively, compared to Na-FAU(X).

In Fig. 7.6 and 7.7 the effect of small O₂ concentrations (0.231 mbar (231 ppm) or (0.723 mbar (723 ppm) in the feed of MeOH) on the production of formaldehyde (CH₂O) and surface formate (HCOO) during methanol oxidation over Cs-FAU(X) is shown (as function of temperature and oxygen content of the feed). Analysis

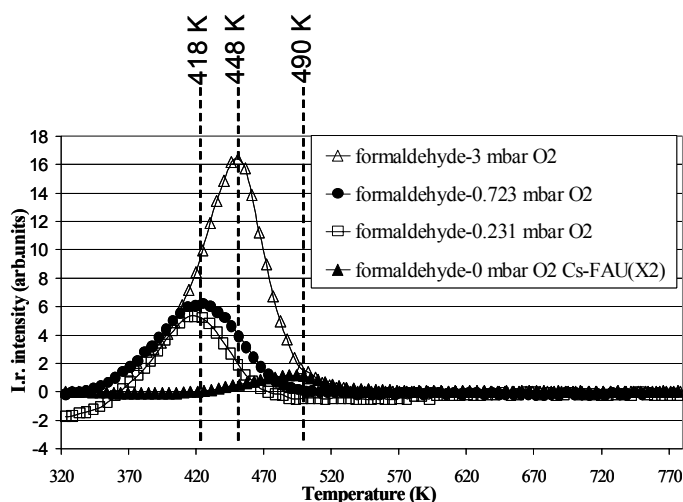


Figure 7.6: Evolution of surface formaldehyde (band at ~ 1713 cm⁻¹) during MeOH reaction over Cs-FAU(X) as a function of temperature and O₂ partial pressure (0.231, 0.723, and 3 mbar O₂). For clarity the formation of formaldehyde over Cs-FAU(X2) in the absence of O₂ is also shown (see Chapter 6).

of the area of surface formaldehyde (between 323-503 K) showed that using a three fold increase of O_2 (0.723 mbar = 6.7 mol% (based on total [MeOH+ O_2] concentration)) in the feed, compared to 0.231 mbar O_2 (= 2.3 mol% (based on total [MeOH+ O_2] concentration)), resulted only in a slight broadening of the band assigned to surface formaldehyde (area increase: 7%); maximum intensity at 418 (0.231 mbar) - 423 K (0.723 mbar). The area of the CH_2O i.r. band when using 3 mbar O_2 (as function of temperature) increased 2 times (compared to the band observed with 0.231 and 0.723 mbar O_2).

While with 3 mbar O_2 only one maximum of the surface formate band was found at 495 K (see Fig. 7.7), two apparent maxima were found during MeOH t.p.o. over Cs-FAU(X) for the surface formate i.r. band with 0.723 and 0.231 mbar O_2 ; at approximately 473 and 554 K in 0.231 mbar O_2 and with 0.723 mbar O_2 the second maximum was shifted to lower temperatures (approximately 523 K). The band assigned to surface formate (between 423 and 673 K), increased approximately 2 times at its maximum intensity when using 0.723 mbar O_2 , compared to using 0.231 mbar O_2 . The i.r. band at the maximum formate intensity was approximately 4 times larger when using 3 mbar O_2 , compared to using 0.231 mbar O_2 .

Also during MeOH oxidation ($p_{O_2} = 3$ mbar) over Cs-FAU(X) no gaseous formaldehyde was detected between 323 and 773 K, even though adsorbed formaldehyde was observed (1717 cm^{-1}). This observation agrees well with the observation made for Na-FAU(X). And as with Na-FAU(X), methyl formate was observed in the gas phase between 370 and 532 K with Cs-FAU(X) (maximum intensity at 450 K, which coincides with the maximum in surface CH_2O i.r. intensity on Cs-FAU(X) (see Fig. 7.5)). The production of methyl formate was found over a wider temperature range on Cs-FAU(X), compared to Na-FAU(X) and agrees well with the i.r. intensity difference of surface formaldehyde and formate between Cs-FAU(X) and Na-FAU(X). Most likely the high production of CO_2 and H_2 on Na-FAU(X) (at these low temperatures) causes this product difference.

Also with low O_2 concentration in the MeOH feed (0.723 and 0.231 mbar), no gas phase formaldehyde was detected but only methyl formate (MF). Methyl formate was observed between 323 and 498 K (max gas phase concentration at 423 K) with 0.231 mbar O_2 and between 323 and 518 K (max gas phase concentration at 438 K) with 0.723 mbar O_2 . When using approximately 3 times more O_2 (i.e., 0.723 mbar O_2) also more MF was produced (1.5 times more), compared to 0.231 mbar O_2 ,

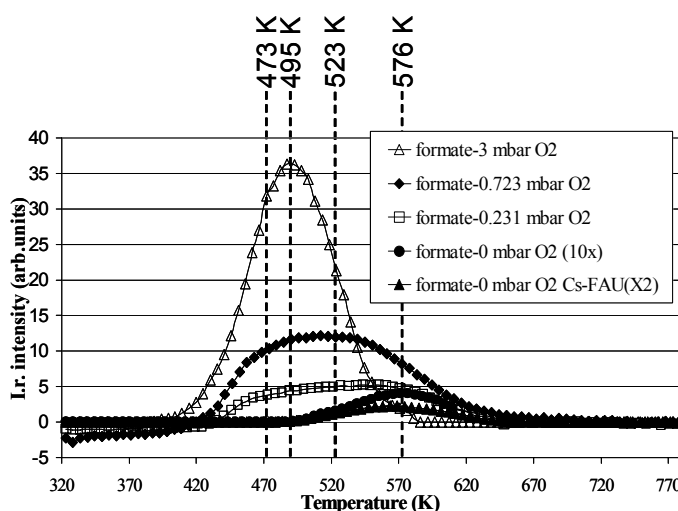


Figure 7.7: Production of surface formate (band at 1607 cm^{-1}) during MeOH reaction over Cs-FAU(X) as a function of temperature and O_2 partial pressure (0 (enlarged 10x), 0.231, 0.723, and 3 mbar O_2). For clarity the formation of surface formate over Cs-FAU(X2) in the absence of O_2 is also shown (see Chapter 6).

with a small shift of its maximum rate of formation to higher temperatures (433 K). This was also observed for the production of surface formaldehyde. However, although the surface concentration of formaldehyde with 3 mbar of O₂ was only 2 times larger the production of methyl formate was approximately 8 times larger compared to 0.231 mbar O₂. Also on the catalysts surface is methyl formate observed (band at 1672 cm⁻¹ [23]); the MF concentration (gas phase and surface) decreases simultaneously with the decreasing i.r. intensity of CH₂O. No adsorbed methyl formate was observed during MeOH oxidation using 3 mbar O₂.

Also a band at 2629 cm⁻¹ was observed on Cs-FAU(X) during MeOH oxydehydrogenation (see Fig. 7.3 at 516 K). The origin is unknown; this band can not be attributed to adsorbed methyl formate, since MF is characterized by a carbonyl stretching vibration at 1672 cm⁻¹ (see before) [23], which is not present at these temperatures. Other forms of adsorbed formaldehyde, e.g., polymerized formaldehyde, characterized by bands at 1486 and 1377 cm⁻¹ [24], were not observed. The bands at 3569, 3460, and 2834 cm⁻¹ in Fig. 7.3 are assigned to chemisorbed methanol.

The increase in water production is almost similar when using 3, 0.723, or 0.231 mbar O₂ at low temperatures (T < 428 K). This coincides with the rate of production of surface formaldehyde, which also did not depend too much on the oxygen concentration. An additional amount of H₂O is adsorbed on the surface of the catalyst (see Fig. 7.3).

As also observed for the production of CO₂ over Na-FAU(X) during MeOH oxidation in 3 mbar O₂ a shoulder at 488 K and a maximum at 654 K were observed, which were not observed in the blank experiment, and are thus attributed to the presence of the catalyst (no indication of adsorbed CO₂ (bands at, e.g., 1690 and 1300 cm⁻¹ (on Cs-FAU(X)) [21]) was found). In Fig. 7.5 the composition of the gas phase during MeOH oxidation over Cs-FAU(X) in the i.r. reactor as function of temperature is shown. The production of DME and H₂ showed also a maximum in the gas phase concentration at 643 and 657 K, respectively (not observed in the blank experiment).

With the smaller O₂ concentrations the production of CO₂, DME and H₂ was observed at much higher temperatures, compared to the reaction in the presence of 3 mbar O₂. Due to the fact that no blank experiment was performed using 0.231 and/or 0.723 mbar O₂, the effect of the heating wires at these low O₂ is not known and will thus not be discussed here.

However, production of CO was not observed in the empty i.r. reactor and is thus attributed to the catalysts performance. The CO production in the presence of the three different O₂ pressures on Cs-FAU(X) was found to start at approximately 598-603 K and increased until 773 K. The production of CO was approximately 3 times higher with 3 mbar, compared to 0.723 and 0.231 mbar O₂ at 773 K.

Also methanol oxidation in a fixed bed reactor was performed to obtain information about the gas phase composition without the catalytic effect of heating wires as observed with the i.r. reactor. The gas phase composition and the product trend did not differ from that observed from the i.r. reactor despite the fact that both are different reactor types (compare gas phase composition during MeOH

23. Feil, F.S.; Van Ommen, J.G.; Ross, J.R.H. *Langmuir* **1987**, *3*, 668.

24. Fisher, I.A.; Bell, A.T. *J. Catal.* **1999**, *184*, 357.

oxidation over Cs-FAU(X) in the i.r. reactor (Fig. 7.5) and Rb-FAU(X) in the fixed bed reactor (Fig. 7.8)). Methanol oxidation over Rb-FAU(X) yielded a small increase in the H₂O content of the gas phase (see Fig. 7.8). From 428 K it increased till 773 K with a jump at 500 K. Methyl formate was observed between 343 and 503 K (maximum gas phase concentration at 413 K). The production of methyl formate in the fixed bed reactor can most likely be used as evidence for the production of surface formaldehyde as shown before.

CO₂ was detected starting at 438 K, and showed a maximum at 683 K with a jump at 493 K (see Fig. 7.8); the simultaneous fast increase of CO₂ and water at 430 K, and the similar jump in the CO₂ and H₂O production curve during methanol oxidation at approximately 493 K could indicate oxidation of formaldehyde. After 490 K the CO₂ production curve showed a very nice correlation with the DME production curve. DME production started at 453 K and showed a maximum at 698 K. The slow increase in both production curves of DME and CO₂ between 510 and 700 K could indicate CH₂O reaction, yielding CO₂ and DME. The shoulder observed in the production of CO₂ and the maxima in the production of DME and CO₂ were also observed in the i.r. reactor with Cs-FAU(X).

Other compounds found in the effluent stream were: CO (start at 618 K, fast increase after 703 K), and H₂ (start 570 K, fast increase after 683 K). The ratio of H₂ and CO at 673 K was found to be approximately 1 (in the absence of O₂ the H₂/CO ratio was 2).

In an isothermal experiment at 773 K approximately 93% MeOH was converted (in the absence of O₂ this was only 71%). The production of methyl formate was smaller in the fixed bed reactor than in the i.r. reactor.

MeOH oxidation over Na⁺ and Cs⁺ exchanged MFI catalysts

As concluded for alkali cation exchanged FAU(X) molecular sieves, the coadsorption of methanol (10 mbar) and oxygen (3 mbar = 23 mol% (based on total [MeOH+O₂] concentration))) on basic MFI catalysts at 323 K also did not result in a marked difference with the i.r. spectrum of adsorbed methanol over MFI catalysts as reported in Chapter 6, and are therefore not shown here. In summary, the stretching vibration of the methanol hydroxyl and methyl group adsorbed on Cs-MFI are

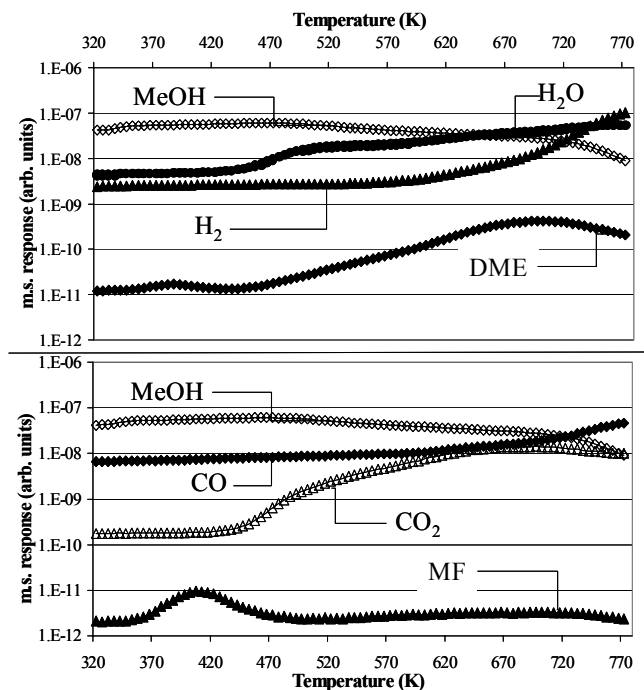


Figure 7.8: Gas phase analysis of the effluent stream after methanol oxidation over Rb-FAU(X). 323-773 K, $T_r = 5 \text{ K.min}^{-1}$. (DME = dimethyl ether; MF = methyl formate)

found at 3624 and 3493 (OH), and 2948 and 2841 (CH_3) cm^{-1} , while on Na-MFI these are found at 3620 and 3439 ($\nu(\text{OH})$), and 2950 and 2844 ($\nu(\text{CH}_3)$) cm^{-1} .

In Fig. 7.9 an i.r. spectrum obtained during the methanol oxidation at 503 K is shown. The bands shown in Fig. 7.9 (at 503 K) at 3618, 3460, 2954, and 2845 cm^{-1} are assigned to chemisorbed methanol. The i.r. bands observed at 1713 and 1742 cm^{-1} in Fig. 7.9 are assigned to adsorbed formaldehyde. A similar pattern for adsorbed formaldehyde was observed during CH_2O sorption (see Chapter 6), indicating two types of adsorbed formaldehyde. Already at 323 K the formation of surface formaldehyde was observed (by an i.r. band at 1713 cm^{-1}) and with increasing temperatures a higher surface concentration was found. No adsorbed H_2O was observed (absence of a band at approximately 1650-1630 cm^{-1} [25]). At 363 K a second band assigned to adsorbed CH_2O was observed at 1742 cm^{-1} (which is also seen in Fig. 7.9).

In Fig. 7.10 the presence of surface formaldehyde (1742 and 1713 cm^{-1}) as a function of temperature is shown. Surface formaldehyde was observed between 323 and 650 K (maximum i.r. intensity at 503 K). It is clear that methanol oxidation over Cs-MFI yields a very stable surface formaldehyde species (i.r. band at 1742 and 1713 cm^{-1}) as is indicated by the wide temperature range (323-650 K) of the surface formaldehyde (much wider compared to basic FAU(X) zeolites ($T < 521$

K)). Simultaneously, with the formation of surface formaldehyde methyl formate (MF) is detected in the gas phase till 618 K showing two maxima at approximately 373 and 463 K (see Fig. 7.10), which agrees well with the temperature range of adsorbed formaldehyde (see Fig. 7.10) [26]. Note that the gas

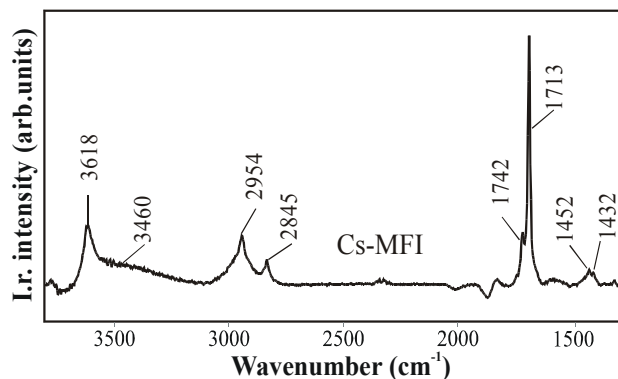


Figure 7.9 Difference i.r. spectrum during MeOH oxidation over Cs-MFI at 503 K yielding surface formaldehyde (band at 1742-1713 cm^{-1}).

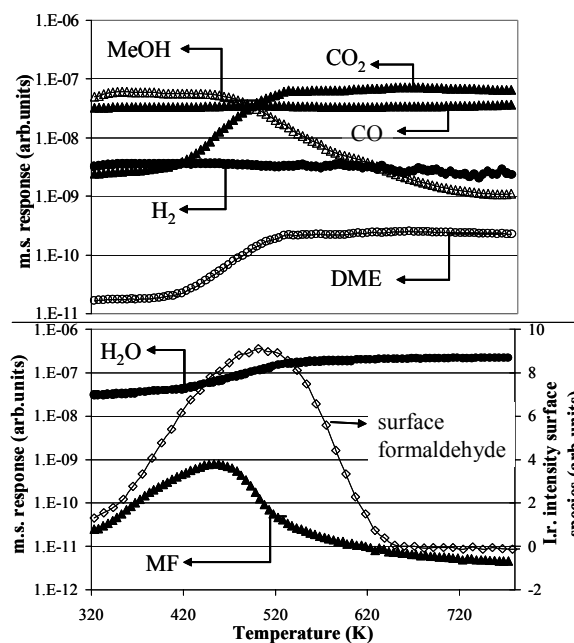


Figure 7.10: Gas phase analysis of the effluent stream after methanol oxidation (in the i.r. reactor) and evolution of the i.r. intensity of surface formaldehyde and formate over the same Cs-MFI (bottom) as function of temperature. 323-773 K, $T_r = 5 \text{ K.min}^{-1}$. (DME = dimethyl ether; MF = methyl formate)

25. Jentys, A.; Warecka, G.; Derewinski, M.; Lercher, J.A. *J.Phys. Chem.* **1989**, 93, 4837.

26. Gaseous methyl formate was also observed during thermal desorption (t.p.d.) of adsorbed formaldehyde on Cs-MFI between 323 and 523 K (maximum at 378 K) (not shown here). Also gaseous formaldehyde and the

phase concentration of methyl formate decreases more rapidly and has a maximum at lower temperature (463 K), compared to surface formaldehyde (503 K). No gaseous formaldehyde was detected at these temperatures during MeOH oxydehydrogenation (as also found for Na- and Cs-FAU(X)). The surface CH₂O concentration decreases after 503 K; however, no observation of surface formate or formaldehyde decomposition into CO and H₂ was observed. This is in sharp contrast to that observed for formaldehyde decomposition over alkali cation exchanged FAU(X) zeolites. It can be seen in Fig. 7.10 that the i.r. intensity of surface formaldehyde decreases with a decrease in MeOH gas phase concentration in the i.r. reactor.

As can be seen in Fig. 7.10 the evolution of CO₂, H₂O, and DME closely resemble that observed in the blank experiment and will thus not be discussed. Interesting result was that H₂ production is present in the oxidation reaction catalyzed by the heating wires, but not during the reaction over Cs-MFI and might indicate that the catalyst is much more active than the heating wires. In an isothermal experiment, approximately 76 and 89% MeOH was converted at 673 and 773 K, respectively. (In the absence of O₂ this was only 55 and 78% at 673 and 773 K, respectively.)

Methanol oxidation over Na-MFI yielded formaldehyde (i.r. band at 1712 cm⁻¹) between 323 and 520 K, showing two maxima at approximately 354 and 428 K (not shown here). The same product distribution was found in the gas phase for MF production (two maxima at 378 and 448 K). The intensity of surface formaldehyde and methyl formate was smaller with Na-MFI than with Cs-MFI and over a much smaller temperature range. Methyl formate was also detected during t.p.d. of adsorbed CH₂O on Na-MFI between 323 and 539 K (maximum at 378 K) [27] (not shown here). No gaseous formaldehyde was detected between 323 and 773 K, and also no production of surface formate and/or gas phase CO and H₂ was observed during MeOH oxydehydrogenation over Na-MFI. A 1.5-2 times increase was observed for CO₂ compared to DME over MFI catalysts, indicating deep oxidation of methanol.

MeOH reaction over basic MFI catalysts in the absence of O₂ did not yield any surface formaldehyde species or gaseous methyl formate (see also Chapter 6). These products in the present study, therefore, are the products of MeOH oxidation over these materials; the appearance of surface formaldehyde shows that these materials are reactive for the oxidative dehydrogenation of methanol in agreement with Gryaznova *et al.* [6].

MeOH oxidation over Na⁺ exchanged FAU(Y), MOR10, and MOR20 catalysts

Methanol adsorption at 373 K in the presence of oxygen on Na-FAU(Y), Na-MOR10 and Na-MOR20 zeolites yielded also surface formaldehyde species. On Na-FAU(Y) the formaldehyde carbonyl stretch vibration ($\nu_{C=O}$) was found at 1709 cm⁻¹; on Na-MOR10 and Na-MOR20 the

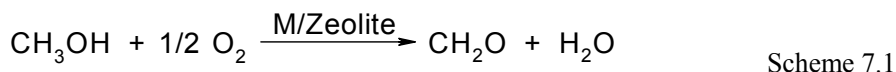
formation of gas phase methanol were observed between 363 and 549 K (maximum 456 K) over Cs-MFI. No CO and/or H₂ was observed. CH₂O adsorption – desorption also did not show the production of surface formate by i.r. spectroscopy (see Chapter 6).

27. Other desorbing gases during formaldehyde t.p.d. from Na-MFI were (not shown here): methanol and formaldehyde between 333 and 513 K (maximum 353 K). No CO and/or H₂ was observed. Also no surface formate was observed during CH₂O adsorption – desorption by i.r. spectroscopy (see Chapter 6).

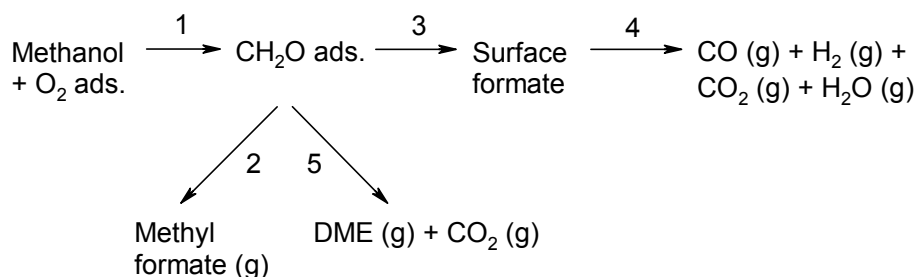
corresponding vibration is found at 1717 and 1712 cm^{-1} , respectively. On all samples also the formation of surface formate is also observed, this in contrast to basic MFI catalysts. The asymmetric C=O stretching vibration of surface formate ($\nu_{\text{as,C=O}}(\text{HCOO})$) was found at 1612 (Na-FAU(Y)), 1610 (Na-MOR10), and 1611 (Na-MOR20) cm^{-1} , respectively. (Due to the overlap at 373 K of the symmetric C=O stretching vibration ($\nu_{\text{s,C=O}}(\text{HCOO})$) at approximately 1370 cm^{-1} with the deformation band of the OH group of molecularly adsorbed methanol (δ_{OH}) at approximately 1400-1390 cm^{-1} , the band assigned to $\nu_{\text{s,C=O}}(\text{HCOO})$ was not observed.) No temperature ramp was performed to analyze any desorbing gases.

7.4 DISCUSSION

The use of molecular oxygen in the feed of MeOH to alkali cation exchanged zeolites resulted in the production of formaldehyde that was adsorbed on the zeolites surface (as observed using i.r. spectroscopy); formaldehyde results from the oxidative dehydrogenation of methanol. The overall reaction equation of the reaction of methanol with molecular oxygen to give formaldehyde is depicted in Scheme 7.1, where M represents the extra framework alkali cations (Na^+ , Cs^+ etc.).



Partial methanol oxidation over alkali cation exchanged FAU(X) and MFI zeolites yielded besides the desired product formaldehyde (CH_2O), a wide variety of other products. At low temperatures the formation of surface formaldehyde, formate (not on MFI), water (not on MFI), and methyl formate was found. The gas phase showed the production of water, methyl formate, CO_2 , H_2 (not on MFI), CO (not on MFI), and dimethyl ether (not on Na-FAU(X)) that increased with reaction temperatures. No gas phase formaldehyde was observed. In light of the i.r. spectroscopic (surface formaldehyde and formate), and gas phase (H_2O , MF, DME, CO_2 , H_2 , CO) results the following reaction pathways are proposed (see Scheme 7.2) and will be discussed here.



Scheme 7.2

ADSORBED METHANOL + OXYGEN

When methanol and O_2 are coadsorbed on the alkali cation exchanged MFI and FAU(X) zeolites, i.r. spectroscopy did not reveal any interaction of the methanol molecule with the oxygen molecule. This would be indicated by a shift of the methanol i.r. bands upon methanol - O_2 coadsorption compared to methanol adsorption on basic zeolites, and thus we conclude that there is no

strong interaction between the oxygen and the methanol molecule. Previous measurements reported isosteric heats of adsorption between 15 and 18 kJ.mol⁻¹ for O₂ on alkali cation exchanged FAU(X) [28] and MFI [29], and silicalite [28a], suggesting that interactions between O₂ and the alkali cations are negligible. Therefore, we suggest that methanol molecules are adsorbed on the extra framework cations (in the supercage and the channels of FAU(X) and MFI, respectively) as reported in Chapter 4 and 5 with a very weak interaction with O₂ [30].

Reaction 1: ADSORBED METHANOL → ADSORBED FORMALDEHYDE

MeOH adsorption (in the absence of O₂) on alkali exchanged FAU(X) and MFI at 323 K showed only i.r. bands related to MeOH (see Fig. 7.2a). Only on basic FAU(X) zeolites was the production of adsorbed formaldehyde (or formate via adsorbed formaldehyde) in the absence of O₂ observed at temperatures above 420 K. Basic MFI zeolites are not active for the production of formaldehyde; they do not possess strong enough basic framework oxygen centers for the abstraction of the methyl hydrogen (see Chapter 6).

Coadsorption of methanol and O₂ at 323 K (p_{MeOH} = 10 mbar; p_{O₂} = 3 mbar), however, results readily in the formation of new i.r. bands (at 1721 (on Na-FAU(X)), 1717 (on Cs-FAU(X)), 1712 (on Na-MFI), and 1742 and 1712 (on Cs-MFI) cm⁻¹ (see Fig. 7.2b)), which are attributed to adsorbed formaldehyde (formaldehyde adsorption at 323 K on basic FAU(X) and MFI zeolites (see Chapter 6) showed i.r bands of the C=O stretching vibration ($\nu_{C=O}$) that resemble well those observed during methanol oxydehydrogenation). For example, during CH₂O adsorption on Na-FAU(X), the $\nu_{C=O}$ band was observed at 1724 cm⁻¹, whereas this band was observed at 1721 cm⁻¹ during methanol oxydehydrogenation. From this result we conclude that the reaction of MeOH with oxygen over alkali cation exchanged FAU(X) and MFI zeolites easily proceeds at room temperature, yielding the desired product formaldehyde. This is also evident from the production of water; the major byproduct formed during methanol oxydehydrogenation over alkali exchanged FAU(X) and MFI zeolites (see Scheme 7.1). Water was observed both in the gas phase (over the whole temperature range (323-773 K) for all zeolites during reaction) and adsorbed on the catalysts surface (with i.r. bands at 3685 and 1651-1646 on Na-FAU(X) (see Fig. 7.2b and 7.3a) and 1646 cm⁻¹ on Cs-FAU(X) (see Fig. 7.3b). Also the other Na⁺ exchanged zeolites, i.e., Na-FAU(Y), Na-MOR10 and Na-MOR20, produced adsorbed formaldehyde during MeOH oxydehydrogenation at 373 K (p_{MeOH} = 10 mbar; p_{O₂} = 3 mbar). The ability of the alkali cation exchanged zeolites to produce surface formaldehyde in the presence of O₂ agrees well with what is reported by Gryaznova *et al.* [6].

The different i.r. wavenumber of the band assigned to surface formaldehyde observed on the different basic FAU(X) and MFI zeolites are attributed to the different adsorption structures and

28. a) Dunne, J.A.; Rao, M.; Sircar, S.; Gorte, R.J.; Myers, A.L. *Langmuir* **1996**, *12*, 5896; b) Jasra, R.V.; Choudary, N.V.; Bhat, S.G.T. *Ind. Eng. Chem. Res.* **1996**, *35*, 4221.

29. Savitz, S.; Myers, A.L.; Gorte, R.J. *Microporous Mesoporous Mater.* **2000**, *37*, 33.

30. Frei *et al.* [11a,12b] reported that such a weak interaction could only be observed by UV-visible absorption measurements, as concluded for alkane-O₂ and alkene-O₂ interactions.

locations of surface formaldehyde on these zeolites (see Chapter 6). Also when comparing the C=O stretching vibration ($\nu_{\text{C=O}}$) of adsorbed CH_2O on the different Na^+ exchanged zeolites (Na-FAU(X): 1722 cm^{-1} ; Na-FAU(Y): 1709 cm^{-1} ; Na-MOR10: 1717 cm^{-1} ; Na-MOR20 1712 cm^{-1} ; Na-MFI: 1709 cm^{-1}) and the zeolite structure (Si/Al ratio (Na-FAU(X) lowest Si/Al and Na-MFI highest Si/Al)) no apparent correlation was found. This is not fully understood; the large difference observed for the $\nu_{\text{C=O}}$ on Na-FAU(X) and Na-FAU(Y) (found at 1722 and 1709 cm^{-1} , respectively) maybe is caused by the presence of Na^+ cations at site III in the supercage of Na-FAU(X). The reason for the different $\nu_{\text{C=O}}$ on the other Na^+ exchanged zeolites is unclear.

When the temperature was increased this resulted in an increase in the surface formaldehyde concentration on all zeolites studied. In Fig. 7.11 the i.r. intensity of the surface formaldehyde i.r. band is plotted as function of temperature. It can be seen that the stability of surface formaldehyde over alkali exchanged zeolites was highest for the Cs^+ exchanged analogues (i.e., that the temperature for observing CH_2O by i.r. spectroscopy was widest for Cs-FAU(X) and Cs-MFI, compared to Na-FAU(X) (see Fig.7.11) and Na-MFI. Furthermore, on Cs-FAU(X) a higher surface formaldehyde concentration at higher temperatures (448 K) was found, compared to Na-FAU(X). This is probably due to side reactions occurring on Na^+ exchanged zeolites at these low temperatures (see later). Also a marked difference can be

observed for the production over the Cs^+ exchanged zeolites; obviously, on Cs-MFI the widest temperature range for the surface CH_2O concentration is observed. From this we conclude that CH_2O was the most stable on Cs-MFI. Isothermally, MeOH conversion over Rb-FAU(X) was slightly higher compared to Cs-MFI at 773 K (93% and 89%, respectively).

Cs-MFI, however, has approximately 12 times less active sites per gram catalyst (0.4 mmol.g^{-1} active sites), compared to Rb-FAU(X) (4.9 mmol.g^{-1} active sites), thus the reactivity per site in Cs-MFI must be much higher.

This higher activity of Cs-MFI, compared to Cs-FAU(X), is explained by the high electrostatic field inside these high silica zeolites [13b]. Chang *et al.* [3] and Kubacka *et al.* [4] reported

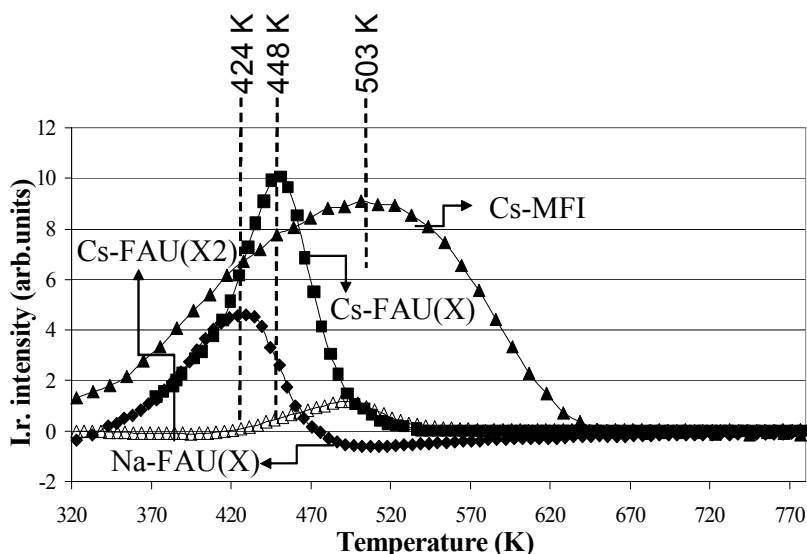


Figure 7.11: Evolution of surface formaldehyde (band at $\sim 1742\text{-}1712\text{ cm}^{-1}$) during MeOH reaction over Na-FAU(X), Cs-FAU(X), and Cs-MFI as a function of temperature ($p_{\text{MeOH}} = 10\text{ mbar}$; $p_{\text{O}_2} = 3\text{ mbar}$). For clarity the formation of formaldehyde over Cs-FAU(X2) in the absence of O_2 is also shown (see Chapter 6).

also higher reactivity for alkane oxidation over MFI zeolites, compared to FAU(Y), however, Gryaznova *et al.* [6] reported higher reactivity for MeOH ODH of FAU(Y), compared to MFI; the reason for this inconsistency is not understood.

From the above it is obvious that with the use of gaseous O₂ the production of CH₂O is much facilitated as is indicated by the lower reaction temperatures where surface formaldehyde is observed (T > 323 K), compared to the reaction in the absence of O₂ (T > 420 K (see Chapter 6)). This is shown in Fig. 7.11. In the absence of O₂, surface formaldehyde was observed between 423 and 583 K (maximum i.r. intensity at 490 K). The maximum i.r. intensity of the CH₂O carbonyl group in the absence of O₂ on Cs-FAU(X2) was thus observed 40 K higher (starting temperature approximately 100 K higher). Additionally, also the surface CH₂O concentration has increased with the use of O₂. This is probably due to the higher CH₂O formation rate and the lower probability of surface formaldehyde disproportionation to surface formate at these lower reaction temperatures, as has been discussed in Chapter 6 (bare in mind that formaldehyde disproportionation, however, already proceeds at 323 K).

Adsorbed formaldehyde was only observed during MeOH dehydrogenation (without O₂) over a specially prepared Cs-FAU(X2) zeolite (containing less Cs⁺ and Na⁺ cations, but with a similar Si/Al ratio (see Chapter 3 and 6) as the molecular sieve used in this study). On the other zeolites used here (Na- and Cs-FAU(X)), no adsorbed formaldehyde was observed in the absence of O₂ (see Chapter 6). This was attributed to the fact that these catalysts were too active for the decomposition of surface formaldehyde (see Chapter 6), due to the high temperatures needed to form it.

It is clear from the similar slope of the surface formaldehyde production curve in Fig. 7.11 at low temperature (T < 424 K) on Na- and Cs-FAU(X) that the nature of the cation in basic FAU(X) does not influence the CH₂O production on Na- and Cs-FAU(X). This is further emphasized by the almost similar temperature window for CH₂O production over these basic FAU(X) zeolites.

A similar observation was made when using O₂ at different partial pressures in the MeOH feed over Cs-FAU(X). The presence of different O₂ concentrations (3, 0.723, or 0.231 mbar O₂) also did not lead to an enhancement of the formation rate of formaldehyde. The slopes of all three CH₂O curves with different O₂ pressures are approximately the same until 418 K (see Fig. 7.6); only a higher surface CH₂O concentration and wider temperature range was observed for the production of CH₂O (see Fig. 7.6) with increasing O₂ concentrations in the MeOH feed. Furthermore, CH₂O formation starts at similar temperatures on Cs-FAU(X) with different O₂ concentrations. The smaller temperature range with decreasing O₂ concentrations might indicate O₂ depletion at low O₂ concentrations in the gas phase due to other fast competing oxidation reactions at low temperatures (see below). O₂ depletion could not be measured by the mass spectrometer, due to the fact that the reactants (MeOH, O₂) and products (CO₂, CO, H₂O) share common molecular and fragment ions of m/z 32 (MeOH, O₂) and 16 (O₂, CO₂, CO H₂O).

The most important observation, however, to be made here is that in the presence of oxygen formaldehyde production can be induced on alkali exchanged MFI zeolites, whereas in the absence of O₂ only DME is produced (see Chapter 6). Thus the first goal has been reached. However, the question

remains, what happens with the surface formaldehyde on the different catalysts as function of O₂ concentration and temperature. This question will be answered in the remaining part of this Chapter.

Reaction 2: ADSORBED FORMALDEHYDE → METHYL FORMATE

During the increase of temperature, no gas phase formaldehyde was observed in the whole temperature range (323-773 K) on all catalysts studied. However, gas phase methyl formate (MF) was observed in the same temperature range with concentration maxima of methyl formate (in the gas phase) at approximately the same temperatures as surface formaldehyde on all catalysts. This is shown in Figures 7.4, 7.5, and 7.10. Furthermore, temperature programmed desorption of CH₂O adsorbed on Na-FAU(X) (see Chapter 6), and Na- and Cs-MFI also showed the presence of methyl formate in the gas phase between 323 and approximately 539 K [31].

Thus it was concluded that surface formaldehyde desorbs as methyl formate; the mechanism at this moment is unclear. Most likely it proceeds via an aldol condensation reaction. This reaction is considered to be very fast (on Cs-FAU(X)), as a 3 times increase of O₂ resulted in a 1.5 times increase of the methyl formate concentration in the gas phase, whereas only a slight

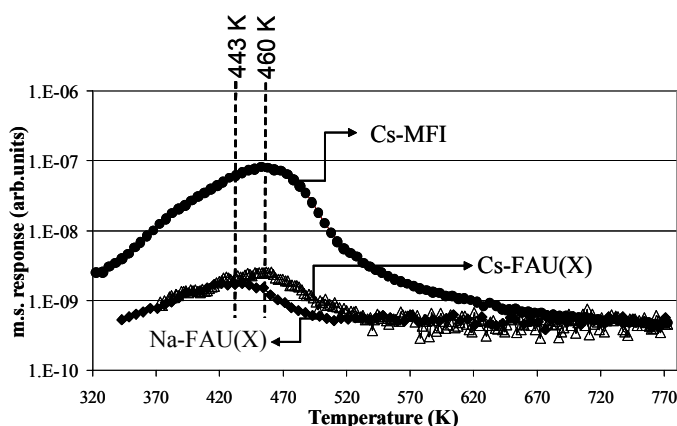


Figure 7.12: Evolution of gaseous methyl formate during MeOH oxidation over Cs-MFI, Na-FAU(X), and Cs-FAU(X) as a function of temperature. 323-773 K, $T_r = 5 \text{ K.min}^{-1}$.

broadening was observed for the surface formaldehyde concentration. Methyl formate was also observed on the surface of Cs-FAU(X) when small concentrations of O₂ were used in the feed and is characterized by an i.r. band at 1672 cm⁻¹.

The gaseous methyl formate concentration was found to be highest and also the temperature range was widest with Cs-MFI (see Fig. 7.12), compared to the other basic zeolites used. This agrees well with the observation made for the surface formaldehyde concentration on these same catalysts, i.e., widest temperature range for surface formaldehyde is observed for Cs-MFI (see before). The methyl formate concentration during MeOH oxydehydrogenation over Cs-FAU(X) was found over a wider temperature range compared to Na-FAU(X) (a similar observation was done for the surface formaldehyde i.r. intensity on Cs-FAU(X)). This is probably due to fast decomposition (oxidation) of surface formaldehyde over Na-FAU(X) at low temperatures (see below). This also explains the difference in methyl formate production over Cs-FAU(X), compared to Cs-MFI. The temperature range difference between Na-MFI (323-520K) and Cs-MFI (323-618 K) can probably be explained by a higher activity towards CH₂O coupling yielding DME and CO₂ over Na-MFI (see below). The

31. On Cs-FAU(X) this product species was not analyzed for during CH₂O adsorption – desorption.

temperature range of methyl formate over Rb-FAU(X) in the fixed bed reactor was smaller than with Cs-FAU(X) in the i.r. reactor. This could be attributed to the different catalyst or to the longer contact times in the fixed bed reactor, leading to higher oxidation of the formed products in the presence of O₂.

Methyl formate was not detected during the MeOH reaction over basic zeolites in the absence of O₂. This is related to the much higher temperatures needed for MeOH dehydrogenation (yielding surface CH₂O) over basic FAU(X) zeolites (approximately 100 K higher) and the high probability for formaldehyde disproportionation at these temperatures. Also with basic MFI the production of methyl formate was not observed during methanol reaction in the absence of O₂; this is due to the fact that basic MFI is not an active dehydrogenation catalyst, i.e., no adsorbed CH₂O is observed (see Chapter 6).

Above 420-460 K on basic FAU(X) the methyl formate gas phase concentration was found to decline simultaneously with the decreasing i.r. intensity of surface formaldehyde (see Fig. 7.4 and 7.5). New i.r. bands were observed at approximately 2814-2810, 1615-1610 and 1371-1344 cm⁻¹ (see Fig. 7.3). This will be discussed below.

Reaction 3 and 4: ADSORBED FORMALDEHYDE → SURFACE FORMATE → CO, H₂, CO₂ and/or H₂O

The new i.r. bands observed during MeOH oxydehydrogenation at approximately 1615-1610 and 1371-1344 cm⁻¹ on Na- and Cs-FAU(X) are attributed to the formation of surface formate and the i.r. band at 2814-2810 cm⁻¹ to surface methoxy, as these results resemble well those observed during formaldehyde adsorption on basic FAU(X) (see Chapter 6). It was shown in Chapter 6, that adsorbed formaldehyde easily decomposes on Na- and Cs-FAU(X) into surface methoxy (2820-2816 cm⁻¹) and surface formate (at T > 323 K) and, subsequently, to CO and H₂ (at T > 530 K); the production of surface formate (i.r. bands at approximately 1613 and 1371-1345 cm⁻¹) and CO are evidence of a *Cannizzaro* type disproportionation reaction [32,[33]]. Also on Na-FAU(Y), Na-MOR10, and Na-MOR20 was surface formate observed during MeOH oxidation.

In Fig. 7.7 and 7.13, the i.r. intensity of the surface formate i.r. band is plotted as function of temperature, O₂ concentration and different basic FAU(X) zeolites. Interestingly, the production of surface formate with small concentrations of O₂ shows two i.r. maxima, of which the high temperature maximum shifts to lower temperatures with increasing O₂ concentrations, and finally completely disappeared (see Fig. 7.7); in the presence of 3 mbar O₂ only one maximum at 495 K was observed. The same observation was made for Na-FAU(X); no overlap of the surface formate in the presence and absence of O₂ was found above 630 K. In the absence of oxygen over Cs-FAU(X), MeOH dehydrogenation yielded surface formate at 490-620 K (maximum surface concentration at 576 K). These temperatures are approximately 100 K higher than in the presence of 3 mbar O₂ (383-585 K (maximum i.r. intensity at 495 K)). The same observation was made for the MeOH reaction in the

32. Venuto, P.B.; Landis, P.S. *Adv. Catal.* **1968**, *19*, 259.

33. Busca, G.; Lamotte, J.; Lavalley, J.C.; Lorenzelli, V. *J. Am. Chem. Soc.* **1987**, *109*, 5197.

presence and absence of O_2 over Na-FAU(X) (see Fig. 7.13). It can be seen that the production of surface formate proceeds over Cs-FAU(X) at lower temperature and is highest (a three times larger surface formaldehyde concentration was observed on Cs-FAU(X)), compared to Na-FAU(X) when using 3 mbar O_2 . This is probably due to higher surface CH_2O concentration on Cs-FAU(X) (see before).

It can be seen that at low O_2 concentrations (0.231 and 0.723 mbar O_2) in the MeOH feed the shape of the formate production curve at $T > 520$ K) and the second maximum at high temperature (at approximately 520-550 K) closely resembles that found for the surface formate in the absence of O_2 (see Fig. 7.7 and 7.13). This might indicate a similar decomposition pathway of methanol. And indeed, further increasing temperatures ($T > 570$ K) resulted in the decrease of the surface formate band and the simultaneous increase in the production of CO and H_2 . The starting temperatures for the formation of CO on Na-, Rb-, and Cs-FAU(X) zeolites (in the i.r. reactor and fixed bed reactor (> 3 mbar O_2)) during MeOH oxidation coincides very nicely with that observed during formaldehyde desorption and MeOH dehydrogenation (see Chapter 6) and indicate that the absence of the surface formate i.r. band at $T > 570$ K (with > 3 mbar) does not imply that this decomposition path way is not used.

The ratio of H_2 and CO at 673 K on Rb-FAU(X) during MeOH oxidation (5 mbar) was found to be approximately 1 (in the absence of O_2 the H_2/CO ratio is 2) and is indicative of formaldehyde decomposition to formate that, subsequently, decomposes to CO and H_2 . Thus (part of) adsorbed formaldehyde decomposes via surface formate (Cannizzaro type disproportionation).

The presence of the additional low temperature maximum (at $T = 470$ K) of the surface formate with 0.231 and 0.723 mbar O_2 and the absence of the high temperature maxima of the surface

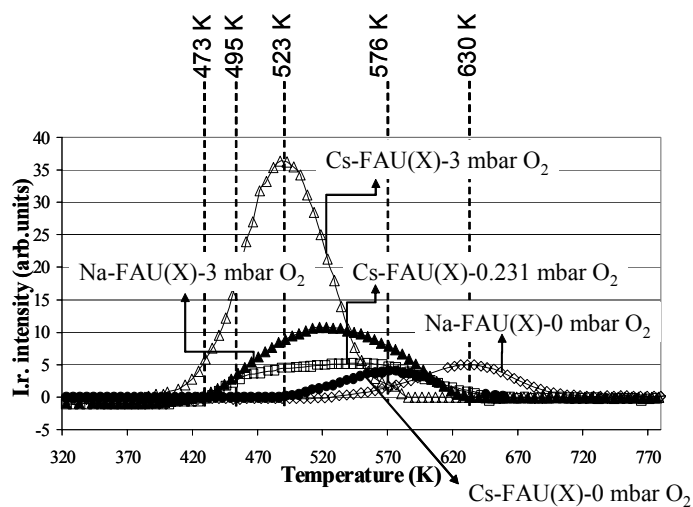


Figure 7.13: Evolution of surface formate (band at ~ 1613 cm^{-1}) during MeOH reaction over Na-FAU(X), and Cs-FAU(X) as a function of temperature, and O_2 pressure ($p_{O_2} = 0, 0.231$ and 3 mbar). For clarity the formation of formaldehyde over Cs-FAU(X) in the absence of O_2 is also shown (see Chapter 6) (enlarged 10x).

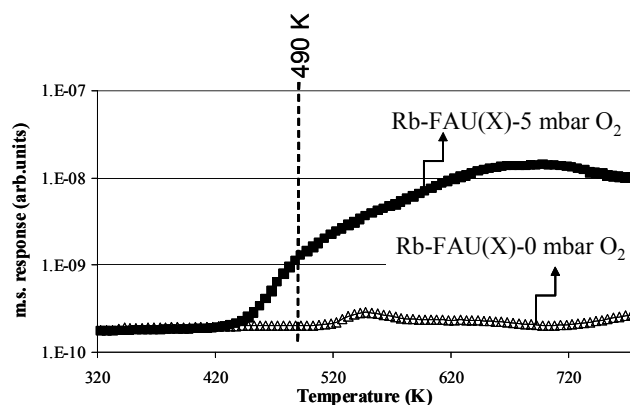


Figure 7.14: Gas phase CO_2 production during methanol reaction and oxidation over Rb-FAU(X) in the fixed bed reactor as function of temperature. 323-773 K, $T_r = 5$ $K \cdot min^{-1}$; $p_{MeOH} = 15$ mbar (see Experimental section).

formate with 3 mbar O₂ on Na- and Cs-FAU(X) compared to 0 mbar O₂, could indicate a different decomposition pathway for the surface formate group or a different surface species on Cs-FAU(X). Close examination of the effluent stream during MeOH oxidation showed that with the surface formate production at low temperatures the simultaneous production of CO₂ and H₂ over Na-FAU(X) (see Fig. 7.4) and CO₂ and H₂O over Rb- and Cs-FAU(X) was observed (see Fig. 7.5 and 7.10) and this might indicate a similar intermediate species. No CO₂ production was observed during the methanol reaction in the absence of O₂ (see Fig. 7.14). Thus the production of CO₂ could indicate surface CH₂O oxidation (deep-oxidation: a commonly encountered problem when using molecular oxygen as oxidant [7b,14b]). Based on the product distribution (CO₂ and H₂) over Na-FAU(X) this could be formic acid (HCOOH); it is known that formaldehyde produced during methanol oxydehydrogenation could, subsequently, also be oxidized resulting in the formation of formic acid [34] and formic acid is thought to be the precursor to the production of CO₂ [35]. Furthermore, it was established that formic acid (HCOOH) adsorption yields similar surface formate groups as observed during MeOH oxidation (see Chapter 6 and Ref. [36]). The appearance of the formate i.r. band at low temperatures would thus be in favor of such assignment. Thus to further aid the identification of the origin of gaseous products formed during the MeOH oxydehydrogenation over basic zeolites, such as CO₂, H₂O and H₂, temperature programmed desorption of adsorbed formic acid on basic FAU(X) and MFI was studied (see Chapter 6).

Analysis of desorbing species during t.p.d. of formic acid adsorbed on basic FAU(X) zeolites (in the absence of O₂) was, however, not conclusive about the possible CH₂O oxidation to formic acid (during MeOH oxydehydrogenation) as a precursor for the production of CO, CO₂, H₂, and H₂O. In present study CO₂ and H₂ were observed at much lower temperatures during MeOH oxidation over Na-FAU(X) (410 K); during HCOOH t.p.d. they were observed above 543 K. Production of CO was only observed at temperatures above 570 K, whereas HCOOH desorption led to the production of CO above 440 K (see Chapter 6). Water was detected over the whole temperature range between 323 and 973 K (see Chapter 6). Non-dissociated HCOOH desorbed from basic FAU(X) between 353 and 623 K; in present study no HCOOH could be detected. Similar observations were done on Rb- [37] and Cs-FAU(X) (see Chapter 6) (for Rb- and Cs-FAU(X), during HCOOH desorption CO was observed at T > 420 K, while H₂ and CO₂ were observed at T > 493 K). Thus the difference of temperature regions for CO, CO₂, and H₂ appears to indicate that formic acid is no precursor to the formation of CO, CO₂ and H₂ formed during MeOH oxydehydrogenation. However, it can not be excluded that formic acid itself in present study is directly oxidized at low temperatures to yield CO₂, H₂O, and/or H₂ (formic

34. Horowitz, A. *J. Phys. Chem.* **1985**, *89*, 1764.

35. Brock, E.E.; Oshima, Y.; Savage, P.E.; Barker, J.R. *J. Phys. Chem.* **1996**, *100*, 15834.

36. Fraissard, J.; Rouabah, D.; Gruia, M. *J. Chim. Phys. Phys.-Chim. Biol.* **1986**, *83*, 681.

37. HCOOH desorption from Rb-FAU(X) showed a similar spectrum as observed for Cs-FAU(X) (not shown here), however, lower desorbing concentrations of H₂ and CO₂ were found at higher temperature for H₂ and CO₂ (at 623 K), compared to Cs-FAU(X) (at 610 K).

acid t.p.d. in the presence of O₂ was not performed). Note that no adsorbed CO₂ was observed on Na- and Cs-FAU(X) during MeOH oxydehydrogenation.

On Na- and Cs-MFI the i.r. intensity of formaldehyde was found to decrease after 430 and 503 K, respectively. However, this cannot be attributed to the formation of surface formate, since no surface formate was observed during MeOH oxidation on Na- and Cs-MFI; this in sharp contrast to basic FAU(X) zeolites. The absence of CO and H₂ as CH₂O decomposition products over basic MFI catalysts during MeOH oxidation is consistent with those findings. The same observations were made during CH₂O t.p.d. [26,27]. The absence of surface formate and CO and H₂ on basic MFI catalysts was explained by 1) the framework oxygens of alkali cation exchanged MFI are not basic enough (to yield dioxymethylene), 2) the low cation concentration, and 3) the sites are too far separated for hydride transfer between neighboring adsorbed formaldehyde molecules (see also Chapter 6), thus preventing a *Cannizzaro* type disproportionation. This indicates higher stability of surface formaldehyde on basic MFI catalysts, due to the fact that CH₂O decomposition to CO and H₂ does not occur.

Also direct oxidation of surface formaldehyde to formic acid on Na- and Cs-MFI could not be established as no i.r. spectroscopic evidence of surface formate or adsorbed formic acid was found between 323 and 773 K. Also in the gas phase no formic acid or CO was observed in present study, whereas during formic acid decomposition from Na-MFI (in the absence of O₂), HCOOH and CO were the most abundant species in the gas phase (see Chapter 6; Appendix 3). In the case of Cs-MFI, H₂ was observed during formic acid decomposition that is not observed during MeOH oxydehydrogenation. No formic acid decomposition experiments, however, have been performed in the presence of O₂.

Reaction 5: ADSORBED FORMALDEHYDE → DME + CO₂

Another product that is increasingly observed upon further increasing temperatures is the production of gas phase dimethyl ether (except on Na-FAU(X)). Very clearly it can be seen in Fig. 7.10 that the production of DME is accompanied by the formation of CO₂ (both increase similar at T > 500 K and show gas phase maxima at approximately the same temperature (T > 673 K)). (Above 673 K the decrease of the m.s. response signals of CO₂ and DME decrease. This might indicate O₂ depletion above 593 K (5 mbar O₂ present at 323 K)). It was shown by Venuto and Landis [32] and Sefcik [38] that formaldehyde (in the absence of O₂) could react intermolecularly to form DME and CO₂ as is represented in Scheme 7.3.



In the case of Na-FAU(X) no gas phase DME is observed. The reason for this is at this moment unclear. It is supposed that the high electrostatic potential of the Na⁺ cation, induces extreme oxidation of formaldehyde and methanol to CO₂. This is obvious from the small temperature range of surface formaldehyde and methyl formate in the gas phase, compared to Cs-FAU(X).

The decrease of the i.r. and m.s. signals of surface formaldehyde and gaseous methyl formate on Na- and Cs-MFI, however, can not be explained by the formation of surface formate or CH₂O

38. Sefcik, M.D. *J. Am. Chem. Soc.* **1979**, *101*, 2164.

oxidation to formic acid (see before). Therefore, another reaction path must be available for the decrease of surface formaldehyde and methyl formate with increasing temperatures. When using Cs-MFI at temperatures higher than 463 K the methyl formate gas phase concentration decreases, while the surface formaldehyde concentration still increases (see Fig. 7.10). No other surface or gas phase species are observed than CO₂ and DME (in the gas phase). This indicates a similar overall reaction as was shown by Sefcik [38] (see Scheme 7.3). Thus it is concluded that the formation of DME and CO₂ over basic MFI catalysts results from the coupling of formaldehyde. A 1.5-2 times increase is observed for CO₂ compared to DME over MFI catalysts, indicating deep oxidation of methanol. (Caution has to be kept in mind due to the fact that the production patterns resemble closely those of the empty reactor.) Than at temperatures higher than 503 K also the surface formaldehyde i.r. intensity decreases. This parallels the decrease of gas phase MeOH concentration (see Fig. 7.10). Thus the high MeOH conversion above 500 K results in the decrease of surface formaldehyde.

A final word: The results shown in this work show that O₂ contamination during methanol adsorption on and/or reaction over basic zeolites can alter the course of the reaction and hence influence the interpretation of results. Therefore, great caution has to be taken into account while investigating methanol adsorption/reaction.

7.5 CONCLUSION

In Chapter 6 the reaction of methanol was studied in the absence of oxygen yielding surface formaldehyde and formate over alkali exchanged FAU(X) zeolites as well. The aim of the study presented here was to determine whether molecular oxygen could be used to yield formaldehyde, which is the supposed intermediate in the side chain alkylation of MeOH with toluene [19], over basic FAU(X) and MFI in the oxydehydrogenation of methanol; this was confirmed in present study.

Partial methanol oxidation over alkali cation exchanged FAU(X) and MFI zeolites yielded the desired product surface formaldehyde (CH₂O) at much lower temperatures (water as by product), compared to the reaction in the absence of O₂ (which was shown in Chapter 6). These results show that the presence of O₂ in the methanol feed MeOH oxidation resulted in a much lower reaction barrier for the formation of surface formaldehyde over active dehydrogenation catalysts, e.g., Cs-FAU(X) and catalysts which are inactive for MeOH dehydrogenation in the absence of O₂, e.g., Cs-MFI. However, no gaseous formaldehyde was observed.

The use of O₂, however, opened also the reaction pathway over basic FAU(X) and MFI to other products at these low temperatures. The formation of adsorbed formaldehyde is limited on Na-Rb-, and Cs-FAU(X) and Na, and Cs-MFI by 1) the production of methyl formate, 2) the decomposition of formaldehyde and/or oxidation of formaldehyde to surface formate (not on basic MFI) and CO₂ and 3) the production of DME (not on Na-FAU(X)) and CO₂.

Methyl formate is supposed to be the product of an aldol condensation reaction. Production of CO, H₂, CO₂, and water results from direct oxidation of surface formaldehyde or *Cannizzaro* type disproportionation of surface formaldehyde to surface formate (not on basic MFI). The production of surface formate was also observed on basic FAU(X) at lower temperatures compared to the reaction in the absence of O₂. Increasing O₂ concentrations resulted in an increase of the direct oxidation of CH₂O. DME was also observed as a product of CH₂O coupling.

Due to the wider temperature range of surface CH₂O (and gaseous methyl formate) on Cs-MFI, which indicates a higher surface stability on Cs-MFI, it is concluded that Cs-MFI is the most selective surface formaldehyde production catalyst in the methanol oxydehydrogenation reaction.

Based on the results described here we propose that MeOH oxidation yielding *in situ* surface formaldehyde for the side chain alkylation reaction of toluene yielding styrene benefits probably the most from Cs-MFI. Since at higher temperatures (T > 463 K) methanol and/or formaldehyde deep oxidation prevails (i.e., CO₂, H₂, and H₂O production) the temperatures for formaldehyde reaction with toluene must be kept low (T < 520 K over Cs-MFI). This means toluene activation at low temperature. If high temperatures are needed this will result in unselective decomposition of methanol, i.e. deep oxidation of methanol to CO_x and H₂O.

Potential use of methanol oxydehydrogenation in toluene side chain alkylation: Recommendation

The major disadvantage of the use of molecular oxygen as oxydehydrogenation reagent of alkanes and/or alcohols is the large production of unwanted side-products (up to 93% of methanol is converted), since the desired alkene and/or aldehyde/ketone products are more reactive towards oxidation than the starting hydrocarbons; the desired products are immediate subject to consecutive reactions, leading to the thermodynamically favored final products CO₂, CO and H₂O. Earlier it was shown [6,47,39] that the oxidative dehydrogenation of lower alcohols on alkali exchanged zeolites is complicated with intramolecular and intermolecular dehydration and deep oxidation to CO₂; ethanol conversion on zeolites in oxidative atmosphere was carried out by following parallel, parallel-consequent and consequent reactions (intermolecular and intramolecular dehydration to C₂H₄ and (C₂H₅)₂O, respectively, partial oxidation to CH₃CHO and full oxidation to CO₂), and also conversion of isobutanol on sodium forms of FAU(Y), erionite and mordenite zeolite types tends toward a deep oxidation and dehydration.

Low reaction temperatures (T < 520 K) can limit by product formation, such as DME, CO₂, CO and H₂ as shown in present study. Also by keeping the conversions low deep oxidation can be overcome [40]. Furthermore, byproduct formation because of highly reactive oxy radicals can thus be reduced. Also milder oxidizing agents have been used to dehydrogenate alkanes and alcohols. For

39. Akhalbedashvili, L.; Mskhiladze, A.; Sidamonidze, Sh. In *Proceedings of the 13th International Zeolite Conference, Montpellier*; Galarneau, A., Di Renzo, F., Fajula, F., and Vedrine, J., Eds.; Elsevier: Amsterdam, 2001; Vol. 135, p 231.

40. Frei, H.; Blatter, F.; Sun, H. *Chem. Tech.* **1996**, *6*, 24.

example, CO₂ was used to dehydrogenate ethylbenzene yielding styrene [41], while, e.g., *tert*-butyl hydroperoxide, was tested in the ODH of alcohols over metal cation exchanged zeolites and yielded selectively aldehydes and ketones [54]. However, the use of CO₂ as oxidizing agent over basic zeolites is limited, since it adsorbs on the basic sites forming surface carbonates that might hinder the reaction [42].

Zeolites exchanged with transition metals for the oxydehydrogenation of methanol during the side chain alkylation could be used, since these zeolites exhibit a higher oxidative dehydrogenation activity and CH₂O selectivity [6,47,39]. Copper exchanged zeolites were used by Lacroix *et al.* [43] for the side chain alkylation of toluene in Ar and N₂. (Also zeotypes, like AlPO₄-18, with small amounts of transition metals as part of the framework were found active for oxydehydrogenation [44]. These materials were, however, not tested in the side chain methylation of toluene.) Also acidic zeolites were found to be active for alcohol oxidation; oxidation of benzyl alcohol over H-FAU(Y) proceeded with 100% selectivity yielding the corresponding benzaldehyde [45], thus being a good alternative to alkali exchanged zeolites. However, under reaction conditions using inert gas, e.g., He, during the reaction of alcohol with toluene, acidic zeolites have a high tendency for ring alkylation [46] and thus it is expected that the reaction of alcohol with toluene under oxidizing conditions will yield ring alkylated products as well.

In Chapter 9 results, obtained during the side chain methylation of toluene in the presence of O₂, will be discussed. From the above it is clear that if *in situ* oxidative dehydrogenation of methanol is to be used during the side chain alkylation of toluene (see Chapter 9) then this reaction should proceed at low reaction temperatures or with small O₂ concentrations in the feed in order to prevent deep oxidation of methanol to CO_x over basic zeolites. If alkylation of toluene can only proceed at temperatures higher than 550 K (indicating difficult toluene activation) then alkylation will have to compete with deep oxidation of MeOH.

Appendix 1 - Nature of the reactive oxygen species

It was shown here that the use of molecular oxygen yielded not only formaldehyde but opened also the route to different reaction products, e.g., methyl formate, CO, CO₂ etc. The remaining part of this Chapter will be addressed to the nature of the oxygen species, the interaction and reactivity of O₂ with methanol inside the zeolite pores and the effect of zeolite topology and basicity.

One possible reactive oxygen species in the oxidative methanol dehydrogenation reaction as mentioned in the Introduction are the oxygen centers of the zeolite framework as also considered in the

41. Mimura, N.; Tuatara, I.; Saito, M.; Hattori, T.; Ohkuma, K.; Ando, M. *Catal. Today* **1998**, *45*, 61.

42. Yagi, F.; Tsuji, H.; Hattori, H. *Microporous Mater.* **1997**, *9*, 237.

43. Lacroix, C.; Deluzarche, A.; Kiennemann, A.; Boyer, A. *Zeolites* **1984**, *4*, 109.

44. Hartmann, M.; Ernst, S. *Angew. Chem. Int. Ed.* **2000**, *39*, 888.

45. Tsuruya, S.; Okamoto, Y.; Kuwada, T. *J. Catal.* **1979**, *56*, 52.

46. a) Sidorenko, Yu.N.; Galich, P.N. *Petrol Chem.* **1991**, *31*, 57; b) Eder-Mirth, G., Lercher, J.A. *Recl. Trav. Chim. Pays-Bas* **1996**, *115*, 157.

oxidative methane coupling reaction [15-17]. However, oxygen isotope exchange experiments, to examine framework oxygen mobility, showed that oxygen exchange between the gas phase and framework oxygen only proceeds at high temperatures (873-973 K) [47]; much higher than the temperature range studied here. Thus it is concluded that (adsorbed) gas phase oxygen is the oxidative dehydrogenation reagent of methanol as studied here.

As said in the Introduction also singlet oxygen can be formed thermally inside the zeolite cages. The singlet, or S_1 , state is only 96 kJ.mol⁻¹ above the ground state [8] and could thus be considered as a reactive species in methanol oxidative dehydrogenation. However, singlet oxygen behaves like a very reactive alkene; it adds to dienes and alkenes in a cycloaddition reaction [48] yielding a peroxide species, which decomposes yielding oxygenates [9,10] instead of dehydrogenating the olefin. Addition of singlet oxygen to alcohols or alkanes (into an O-H or C-H bond) has not been reported [9,10]. Therefore, we do not consider singlet oxygen as active species for the observed dehydrogenation of methanol.

Additionally, also the formation of O_2^- species has been postulated and observed for basic zeolites. Superoxide anions could be formed during reaction of gas phase oxygen with trapped holes on Si-O-Al groups (T = Si or Al) in the framework composite [49]. Thermal formation of O_2^- species at temperatures higher than 293 K was reported for Li⁺, Na⁺, and K⁺ exchanged FAU(Y) zeolites containing incorporated transition metal cation impurities [50]; O_2^- formation distinctly increased upon adding of iron and copper ions to the zeolites. Furthermore, they showed that the presence of M⁺ cations in a FAU(Y) zeolite stabilized the formation of those superoxide anions (M⁺ = Li⁺, and Na⁺), most likely via an M⁺- O_2^- base pair interaction induced by the high electrostatic field properties [50]. XRF analysis of the samples used here also revealed the presence of Fe impurities (Na-FAU(X): 0.07wt% Fe; Na-MFI: 0.06wt% Fe (on dry basis)). The existence of such O_2^- species in the present study can, therefore, arise either from the presence of such impurities (in Na⁺ exchanged zeolites) and/or from the chemical interaction with the hydrocarbons (in Na⁺ and Cs⁺ exchanged zeolites), a so-called O_2 -hydrocarbon charge-transfer complex, as also concluded by Frei *et al.* [11-14]. No experimental work was done here (and no spectroscopic evidence was found during experimental work) to support such hypothesis.

Appendix 2 - Reaction of oxygen with methanol over basic molecular sieves

Although no indication of the type of interaction between methanol and oxygen can be given based on our results, it is widely accepted that molecular gas phase oxygen in the ground state is a highly polarizable diradical, having two unpaired electrons and so it is a triplet-state molecule ($X^3\Sigma_g^-$)

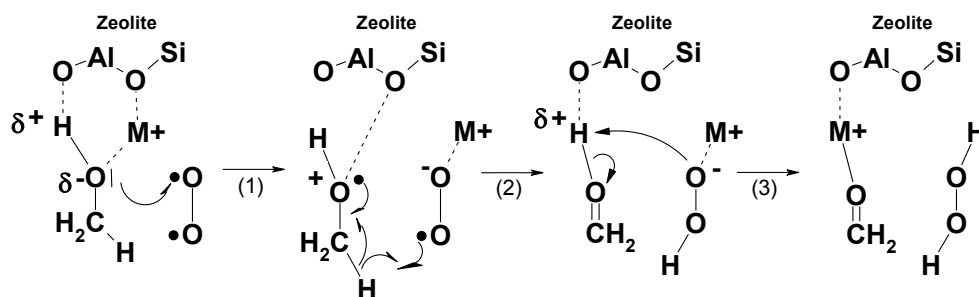
47. Zulfugarova, S. In *Proceedings of the 13th International Zeolite Conference, Montpellier*; Galarneau, A., Di Renzo, F., Fajula, F., and Vedrine, J., Eds.; Elsevier: Amsterdam, 2001; Vol. 135, p 367.

48. Lowry, T.H.; Schueller Richardson, K. *Mechanism and Theory in Organic Chemistry*, 3rd Edition; Harper Collins Publishers: New York, 1987; p 912.

49. a) Wang, K.M.; Lunsford, J.H. *J. Phys. Chem.* **1970**, *74*, 1512; b) Abou-Kais, A.; Vedrine, J.C.; Massardier, J. *J. Chem. Soc., Faraday Trans. 1* **1975**, *71*, 1697; c) Narayana, M.; Kevan, L. *Chem. Phys. Lett.* **1982**, *90*, 235.

50. Imai, T.; Habgood, H.W. *J. Phys. Chem.* **1973**, *77*, 925.

[51]. Because of this unusual feature, molecular oxygen reacts slowly with organic compounds. Reaction of alcohols with oxygen in the presence of a base (e.g., NaOH) yields aldehydes and ketones by creating alkoxy radicals [52]. In the present study, the zeolite host acts as the basic environment and, in analogy to the mechanism in NaOH solution, a similar mechanism might exist inside the pores of alkali exchanged zeolites (see Scheme 7.4, where $M^+ = Na^+, Cs^+$). However, the zeolite is a weak base and not capable to abstract the hydroxy proton (see also Chapter 6). Interaction of the hydroxy proton with the zeolite framework yields partial negatively charged oxygen, which can transfer an electron to the oxygen molecule (Scheme 7.4: step 1). This forms a positively charged methanol molecule and a superoxide anion, which then recombine to a hydroperoxide anion and a protonated formaldehyde molecule by hydrogen transfer (Scheme 7.4: step 2). Proton transfer to the hydroperoxide anion yields hydrogen peroxide and formaldehyde (Scheme 7.4: step 3). These last two steps occur most likely concerted. Rice and coworkers have reported on the observation of hydrogen peroxide during the oxidation of methanol by molecular oxygen [53]. Note that the first two steps resemble the formation of an O_2 -hydrocarbon charge-transfer complex [11-14]. However, in contrast to Ref. [11-14] a recombination of the peroxide anion with the protonated formaldehyde is not expected due to the high stability of the formaldehyde product and thus proton abstraction to form hydrogen peroxide is favored.



Scheme 7.4

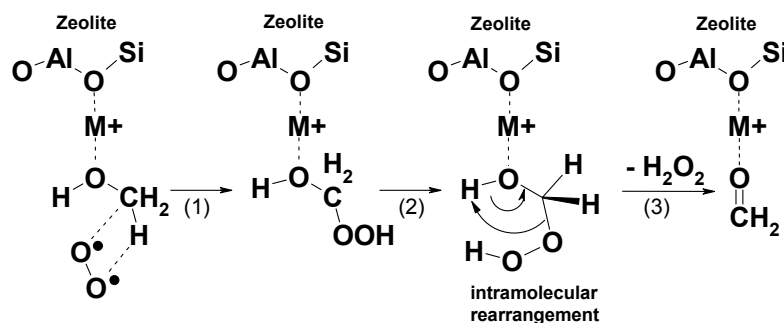
Another possible reaction of molecular oxygen with alcohols involves the replacement of hydrogen atoms bonded to carbons that are adjacent to the oxygen atom in alcohols and ethers by hydroperoxide groups [52] (Scheme 7.5: step 1). The formed hydroperoxide-alcohols can intramolecularly rearrange (Scheme 7.5: step 2) to yield hydrogen peroxide and formaldehyde (Scheme 7.5: step 3). In Ref. [9-14] this process is described for alkanes and benzylic and allylic compounds yielding hydroperoxides and is catalyzed by light. (This process occurs also in the absence of a catalyst via free radical chain reactions and is called *autoxidation*.) Hydrogen bonding between framework oxygens and methyl (CH_3) hydrogens of methanol adsorbed on Cs-FAU(X) (see also Chapter 6) most likely facilitates O_2 insertion into the C-H bond of the methanol methyl group. Insertion of O_2 into the C-H bond of the methyl group of methanol adsorbed on Cs-FAU(X) most likely occurs at higher temperatures. This could account for the first maximum observed with i.r. spectroscopy in the

51. a) Atkins, P.W. *Physical Chemistry*, 4th Edition; Oxford University Press: Oxford, 1990; p 399; b) Poulsen, T.D.; Ogilby, P.R.; Mikkelsen, K.V. *J. Phys. Chem. A* **1998**, *102*, 8970.

52. Ege, S. *Organic Chemistry*, 2nd Edition; D.C. Heath and Company: Lexington, 1989; pp 842-853.

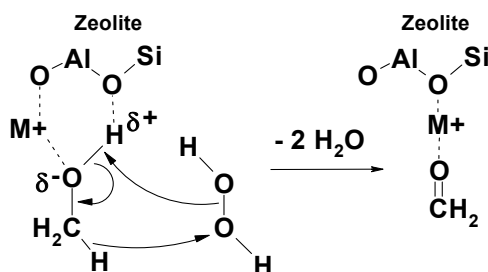
53. a) Rice, S.F.; Hunter, T.B.; Rydén, Å.C.; Hanush, R.G. *Ind. Eng. Chem. Res.* **1996**, *35*, 2161; b) Croiset, E.; Rice, S.F. *Ind. Eng. Chem. Res.* **1998**, *37*, 1755.

formation of surface formate (at approximately 500 K). The second maximum most likely appears to be the decomposition of adsorbed formaldehyde via a *Cannizzaro* type disproportionation.



Scheme 7.5

The formed hydrogen peroxide (in Scheme 7.4 and 7.5) then oxidizes an additional methanol molecule in a concerted reaction to form water and formaldehyde [53] (Scheme 7.6). The reactions of an alcohol and hydroperoxide over alkali cation exchanged zeolites have been reported in literature [54] and shown to proceed rapidly at 353 K.



Scheme 7.6

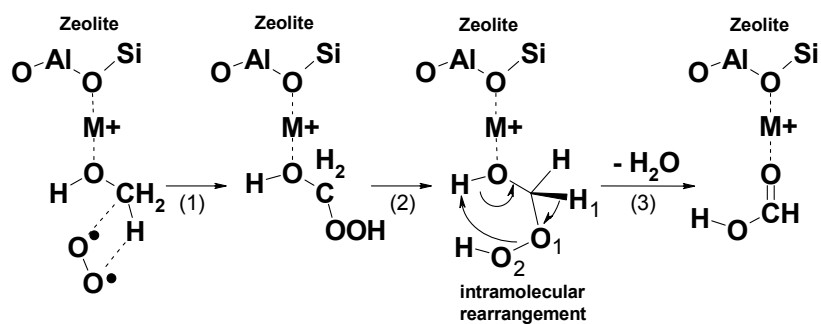
Experimental observation of the formed hydrogen peroxide intermediate in the alkali cation exchanged zeolites is difficult, because of the overlap of the OH stretching vibration of the hydroperoxide intermediate and of the methanol molecule. Peroxide species have been observed following cyclohexane and isobutane oxidation in Na-FAU(Y) [11a] and Ba-FAU(Y) zeolites [14a], respectively, and exhibited a broad OH stretching vibration near 3200-3250 cm^{-1} . The formation of water with the simultaneous formation of surface formaldehyde during methanol oxidation over Na- and Cs-FAU(X) is in agreement with above proposed mechanisms (Scheme 7.2-7.4).

The in Scheme 7.2-7.4 produced formaldehyde desorbs as methyl formate from the catalyst surface (maxima coincide with that of formaldehyde production during methanol oxydehydrogenation). Methyl formate is produced via a *condensation* type reaction maybe as a result of the high density (~ 5 mmol active sites/g zeolite) and high proximity of active sites (distance between site II and III' in the supercage of FAU(X) approximately 4.7-4.8 Å [55] (see also Chapter 5)). A similar conclusion was reached by Palombi *et al.* [54b,c]; oxidative dehydrogenation of alcohols with hydroperoxides over commercial Na-FAU(X) zeolite promoted the undesired coupling of products (other side reactions reported in Ref. [54b,c] were rearrangements and oxidative fission of reactants and products).

54. a) Floor, M., Kieboom, A.P.G.; Van Bekkum, H. *Recl. Trav. Chim. Pays-Bas* **1988**, *107*, 362; b) Palombi, L.; Bonadies, F.; Scettri, A. *tetrahedron* **1997**, *53*, 15867; c) Palombi, L.; Bonadies, F.; Scettri, A. *J. Mol. Catal. A: Chemical* **1999**, *140*, 47.

55. Zhu, L.; Seff, K. *J. Phys. Chem. B* **1999**, *103*, 9512.

The hydroperoxide-alcohol formed in Scheme 7.5 (see also scheme 7.7 after step 1) also can decompose intramolecularly (Scheme 7.7: step 2) to yield carboxylic acid (formic acid) and water (Scheme 7.7: step 3). (An oxygen-oxygen bond is weak, $\sim 197 \text{ kJ.mol}^{-1}$, and thus not difficult to break [56].) However, we did not find any evidence for the production of formic acid that might lead us to the assumption that this happens.



Scheme 7.7

56. Idem as Ref. [52], pp 606-607.

Chapter 8

Alkylation of Toluene over Basic Catalysts – Key Requirements for Side Chain Alkylation

Abstract:

In situ infrared spectroscopy was used to study sorption and reaction of toluene and methanol over various basic catalysts (MgO, hydrotalcites and basic zeolites). The larger the metal cation in the basic zeolite the higher the preference for toluene adsorption compared to methanol. The key requirements for a good catalyst for side-chain alkylation are (i) sufficient base strength to dehydrogenate methanol to formaldehyde, (ii) stabilization of sorbed toluene and sufficient base strength to polarize its methyl group and (iii) balanced sorption stoichiometry of the two reactants. The formation of the carbon-carbon bond mechanistically resembles an aldol condensation.

8.1 INTRODUCTION

Because of its theoretical potential as novel route to styrene, alkylation of toluene with methanol over basic materials has been studied frequently over the past years [1,2,3,4,5,6]. Despite these efforts, a consensus has not been reached so far concerning the mechanism of the reaction and the role of the catalyst in directing the selectivity toward side chain or ring alkylated products. It is known that basic materials such as Cs^+ and Rb^+ exchanged FAU(X) zeolites catalyze the side chain alkylation of toluene with methanol to styrene which subsequently can be hydrogenated to ethylbenzene [7,8,9]. Acid materials, i.e., H-FAU(Y), H-ZSM5, etc., selectively catalyze ring alkylation to xylenes [10,11,12]. While the rates for ring alkylation are quite high, the rates and yields for side chain alkylation are still unsatisfactory, especially from the point of methanol utilization. A recent study indicated, however, that alkali metal (hydr)oxides supported in zeolite strongly improve the yield of the side chain alkylation products [13]. Also the addition of boron [14] or zinc oxides [15] have a promoting effect on the side chain alkylation.

Several factors have been suggested to be crucial to catalyze selectively side chain alkylation: (i) the presence of active (basic) sites capable to dehydrogenate methanol to formaldehyde and stabilize the formed formaldehyde on the catalyst [8,16,17], (ii) spatial constraints as found within zeolite pores and inhibition of toluene rotation in the zeolite cavity (13,17,18,19). It was also suggested that specific steric configurations of acidic and basic sites are crucial for the formation of the required reaction complexes on the zeolite surface (15,20,21,22,23,24,25,26,27). The base sites activate the carbon atom

1. Hattori, H. *Chem. Rev.* **1995**, *95*, 537.
2. Dartt, C.B.; Davis, M.E. *Catalysis Today* **1994**, *19*, 151.
3. Kollar, J. (Ed.), *Adv. Chem. Technol.* **1979**, *1*, 1.
4. Pines, H.; Arrigo, J.T. *J. Am. Chem. Soc.* **1957**, *79*, 4958.
5. Garces, J.M.; Vrieland, E.; Bates, S.I.; Scheidt, F.M. *Stud. Surf. Sci. Catal.* **1985**, *20*, 67.
6. Giordano, N.; Pino, L.; Cavallaro, S.; Vitarelli, P.; Rao, B.S. *Zeolites* **1987**, *7*, 131.
7. Yashima, T.; Sato, K.; Hayasaka, T.; Hara, N. *J. Catal.* **1972**, *26*, 303.
8. Sidorenko, Y.N.; Galich, P.N.; Gutryra, V.S.; Ilin, V.G.; Neimark, I.E. *Dokl. Akad. Nauk. SSSR* **1967**, *173*, 132.
9. Engelhardt, J.; Szanyi, J.; Valyon, J. *J. Catal.* **1987**, *107*, 296.
10. Chen, N.Y.; Kaeding, W.W.; Dwyer, T. *J. Am. Chem. Soc.* **1979**, *101*, 6783.
11. Kaeding, W.W.; Chu, C.; Young, L.B.; Butter, S.A. *J. Catal.* **1981**, *67*, 159.
12. Young, L.B.; Butter, S.A.; Kaeding, W.W. *J. Catal.* **1982**, *76*, 418.
13. Hathaway, P.E.; Davis, M.E. *J. Catal.* **1989**, *119*, 497.
14. Wieland, W.S.; Davis, R.J.; Garces, J.M. *Catalysis Today* **1996**, *28*, 443.
15. Archier, D.; Coudurier, G.; Naccache, C. In *Proceedings of the 9th International Zeolite Conference, Montreal*; Von Ballmoos, R., Higgins, J.B., and Treacy, M.M.J., Eds.; Butterworth-Heinemann: Boston, 1992; Vol. 2, pp 525-533.
16. King, S.T.; Garces, J. *J. Catal.* **1987**, *104*, 59.
17. Phillippou, A.; Anderson, M.W. *J. Am. Chem. Soc.* **1994**, *116*, 5774.
18. Unland, M.L.; Barker, G.E. In *Chem. Ind. Ser., Catalysis of Organic Reactions*; Moser, W.R., Ed.; Dekker: New York, 1981; Vol. 5, pp 51-71.
19. Sefcik, M.D. *J. Amer. Chem. Soc.* **1979**, *101*, 2164.
20. Rakoczy, J. *React. Kinet. Catal. Lett.* **1992**, *48*, 401.
21. Itoh, H.; Miyamoto, A.; Murakami, Y. *J. Catal.* **1980**, *64*, 284.
22. Lacroix, C.; Deluzarche, A.; Kiennemann, A.; Boyer, A. *J. Chim. Phys.* **1984**, *81*, 481.
23. Itoh, H.; Hattori, T.; Suzuki, K.; Miyamoto, A. *J. Catal.* **1983**, *79*, 21.
24. Eder-Mirth, G.; Wanzenbock, H.D.; Lercher, J.A. *Stud. Surf. Sc. Catal.* **1995**, *94*, 449.
25. Mielczarski, E.; Davis, M.E. *Ind. Eng. Chem. Res.* **1990**, *29*, 1579.
26. Eder-Mirth, G.; Lercher, J.A. *Recl. Trav. Chim. Pays-Bas* **1996**, *115*, 157.

of the side chain of toluene and the acid sites adsorb and stabilize the toluene [21]. Then, the active center is the assemble of an acid and base sites in a cooperative action. In contrast to these quite complex requirements, Giordano *et al.* [6] suggests that the primary factor governing zeolite activity and selectivity is the overall acid-base strength expressed as the averaged Sanderson electronegativity of the oxide.

In a previous communication [28], we have reported an *in situ* i.r. spectroscopic study of the surface chemistry on different alkali exchanged FAU(X) zeolites during toluene alkylation. We concluded that in addition to requirements listed above, the balanced sorption stoichiometry of the two reactants and a strong polarization of the methyl group of toluene are indispensable to catalyze side chain alkylation of toluene.

The purpose of the present contribution is to compare the surface chemistry of other basic materials with varying activity (Cs^+ solid state exchanged FAU(Y) zeolite, MgO and hydrotalcites with different Al/(Al+Mg) ratio) with that of alkali exchanged FAU(X) zeolites and to show that high base strength alone is insufficient for good catalytic properties. It is our goal to outline the requirements of the working catalysts during toluene alkylation. *In situ* i.r. spectroscopy and kinetic measurements are used to show, how chemisorption and stabilization of the reactants at the surface of the different basic materials relate to their catalytic properties.

8.2 EXPERIMENTAL

Materials

Materials used were alkali metal cation exchanged FAU(X) (Na^+ , Rb^+ , and Cs^+), as prepared and described in Chapter 3. Detailed specifications of the used molecular sieves are compiled in Table 3.1 of Chapter 3. Comparison was made with cesium solid state ion exchanged zeolite FAU(Y), hydrotalcite, and MgO. The Si/Al ratio of the zeolite was 2.6 and 100% of Cs^+ exchange was reached. The hydrotalcites used had Al/(Al+Mg) ratios of 0.33 or 0.2 and MgO with a specific surface area of 200 m²/g was used.

Sorption and coadsorption experiments

Experiments were performed according to the procedures described in Chapter 3. Infrared spectra were taken using a BRUKER IFS88 FTIR spectrophotometer. The activated sample wafer was contacted with the appropriate pressure of methanol or toluene (between 10⁻⁴ and 1 mbar) at constant temperature (T=308 K) until adsorption-desorption equilibrium was achieved. The adsorption capacity for toluene and methanol (measured in a modified SETARAM TG-DSC 111 instrument) was determined at 5.10⁻³ mbar under the same conditions as used for the infrared measurements (unless

27. Eder-Mirth, G. *Collect. Czech. Chem. Commun.* **1995**, *60*, 421.

28. Palomares, A.E.; Eder, G.; Lercher, J.A. *J. Catal.* **1997**, *168*, 442.

otherwise stated). The accuracy of the gravimetric measurements was $\pm 5\%$: the accuracy of the calorimetric measurements was $\pm 2 \text{ kJ}\cdot\text{mol}^{-1}$.

Reaction studies

In situ reaction studies were performed in an i.r. reactor cell (see Chapter 3 for details). To characterize the species sorbed in the material during the catalytic reaction, i.r. spectra were recorded time resolved at different reaction temperatures (from 373 to 723 K) as the activated material was contacted with the reactant stream. The feed gas composition had a partial pressure ratio of toluene/methanol = 45/15 (expressed in mbar) and He was added to 1 bar. The overall flow was 3.5 ml/min. This corresponds to a W/F ratio of $1.8 \cdot 10^4 \text{ g}$ of catalysts/mol of toluene+methanol. Simultaneously, samples of the effluent gas stream were collected in sample loops of a multi-port valve and subsequently analyzed by gas chromatography (HP5890 II capillary column DBWAX 30m, FID, He as carrier gas).

Because of the low reactivity of the catalysts and the small weight permissible for an *in situ* infrared experiment and the minimum flow rates for good backmixing only low conversions and yields could be achieved in the i.r. reactor. Therefore, parallel experiments were performed replacing the i.r. reactor with a tubular quartz reactor (4 mm. inner diameter), in order to be able to direct compare the data to those reported in the literature [7,9,13,14]. In these experiments, catalyst powders were loaded into the fixed bed quartz reactor and heated *in situ* at 723 K in flowing He for 2 hours before cooling to the reaction temperature (698 K). A liquid mixture of toluene and methanol at a 3:1 molar ratio was then pumped into the reactor system. The reactants were vaporized (partial pressure ratio 45/15 (expressed in mbar)) and then mixed with flowing He to obtain a constant reactor space-time. It was chosen a W/F of $1.2 \cdot 10^5 \text{ g}$ of catalysts/mol toluene+methanol and the reaction was tested at 698 K. The yield was calculated referred to the methanol feed (mol styrene+mol ethylbenzene in the outlet per mol of methanol in the feed) and to the aromatic feed (mol styrene+mol ethylbenzene in the outlet per mol of toluene in the feed). The selectivity was defined as moles of styrene+ethylbenzene formed per moles of toluene reacted (selectivity to side chain alkylation) or moles of xylenes formed per moles of toluene reacted (selectivity to ring alkylation). Other products detected were dimethyl ether (DME), formaldehyde, CO and H₂O.

8.3 RESULTS

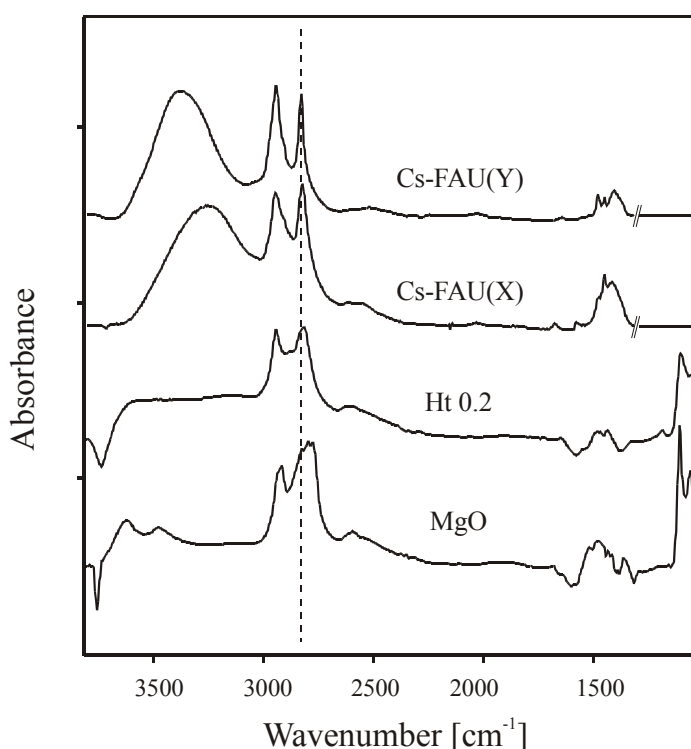
Adsorption of the individual reactants

The i.r. spectra of methanol sorbed on different samples are shown in Figure 8.1. Table 8.1 compiles the wavenumbers of the bands of methanol sorbed on the various samples. All the spectra shown in this paper are difference spectra. In this mode of presentation, the bands increasing in intensity after exposing the activated material to the sorbate point upwards, the bands decreasing in intensity point downwards.

TABLE 8.1: I.r. bands of methanol sorbed on Na-FAU(X), Rb-FAU(X), Cs-FAU(X), Cs-FAU(Y), hydrotalcite and MgO at $5 \cdot 10^{-3}$ mbar and 308 K

Sample	$\nu_{\text{O-H}} \text{ (cm}^{-1}\text{)}$	$\nu_{\text{C-H methyl}} \text{ (cm}^{-1}\text{)}$
Na- FAU(X)	3336	2956, 2839
Rb-FAU(X)	3216	2942, 2825
Cs- FAU(X)	3244	2941, 2820
Cs- FAU(Y)	3375	2940, 2829
Hydrotalcite 0.33 (Ht 0.33)	3600-2900	2940, 2817
	3739 (negative band)	
Hydrotalcite 0.2 (Ht 0.2)	3600-2900	2941, 2815
	3740 (negative band)	
MgO	3600-2900, 3617, 3481	2939, 2917,
	3758 (negative band)	2824, 2795, 2772

After equilibration at $5 \cdot 10^{-3}$ mbar, the stretching vibration of the hydrogen bonded OH group of methanol appeared as a broad band (between 3500 and 3200 cm^{-1}) with the alkali exchanged zeolites, and as a combination of several broad bands (between 3600 and 2900 cm^{-1}) with hydrotalcites and MgO. With MgO, additionally, two relatively small bands super positioned on the broad band between 3600 and 2900 cm^{-1} were observed at 3475 and 3618 cm^{-1} . With the non-zeolitic materials a negative peak appeared between 3734 - 3760 cm^{-1} , characteristic of oxide surface hydroxyl groups in interaction with the sorbate. The C-H stretching vibration bands appeared between 2917 - 2955 cm^{-1} and 2771 - 2839 cm^{-1} (asymmetric and symmetric vibration), the C-H deformation vibration bands between 1451 - 1480 cm^{-1} and the C-O-H deformation vibration between 1400 - 1420 cm^{-1} . With MgO and hydrotalcite two peaks assigned to C-O stretching vibrations were observed at 1098 - 1105 and 1045 - 1065 cm^{-1} . Note that these bands could not be seen with the zeolite samples due to the strong absorption

**Figure 8.1:** Difference i.r. spectra of methanol sorbed on MgO, hydrotalcite, Cs-FAU(X) and Cs-FAU(Y): $p = 5 \cdot 10^{-3}$ mbar, $T = 308 \text{ K}$.

of their Si-O vibrations. All these observed bands for methanol adsorbed on zeolites and metal-oxides agree well with results obtained by other research groups [25,29,30,31].

The temperature of the desorption maximum of methanol during t.p.d. of methanol decreased in the order MgO, hydrotalcites>Na-FAU(X)>Rb-FAU(X), Cs-FAU(X)>Cs-FAU(Y). With MgO and hydrotalcites the interaction between methanol and the surface was so strong that even at temperatures higher than 773K some methanol derived compounds remained adsorbed. Analyses of the curves of desorption the same trend was observed, i.e., higher desorption rates were observed for Cs-FAU(X) and Cs-FAU(Y) at low temperatures.

The bands of the i.r. spectra of adsorbed toluene are compiled in Table 8.2. For toluene sorbed on the zeolitic materials only minor differences in the wavenumbers of the C-C and the ring deformation vibrations (1598, 1494 and 1465 cm^{-1}) were observed. The C-H stretching vibration bands of the aromatic ring (3058-3048 and 3024-3019 cm^{-1}) and the methyl group (2921-2912 and 2874-2857 cm^{-1}) slightly shifted to lower wavenumbers as the size of the cation increased [25]. The characteristic bands of the out of plane vibrations were observed between 1700 and 2000 cm^{-1} [32], and were especially well resolved for toluene sorbed on Cs-FAU(Y). With the hydrotalcites and MgO the concentrations of toluene sorbed were small compared to the other samples studied. A negative band at 3725-3747 cm^{-1} and a positive band between 3670-3700 cm^{-1} were observed in the difference spectra which varied parallel in intensity. During t.p.d. of toluene the temperature of the desorption rate maximum increased in the order MgO<hydrotalcite<Na-FAU(X)<Rb,Cs-FAU(X)<Cs-FAU(Y). Further analysis of the shape of the desorption curves showed that at low temperatures hydrotalcite and MgO released toluene easier. The toluene desorption curve of Cs-FAU(X) showed multiple maxima, indicating site heterogeneity.

TABLE 8.2: I.r. bands of toluene sorbed on Na-FAU(X), Rb-FAU(X), Cs-FAU(X), Cs-FAU(Y), hydrotalcite and MgO at $5 \cdot 10^{-3}$ mbar and 308 K

Sample	$\nu_{\text{C-H aromatic}} (\text{cm}^{-1})$	$\nu_{\text{C-H aliphatic}} (\text{cm}^{-1})$
Na-FAU(X)	3055, 3024	2921, 2859
Rb-FAU(X)	3049, 3022	2916, 2858
Cs-FAU(X)	3048, 3021	2916, 2857
Cs-FAU(Y)	3048, 3021	2912, 2874, 2858
Ht 0.2, Ht 0.33	3083, 3053, 3024	2950, 2926, 2871
MgO	3082, 3052, 3025	2958, 2926, 2873

29. Ziolk, M.; Czyzniewska, J.; Lamotte, J.; Lavalley, J.C. *Catal. Lett.* **1996**, *37*, 223.

30. Unland, M.L. *J. Phys. Chem.* **1978**, *82*, 580.

31. Tench, A.J.; Giles, D.; Kibblewhite, J.F.J. *Trans. Far. Soc.* **1971**, *67*, 854.

32. Dzwigaj, S.; De Mallmann, A.; Barthomeuf, D. *J. Chem. Soc., Faraday Trans.* **1990**, *86*, 431.

The adsorption isotherms of toluene on Na-FAU(X) and Cs-FAU(X) shown in Figure 8.2, show that the amount of toluene sorbed on Cs-FAU(X) is larger than on Na-FAU(X). In Chapter 4 it was shown that this was the opposite for the adsorption of methanol; the MeOH uptake was found to be larger on Na-FAU(X). The heats of adsorption for Na-FAU(X) and Cs-FAU(X) (extrapolated to zero loading) are 76 kJ.mol⁻¹ and 92 kJ.mol⁻¹ respectively (a similar trend was observed by Xie *et al.* [33]); for MgO it is much lower (50 kJ.mol⁻¹).

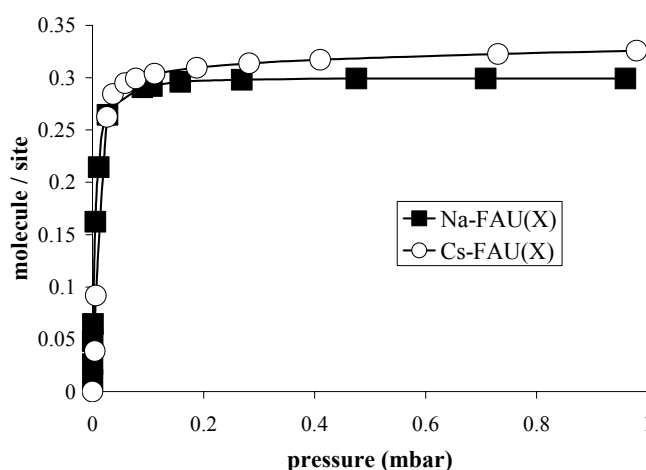


Figure 8.2: Adsorption isotherm (pressure vs molecule / site) of toluene on Na-FAU(X) and Cs-FAU(X) zeolites. $T = 323\text{ K}$; $p = 10^{-3}\text{-}1\text{ mbar}$.

Coadsorption of the reactants

The i.r. spectra recorded after coadsorption of the two reactants are compiled in Figure 8.3. Only bands characteristic for sorbed toluene and methanol were observed. The bands typical for sorbed toluene (CH stretching vibrations of the aromatic ring at 3055-3045 and 3025-3020 cm⁻¹, CH stretching vibrations of the methyl group at 2918-2916 and 2869-2859 cm⁻¹ and C-C ring vibrations at 1495 and 1598 cm⁻¹) were the main spectral features with the Cs⁺ exchanged zeolites. On the other hand, the bands characteristic for sorbed methanol (the OH stretching vibration at 2900-3600 cm⁻¹ and the CH stretching vibrations of the methyl group at 2815-2771 and 2945-2917 cm⁻¹) were the most

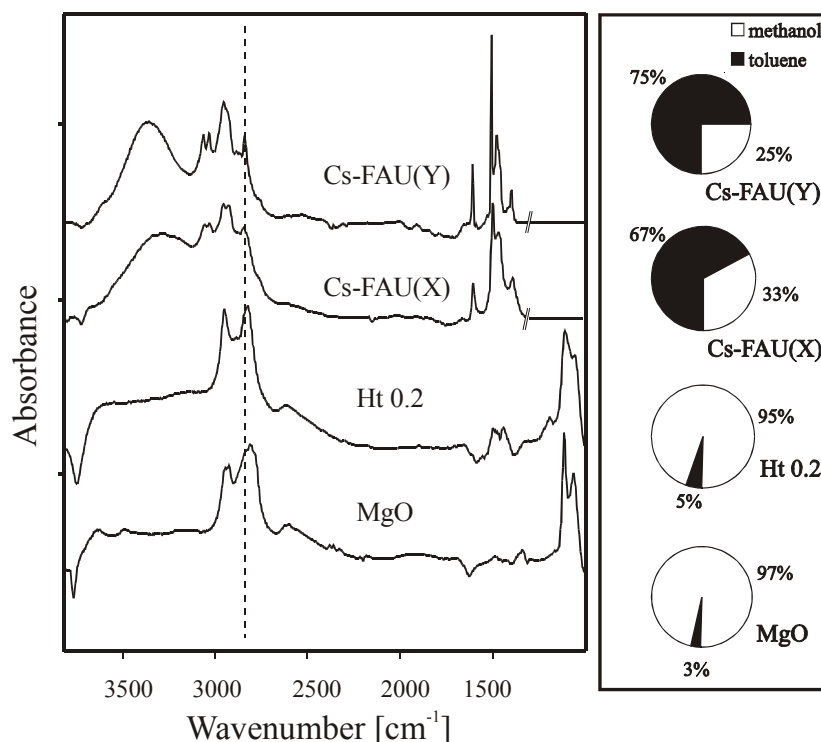


Figure 8.3: Difference i.r. spectra and quantitative evaluation of toluene methanol occupation after coadsorption of toluene and methanol on MgO, hydrotalcite, Cs-FAU(X) and Cs-FAU(Y): $p = 5.10^{-3}\text{ mbar}$, $T = 308\text{ K}$.

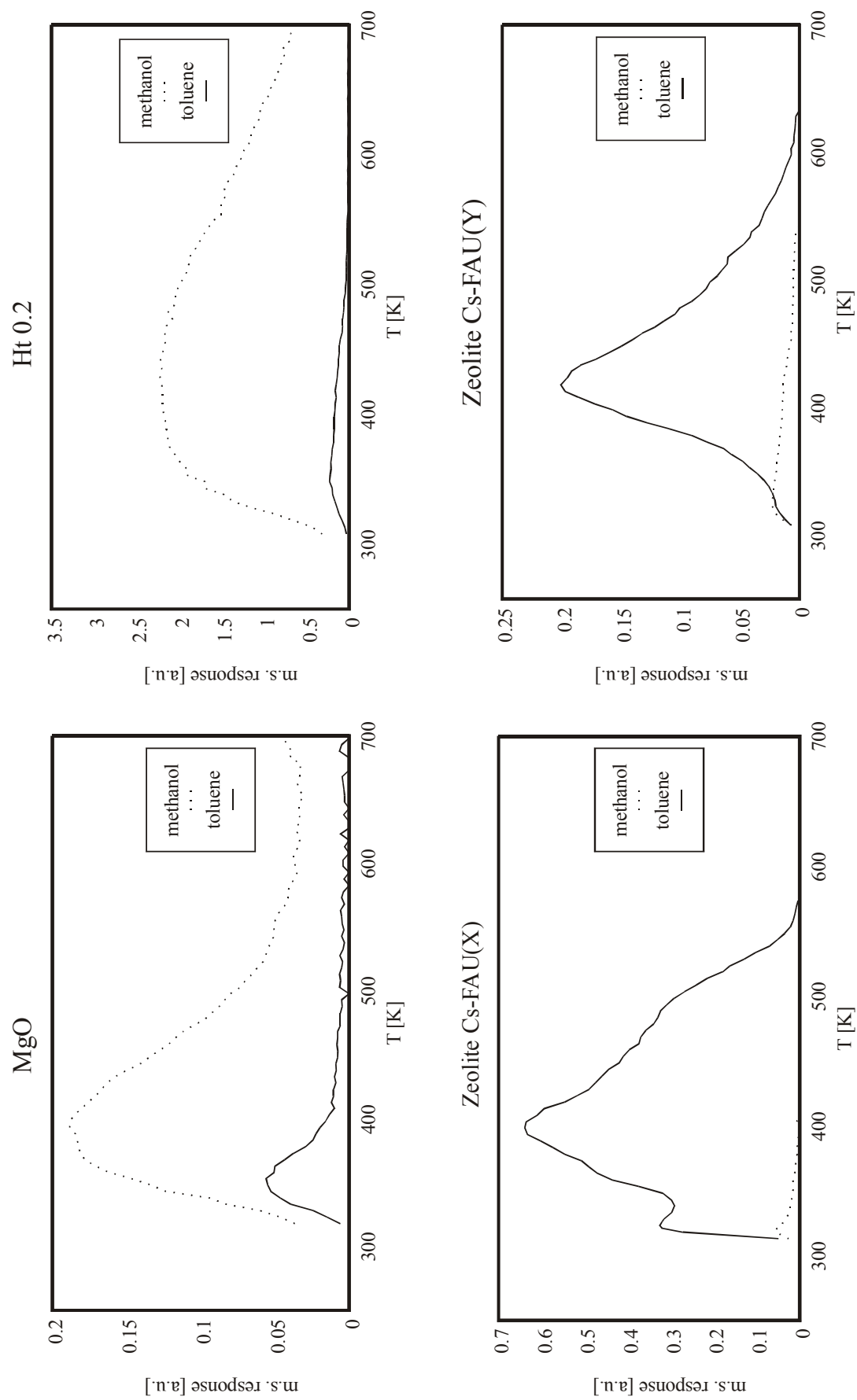


Figure 8.4: T.p.d. of toluene and methanol coadsorbed on MgO, hydrotalcite, Cs-FAU(X) and Cs-FAU(Y) ($m/z = 31$ for methanol, and $m/z = 91$ for toluene).

the CH stretching vibrations of the methyl group at 2815-2771 and 2945-2917 cm^{-1}) were the most important ones after coadsorption of methanol and toluene on hydrotalcite and MgO. Indeed, the quantitative evaluation of the i.r. spectra showed that the ratio of toluene: methanol in the sorbed phase was 1:30 with MgO, 1:19 with hydrotalcite, 2:1 with Cs-FAU(X) and 3:1 with Cs-FAU(Y). T.p.d. of coadsorbed toluene and methanol from the various materials (Figure 8.4) also indicated that methanol was the main desorbing species at every temperature with hydrotalcite and MgO, while it was toluene with Cs-FAU(X) and Cs-FAU(Y).

Reaction studies

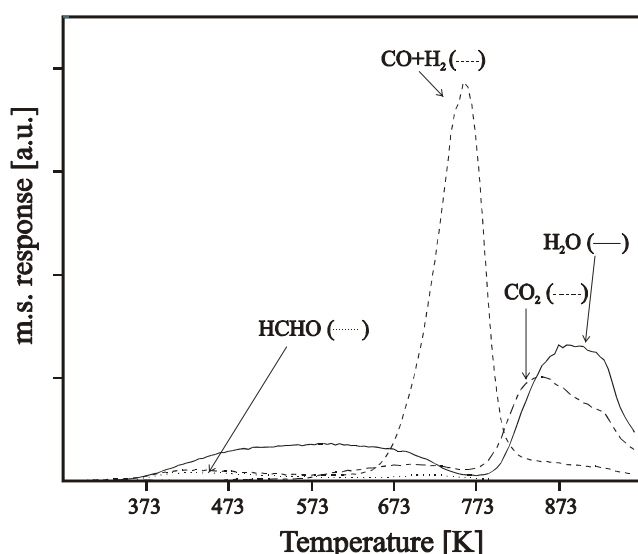


Figure 8.5: Products formed during temperature programmed reaction of toluene and methanol over hydrotalcite with an Al/Al+Mg ratio of 0.2. (47 mg of sample, 10 K/min, 6 mbar toluene, 3 mbar methanol).

formaldehyde, dimethylether, CO, H₂ and water up to 673 K, H₂ and CO between 673 and 823 K, and

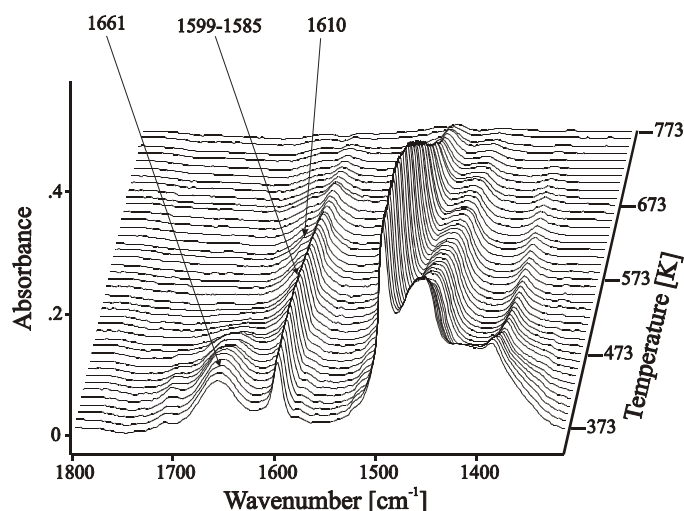


Figure 8.6: Difference i.r. spectra of Cs-FAU(X) during the reaction of toluene and methanol as function of the reaction temperature ($T = 373\text{--}773\text{ K}$).

With zeolitic materials reaction products were not detected in the gas phase below 523 K. Above 523 K, the formation of formaldehyde was observed. Products of the alkylation of toluene with methanol appeared between 573 and 593 K. Depending on the zeolite, side chain alkylated (Cs-FAU(X)) or ring alkylated products (Cs-FAU(Y)) were formed (Table 8.4). The situation was different with the hydrotalcites and MgO. In this case, side chain alkylated products were only observed in very low concentrations, the main reaction products being formaldehyde, dimethylether, CO, H₂ and water up to 673 K, H₂ and CO between 673 and 823 K, and CO₂ and H₂O at higher temperatures (see Figure 8.5). Note that yields obtained in the fixed bed reactor are in excellent agreement with the values reported in the literature (Table 8.3), while the selectivities between the two reactors used in the present study (i.e., the i.r. reactor and the tubular reactor) were almost identical (Table 8.4).

The *in situ* i.r. spectra obtained in the temperature programmed reaction of toluene and methanol over Cs-FAU(X) and

hydrotalcite are shown in Figures 8.6 and 8.7, respectively. With Cs-FAU(X), at low temperatures, the main bands were characteristic for sorbed toluene, while a new band was observed at 1661 cm^{-1} . This band reached its maximum intensity around 433 K and disappeared completely at 523 K. At higher temperatures another new band (as a shoulder) was observed with Cs-FAU(X) at 1610 cm^{-1} (as it was previously reported [28] for Na-FAU(X)). The presence of this band is difficult to unequivocally establish due to the overlap with the band of sorbed toluene at 1600 cm^{-1} . For clarification, Cs-FAU(X) was exposed only to methanol. It was seen (Figure 8.8, line c) that also in this case a band appeared around 1610 cm^{-1} . Note that the shoulder at 1610 cm^{-1} was observed in the spectra during reaction over Cs-FAU(X) zeolite (Figure 8.8, line a) but not during reaction over Cs-FAU(Y) (Figure 8.8, line b).

TABLE 8.3: Yields reported in the literature for the side chain alkylation of toluene with methanol on Cs- and Rb-FAU(X) ($T=698\text{ K}$).

Reference	W/F (g's/mol)	% Yield (mol styrene + ethylbenzene / mol methanol)	% Yield (mol styrene + ethylbenzene / mol of toluene)
our work	$1.2 \cdot 10^5$	7.6	2.5
[7]	$1.8 \cdot 10^5$	10	
[9]	$6 \cdot 10^5$	10-20	
[13]	$1 \cdot 10^5$		0.4-2.75
[14]	$1.1 \cdot 10^5$	13	

TABLE 8.4: Comparison between the selectivity (mol %) obtained in the side chain alkylation of toluene with methanol in the tubular quartz reactor ($W/F=1.2 \cdot 10^5\text{ g's/mol}$ toluene+methanol, toluene/methanol=3) and in the i.r. reactor ($W/F=1.8 \cdot 10^4\text{ g's/mol}$ toluene+methanol) at 698 K over different materials.

Sample	Selectivity to side chain alk. ($W/F=1.2 \cdot 10^5\text{ g's/mol}$)	Selectivity to ring alk. ($W/F=1.2 \cdot 10^5\text{ g's/mol}$)	Selectivity to side-chain alk. ($W/F=1.8 \cdot 10^4\text{ g's/mol}$)	Selectivity to ring alk. ($W/F=1.8 \cdot 10^4\text{ g's/mol}$)
Hydrotalcite	Traces		Traces	
MgO	Traces		Traces	
Cs-FAU(X)	78	14	82	10
Rb-FAU(X)	65	22	70	20
K-FAU(X)	46	43	41	39
Na-FAU(X)	3	97	5	95
Cs-FAU(Y)	-	-	17	83

With hydrotalcite (Figure 8.7) and MgO, methanol was the main adsorbent and, thus, nearly all bands were related to methanol and its reaction products. The most intense band appeared at 1602 cm^{-1} , together with two other bands at 1380 and 1369 cm^{-1} [34]. These bands (especially that at 1602 cm^{-1}), appeared already at very low temperatures (333 K) and increased in intensity until 673 K . Then, their intensity decreased, but the bands were still visible at 773 K . A new band was also observed at 1089 cm^{-1} and 1118 cm^{-1} (starting from 473 K), reaching its maximum intensity at 673 K , when the bands at 1109 and 1060 cm^{-1} disappeared (see Fig. 8.7).

8.4 DISCUSSION

Adsorption and coadsorption of the reactants

When methanol is sorbed on the alkali cation exchanged zeolites [28], all bands typical for hydroxyl and methyl group stretching vibrations shift to lower wavenumbers indicating a weakening of the OH and CH bands due to the interactions with the catalyst. The wavenumbers of the OH stretching vibration band decreased in the order Cs-FAU(Y)>Na-FAU(X)>Cs-FAU(X)>Rb-FAU(X). This shift results from two effects, i.e., the increasing interaction between the OH groups and the oxygen of the zeolite lattice and the increasing intermolecular interactions between sorbed methanol molecules [35] (see also Chapter 4). In the case of methanol sorbed on MgO and hydrotalcites several overlapping broad bands appear indicating strong hydrogen bonded hydroxyl groups of the surface and of sorbed methanol. The most important suggestion from these results is that the hydrogen bonds of a molecule like methanol become stronger the more polar (in case of the oxygen, the more basic) the surface is.

Note that the wavenumber of the symmetric methyl stretching band decreased in the order: Na-FAU(X)>Cs-FAU(Y)>Rb-FAU(X)>Cs-FAU(X)>hydrotalcite>MgO. In line with an earlier paper of Takezawa and Kobayashi [36] this indicates increasing strength of interaction between the lattice oxygens of the catalyst and the hydrogen atoms of the methyl group of methanol. It suggests that MgO ($\nu_{\text{s C-H}} 2795\text{ cm}^{-1}$) is the most basic and Na-FAU(X) ($\nu_{\text{s C-H}} 2839\text{ cm}^{-1}$) the least basic material. This

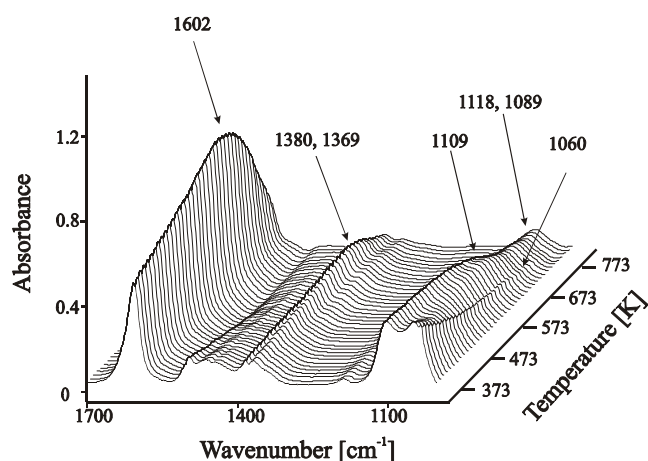


Figure 8.7: Difference i.r. spectra of a hydrotalcite with an $Al/Al+Mg = 0.2$ during the reaction of toluene and methanol as function of the reaction temperature ($T = 373\text{--}773\text{ K}$).

34. Busca, G.; Lamotte, J.; Lavalley, J.C.; Lorenzelli, V. *J. Am. Chem. Soc.* **1987**, *109*, 5197.

35. Rep, M.; Palomares, A.E.; Eder-Mirth, G.; Van Ommen, J.G.; Rösch, N.; Lercher, J.A. *J.Phys. Chem. B* **2000**, *104*, 8624.

36. Takezawa, N.; Kobayashi, H. *J.Catal.* **1973**, *28*, 335.

correlation of the C-H stretching vibration with framework basicity is not as clearly observed with the asymmetric methyl stretching band (see Table 8.1). The small difference observed in the trend between the shifts of the i.r. band of methanol hydroxy and methyl group (see Table 8.1) as a function of basicity of the zeolite samples (Cs-FAU(Y) and alkali cation exchanged FAU(X)) are attributed to interaction with basic framework oxygens in different environments in FAU (X and Y) and the additional occurrence of intermolecular methanol hydrogen bonding in FAU(X) (see Chapter 4 and 5) in FAU (X and Y) molecular sieves whereas the C-H stretching vibration of the methyl group is mostly related to its interaction with the framework oxygens.

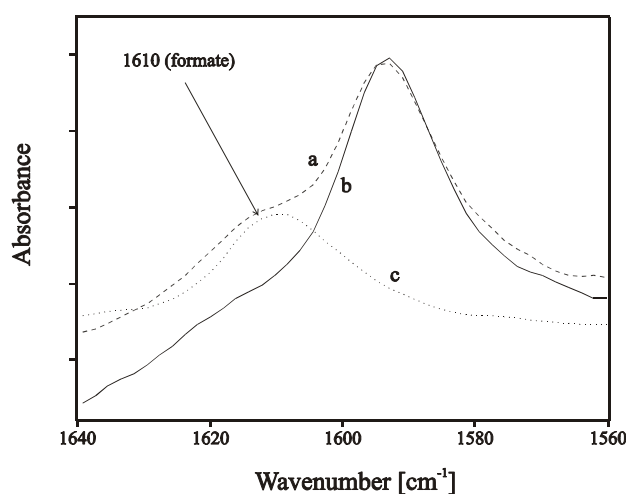


Figure 8.8: Difference i.r. spectra at 643 K of (a) methanol and toluene on Cs-FAU(X), (b) methanol and toluene on Cs-FAU(Y), (c) methanol on Cs-FAU(X)X.

In the case of the hydrotalcite, the presence of a combination of several broad OH stretching vibrational bands (between 3600 and 2900 cm^{-1}) reflects well the contribution of the perturbed surface OH groups and the OH group of methanol. An exact contribution is not possible at this point, but previous experience with sorption on acidic zeolites, indicates the existence of cyclic sorbed species [37].

For MgO the case is more complex and the relatively narrow bands that appear with the broad bands, show dramatically lower hydrogen bonding strength and/or dissociation of methanol and the formation of new hydroxyl bands [31,38]. Moreover a significant fraction of the molecules is concluded to be sorbed on Mg^{2+} cations which also should lead to a relatively sharp OH band. The C-H stretching vibrations at 2939 and 2824 cm^{-1} , appearing as shoulders in Figure 8.1, are attributed to a methyl group vibrating rather free, probably related with the narrow O-H bands observed at higher wavenumber.

The results from the t.p.d of methanol show that it is bound strongly when the radius of the accessible metal cation is small (MgO, hydrotalcite and Na-FAU(X)) and the interaction becomes very weak when the radius is large (Cs-FAU(X), Cs-FAU(Y)). Similar results were obtained in Chapter 4. Thus, we conclude that methanol is coordinately bound *via* the lone pair of its oxygen to the metal cation and the strength of the interaction between methanol and the catalyst is mainly determined by this bonding. This is clearly seen when considering the decreasing strength of methanol sorption with increasing size of the cation in a series of alkali exchanged FAU(X) zeolites [28]. The increasing base strength of the lattice oxygen in this series leads to more pronounced hydrogen bonding between the

37. Van Santen, R.A.; Kramer, G.J. *Chem. Rev.* **1995**, *95*, 637.

38. Kagel, R.O.; Greenler, R.G. *J. Chem. Phys.* **1968**, *49*, 1638.

methanol hydroxyl group and the lattice oxygen. However, the contribution of that interaction to the overall strength of sorption is minor. Note that these interactions are most pronounced for the most basic catalysts of this study, i.e., MgO and the hydrotalcites.

The infrared spectra of sorbed toluene show a slightly downward shift of the C-H stretching vibration bands of the aromatic ring and the methyl group as the size of the cation increases. These shifts to lower wavenumbers are attributed to a combination of the strong interactions of the aromatic ring with the cation (acting as electron withdrawing, i.e., electron pair acceptor [39] sites) and to direct interactions with the lattice oxygen. These observations are in line with reports by Barthomeuf *et al.* [40] and Jobic *et al.* [41] on the adsorption of benzene on Na-FAU(Y) zeolite.

With MgO and the hydrotalcites, only traces of toluene were adsorbed on the hydroxyl groups giving rise to a band at 3743 cm⁻¹. Upon contact with toluene a band appears at 3670 cm⁻¹ (in parallel to the decrease of the band at 3743 cm⁻¹) attributed to the perturbed OH groups hydrogen bonding toluene. Such hydrogen bonding interactions with aromatic molecules have been shown to be very weak [42], even when adsorbed on very acidic hydroxyl groups. For the current sample of MgO the low uptake and the dominance of this type of interaction suggests that only few hydroxyl groups and partially unsaturated Mg²⁺ exist on the surface of the sample studied.

In contrast to methanol, the sorption strength of toluene increased with increasing size of the metal cation, as seen from the increasing thermal stability during t.p.d. of toluene when going from MgO, hydrotalcite and Na-FAU(X) to Cs-FAU(X) and Cs-FAU(Y). Although toluene desorption was already found at low temperatures from Cs-FAU(X) (see Fig. 8.4), it also contains sites that interact strongly with toluene as indicated by the second maximum at approximately 500 K. The stronger bonding results from the specific interaction of the aromatic ring with the metal cation. The better the match of the delocalized π -orbitals of toluene (Lewis-base) and the orbitals of the electron pair accepting alkali cation (Lewis-acid), the higher the stability of the bond. Note that this is clearly observed also in more complex systems, like the K⁺-channels used by Dougherty *et al.* [43,44]. In consequence, this leads to a low mobility of the aromatic molecules sorbed in alkali exchanged FAU(X) zeolites with large cations as suggested also from earlier NMR studies [19,45]). This low mobility, however, is not the result of the steric constraints in the zeolite pores induced by the larger size of the metal cation as shown from the similar uptake rates on all samples studied. Note in this context that Bellat *et al.* [46] reported even higher uptake rates for the K-FAU(Y)/p-xylene system, than for the Na-FAU(Y)/p-xylene system. The stronger interaction of the larger cations is reflected

39. McMurry, J. *Organic Chemistry*, 2nd Edition; Brooks/Cole: Pacific Grove, 1988.

40. De Mallmann, A.; Barthomeuf, D. *Zeolites* **1988**, *8*, 293.

41. Fitch, A.N.; Jobic, H.; Renouprez, A. *J. Phys. Chem.* **1986**, *90*, 1311.

42. Derewinski, M.; Haber, J.; Ptaszynski, J.; Lercher, J.A.; Rumplmayer, G. *Stud. Surf. Sci. Catal.* **1986**, *28*, 957.

43. Kumpf, R.A.; Dougherty, D.A. *Science* **1993**, *261*, 1708.

44. Dougherty, D.A. *Science* **1996**, *271*, 163.

45. Borovkov, V.Y.; Hall, W.K.; Kazanski, V.B. *J. Catal.* **1978**, *51*, 437.

46. Bellat, J.-P.; Simonot-Grange, M.-H. *Zeolites* **1995**, *15*, 124.

clearly in the heats of toluene adsorption ($76 \text{ kJ}\cdot\text{mol}^{-1}$ with Na-FAU(X) and $92 \text{ kJ}\cdot\text{mol}^{-1}$ with Cs-FAU(X)).

The coadsorption experiments fully confirm the results and discussion. MgO and hydrotalcite adsorb preferentially methanol, while Cs-FAU(X) and Cs-FAU(Y) adsorb mainly toluene. For the hydrotalcites and MgO, 95-97 % of sorption capacity is taken up by methanol; with Cs-FAU(Y) 75% of the sorbed molecules is toluene.

Reaction studies

Previous reaction studies demonstrated that depending on the alkali ion exchanged into the FAU(X)-zeolite, side chain or ring alkylation is preferred. FAU(X)-zeolites with the larger cations (preferentially adsorbing toluene over methanol) show high selectivity to styrene and ethylbenzene. The more acidic FAU(X) zeolites (i.e., those with smaller metal cations and preferentially sorbing methanol over toluene) show high selectivity to xylenes (see, e.g., Palomares *et al.* [28]).

Hydrotalcites and MgO readily catalyze methanol dehydrogenation, i.e., formaldehyde and its decomposition products were observed in adsorbed state and in the gas phase. After contact with the reactant mixture chemisorbed formaldehyde (formate band at 1602 cm^{-1} [38]) was the most abundant surface species. The formation of CO and H₂ was observed as the formate decomposed (673 K). Other CO containing compounds adsorbed at different positions (as evidenced by bands at 1109 and 1060 cm^{-1}) were also seen. With increasing temperature these compounds transform to surface species characterized by bands at 1089 and 1118 cm^{-1} (mixture of carbonate, methoxy, etc.) [31] and finally decompose into CO₂ and H₂O at high temperatures (773 K). In the temperature interval monitored the surface concentration of toluene was minimal. Thus, we conclude that the low toluene concentration prevents an appreciable production of ethylbenzene.

In contrast, with Cs-FAU(Y) strong sorption of toluene was observed (see Figs. 8.3 and 8.4). However, while formate type species are present after sorption of methanol on Cs-FAU(X) (see Chapter 6 and, e.g., Ref. [30]), they were not observed with Cs-FAU(Y) (see Fig. 8.8). This implies that Cs-FAU(Y) was unable to dehydrogenate/activate methanol. Thus, we attribute the absence of catalytic activity for side chain alkylation to the absence of chemisorbed formaldehyde. This contrasts with earlier reports of Yashima *et al.* [7] and Wieland *et al.* [47], who reported formaldehyde formation and subsequent side chain alkylation of toluene. We attribute this different behavior to the existence of CsO-moieties in the zeolites used by the above mentioned authors [7,47], in accordance with Hathaway *et al.* [48]. The absence of such very basic oxide clusters leaves the parent Cs-FAU(Y) zeolite inactive for methanol dehydrogenation. In our case, CO₂ adsorption experiments at 323 K on Na- and Cs-FAU(X) and Cs-FAU(Y) did not show any i.r. bands attributed to CO₂ adsorption on occluded

47. Wieland, W.S.; Davis, R.J.; Garces, J.M. *J. Catal.* **1998**, *173*, 490.

48. a) Hathaway, P.E.; Davis, M.E. *J. Catal.* **1989**, *116*, 263; b) Hathaway, P.E.; Davis, M.E. *J. Catal.* **1989**, *116*, 279.

alkali oxide clusters (i.r. bands at 1570 and 1380 cm^{-1} [48a]). Note in this context that Lavalley *et al.* [29] did not mention any formaldehyde formation on Cs-FAU(Y) at elevated temperatures (623 K).

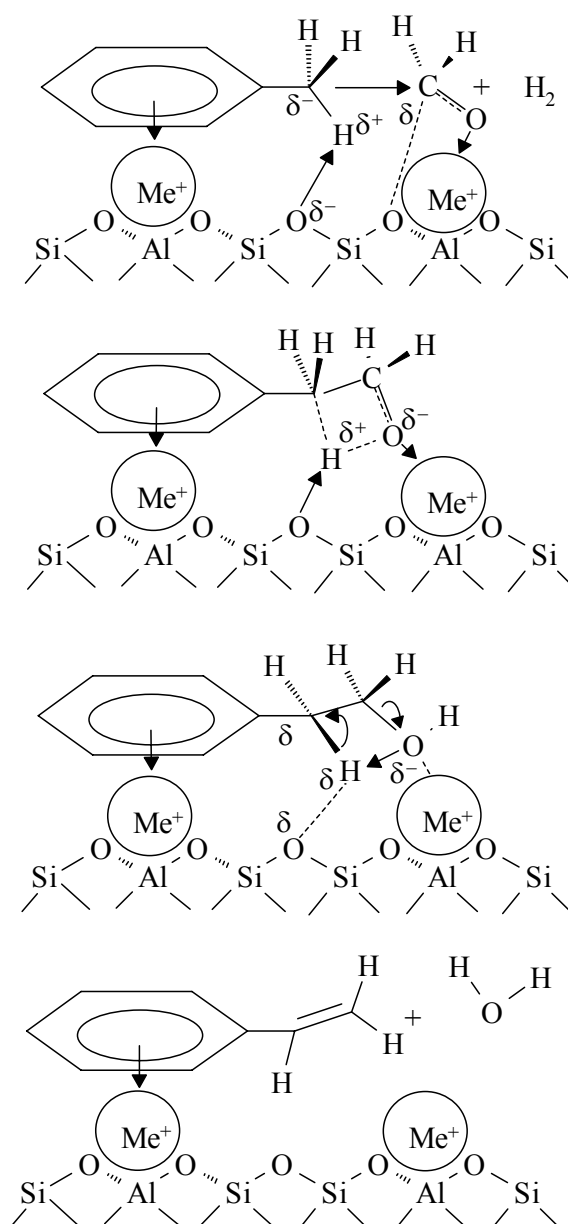
It should be emphasized that with Rb- (see Ref. [28]) and Cs-FAU(X) zeolite a significant fraction of the sites were interacting with toluene (see Figs. 8.3 and 8.4) and adsorbed formate species were observed. Both materials showed an appreciable activity for side-chain alkylation (see Table 8.3 and 8.4). Thus, we conclude that from the basic materials reported in this work, only Rb- and Cs-FAU(X) possess the adequate balance of both catalytic functions to catalyze the side-chain alkylation of methanol. MgO, hydrotalcites and Cs-FAU(Y), were either unable to bind toluene sufficiently or did not transfer methanol into its dehydrogenated state.

8.5 CONCLUSIONS

The present study, demonstrates that several requirements have to be met to successfully catalyze the side chain alkylation of methanol. The catalyst needs to (i) have sufficient base strength to dehydrogenate methanol to formaldehyde, (ii) stabilize toluene on the surface or in the pores and activate its methyl group and (iii) establish adequate sorption stoichiometry between toluene and methanol. Only materials which provide all these characteristics show appreciable catalytic activity.

These requirements lead us to suggest a pathway for the reaction (Scheme 8.1) similar to an aldol type condensation which was discussed in detail in ref. [28], as also postulated by Itoh *et al.* [21]. One elementary step is the abstraction of the hydrogen from methanol adsorbed on the basic materials leading to the formation of formaldehyde and formates with a C-atom positively polarized. Note that this does not require redox properties in the oxide catalysts (see e.g., ref. [49]). In a parallel reaction step, toluene is strongly retained on the large cations due to the interactions of the toluene π -electrons (electron pair donor) and the cation (electron pair acceptor). This interaction withdraws electron from the aromatic ring and facilitates the polarization of the methyl C-H, much like an electron withdrawing substituent (e.g., a nitro group) on the aromatic ring would [39,49]. Additionally the methyl group of toluene interacts with the oxygen atoms of the basic framework further polarizing the methyl C-H bond. Note that this leads in the transition state (when the hydrogen is being split off as H^+) to a negatively charged methyl carbon. Under these conditions, the positively charged C-atom of formaldehyde, would react with the activated carbon atom of toluene to form the new carbon-carbon bond at the methyl group. Most likely the reaction would proceed *via* a concerted mechanism avoiding the existence of long lived ionic intermediates. We would emphasize the strong analogy to a classical aldol condensation by stressing the improved ease of that reaction if an electron withdrawing group is placed on the aromatic ring [49].

49. March, J. *Advanced Organic Chemistry*, 4th Edition; Wiley Interscience Publication: New York, 1992.



Scheme 8.1

The elementary step mentioned first may proceed on alkali cation exchanged FAU(X) zeolites, hydrotalcite and MgO, but not with Cs-FAU(Y) (as it has an insufficient base strength), the other is only possible with basic materials having large accessible cations, such as the Cs⁺ cations in the exchanged FAU(X) and FAU(Y) zeolites, but not with hydrotalcite and the MgO studied in the present report. This is not so much related to the base strength of the lattice oxygen, but to the inability to retain and polarize toluene under reaction conditions. Note that Rb- (see Ref. [28]) and Cs-FAU(X) are the only materials reported here that fulfill both conditions. These results also demonstrate that side chain alkylation does not solely depend on basic properties of a catalytic material and is, hence, inadequate for probing the base strength of unknown materials.

It needs to be said that Scheme 8.1 implies that Lewis acid site proximity could be an important factor during the side chain alkylation reaction since two neighboring sites are needed for activation of toluene and formaldehyde. However, calculations have shown that proximity of base sites interacting with the toluene side chain was a more important factor than proximity of acid sites [21,50]; this means that the closer the base sites the higher the probability for activating the toluene methyl group and thus facilitating reaction with formaldehyde. The higher proximity of base sites in turn indicates a higher proximity of Lewis acid sites as found for alkali exchanged FAU(X), but that was considered less important.

Acknowledgments. The financial support of the European Community, Human Capital and Mobility Project, under grant Nr. CIPA-CT94-0184 is acknowledged. We thank Dr. Florian Eder and Drs. G. Nivarthi for the gravimetric measurements and Prof. Dr. H.G. Karge and Prof. A. Corma for providing the samples used in this study.

50. Miyamoto, A.; Iwamoto, S.; Agusa, K.; Inui, T. In *Acid-Base Catalysis*; Tanabe, K., Hattori, H., Yamaguchi, T., and Tanaka, T., Eds.; Verlag Chemie: Weinheim, 1989; pp 497-504.

Chapter 9

Side Chain Methylation of Toluene: The Effect of Oxygen

Abstract:

Previously, it was shown that the addition of molecular oxygen to a methanol feed induced the formation of formaldehyde over alkali cation exchanged zeolites (FAU(X) and MFI). In this Chapter, the effect of oxygen was investigated in the methylation of toluene. It was concluded that oxygen had an overall negative effect on the side chain alkylation, although small increases in styrene and ethylbenzene yield were observed. However, major byproducts were CO, H₂, CO₂, H₂O, benzene. These byproducts are the result of methanol and toluene oxidation.

9.1 INTRODUCTION

The best catalysts for the side chain alkylation of toluene with methanol yielding styrene are Rb^+ and Cs^+ exchanged FAU(X) zeolites at 698 K [1]. The side chain alkylation of toluene with methanol has potential to replace the current industrial styrene processes used by UOP, DOW and SHELL [2]. Yashima *et al.* have shown that the intermediate could be formaldehyde, resulting from the methanol dehydrogenation over basic sites [3] (see also Chapter 6). A mayor problem still to overcome is the unselective methanol and formaldehyde decomposition over these basic zeolites to CO and H_2 [1]. Less basic zeolites like Na-FAU(X) and Cs-MFI, however, were found to be not active for the formation of formaldehyde, and, subsequently, yield mainly xylenes [1,4].

Previous research has shown that oxidation of methanol with O_2 (oxidative dehydrogenation, ODH) over alkali cation exchanged zeolites yield formaldehyde in high yields [5]. Also in Chapter 7 it was shown that the reaction of methanol with molecular oxygen yielded surface formaldehyde over alkali cation exchanged MFI and FAU(X) zeolites. It was concluded that Cs-MFI of all the catalysts studied (Na-, Rb- and Cs-FAU(X) and Na- and Cs-MFI) was the most promising as it yielded surface formaldehyde over the widest temperature range (323-620 K). Only on Cs-MFI was adsorbed formaldehyde detected above 500 K.

Since ODH of methanol over alkali cation exchanged MFI and FAU(X) zeolites yielded surface formaldehyde (see Chapter 7) we were interested to study the methylation of toluene over these zeolites in the presence of molecular oxygen. The objective was to increase the surface concentration and stability of surface formaldehyde *in situ* during methylation of toluene over alkali metal cation exchanged MFI and FAU(X) by adding molecular oxygen. Since these MFI materials are weakly basic, concomitant production of CO and H_2 as a result of formaldehyde decomposition may be small and thus high methanol selectivity is expected (see also Chapter 7). The use of O_2 could thus improve the selectivity towards styrene.

The other catalyst tested here was Rb-FAU(X). This catalyst has proven to be a very selective catalyst for the alkylation with methanol (methylation) of the side chain of toluene yielding styrene and ethylbenzene (selectivity 70 mol% (based on converted toluene)) [1] in the absence of O_2 . Due to the lower basicity of the framework oxygen centers of Rb-FAU(X), this catalyst is less active for the unselective decomposition of formaldehyde into CO and H_2 , compared to Cs-FAU(X) (see also Chapter 6).

To our knowledge, this is the first detailed alkylation study over single alkali cation exchanged zeolites in which oxygen is used to yield formaldehyde *in situ*.

-
1. a) See Chapter 8 of this thesis; b) Palomares, A.E.; Eder-Mirth, G.; Rep, M.; Lercher, J.A. *J. Catal.* **1998**, *180*, 56.
 2. Weissermel, K.; Arpe, H.J. *Industrial Organic Chemistry, Third Completely Revised Edition*; VCH Verlagsgesellschaft mbH: Weinheim, 1997; pp 335-342.
 3. Yashima, T.; Sato, K.; Hayasaka, T.; Hara, N. *J. Catal.* **1972**, *26*, 303.
 4. Vinek, H.; Derewinski, M.; Mirth, G.; Lercher, J.A. *Appl. Catal.* **1991**, *68*, 277.
 5. Gryaznova, Z.V.; Nefjodova, A.R.; Sidamonidze, Sh.I.; Akhalbedashvili, L.G. *Zeolites* **1987**, *7*, 123.

9.2 EXPERIMENTAL

In Chapter 3 a detailed description of the experimental equipment has been given as well as the procedure for evaluation of the obtained reactor data. Zeolite materials and activation procedures used are described also in Chapter 3.

At 323 K approximately 50 mg of Rb-FAU(X) or Cs-MFI catalysts were allowed to equilibrate in 19 ml.min⁻¹ argon containing MeOH, toluene and O₂, continuously (10, 30, and 3.3 mbar, respectively). This corresponds with a W/F of 94 g.h.mol⁻¹ based on MeOH. After 80 minutes heating of the catalyst in Ar/MeOH/toluene/O₂ flow was started to 773 K (heating rate of 5 K.min⁻¹). Other gas flows used in the fixed bed reactor were (composition can vary): 1) MeOH/toluene (molar ratio = 1/3), 2) MeOH/toluene/O₂ (9/3/1), and 3) toluene/O₂ (9/1). Temperature programmed reaction (t.p.r.) experiments were chosen because of the ability to quickly scan for alkylation products at different temperatures in one experiment and to obtain information about subsequent products (that are related *via* their (surface) intermediates). This was measured using a Balzers OMNISTAR GSD 300 O2 mass spectrometer (online continuously). Conversion, yield and selectivity were measured at 673 and 773 K isothermally using a Varian 3300 gas chromatograph (samples taken at 323, 673, and 773 K, respectively).

Evaluation of the gas composition of the effluent gas stream (conversions (*X*), yields (*Y*) and selectivities (*S*)) were performed as described in Chapter 3. Briefly, the MeOH and toluene conversion were calculated using Equation 9.1a and b. Yields and selectivities are based on methanol and were calculated using Equations 9.2 and 9.3:

$$X_{MeOH} = ((N_{MeOH,in} - N_{MeOH,out}) / N_{MeOH,in}) \times 100\% \quad (\text{Eq. 9.1a})$$

$$X_{toluene} = ((N_{toluene,in} - N_{toluene,out}) / N_{toluene,in}) \times 100\% \quad (\text{Eq. 9.1b})$$

$$Y_{product} = N_{product} / N_{MeOH,in} \times 100\% \quad (\text{Eq. 9.2})$$

$$S_{product} = Y_{product} / X_{MeOH} \times 100\% \quad (\text{Eq. 9.3})$$

where N_i is calculated from the GC response signal using the response factors for individual components (*i*) and converted into mols. The response signal of the gas chromatograph attributed to toluene or methanol in the reactor feed was very stable (deviation: less than 1%). However, due to the very low toluene conversion, the error in conversion, yield and selectivity based on toluene was significant (over 66% at 773 K). The error in MeOH conversion was approximately between 15 (673 K) and 33% (773 K).

To quantify the amount of carbon deposition during toluene alkylation a coking experiment was performed using Rb-FAU(X). Catalyst loading, activation, equilibration with the MeOH and toluene mixture in Ar (molar ratio toluene/methanol = 3/1), and heating ramp (5 K.min⁻¹) was performed as described above. At 698 K, heating was stopped and the catalyst was kept for two days constant at 698 K in flowing MeOH and toluene (toluene/methanol = 3/1). After approximately two days, the coke deposition was measured by analyzing the weight loss during oxidation in a TGA apparatus (Mettler Toledo TGA/SDTA851^e). Approximately 44 mg coked Rb-FAU(X) was loaded in a

70 μl aluminum sample holder and heated in 10 mbar oxygen (Ar was added to 1 bar) with $5 \text{ K}\cdot\text{min}^{-1}$ up to 873 K (at this temperature no more weight loss was recorded). The total gas flow was $20 \text{ ml}\cdot\text{min}^{-1}$.

Blank experiments in an empty (no catalyst) reactor were carried out in order to examine the contribution of the reactor wall and thermal gas phase reactions (further referred to as thermal non-catalytic oxidation reactions). Experiments in an empty fixed bed reactor showed a small contribution of the empty reactor to the catalytic performances above 600 K (benzene, benzaldehyde, benzoic acid, CO, and CO₂) and increased with increasing temperatures. In a MeOH/toluene/O₂ flow, the MeOH conversion was found to be 8.8% at 673 K and 28.1% at 773 K with GC. Toluene conversion was found to be 5% at 773 K. However, it should be noted that the toluene conversion was very small and thus the selectivity could not be measured properly due to large experimental error. Benzene yield at 773 K was 0.75 mol% (selectivity (based on MeOH converted) = 2.7 mol%). Methanol oxidation in the empty reactor has been described in Chapter 7. Above 673 (H₂ and dimethyl ether (DME)), 743 (H₂O) and 773 (CO₂) K thermal non-catalytic oxidation reactions took place, but their gas phase concentrations were too low to be detected by gas chromatograph. No CO was found during oxidation of MeOH. No detectable gaseous products, other than MeOH and toluene, were found when this mixture in the absence of O₂ was fed to the empty fixed bed reactor at 673 and 773 K.

Zeolite Cs-FAU(X) was pressed into self-supporting wafers and loaded into the i.r. spectrophotometer, where it was analysed *in situ* during all treatments. Activation procedures were performed in 19 ml/min He flow. After activation the zeolite was brought into contact with a toluene/O₂ mixture (molecular ratio 45/5 (expressed in mbar)) and was allowed to equilibrate. He was added to 1 bar (total flow 19 ml/min). Then the sample was heated under continuous methanol / toluene and oxygen flow. Gas phase analysis was performed using a Balzers OMNISTAR GSD 300 O₂ mass spectrometer. In Chapter 7, it was shown that MeOH was readily converted to H₂O, CO₂, H₂, and DME over the heating wires in the empty i.r. reactor. No blank experiments were performed to assess the heating wires of the i.r. reactor ability to convert toluene in the presence of O₂. However, due to the lower reactivity of toluene compared to MeOH we do not expect significant toluene conversion below 673 K over the heating wires.

9.3 RESULTS

MeOH and toluene reaction in the presence of molecular oxygen

Cs-MFI

To obtain information about the temperature range in which alkylation of toluene with methanol in the absence and presence of O₂ was found to proceed, first a temperature scan (by mass spectrometer) was performed between 323 and 773 K in the fixed bed reactor (a heating rate of $5 \text{ K}\cdot\text{min}^{-1}$ was used). In Fig. 9.1 the temperature dependence of the toluene alkylation with methanol is

shown; the mass spectrometers response to m/z 104 is represented, which is attributed to the molecular ion peak of ionized styrene. Also other aromatic products analyzed in this Chapter can be represented by m/z 104, as these can be fragments of ethylbenzene, and xylene. Thus any increase of the m/z 104 signal is concluded to indicate toluene alkylation products (styrene, ethylbenzene and xylene) or desorption of alkylation products adsorbed on the surface.

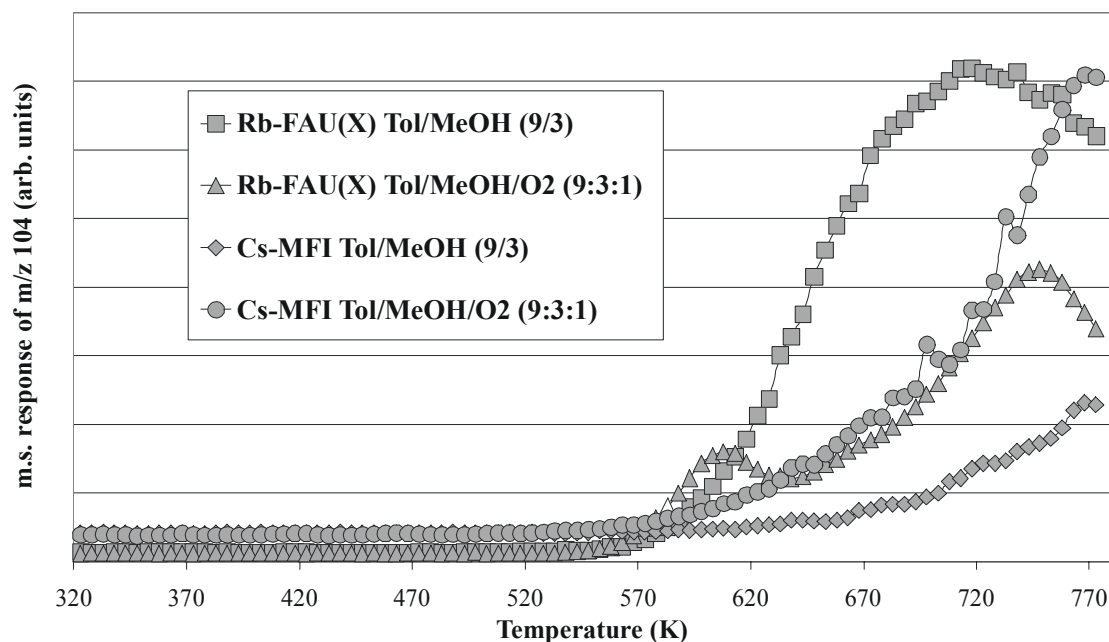


Figure 9.1: Alkylation profile of toluene with methanol over Rb-FAU(X) and Cs-MFI in the absence of O_2 and in the presence of O_2 (7.7 mol% O_2 (based on total [MeOH+toluene+ O_2] concentration) as a function of temperature monitored by mass spectrometry. The scanned mass is m/z 104 (styrene).

It can be seen in the temperature scan presented in Fig. 9.1 that alkylation only started at temperatures higher than 570 K. At temperatures where surface formaldehyde was observed (at $T < 620$ K (maximum intensity at 490 K) (see Chapter 7)) almost no alkylation took place. Therefore, alkylation experiments were performed at temperatures above 620 K. Other products observed in the gas phase were CO, CO_2 , H_2O , etc. (see below).

In Table 9.1 the conversion and selectivity obtained (based on MeOH) during toluene alkylation over Cs-MFI, in the absence and presence of molecular oxygen isothermally at 673 and 773 K are compiled.

As can be seen in Table 9.1 the conversion of MeOH remained almost constant (from 32.8 to 31.8%) at 673 K. MeOH conversion increased from 43.6% to 52.4% with the addition of O_2 at 773 K (see Fig. 9.2) to the feed. Compared to the reaction in the presence of O_2 at 673 K, the MeOH conversion had also increased. Overall it is clear from Table 9.1 that most methanol is converted to other products that could not be detected quantitatively in the gas phase (e.g., H_2O , CO, CO_2 , etc.) due to the characteristics of the chosen gas chromatograph analysis columns (with the mass spectrometer it was possible to measure them qualitatively). Additionally, the formation of coke was observed.

TABLE 9.1: Methanol (MeOH) conversion (%) over Cs-MFI in the absence and presence of molecular oxygen isothermally at 673 and 773 K. Selectivities (mol%): alkylation (SCA or RA)^{a,b}, DME, and H₂ based on MeOH converted.

Reaction	Reaction conditions (molar ratio + reaction temperature)				
	C ₇ H ₈ /MeOH = 9/3; 673 K	C ₇ H ₈ /MeOH/O ₂ = 9/3/1; 673 K	C ₇ H ₈ /MeOH = 9/3; 773 K	C ₇ H ₈ /MeOH/O ₂ = 9/3/1; 773K	C ₇ H ₈ /MeOH/O ₂ = 3/9/1; 773K
MeOH conv.	32.8	31.8	43.6	52.4	56.6
SCA ^a select.	0.2	0.09	0.3	0.4	0.02
RA ^b select.	2.3	3.8	2.6	1.5	3.2
DME select.	11.5	7.7	11.5	1.71	n.d.
H ₂ select.	n.d.	5.9	n.d.	15.51	n.d.

^a SCA is side chain alkylation (= total styrene+ethylbenzene).

^b RA is ring alkylation (= total *o*-+*m*-+*p*-xylene).

In the absence of O₂, Cs-MFI is a catalyst found to alkylate solely the ring of toluene with methanol (methylation) yielding *ortho*-, *meta*-, and *para*-xylene [4]. With the presence of O₂ (3.3 mbar) in the MeOH+toluene feed at 673 K (molar ratio of toluene/methanol/oxygen feed: 9/3/1), the ring alkylation yield and selectivity (based on MeOH conversion) were found to have slightly increased (see Table 9.1). The side chain alkylation selectivity had dropped slightly, compared to the MeOH/toluene reaction in the absence of O₂.

The addition of molecular oxygen to the toluene/methanol feed at 773 K (molar ratio toluene/methanol/oxygen: 9/3/1) decreased the ring alkylation (i.e., xylene) yield and selectivity, but

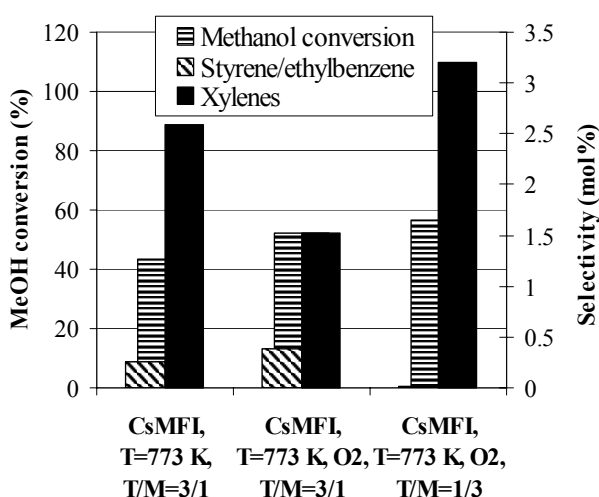


Figure 9.2: Methanol conversion (%) and alkylation selectivities (mol%) obtained during methylation of toluene in the absence and presence of oxygen over Cs-MFI at 773 K.

increased a little the side chain alkylation (i.e., styrene and ethylbenzene) yield and selectivity (see Table 9.1). This is also shown in Fig 9.2, where the reaction selectivity in the absence of O₂ is shown. Preliminary results showed that increasing O₂ concentrations (from 7.7 to 14 mol% O₂ (based on total [MeOH+toluene+O₂] concentration) during the methylation of toluene over Cs-MFI at 773 K led to lower xylene yield (approximately 0.5 times lower), but to higher styrene and ethylbenzene yield (approximately 1.7 times higher). DME yield decreased approximately 2.5 times with higher O₂ concentration in the MeOH+toluene feed. Increasing O₂ concentrations led also to increased benzene production and more benzaldehyde, resulting from gas phase toluene oxidation.

The product distribution of *o*-xylene and *m*- and *p*-xylene did not change with the addition of O₂; thus the *o*-xylene : *p*-xylene+*m*-xylene ratio of 1:2 was maintained (see also Appendix 1). Gas phase analysis could not separate *m*- and *p*-xylene. When a higher methanol concentration was used at 773 K (molar ratio toluene/methanol/oxygen: 3:9:1) the total xylene selectivity further improved (see Table 9.1 and Fig. 9.2): the xylene selectivity had increased approximately 2 times (see Fig. 9.2). The styrene and ethylbenzene selectivity decreased dramatically (from 0.4 to 0.02%).

In Table 9.1 the results obtained for the production of DME as function of temperature and the absence and presence O₂ concentration is compiled. DME yield at 673 K (molar ratio toluene/methanol/oxygen: 9/3/1) decreased with the addition of O₂ from 3.8 to 2.0 mol% mainly caused by the reduction of the selectivity at 673 K from 11.5 mol% in the absence of O₂ to 7.7 mol% in the presence of O₂ (based on MeOH). Also at 773 K in the presence of O₂ was the DME production lower (see Table 9.1). Overall, the DME selectivity was 33% and 85% lower in the presence than observed in the absence of O₂ at 673 and 773 K, respectively.

Furthermore, also benzene, benzaldehyde, benzoic acid, CO, CO₂, H₂, and H₂O were found in the gas phase during toluene and methanol reaction over Cs-MFI in the presence of O₂. Analysis of the effluent gas stream did not show any gaseous formaldehyde (this agrees well with Chapter 7) and/or methyl formate. H₂O was found in the gas phase at starting temperatures of approximately 450 K (see Fig. 9.3). CO₂ was observed at 580 K. In the absence of O₂ no CO₂ is formed. CO and H₂ were found at 623 K. Due to the properties of the chosen gas phase analysis columns in the gas chromatograph (see Chapter 3), no quantitative analysis of the CO, CO₂, and H₂O gas phase concentrations can be given. Furthermore, at 773 K also a high concentration of benzaldehyde and benzene (36x increase compared to the reaction without O₂) were found. At 673 K, the production of benzaldehyde (not shown here) and benzene (see Fig. 9.3) is almost negligible.

However, heating the toluene/methanol/oxygen mixture (ratio 9/3/1) in an empty (fixed bed) reactor also yielded benzene and benzaldehyde above 620 K with the same temperature dependence as observed during toluene alkylation with methanol over Cs-MFI in the presence of O₂. These thermal non-catalytic gas phase oxidation reactions contribute heavily to the oxidation reactions when using Cs-MFI above 620 K.

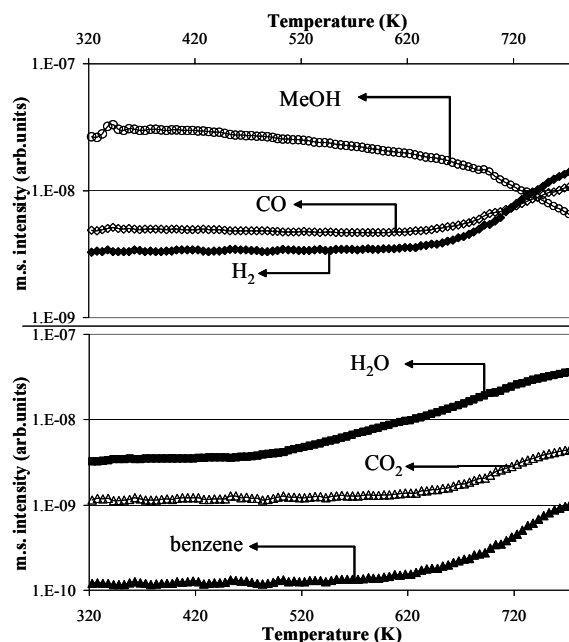


Figure 9.3: Gas phase analysis of the effluent stream after toluene alkylation with methanol in O₂ over Cs-MFI as function of temperature. 323-773 K, $T_r = 5 \text{ K}\cdot\text{min}^{-1}$. (Molar ratio toluene/MeOH/O₂ = 9/3/1)

Rb-FAU(X)

In Fig. 9.1 a temperature scan (by mass spectrometer) is shown for Rb-FAU(X). From this Figure it is clear that at low temperatures, where formaldehyde and/or formate are expected to exist on the surface ($T < 500$ K (see Chapter 7)), no toluene alkylation activity was found (Fig. 9.1). Only water resulting from the oxidative dehydrogenation of methanol was found in the gas phase at low temperatures (this will be discussed later). Therefore, alkylation experiments using Rb-FAU(X) were conducted at temperatures above 600 K.

The small increase of mass 104 (see Fig. 9.1) observed between 578 and 633 K (maximum intensity at 608 K) during the reaction of methanol with toluene in the presence of O_2 over Rb-FAU(X) can not be assigned to the production of styrene, since no alkylation products were found with the gas chromatograph. The origin of this low temperature maximum is not understood. The low temperature maximum is not observed with Cs-MFI (see Fig. 9.1).

In Table 9.2, the results from the fixed bed reactor, which were obtained isothermally at 673 and 773 K in the absence and presence of O_2 with Rb-FAU(X), are compiled.

MeOH conversion at 673 K increased from 14.9% to 23.9%, with the use of oxygen (3.3 mbar O_2). With the use of O_2 at 773 K methanol conversion increased slightly from 75.3% (no O_2) to 79.3% (in the presence of 3.3 mbar).

TABLE 9.2: Methanol (MeOH) conversion (%), and alkylation (SCA or RA)^{a,b}, DME and H_2 selectivity^c (mol%) over Rb-FAU(X) in the absence and presence of molar oxygen isothermally at 673 and 773 K.

Reaction	Reaction conditions (molar ratio + reaction temperature)				
	$C_7H_8/MeOH = 9/3; 673$ K	$C_7H_8/MeOH/O_2 = 9/3/1; 673$ K	$C_7H_8/MeOH = 9/3; 773$ K	$C_7H_8/MeOH/O_2 = 9/3/1; 773$ K	$C_7H_8/MeOH/O_2 = 3/9/1; 773$ K
MeOH conv.	14.9	23.9	75.6	79.6	60.2
SCA ^a select. ^c	5.1	4.4	4.3	3.1	0.9
RA ^b select.	0.3	0.5	0.3	0.06	0.01
H_2 select.	4.4	1.6	38.5	46.4	40.5
DME select.	8.7	5.4	2.6	1.0	2.1

^a SCA is side chain alkylation (= total styrene+ethylbenzene).

^b RA is ring alkylation (= total *o*-+*m*-+*p*-xylene).

^c Selectivity: based on converted MeOH.

In the presence of molecular oxygen (molar ratio toluene/methanol/oxygen: 9/3/1) at 673 K the toluene alkylation with methanol yielded over Rb-FAU(X) yielded selectively styrene and ethylbenzene as expected, and the side chain alkylation (i.e., styrene and ethylbenzene) yield had increased slightly (from 0.7% to 1%) when using O_2 in the feed. The observed side chain alkylation

selectivity in the presence of O₂ had decreased with from 5.1% to 4.4% (based on methanol); the production of styrene appeared to be slightly more favored (styrene : ethylbenzene ratio = 4:1). The selectivity for ring alkylation (i.e., xylene production (all isomers)), increased slightly (from 0.3% to 0.5%) with the use of oxygen at 673 K.

At 773 K the reaction of toluene with methanol in the presence of O₂ yielded styrene and ethylbenzene as well (see Table 9.2). Compared to the reaction at 673 K the side chain alkylation yield at 773 K had increased by a factor of 2.5 in the presence of O₂. The side chain alkylation selectivity (based on methanol) at 773 K was also lower in the presence of O₂ compared to the absence of O₂; it decreased from 4.3 to 3.1 mol% (the same trend for the side chain alkylation selectivity was observed at 673 K). This is shown in Fig. 9.4. With the use of O₂ in the MeOH+toluene feed at 773 K, Rb-FAU(X) was more selective to side chain alkylation; ring alkylation yield decreased slightly from 0.3 to 0.05%. The ratio of styrene : ethylbenzene was found to be 3/2. In the absence of O₂ the styrene : ethylbenzene ratio was 2/3).

When the concentration of methanol in the presence of oxygen was increased (molar ratio toluene/methanol/oxygen: 3:9:1) the yield of styrene and ethylbenzene was 5 times lower (MeOH conversion dropped to 60.2%). This is mainly attributed to the low concentration of toluene in the feed (toluene conversion increased from 5.0 to 8.8%).

Table 9.2 compiles the H₂ yield and selectivity obtained during toluene alkylation in the absence and presence of

O₂ over Rb-FAU(X) at different temperatures and different MeOH concentrations. H₂ was found in the gas phase starting at 640 K. The production of H₂ at 673 K (molar ratio toluene/methanol/oxygen: 9/3/1) decreased with the addition of O₂ from 0.7 to 0.4 mol%; the selectivity at 673 K in the presence of O₂ was 1.6 mol% (based on MeOH). However, the H₂ selectivity had increased with the addition of O₂ at 773 K from 38.5 to 46.4 mol% based on MeOH. When the methanol concentration in the feed was increased (molar ratio toluene/methanol/oxygen: 3:9:1) at 773 K the production of H₂ decreased to 40.5 mol%.

In Table 9.2 the DME selectivity obtained during toluene alkylation in the absence and presence of O₂ over Rb-FAU(X) at different temperatures and different MeOH concentrations is compiled. DME selectivity at 673 K (molar ratio toluene/methanol/oxygen: 9/3/1) decreased in the presence of O₂ to 5.4 mol%; in the absence of O₂ this was 8.7 mol%. The DME selectivity at 773 K had decreased with the addition of O₂ from 2.6 to 1.0 mol%. The DME yield was 56% lower than observed

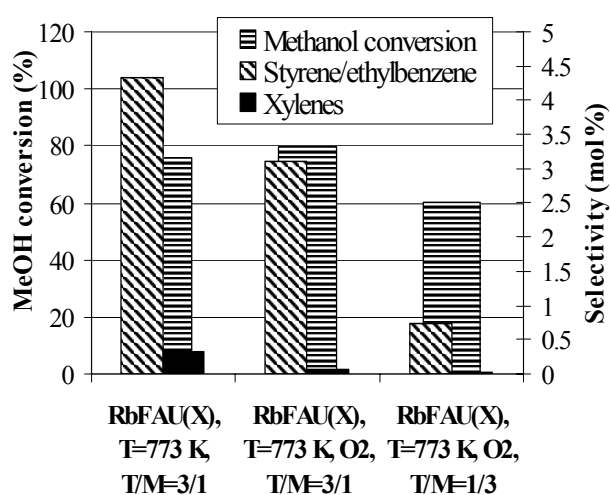


Figure 9.4: Methanol conversion (%) and alkylation selectivities (mol%) obtained during methylation of toluene in the absence and presence of oxygen over Rb-FAU(X) at 773 K.

in the absence of O_2 at 773 K. When the methanol concentration in the feed was increased (molar ratio toluene/methanol/oxygen: 3:9:1) at 773 K the selectivity of DME increased approximately two times, compared to lower MeOH concentrations at 773 K (the selectivity to DME also increased twice).

Other gaseous species detected in the effluent stream during toluene and methanol reaction over Rb-FAU(X) in the presence of O_2 (besides H_2 , DME) were CO, CO_2 , and H_2O . In Fig. 9.5 part of the gas phase composition of the effluent gas stream is shown (toluene, styrene, ethylbenzene, and xylene are not shown). Analysis of the effluent gas stream did not show any formaldehyde in the gas phase during toluene alkylation with methanol in the presence of O_2 (as also reported for Cs-MFI) and/or methyl formate. H_2O was found in the gas phase at starting temperatures of approximately 398 K and showed a maximum at 488 K after which it first decreased until 588 K before it increased again to 773 K (see Fig. 9.5). CO_2 was detected in the gas phase from $T > 538$ K and increased until approximately 720 K, after which the CO_2 gas phase concentration decreased again. Gas phase analysis using mass spectrometry indicated a 5 times increase of the CO_2 production. In the absence of O_2 almost no CO_2 is formed. CO was found starting at approximately 620 K. Similar observations were made in Chapter 7. Note that the CO_2 and CO gas phase concentrations also include contributions of the non-thermal gas phase oxidation reaction. Due to the properties of the gas chromatography columns, no quantitative analysis of the CO, CO_2 , and H_2O concentrations can be given.

Besides the production of above mentioned products (styrene, ethylbenzene, CO_2 , etc.) also a small amount of benzene was found (above 570 K). At approximately 620 K a jump is clearly seen (see Fig. 9.5), which was not present in the benzene production curve for Cs-MFI (see Fig. 9.3). Increasing O_2 concentrations (from 7.7 to 14 mol% O_2 (based on total [MeOH+toluene+ O_2] concentration) added during the reaction of toluene with methanol at 673 K over Rb-FAU(X) yielded mainly increasing concentrations of benzene. This observation agrees well with results obtained by others [6].

Due to the lower reaction temperature for the production of benzene (600 K) during toluene alkylation in the presence of O_2 compared to the empty fixed bed reactor ($T > 673$ K), it was decided to study the reaction of toluene with O_2 solely. The reaction of toluene and O_2 (molar ratio = 9:1) over

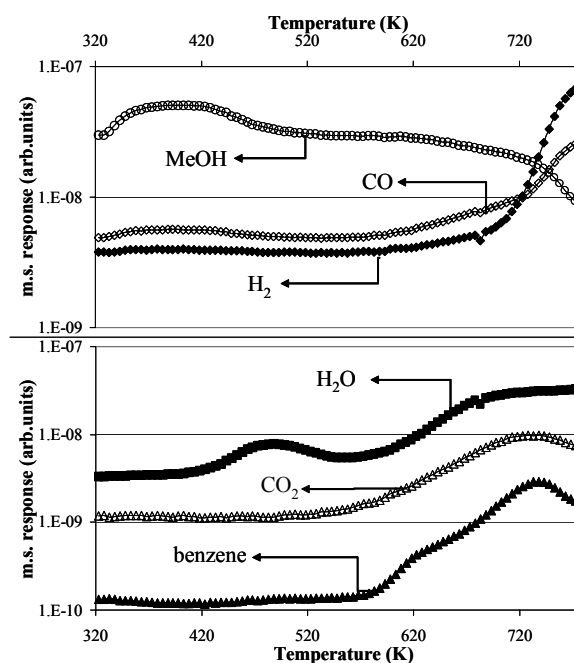


Figure 9.5: Gas phase analysis of the effluent stream after toluene alkylation with methanol in O_2 over Rb-FAU(X) as a function of temperature. 323–773 K, $T_r = 5 \text{ K}\cdot\text{min}^{-1}$. (Molar ratio toluene/MeOH/ $O_2 = 9/3/1$)

6. Itoh, H.; Miyamoto, A.; Murakami, Y. *J. Catal.* **1980**, *64*, 284.

Rb-FAU(X) yielded mainly benzene, water, CO and CO₂ at reaction temperatures above 600 K (see Fig. 9.6). Toluene conversion at 773 K was 5.6 mol% (± 4 mol%), which was a little higher ($\sim 10\%$) than that observed in the reaction of methanol (toluene conversion = 5 mol%), and the empty fixed bed reactor (toluene conversion = 5 mol%). Also small concentrations of xylene, ethylbenzene and styrene were found, even though no MeOH is present in the feed stream. The decrease in benzene production at 720 K is attributed to O₂ depletion from the gas phase (see Fig. 9.6). Increasing O₂ concentration at 773 K yielded more benzene (3.3 mbar O₂: 0.6 mol%; 6.6 mbar: 1.2 mol%; 13.2 mbar: 2.3 mol% based on toluene), water, CO and CO₂. Water was observed at 573 K, CO₂ at 563 K, and CO at 620 K. Also the styrene yield increased slightly with increasing O₂ pressure (four times increase in O₂ yielded approximately 2 times more styrene) and by increasing the reaction temperatures: the styrene yield increased from 773 K to 923 K with 50%. The toluene conversion at 925 K was 7 mol%.

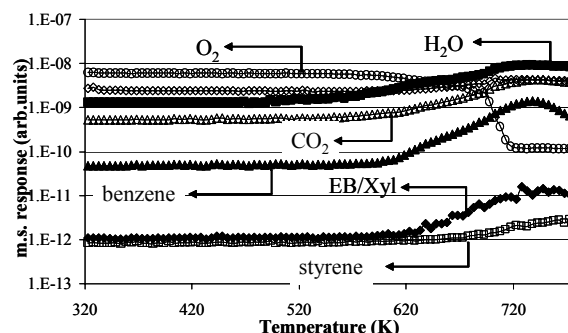


Figure 9.6: Gas phase analysis of the effluent stream after toluene oxidation over Rb-FAU(X) as function of temperature. 323-773 K, $T_r = 5 \text{ K.min}^{-1}$. (Molar ratio toluene/O₂ = 9/1) (EB/Xyl = ethylbenzene and/or xylene)

I.r. experiments performed during oxidation of toluene over Cs-FAU(X) in an i.r. CSTR reactor showed the formation of surface benzaldehyde (band at 1680 cm⁻¹) between 523 and 703 K (maximum intensity at 621 K). In Fig. 9.7 the obtained i.r. spectrum during toluene oxidation over Cs-FAU(X) as a function of temperature is shown. The band observed at 1680 cm⁻¹ agrees well with that reported by others [7]. The decrease of the i.r. bands (at $T > 660 \text{ K}$) observed for benzaldehyde is accompanied by the appearance of surface benzoate (bands at 1579 and 1357 cm⁻¹: between 700 and 773 K). This result agrees well with the result reported in Chapter 7 for the decomposition and oxidation of surface formaldehyde. Furthermore, during the decrease of the i.r. bands observed for surface benzaldehyde, the gas phase appearance of benzene and CO was detected. Final decomposition of surface benzoate yielded also benzene and CO₂. Please note that the oxidation of toluene in the empty i.r. reactor as function of temperature

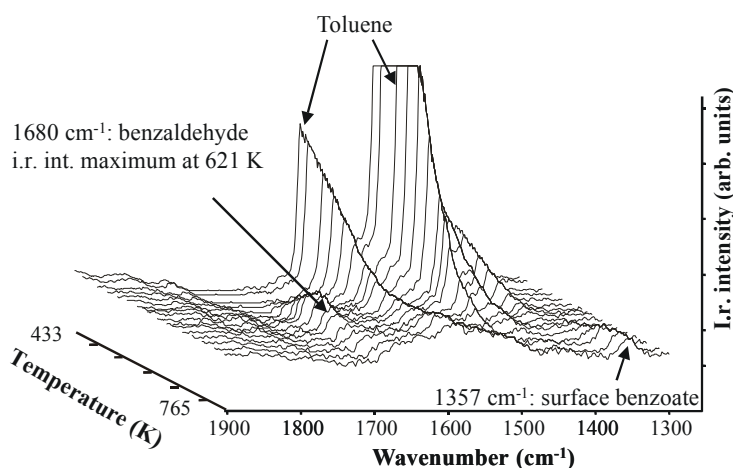


Figure 9.7: I.r. spectra recorded during the oxidation of toluene with O₂ (toluene/O₂ ratio = 9/1) over Cs-FAU(X). $T = 433\text{-}765 \text{ K}$; $T_r = 5 \text{ K.min}^{-1}$.

was not studied. No benzaldehyde and benzoate (as benzoic acid) were found in the gas phase during toluene oxidation over Cs-FAU(X) and Rb-FAU(X).

Additionally, during the reaction the production of coke was observed. This is also a major problem during toluene alkylation (see Appendix 1) and MeOH reaction (see Chapter 6) in the absence of O₂. Thus the stability of the catalyst was checked in a duration experiment (two days) at 698 K in the absence of O₂. The results are shown in Fig. 9.8. It can be seen that with time on stream the MeOH conversion and the yield of H₂, styrene and ethylbenzene decreased. Only the DME yield was found to slightly increase with time on stream. After reaction the catalyst was found to be black, indicating large carbon deposits. In an attempt to analyze the amount of carbon deposit, the deposit was oxidized in a TGA experiment. The weight loss during oxidation indicated that 6.32 mg of coke had been accumulated on 50 mg of catalyst. When a similar experiment was performed in the presence of O₂ a small increase in catalyst lifetime was observed of only 15%.

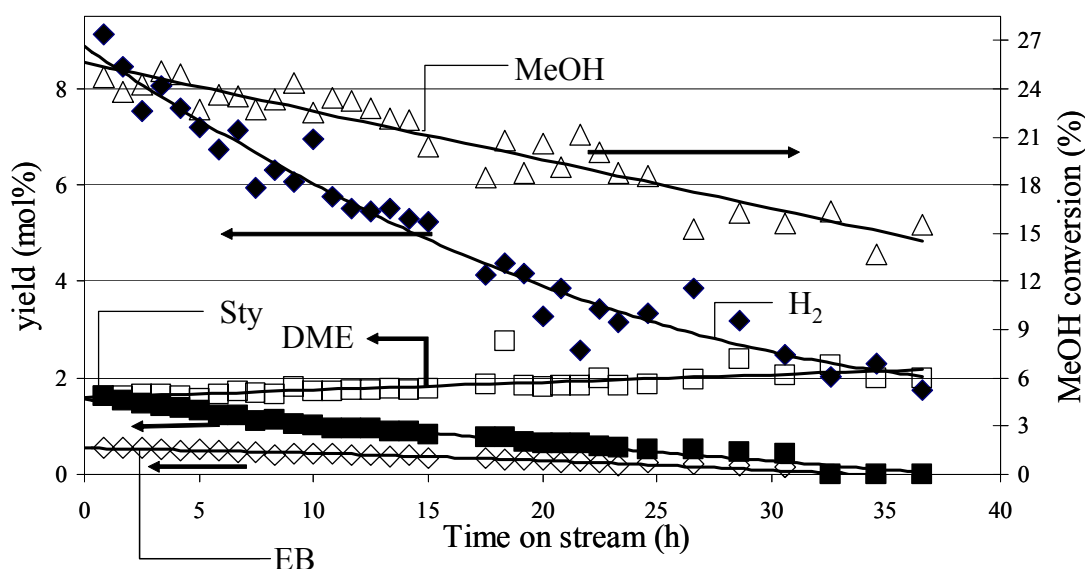


Figure 9.8: MeOH conversion (right axis) and yield of various gaseous products (left axis) with time on stream during toluene alkylation with methanol (toluene/MeOH = 3/1) over Rb-FAU(X) at 698 K.

9.4 DISCUSSION

Toluene methylation in the presence of oxygen

The higher temperatures needed for the alkylation of toluene (see Fig. 9.1), compared to the temperatures where surface formaldehyde was detected (at $T < 600$ K (see Chapter 7)), indicate that the activation of toluene is also a very important factor in the alkylation. Temperatures lower than 600 K are probably not sufficient. The temperatures chosen in Chapter 7 for the selective oxidation of MeOH to the side chain alkylation intermediate formaldehyde, i.e., reaction temperatures below 520 K (Cs-MFI) and below 450 K (Rb-FAU(X)), as the most promising due to formaldehyde stability thus proved not to be useful for the toluene alkylation. Activation of the side chain of toluene at lower

temperatures could possibly be achieved by, e.g., incorporating transition metals like iron and molybdenum. It was shown by Das and Pramanik [8] that incorporation of Fe-Mo oxide clusters in Cs⁺ exchanged FAU(X) zeolites resulted in lower alkylation temperatures (598 K) compared to single Cs⁺ exchanged FAU(X) zeolites (648 K). The incorporated Fe-Mo clusters are supposed to activate the toluene methyl group by hydrogen abstraction [9]. Thus *in situ* production of formaldehyde at lower temperatures, without the simultaneous activation of the methyl group of toluene does not result in a larger styrene production on the here used catalyst, Cs-MFI and Rb-FAU(X).

As can be seen in Tables 9.1 and 9.2 the addition of O₂ had only minor effects on the side chain alkylation yield. With Cs-MFI side chain alkylation yield had slightly increased at 773 K (Cs-MFI remained a very selective ring alkylation catalyst) whereas with Rb-FAU(X) side chain alkylation yield had slightly increased at 673 K. In the case of Rb-FAU(X) smaller yield and selectivity (based on MeOH) was found at 773 K, compared to 673 K. This is explained as follows. On Rb-FAU(X) decomposition and oxidation of methanol/formaldehyde to CO, H₂, CO₂, and H₂O at 673 K is probably smaller, compared to 773 K, and therefore more formaldehyde can react with toluene (O₂ was shown to increase surface formaldehyde formation, compared to the reaction in the absence of O₂ (see Chapters 6 and 7)). The lower side chain alkylation yield at 773 K is thus explained by a higher decomposition/oxidation rate of methanol/formaldehyde as indicated by the higher MeOH conversion and H₂ yield at 773 K in the presence of O₂. Addition of more MeOH at 773 K only resulted in much lower side chain alkylation yields and selectivities, but higher H₂ and DME yields. The higher H₂ yield can be the result of the higher formaldehyde decomposition over basic framework oxygen centers (see Chapter 6 and 7 and Ref. [10], while the higher DME yield can be the result of formaldehyde coupling to DME and CO₂ (see Chapter 7).

When using O₂ in the feed during reaction of toluene and methanol over Rb-FAU(X) at 673 and 773 K more styrene was produced. The ratio styrene:ethylbenzene at 673 K was 4:1 in the presence of O₂ (3:1 in the absence of O₂ (see Appendix 1)); at 773 K the ratio styrene:ethylbenzene was 3:2 (in the absence of O₂ this was 2:3). The lower ethylbenzene yield could be related to H₂ removal from the gas phase by the presence of O₂ (combustion) and thus preventing the hydrogenation of styrene by surface or gas phase hydrogen [11]: in the presence of O₂ less H₂ was found in the gas phase at 673 K (see Table 9.2). Another possibility could be oxidative dehydrogenation of ethylbenzene yielding styrene [12]. A third possibility might be that the selective methanol oxidation to formaldehyde and/or the unselective methanol oxidation to CO₂, etc. limits the direct alkylation of methanol with toluene

8. Das, N.K.; Pramanik, K. *J. Indian Chem. Soc.* **1997**, *74*, 705.

9. a) Yoo, J.S. *Appl. Catal. A: General* **1996**, *143*, 29; b) Yoo, J.S. *Catal. Today* **1998**, *41*, 409.

10. Hunger, M.; Schenk, U.; Weitkamp, J. *J. Mol. Catal.* **1998**, *134*, 97.

11. Sooknoi, T.; Dwyer, J. *Stud. Surf. Sci. Catal.* **1995**, *97*, 423.

12. a) Zhou, L.; Li, W.; Su, M.; Li, H.; Tao, K.; Hattori, H. *Appl. Catal. A: General* **1999**, *181*, L1; b) Zhou, L.; Li, W.; Fu, Q.; Guan, N.; Zheng, S.; Tao, K. In *Proceedings of the 12th International Zeolite Conference, Baltimore*; Treacy, M.M.J., Marcus, B.K., Bisher, M.E., and Higgins, J.B., Eds.; Materials Research Society: Boston, 1999; Vol. 4, pp 2585-2588.

(hydrocondensation) yielding less ethylbenzene [11]. No experiments were performed to answer this question.

The higher reaction temperatures needed for the side chain alkylation over Cs-MFI, compared to Rb-FAU(X), could follow from the low basicity of the framework oxygen centers of the Cs-MFI zeolite ($-\delta_{\text{O}} = 0.168$), compared to Rb-FAU(X) ($-\delta_{\text{O}} = 0.378$). These oxygen centers interact with the methyl group of the toluene (see Chapter 8). These results, however, indicate that Cs-MFI is a catalyst that can alkylate toluene at its side chain. However, no large yields could be obtained probably due to high formaldehyde coupling to DME and CO_2 (see Chapter 7). Addition of more MeOH decreased the side chain yield again and increased the ring alkylation. This could result from the fact that no more O_2 was present in the gas phase after reaction with these high methanol loadings. No experiments with intermediate MeOH partial pressures were tried to increase side chain alkylation yield. The results reported here show that alkylation in the presence of O_2 have a small positive effect on the side chain alkylation of the toluene with methanol over Cs-MFI and Rb-FAU(X). Side chain alkylation can even be induced on an otherwise inactive Cs-MFI catalyst. The presence of large alkali metal cations, i.e., Cs^+ , together with the weakly basic framework oxygens in MFI appear to activate the toluene side chain enough for some alkylation.

At temperatures above 670 K alkylation selectivity is low due to 1) the high decomposition of methanol and the alkylation intermediate, formaldehyde, at these high temperatures, which is evident from the increased H_2 production over Rb-FAU(X) in the presence of O_2 (see Table 9.2), 2) formaldehyde coupling to DME and CO_2 (see Chapter 7) and 3) oxidation rate of the surface formaldehyde to CO , CO_2 , H_2 , and H_2O . The high rate of decomposition of methanol in the presence of O_2 is also evident from the decreased production of dimethyl ether over Cs-MFI and Rb-FAU(X) and the higher methanol conversion (see Table 9.1 and 9.2).

The remaining part of this Chapter will therefore be devoted to the discussion of the side products observed during alkylation in the presence of O_2 , i.e., CO , CO_2 , H_2 , H_2O , benzene, benzaldehyde, and benzoic acid and coke. In the presence of O_2 approximately 28.1% (673 K) and 51.1% (773 K) over Cs-MFI, and approximately 21.2% (673 K) and 39.4% (773 K) over Rb-FAU(X) could not be accounted for in the measured gaseous products (ethylbenzene, styrene, xylene, H_2 and DME). The missing carbon could be carbon deposition, CO , or CO_2 , which are not measured quantitatively.

Byproduct formation

The first main problem that arises during the alkylation of toluene is the formation of coke with Cs-MFI and Rb-FAU(X). The effect of coke formation on the catalysts performance and selectivity was checked for the reaction over Rb-FAU(X) in the absence of O_2 . However, with the use of O_2 the catalysts life time had only increased approximately 15%. The catalyst deactivated with time on stream (less MeOH conversion) and was less selective towards toluene alkylation, while the DME production increased. After 35 hours on stream approximately 13wt% of coke had accumulated on the

catalyst. This is a lot of carbon; however, it does not account for more than 28% of the total amount of MeOH that is missing. The formation of coke could arise from 1) a Boudouard type of reaction whereby CO molecules decompose into solid carbon and CO₂, or 2) production of olefins that combine to aromatics and are dehydrogenated to solid carbon. However, no experiments were performed to confirm these assumptions. The reason for the increased DME production with time on stream is not clear, but the decrease in ring and side chain alkylation yield could enhance the surface methoxy concentration and hence increase the DME formation.

In Chapter 7 the production of methyl formate was used as evidence for the production of surface formaldehyde. Analysis of the effluent gas stream during toluene alkylation with methanol in the presence of O₂ over Cs-MFI or Rb-FAU(X) (between 323 and 773 K), however, did not show any methyl formate. The reason for this might be found in the high toluene concentration used in these experiments (toluene/methanol = 3/1), and the already low methanol adsorption capacity of Rb-FAU(X) during coadsorption experiments [13]. This probably results in low surface formaldehyde yield. The high toluene partial pressure in the feed was done due to the fact that toluene alkylation with methanol (in the absence of O₂) proceeds most selective with this ratio [3,11]. The observation of water at low temperatures with Cs-MFI and Rb-FAU(X) (below 498 K) is, however, indication of methanol oxidation yielding surface formaldehyde. Also the higher H₂ yield during alkylation over Rb-FAU(X) in the presence of O₂ is indicative of a higher surface formaldehyde yield.

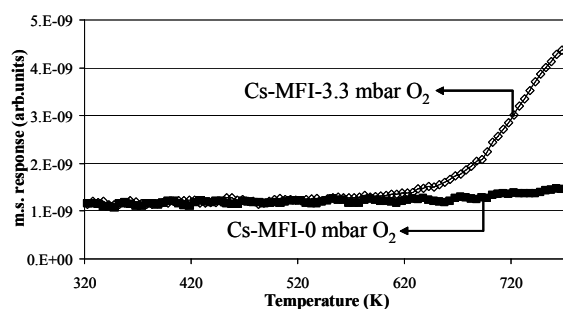


Figure 9.9: Gas phase CO₂ production during toluene alkylation over Cs-MFI in the presence and absence of O₂ as function of temperature. 323-773 K, T_r = 5 K.min⁻¹. (Molar ratio toluene/methanol/O₂ = 9/3/1)

No gaseous formaldehyde was found (this agrees well with Chapter 6 and 7), indicating that formaldehyde observed using i.r. spectroscopy is only a surface species (see Chapter 7), which immediately decomposes over strong basic sites to CO and H₂ [14] or is oxidized to form surface formate, which, subsequently, decomposes into CO₂, CO, H₂, and H₂O at high temperatures (see Chapter 7).

The production of H₂O in present study was not observed below 570 K with Rb-FAU(X) and below 530 K with Cs-MFI in the absence of O₂. In the presence of O₂ this was shifted to lower temperatures and is related to the oxidative dehydrogenation of methanol to surface formaldehyde. Furthermore, when O₂ was used (at 673 K) on Rb-FAU(X) and Cs-MFI an increase of the water gas phase concentration was observed. This is also an indication of the oxidation of MeOH and toluene.

The increase of the gaseous CO₂ concentration until 720 K and the decrease after 720 K in present study was also observed for CO₂ during MeOH oxidation over Rb-FAU(X) in the absence of

13. Palomares, A.E.; Eder-Mirth, G.; Lercher, J.A. *J. Catal.* **1997**, *168*, 442.

toluene (see Chapter 7). The CO_2 increase in Chapter 7, however, was more pronounced when no toluene was added to the feed (a 40 times increase was observed in Chapter 7) compared to the present study where only a 5 times increase was observed. This agrees well with the previous discussion about the high toluene pressure in the present study. During the reaction of toluene with methanol in the absence of O_2 over Cs-MFI no CO_2 was observed (see Fig. 9.9). With the use of O_2 , however, an increase was observed for the CO_2 production (approximately 3.7 times at 773 K). Note that CO_2 production in the empty fixed bed reactor was not observed below 773 K. No increase was found for the production of CO in the presence of O_2 over Rb-FAU(X), compared to the reaction in the absence of O_2 . The reason for this is not clear. The newly observed product CO_2 , the increased gas phase concentrations of CO_2 , H_2 and H_2O , the increasing MeOH conversion, and decreasing alkylation yield indicate that deep-oxidation of MeOH and formaldehyde decomposition are faster than alkylation. Also in the reaction of methanol with toluene in the absence and presence of O_2 H_2 and CO were observed. These products are related to coke formation; since these products were not observed during MeOH reaction and oxidation over Cs-MFI in an i.r. reactor (see Chapter 6 and 7), probably due to the short measuring time. Another possibility could be partial oxidation of DME yielding H_2 and CO. No experiments were performed to confirm this.

During the alkylation experiments over Rb-FAU(X) and Cs-MFI in the absence and presence of O_2 we also found small amounts of benzene (see Fig. 9.10). This is supposed to be related to toluene disproportionation yielding xylene and benzene [15].

With O_2 Cs-MFI yielded also gaseous benzaldehyde and benzoic acid above 620 K (see Fig. 9.10). Reaction of toluene with O_2 in an empty fixed bed reactor yielded also gaseous benzene, benzaldehyde and benzoic acid above 620 K (without O_2 no benzene, benzaldehyde and benzoic acid was found). Furthermore, the same yield and temperature profile were found using an empty reactor (above 620 K). Thus the observation of benzene, benzaldehyde and benzoic acid with Cs-MFI was concluded to be related to gas phase oxidation.

During toluene alkylation in the presence of O_2 over Rb-FAU(X) benzene was already found at 560 K with a jump in the production curve of benzene at approximately 623 K (see Fig. 9.10) that was not observed with Cs-MFI (see Fig. 9.10) or with the empty fixed bed reactor (not shown here). Toluene oxidation in the absence of MeOH yielded the same products and production curve as in

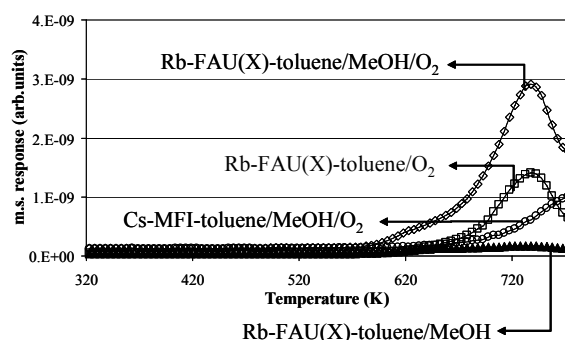


Figure 9.10: Gas phase benzene production during toluene alkylation and/or oxidation over Rb-FAU(X) and Cs-MFI in the presence and absence of O_2 as function of temperature. 323-773 K, $T_r = 5 \text{ K.min}^{-1}$. (Molar ratio toluene/methanol/ $\text{O}_2 = 9/3/1$) The lower intensity of the benzene signal of toluene/ O_2 compared to toluene/MeOH/ O_2 over Rb-FAU(X) is due to a lower SEM voltage of the mass spectrometer apparatus.

the presence of MeOH (see Fig. 9.5, 9.6, and 9.10) and showed the production of surface benzaldehyde and benzoate (see Fig. 9.7). No gaseous benzaldehyde and benzoic acid was found. Additionally, increasing O₂ concentrations added during the reaction of toluene with methanol at 673 K over Rb-FAU(X) yielded increasing concentrations of benzene, which agrees well with the work of Itoh *et al.* [6]. The production of benzene can be explained by assuming toluene oxidation [7,16] and possible decomposition of the oxidation products, as observed for MeOH oxidation (see Chapter 7).

Furthermore, also styrene and ethylbenzene were found during toluene oxidation over Rb-FAU(X) and their gas phase concentrations increased with increasing O₂ concentrations and temperature. This can probably be understood by assuming oxidative coupling of toluene yielding 1,2-diphenylethane and stilbene [17,18,19], which subsequently decompose into ethylbenzene and styrene and benzene.

9.5 Conclusion

The use of O₂ as reagent to increase *in situ* the surface formaldehyde concentration during toluene alkylation with methanol over Cs-MFI and Rb-FAU(X) led to small increases of the production of styrene and ethylbenzene. Most interestingly the Cs-MFI catalyst in the presence of O₂ showed a small catalytic activity towards side chain alkylation (with very low selectivities), whereas it gives almost exclusively ring alkylation in the absence of O₂.

However, the use of O₂ mostly converts MeOH and toluene to products other than styrene, ethylbenzene and/or xylene. Those products are CO, CO₂, H₂, H₂O, benzene (benzaldehyde and benzoic acid). These products have a much higher gas phase concentration, compared to the alkylation products. Alkylation of toluene at lower temperatures is not possible due to the required toluene activation.

Furthermore, it was shown that experiments with long time on stream are limited in possible industrial use due to the high coking observed in our experiments in the absence of O₂. In the presence of O₂ the catalysts lifetime was enlarged with approximately 15%.

It is thus concluded that the addition of O₂, has a large overall negative effect (despite the small increase in styrene and ethylbenzene). Still a large amount of research has to be done to improve the methanol selectivity, and the toluene activation. If selectivity and yield of the side chain alkylation reaction over alkali cation exchanged FAU(X) zeolites could be increased, then maybe a riser reactor could be of help.

15. Tsai, T.-C.; Liu, S.-B.; Wang, I. *Appl. Catal. A: General* **1999**, *181*, 355.

16. Sun, H.; Blatter, F.; Frei, H. *J. Am. Chem. Soc.* **1994** *116*, 7951.

17. a) Arishtirova, K.; Kovacheva, P.; Davidova, N. *Appl. Catal. A: General* **1998**, *167*, 271; b) Kovacheva, P.; Arishtirova, K.; Davidova, N. *Appl. Catal. A: General* **1999**, *178*, 111.

18. Kovacheva, P.; Arishtirova, K.; Davidova, N. *Appl. Catal. A: General* **1997**, *149*, 277.

19. Scheeline, H.W.; Ma, J.J.L. *U.S. Pat. 3,965,206*, 1976, assigned to Monsanto Company, USA.

Recommendations

Based on above results it is recommended that low temperature methylation of the side chain of toluene (to suppress formaldehyde decomposition) over Rb- and Cs-FAU(X) in the presence of oxygen (*via* the intermediate formaldehyde) can only occur when the toluene molecule is enough activated. This might be obtained by incorporation of Fe-Mo clusters [8].

The reaction of toluene with molecular oxygen yielding benzaldehyde, however, could open up new routes for the production of styrene. It was reported that benzaldehyde (*in situ* prepared from toluene oxidation) reacted with dihalomethane reagents to yield styrene [20]; however, the use of dihalomethane reactants is no real option for industrial practice, due to the halogenated byproducts.

Appendix 1 – Toluene alkylation in the absence of oxygen: The influence of the catalyst

The reaction of toluene with methanol in the absence of O₂ over Cs-MFI and Rb-FAU(X) has been investigated by Vinek *et al.* [4] and Palomares *et al.* [1] and many others. In Chapter 8 the alkylation of toluene over basic FAU(X) catalysts has been discussed with regard to toluene. In light of present shortcomings of the experimental setup and low toluene conversions, the yields and selectivities of alkylated products were based on MeOH. Therefore, we will discuss here the results of the alkylation reaction over Cs-MFI and Rb-FAU(X) in the absence of O₂ based on MeOH

The alkylation selectivities observed for both catalysts are in agreement with literature: Cs-MFI is an active catalyst for the alkylation of the toluene ring, whereas Rb-FAU(X) is an active catalyst for the alkylation of the toluene side chain (see Fig. 9.11).

In Table 9.A, the results from the fixed bed reactor, which were obtained isothermally at 673 and 773 K with Cs-MFI and Rb-FAU(X), are compiled. MeOH conversion in the absence of O₂ over Cs-MFI had increased at 773 K from 32.8 to 43.6%, probably due to increased DME production. (DME is the product of methanol intermolecular dehydration over Lewis acid sites (see also Chapter 6)). The DME selectivity remained constant at 673 and 773 K (11.5 mol%); however, due to increased MeOH conversion the DME yield increased from 673 to 773 K with 36%. Overall it is clear from Table 9.A that most methanol is converted to other

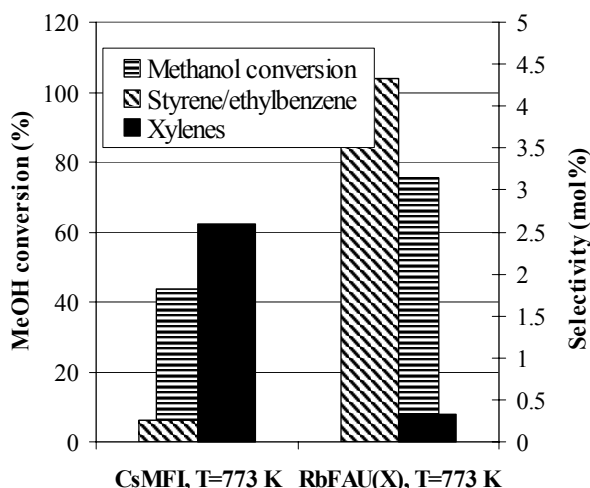


Figure 9.11: Methanol conversion (%) and alkylation selectivities (mol%) obtained during methylation of toluene over Cs-MFI and Rb-FAU(X) at 773 K.

20. Kaeding, W.W. *Catal. Rev.* **1973**, 8, 307.

products that could not be detected quantitatively in the gas phase (e.g., H₂O, CO, CO₂, etc.) due to the characteristics of the chosen gas chromatographs analysis columns. An additional amount of lost MeOH is attributed to coke formation as also was concluded in Chapter 6 and is supported by the fact that the catalyst was black after an alkylation run.

MeOH conversion in the absence of O₂ over Rb-FAU(X) had increased at 773 K from 14.9 to 75.6%, this is due to increased H₂ and DME production. H₂ is the product of MeOH dehydrogenation and decomposition over Lewis acid-base sites (see Chapter 6). The H₂ selectivity at 673 K was 4.4 mol%; at 773 K this was 38.5 mol%. Due to increased MeOH conversion, the H₂ yield increased from 673 to 773 K 40 times. The DME selectivity at 673 K was 8.7 mol%; at 773 K this was 2.6 mol%. While the DME selectivity was lower at 773 K, compared to 673 K, the DME yield still increased from 673 to 773 K with 25%, due to the higher MeOH conversion.

TABLE 9.A: Reaction of toluene with methanol over Cs-MFI and Rb-FAU(X) isothermally at 673 and 773 K. Conversion (%) of methanol (MeOH). Selectivities (mol%): per cent of MeOH converted into alkylation (SCA or RA)^{a,b} products, DME, or H₂.

Reaction	Reaction conditions (molar ratio + reaction temperature)				
	Cs-MFI		Rb-FAU(X)		Cs-FAU(X)
	C ₇ H ₈ /MeOH = 9/3; 673 K	C ₇ H ₈ /MeOH = 9/3; 773 K	C ₇ H ₈ /MeOH = 9/3; 673 K	C ₇ H ₈ /MeOH = 9/3; 773 K	C ₇ H ₈ /MeOH = 9/3; 773 K
MeOH conv.	32.8	43.6	14.9	75.6	37
SCA ^a Select.	0.2	0.3	5.1	4.3	0.92
RA ^b Select.	2.3	2.6	0.3	0.3	0.38
DME Select.	11.5	11.5	8.7	2.6	n.d.
H ₂ Select.	n.d.	n.d.	4.4	38.5	n.d.

^a SCA is side chain alkylation (= total styrene+ethylbenzene).

^b RA is ring alkylation (= total *o*-+*m*-+*p*-xylene).

It can be seen in Table 9.A that toluene alkylation with methanol (molar ratio toluene/methanol: 3/1) over alkali exchanged MFI zeolites in the absence of O₂ yielded mainly xylene (toluene ring alkylation). The xylene selectivity (based on MeOH conversion) had slightly increased at 773 K, compared to 673 K (ring alkylation selectivity increased from 2.3 to 2.6 mol%). The *o*-xylene : *p*-xylene+*m*-xylene ratio was found to be approximately 1:2 (no separation could be obtained between *m*- and *p*-xylene here) at 773 K and agrees well with results obtained by Vinek *et al.* [4], who reported at 773 K a xylene ratio of *o*-xylene : *p*-xylene : *m*-xylene = 33:39:28.

With increasing temperature a higher ring alkylation yield and selectivity was found with Cs-MFI. Also a higher DME yield (see before) was found at 773 K. This is supposed to be related to a higher rate of formation of surface methoxy groups with higher temperatures (see also Chapter 6) that are the supposed intermediates for DME and xylene. Also small concentrations of mesitylene

(= 1,3,5-trimethylbenzene) (approximately 10% of the xylene yield), and styrene and ethylbenzene were found (see Table 9.A).

Toluene alkylation with MeOH in the absence of O₂ (molar ratio toluene/methanol: 3/1) over Rb-FAU(X) yielded selectively side chain alkylation (styrene and ethylbenzene) at 673 and 773 K (see Table 9.A), which agrees well with results obtained by others [3,13]. The styrene alkylation selectivity decreased from 5.1 to 4.3 mol% with increasing temperatures, whereas the styrene and ethylbenzene yield had slightly increased at 773 K, compared to 673 K, due to higher MeOH conversion (side chain alkylation yield increased with 48%). The styrene : ethylbenzene ratio was found to be approximately 3:1 at 673 K (at 773 K this ratio was reversed (approximately 2:3)). Other products detected in the effluent stream were small concentrations of cumene (= isopropylbenzene) (approximately 5-10% of the styrene yield), xylene (see Table 9.A) and mesitylene (less than 10% of the total xylene yield).

In the case of Rb-FAU(X) it was noted that the side chain alkylation yield increased with increasing temperatures (in the absence of O₂), while the selectivity at higher temperatures decreased. This result agrees well with results reported by Palomares *et al.* [1]. The decreasing selectivity is attributed to the high methanol decomposition at 773 K, resulting in the formation of CO and H₂ (a commonly encountered problem with these very basic zeolites [1]). Indeed the production of H₂ at 773 K had increased (approximately 9 times) compared to side chain alkylation (approximately 4.5 times), and also the production of DME had decreased. The H₂ yield increased due to a higher MeOH dehydrogenation rate and decomposition rate of the intermediate formaldehyde (see also Chapter 6). At 673 K the styrene : ethylbenzene ratio was found to be 3:1; at 773 K this was vice versa (styrene : ethylbenzene ratio = 2:3). Two explanations are possible; 1) direct styrene hydrogenation by H₂ (gaseous or surface) formed during MeOH dehydrogenation/decomposition, or 2) direct toluene alkylation with methanol (dehydrocondensation) [3,11].

Although the trends and overall selectivities (ring alkylation *vs* side chain alkylation) are similar to those reported in literature, it is clear from Table 9.A that the yields and selectivity based on methanol were very low. Yashima *et al.* [3] reported 3 to 10 times higher styrene and ethylbenzene yield over Rb-FAU(X) between 673 and 773 K. Conversion of toluene was also very low and yields and selectivity based on toluene could not be measured without a significant experimental error. Low toluene conversions and alkylation yields (based on MeOH) are a commonly encountered problem [3,21]. Alkylation yields based on toluene usually give a more encouraging result. From the above it is clear that MeOH selectivity towards alkylation products over either Cs-MFI or Rb-FAU(X) is extremely low, compared to DME production and/or MeOH decomposition (yielding CO and H₂). A similar observation was made by Archier *et al.* [22] who reported 5% selectivity to side chain alkylation (based on MeOH conversion) over Cs-FAU(X), whereas 39% and 34% selectivity to DME

21. Giordano, N.; Pino, L.; Cavallaro, S.; Vitarelli, P.; Rao, B.S. *Zeolites* **1987**, 7, 131.

22. Archier, D.; Coudurier, G.; Naccache, C. In *Proceedings of the 9th International Zeolite Conference, Montreal*; Van Ballmoos, R., Higgins, J.B., and Treacy, M.M.J., Eds.; Butterworth-Heinemann: Boston, 1992; Vol. 2, pp 525-533.

and CO were found. In the absence of O₂ approximately 28.2% (673 K) and 37.3% (773 K) over Cs-MFI, and approximately 12.1% (673 K) and 41.4% (773 K) over Rb-FAU(X) could not be accounted for in the measured gaseous products (ethylbenzene, styrene, xylenes, H₂ and DME).

This is mainly caused by coke formation on the catalysts as was shown for Rb-FAU(X). Also the white color of the Cs-MFI catalyst particles had transformed into a dark color after reaction indicating large carbon deposits (not shown here). This leads to catalyst deactivation for toluene alkylation as was shown in Fig. 9.8 with Rb-FAU(X) and agrees well with Yashima *et al.* [3], who also observed a decreasing alkylation yield with time on stream.

Also higher alkylated products were found as mesitylene (1,3,5-trimethylbenzene) and cumene (isopropylbenzene). These observations are in agreement with those reported by others [21,23].

23. Beltrame, P.; Fumagalli, P; Zuretti, G. *Ind. Eng. Chem. Res.* **1993**, 32, 26.

Acknowledgements

One of the most difficult parts during the finishing of a PhD is the writing of the acknowledgment. Where do you start; what will be the order in thanking people who have been part of your life during the PhD, without giving them the feeling that they were less important. Do you start with the professors that have given you the opportunity to be here, or with your colleagues, or with the technical staff, or your parents etc.

Well, to me the most important people are the ones who have made this possible. These are my parents, my brother and Mónica. First of all I would like to express my deepest respect and love to my parents. Your strength, belief and love (even at the darkest hour of the day) kept me on going. To my brother; our quarrels and fun in our younger years shaped me as I am today. To Monica; for loving me all the way from the bottom to the top of my PhD (muchas gracias por todo). And Kitty; may chemistry ever be one of your topics when teaching at school.

Second on my list are my two great *paranymfs*, Marc and Jean-Pierre and their wonderful wives Kim and Arja. Without you guys today would not be the day it has to be. Pierre, thanks a lot as well for the evening hours we spent together in the Mensa, “De Geus”, the Munich lab and the Faculty. Marc, without your fun and enthusiasm the last two years would have been very boring.

Jan, working with you was a great experience! Our discussions always were a mixture of my work and the work of the other group members or the field we both liked, homogeneous catalysis. Thanks a lot for the hours we spent together when finishing the conference presentations and the concept of the thesis and of course for introducing me to your sports club for our mutual interest, diving. I will miss our discussions!

What would be the value of this work without the enthusiastic help of my amazing students? Thus, Christian, Manja, Pepi, Uli, and Thomas; you guys have been the driving force of this work. Christian; good luck with your coming promotion and thanks for the hours we spent together in Munich. Manja; you did a great job when I was on the other side of the world. Pepi; your laugh still echoes in the building and your enthusiasm for going out was indestructible. Uli; the godfather of the young, lonely cat: She is doing fine! Thomas, you probably had the shittiest job of all, but you managed to finish it with a smile. To all of you I would like to say: Thanks a lot and see you all very soon again somewhere!!!!

Bertolino, my goeroe, you were the best in the group. With computer trouble, OIO facility matters etc. you always had the cure. Your very valuable help with the final concept is gratefully acknowledged! Karin, you were always there to change my gas bottles and to remind me of my glasses and safety regulations. All your stories about holidays and the dog were a pleasure. Bertje Kamp, you always had a generous smile during the countless times you repaired my GC. To *onze vakgroep moeder* Cis, you never felt tired of sending emails, letters, arranging tickets etc. Jan Talman (ELTN), always a helping hand with the vacuum pumps. To Louise, lots of fun with the infrared machines and to Vilmos for making me realize that there is also music called “Klassiek” and “Barok”.

Of course I cannot forget my old roommates, Sergio en Renate. We shared the room a short time, but nevertheless it was a great time. Sergio; always a smile even when things got out of hand. Renate, after leaving the room for going back to Munich for a PhD, you decided to work on basic zeolites as well. Did I infect you? And to my neighbor, Manon, we shared fun and the same wall.

Takeshi, I will never forget our biking in the snow when we came back from “De Geus”. Laurent (for having me run around in a dress and kissing Bertolino), Gerhard (together with Pierre you introduced me to the nightlife of downtown Enschede), Laszlo D. (our discussions were always lengthy), Laszlo L., Martin, Victor, Sheila, Andre, Katia, Bertha, Gautam, Martijn, Sepp (we both shared the love for German white beer), Dejan, Seshan, Olivier and Eva G.

To my (former) colleagues from Munich, Fred, Thomas, Anil, Andreas, Andreas J., Adam, Alex, Hilton etc.: we shared a great time in the lab and bars of Munich. To all my Spanish friends, Itziar, Eduardo, Belen, Montse, Eva, Marta U., Xavi, David, Diego, Carmen, Franqui (ex-CPM), Olga, Michel and Marta R. (the SMCT freaks) muchas gracias por las vacaciones en España y las canciones, las borracheras y los buenos ratos. Gracias a la familia López-Lorenzo por su acogimiento y cariño: José, María del Carmen, abuelo Manuel y abuela Sofia. Jose M. y Ana, sois los mejores. Con vosotros la diversión está asegurada. No me olvido de ti, Thor.

Gerald and Nieck, thanks a lot for the great sailing trips in Friesland. They were a pleasant break during the work. My other colleagues from IMS, Arian, Samuel, Peter, Thomas, Monse, Mercedes, Louis, Matthijs, Fiona, Riaan, Frederic, Cindy, Attila, Natascha, Marjan, etc. It was a great pleasure to work with all of you and to share all the other assets of life in Enschede (the Batavierenrace, the volleyball team, and the soccer teams).

To my present colleagues, Valer, Igor, Robert, Sune, Barbara, Rahuman, Nabeel, Li, Jiang, Zhu, and Vijay: Guys I count on you in keeping the name of the CPM group high in Catalysis, Volleyball and Soccer.

To all the others who are looking for their names in this list and do not find it, I may have forgotten you, but that does not mean that you are of much less importance to the final result of what lies before you. Working with you short or long has had a definite impact on my work (and Enschede life).

Good luck to all of you!!

And finally, of course I would like to thank my two supervisors for their enthusiasm and knowledge regarding this work. Just your interest made this project already unforgettable. Thanks a lot, Johannes, for giving me the opportunity to work on this specific subject and Leon for taking over the guidance from Johannes after two years. Our discussions sometimes did not go over a bed of roses, but that is part of the job.... and finally resulted in this thesis.

Marco

Curriculum Vitae

Marco Rep werd geboren op 30 december 1970 te Zaandam (Noord-Holland). Na het afsluiten van de MAVO te Zaandijk in 1987 vervolgde hij zijn studie aan de Scholengemeenschap Rooswijk te Zaandijk voor twee jaar HAVO en twee jaar VWO en stapte vervolgens in 1991 over naar de Universiteit van Amsterdam voor een studie Scheikunde. Na een buitenland stage bij Prof. dr. K. Mach aan de Czech Academy of Sciences in Praag, Tsjechië, waarbij hij meewerkte aan onderzoek naar de reactiviteit van verschillende cyclopentadienyl-titaan complexen met diaceton azine en een afstudeer periode in de vakgroep Anorganische Chemie onder leiding van Prof. dr. K. Vrieze en Prof. dr. C.J. Elsevier naar palladium complexen met bidentaats stikstof liganden met een grote bite-angle behaalde hij zijn diploma in 1997 na het schrijven van een literatuur scriptie over de katalytische eigenschappen van metaal complexen in dendrimeren en micellen. Vervolgens begon hij in november 1997 een promotie onderzoek bij de vakgroep Katalytische Processen en Materialen binnen de faculteit Chemische Technologie van de Universiteit Twente te Enschede onder leiding van Prof. dr. J.A. Lercher, waarna de leiding in augustus 1999 werd overgenomen door Prof. dr. ir. L. Lefferts. De resultaten van dit onderzoek naar methanol adsorptie en activering en toluen alkylering over basische zeolieten en de invloed van zuurstof staan beschreven in dit proefschrift.

List of Publications

Coordination Modes of the Novel Bifunctional Nitrogen Ligands 8-(2-Pyridyl)Quinoline and 8-(6-Methyl-2-Pyridyl)Quinoline towards Palladium and Platinum. X-ray Crystal Structures of 8-(2-Pyridyl)QuinolinePd(Me)Cl, 8-(2-Pyridyl)QuinolinePd(C(O)Me)Cl and 8-(2-Pyridyl)QuinolinePd(PEt₃)Cl₂

Delis, J.G.P.; Rep, M.; Rülke, R.E.; Van Leeuwen, P.W.N.M.; Vrieze, K.; Fraanje, J.; Goubitz, K.
In *Inorg. Chim. Acta* **1996**, *250*, 87.

Titanium-Catalyzed [4+2] and [6+2] Cycloadditions of 1,4-Bis(Trimethylsilyl)Buta-1,3-Diene

Kaagman, J.-W.F.; Rep, M.; Horáček, M.; Sedmera, P.; Čejka, J.; Varga, V.; Mach, K.
In *Collect. Czech. Chem. Commun.* **1996**, *61*, 1722.

Trans-4,5-Bis(2-Pyridyl)Norborene: A Bidentate Nitrogen Ligand with a Potentially Large Bite Angle

Delis, J.G.P.; Rep, M.; Kranenburg, M.; Vrieze, K.; Van Leeuwen, P.W.N.M.; Veldman N.; Spek, A.L.
In *J. Organomet. Chem.* **1998**, *564*, 29.

Alkylation of Toluene over Basic Zeolites – Key Requirements for Side Chain Alkylation

Palomares, A.E.; Eder-Mirth, G.; Rep, M.; Lercher, J.A.
In *J. Catal.* **1998**, *180*, 56.

On Selectivity Aspects of the Alkylation of Toluene with Methanol over Zeolites

Rep, M.; Palomares, A.E.; Eder-Mirth, G.; Van Ommen, J.G.; Lercher, J.A.
In *Proceedings of the DGMK-conference "The Future Role of Aromatics in Refining and Petrochemistry"*, *Tagungsbericht 9903, Erlangen*; Emig, G., Rupp, M., and Weitkamp, J., Eds.; DGMK: Hamburg, 1999; pp 279-286.

Reactions of Methyl-substituted Titanocene-Bis(Trimethylsilyl)Acetylene Complexes with Acetone Azine: Crystal Structures of $\eta^5:\eta^1\text{-C}_5\text{HMe}_2\text{CH}_2\text{CMe}_2\text{NH}_2\text{Ti}$ and $(\text{C}_5\text{Me}_5)_2\text{Ti}(\text{N}=\text{CMe}_2)$

Rep, M.; Kaagman, J.-W.F.; Elsevier, C.J.; Sedmera, P.; Hiller, J.; Thewalt, U.; Horáček, M.; Mach, K.
In *J. Organomet. Chem.* **2000**, *597*, 146.

Sorption of Methanol in Alkali Exchanged Zeolites

Rep, M.; Palomares, A.E.; Van Ommen, J.G.; Lefferts, L.; Lercher, J.A.
In *Proceedings of the 12th International Congress on Catalysis, Granada*; Corma, A., Melo, F.V., Mendioroz, S., Fierro, J.L.G., Eds.; Elsevier: Amsterdam, 2000; Vol. C, pp 2957-2962.

Interaction of Methanol with Alkali Metal Exchanged Molecular Sieves. 1. IR Spectroscopic Study

Rep, M.; Palomares, A.E.; Eder-Mirth, G.; Van Ommen, J.G.; Rösch, N.; Lercher, J.A.

In *J. Phys. Chem. B* **2000**, *104*, 8624.

I.r. Study on the Reaction Path of Methanol Decomposition over Basic Zeolites

Rep, M.; Van Ommen, J.G.; Lefferts, L.; Lercher, J.A.

In *Proceedings of the 13th International Zeolite Conference, Montpellier*; Galarnau, A., Di Renzo, F., Fajula, F., and Vedrine, J., Eds.; Elsevier: Amsterdam, 2001; Vol. 135, p 316.

Thiophene Decomposition on Pt-Supported Zeolites: A TPD study

Simon, L.J.; Rep, M.; Van Ommen, J.G.; Lercher, J.A.

In *Appl. Catal. A: General* **2001**, *218*, 161.